

Synthesis, Optimization, and Evaluation of Thiophilic Peptidomimetics as Novel AD Therapies

BY

ISAAC T. SCHIEFER

B.S., University of Toledo, Ohio, 2007

DISSERTATION

Submitted as partial fulfillment of the requirements for the degree of Doctor of
Philosophy in Medicinal Chemistry in the Graduate College of the University of Illinois
at Chicago, 2012

Chicago, Illinois

Defense Committee:

Gregory R. J. Thatcher, Ph.D, Advisor and Chair

Pavel A. Petukhov, Ph.D

Karol S. Bruzik, Ph.D

Douglas D. Thomas, Ph.D

Thomas G. Driver, Ph.D, Chemistry Department

DECLARATION OF ORIGINALITY

I certify that, to the best of my knowledge, this document does not infringe upon nor violate any copyrighted or proprietary materials. The ideas, techniques, and other materials included in this dissertation, published or otherwise, are fully acknowledged in accordance with standard referencing practices. The efforts of colleagues and collaborators are clearly defined within the acknowledgments section. Specific personal contributions are catalogued briefly below:

Chapters 1-2: Design and synthesis of epoxide peptidomimetics for evaluation as AD therapies.

- Conceptualized and synthesized 2nd and 3rd generation calpain inhibitors. Including the optimized preclinical candidate (**NYC-438**)
- Completed characterization and iterative synthesis of entities created by colleagues
- Analyzed literature precedents, x-ray structures, binding motifs and docking results from computational chemistry team to design potent and selective inhibitors
- Assessed structure activity relationship (SAR) based on inhibition results to aide in designing subsequent analogs
- Utilized novel click chemistry approach to quickly generate the 3rd generation library
- Carried out efficient gram-scale synthesis of selected inhibitors for *in vivo* testing
- Carried out all Chapter 2 experiments and analysis of epoxide prodrug reactivity

Chapter 3: Furoxans as novel NO mimetic neuroprotective agents

- Carried out synthesis of the compounds reported in the document.
- Designed peptidomimetic scaffolds for furoxan incorporation
- Carried out reactivity analysis following training and initial reactivity profiling by a post-doctoral colleague
- Examined furoxans for NO₂⁻ production and thiol depletion

I am solely responsible for the composition of the thesis document, which was modified in accordance with recommendations from the defense committee. The document contains modified adaptations of annual project reports, to which I personally contributed. Provisional patent disclosures have been filed for the work presented. Chapter 3 has been accepted for publication (Schiefer, I.T. et al, *J Med Chem*, **2012**, DOI: 10.1021/jm201504).

ITS

ACKNOWLEDGMENTS

I would like to thank all those who contributed to the enclosed work: Dr. Subhasish Tapadar- for his involvement in the synthesis of novel 1st and 2nd generation calpain inhibitors; Dr. Esala Chandrasena and Dr. Gihani T. Wijewickrama- for their experiments utilizing LC-MS/MS in lead optimization and measuring IC₅₀ values of calpain inhibitors, their guidance in operating and utilizing HPLC-MS/MS in my own experiments is greatly appreciated; Dr. Vaishali Sinha & Dr. Robert Scism for their collection of free enzyme inhibition data; Dr. Michael Brunstetter for his efforts in molecular modeling and docking studies; Dr. Pavel A. Petukhov for his continued guidance and support in medchem/synthesis throughout the entirety of the project; and our collaborator at Columbia University, Dr. Ottavio Arancio and his lab for assaying our compound in the LTP paradigm and in behavioral/toxicity studies (Dr. Mauro Fa`, Dr. Hong Zhang, and Dr. Agnieszka Staniszeewski).

Most importantly, I would like to thank my advisor Prof. Gregory R. J. Thatcher. His enthusiasm is contagious, and his no-nonsense approach to troubleshooting problems in chemical biology is inspiring. His capacity to apply his expertise in physical chemistry to all phases of medicinal chemistry is a characteristic that I will strive to mimic and employ throughout my scientific research career.

Last, but certainly not least, I would like to thank my wife, Ashley, for her continued support throughout my academic career. Through the highs and lows of research and academics, her support has been constant and unwavering. She is the light.

ITS

TABLE OF CONTENTS

DECLARATION OF ORIGINALITY	II
ACKNOWLEDGMENTS	III
LIST OF FIGURES	VII
LIST OF TABLES	XI
LIST OF SCHEMES	XII
ABBREVIATIONS	XIII
SUMMARY	XV
CHAPTER 1. CALPAIN AS A THERAPEUTIC TARGET FOR ALZHEIMER'S DISEASE	1
1. INTRODUCTION	1
1.1 Alzheimer Disease: An Approaching Epidemic.....	1
1.2 Brief History of AD.....	2
1.2 Pathophysiology	4
1.2.1 Neurofibrillary Tangles (NFT's).....	4
1.2.2 Senile plaques	5
1.2.3 Current clinical approaches.....	7
1.3 Calpain as a Therapeutic Target for AD.....	8
1.3.1 The Calpain System	8
1.3.2 A Brief Review of Calpain Inhibitors in the Literature	18
1.3.3 Potential of Epoxide Peptidomimetic Calpain Inhibitors in AD Therapy	24
2. RESULTS	32
2.1 Assay Development & Lead Optimization.....	32
2.1.1 Evaluating Calpain Inhibition using a FRET substrate.....	32
2.1.2 Employing LC-MS/MS in Lead Optimization of Calpain Inhibitors	38
2.2 2 nd generation inhibitors: gaining selectivity	47
2.3 3 rd generation inhibitors: P3 refinement and molecular diversity	58
2.4 Ex vivo and in vivo evaluation of efficacy and safety.....	61
3. DISCUSSION.....	75
3.1 In Vitro Assay Directed Drug Discovery.....	75
3.2 SAR of Calpain Inhibitors.....	80
3.3 In vivo evaluation and potential in AD therapy	81
4. SUMMARY	84
5. MATERIALS AND METHODS.....	86
5.1 Synthesis	86
5.2 FRET assay of calpain inhibition	95
5.3 LC-MS/MS approach.....	96
5.4 Calpain vs cathepsin B: preference assay	96
5.5 LTP	97
5.6 Calpain dependent spectrin cleavage in brain homogenates.....	97
5.7 Cognition Enhancement	97
5.8 Pharmacokinetics	98

TABLE OF CONTENTS (continued)

5.9 Acute Toxicity	98
5.10 Chronic Toxicity	98
CHAPTER 2. EPOXIDE PRODRUGS: DISCOVERY OF AN UNREPORTED MECHANISM OF PRODRUG BREAKDOWN	100
1. INTRODUCTION	100
2. RESULTS	102
2.1 Prodrug Aqueous Stability	102
2.2 Prodrug reactivity with GSH: competing breakdown pathways	107
3. DISCUSSION	115
3.1 Impact on NYC-438 prodrug development	115
3.2 Implications on mechanism of action of clinical candidate E-64d	117
4. CONCLUSIONS	118
5. MATERIALS AND METHODS	118
5.1 Materials	118
5.2 Synthesis	118
5.3 HPLC analysis of stability/reactivity	119
CHAPTER 3. DEVELOPMENT OF ATTENUATED FUROXANS AS NOVEL NEUROPROTECTIVE AND PROCOGNITIVE THIOPHILIC NO-MIMETICS	120
1. INTRODUCTION	120
2. RESULTS	124
2.1 Design and Synthesis	124
2.2 Furoxan Reactivity	129
2.3 NO ₂ ⁻ production	144
2.4 Thiol oxidation	146
2.5 Neuroprotection	150
2.6 Restoration of Synaptic Function	155
3. DISCUSSION	157
3.1 Correlating NO _x release and Neuroprotection	157
3.2 Potential of Attenuated Furoxans as Novel Neuroprotective Agents	159
4. CONCLUSIONS	159
5. MATERIALS AND METHODS	160
5.1 Materials	160
5.2 Synthesis	160
5.3 Crystallography	160
5.4 Reactivity Analysis	161
5.5 Griess Assay	161
5.6 Cysteine Reactivity	162
CITED LITERATURE	163
APPENDIX A. EXPERIMENTAL PROCEDURES AND CHARACTERIZATION	174
APPENDIX B. COMPOUND CHARACTERIZATION SPECTRA	223

TABLE OF CONTENTS (continued)

VITA.....	262
STATEMENT OF TEACHING PHILOSOPHY	266

LIST OF FIGURES

<u>FIGURE</u>	<u>PAGE</u>
1. 1st characterization of AD	3
2. NFT's and senile plaques.....	3
3. APP proteolytic degradation by secretases	6
4. Schematic of Cal1 and Cal2 structure motifs	11
5. Schematic of calpains involvement in AD related pathologic pathways	16
6. Non-active site directed inhibitors	20
7. Examples of cysteine reactive “warheads”	20
8. Aldehyde incorporating peptidomimetic calpain inhibitors	21
9. α -ketoamide incorporating peptidomimetic calpain inhibitors	21
10. Epoxide containing peptidomimetic calpain inhibitors	26
11. Review of cysteine protease substrate and inhibitor nomenclature	29
12. Representative examples of reported epoxide peptidomimetics.....	30
13. Lead optimization strategy.....	31
14. Structures and Inhibition curves from end point analysis using the FRET assay.....	35
15. Inhibition curves of potent inhibitors at concentration near the IC ₅₀ values	36
16. Resulting TIC from tryptic digest of Cal1 and Cal1 _{cat}	42
17. Resulting EIC for the treatment of Cal1 _{cat} with E-64 and 5	43
18. Calibration curve of active site modification at varying inhibitor concentration	44
19. Structures of 1 st generation inhibitors examined in LC-MS/MS assay.....	45
20. Rationalization of potential for calpain selectivity via the P2 moiety	49
21. Competition experiment examining relative Cal1 _{cat} vs CathB modification ^a	53

LIST OF FIGURES (continued)

<u>FIGURE</u>	<u>PAGE</u>
22. Examination of inhibition kinetics of selected inhibitors against Cal1 _{cat} and papain.	56
23. Docking results illustrating predicted binding poses of novel inhibitors	57
24. Tentative correlation between Nsig values and observed IC ₅₀ values	60
25. Determination of ED ₅₀ of synaptic rescue in LTP by E-64.....	63
26. Ratio of LTP restoration by epoxide peptidomimetic calpain inhibitors.....	64
27. Lack of a correlation between Cal1 IC ₅₀ and LTP restoration	65
28. Contextual fear memory following 30 d treatment to 2 month old APP/PS1 mice....	67
29. Spatial-working memory following 30 d treatment to 2 month old APP/PS1 mice...	68
30. Contextual fear memory following 5 month treatment to APP/PS1 mice	69
31. Spatial-working memory following 5 month treatment to APP/PS1 mice.....	70
32. Reduction in calpain dependent spectrin degradation products in the brain	71
33. Plasma concentrations of calpain inhibitors following IP administration	73
34. Photographic examination for signs of <i>in vivo</i> toxicity	74
35. Determination of 2 nd order rate constant k_i/K_i	78
36. Prodrug ester approach for epoxysuccinate containing peptidomimetics.....	101
37. Effect of pH on prodrug ester saponification in PB (50 mM) at 25 °C	104
38. NYC-438E ester saponification in phosphate buffer (50 mM, pH 7.4) at 37 °C.....	105
39. E-64d ester saponification in phosphate buffer (50 mM, pH 7.4) at 37 °C	106
40. Analysis of the reaction between epoxide prodrug esters and GSH	108
41. HPLC time course of the products from reaction of NYC-438E and GSH.....	109
42. Graphic representation of reaction products of NYC-438E with GSH	110

LIST OF FIGURES (continued)

<u>FIGURE</u>	<u>PAGE</u>
43. HPLC time course of the products from reaction of NYC-539E and GSH.....	111
44. Graphic representation of reaction products of NYC-539E with GSH	112
45. HPLC time course of the products from reaction of E-64d and GSH	113
46. Graphic representation of reaction products of E-64d with GSH.....	114
47. The ideal prodrug scenario for epoxyacids.....	116
48. X-ray structure of the <i>p</i> -NO ₂ containing furoxan triazole peptidomimetic 6c	128
49. Observed trend in furoxan reactivity	131
50. Chromatogram of products from reaction between the furoxan 6a and cysteine	133
51. Chromatogram of products from the reaction of the furoxan 6c and cysteine	134
52. Comparison of reaction products from 6c and 7c with cysteine.....	136
53. Mass spectrum of proposed keto-oxime product from 6c and 7c	137
54. Comparison of reaction products from 6a and 7a with cysteine.....	138
55. Mass spectrum of proposed keto-oxime product from 6a and 7a	139
56. Chromatogram of products from reaction between the furoxan 11 and cysteine	140
57. Mass spectrum demonstrating incorporation of ¹⁸ O into keto-oxime product of 6c	142
58. Mass spectrum demonstrating incorporation of ¹⁸ O into keto-oxime product of 7c	143
59. Depletion of reduced cysteine in the presence of furoxans	147
60. Correlation between cysteine depletion and NO ₂ ⁻ production.....	149
61. Neuroprotection by furoxans in primary neurons following OGD.....	152
62. Tentative correlation between NO ₂ ⁻ production and neuroprotection	153
63. Neuroprotection by furoxans in the presence of ODQ	154

LIST OF FIGURES (continued)

<u>FIGURE</u>	<u>PAGE</u>
64. LTP restoration by the furoxan 9a following co-perfusion with oligomeric A β	156
65. Correlation of NO $_2^-$ production and neuroprotection including 6c NO $_x$ product	158

LIST OF TABLES

<u>TABLE</u>	<u>PAGE</u>
I. MAIN MEMBERS OF “THE CALPAIN SYSTEM” IN HUMANS ^a	10
II. STRUCTURES AND IC ₅₀ VALUES OF 1ST GENERATION CALPAIN INHIBITORS ^a	37
III. ACTIVE SITE MODIFICATION FOLLOWING COMPETITION WITH E-64 ^a	45
IV. STRUCTURES AND IC ₅₀ VALUES OF 2 ND GENERATION CALPAIN INHIBITORS ^a	50
V. INHIBITION RATE CONSTANTS VERSUS CAL1 AND PAPAIN ^a	56
VI. 3 RD GENERATION INHIBITORS WITH VARYING P3 CAP GROUPS ^a	59
VII. COMPARISON OF CAL1 AND CAL1 _{CAT} INHIBITION RATE CONSTANTS ^a ...	78
VIII . EFFECT OF DIPEA ON INITIAL PEPTIDE COUPLING REACTION ^a	89
IX. EFFECT OF DIPEA ON INITIAL PEPTIDE COUPLING ^a	91
X. EFFECT OF DIPEA ON EPOXIDE ESTER COUPLING REACTION ^a	92
XI. STRUCTURE DESIGNATIONS OF SCHEME 5 ANALOGS	94
XII. STRUCTURE DESIGNATIONS OF SCHEME 7 ANALOGS	95
XIII. NO ₂ ⁻ PRODUCTION FROM FUROXANS AFTER 24 H WITH EXCESS CYSTEINE ^a	145
XIV. CYSTEINE REMAINING AFTER 2 H INCUBATION WITH FUROXANS UNDER HYPOXYIC CONDITIONS ^a	148

LIST OF SCHEMES

<u>SCHEME</u>	<u>PAGE</u>
1. Chemical mechanism of calpain proteolytic activity ^a	12
2. Methodology used to examine active site modification by LC-MS/MS ^a	41
3. Schematic of competition assay methodology using Cal _{cat} and CathB ^a	52
4. Stereo-specific synthesis of the epoxide monoester	87
5. Peptide coupling and hydrolysis reactions to afford the desired peptidomimetics.....	88
6. Divergent synthetic route utilizing click chemistry	91
7. Novel synthesis of the triazole incorporating epoxide peptidomimetics	93
8. Potential mechanisms of furoxan bioactivation and neuroprotection ^a	123
9. Synthesis of furoxan-triazole incorporating peptidomimetics ^a	126
10. Synthesis of furoxan peptidomimetics continued ^a	127
11. Putative mechanism describing products observed from the reaction of the furoxan 9a with cysteine ^a	132

ABBREVIATIONS

AD	Alzheimer's Disease
APP	amyloid precursor protein
APP/PS1	A β overexpressing mice APP (K670N:M671L) & PS1 (M146L) mutants
A β	amyloid beta
β secretase	β -site of APP cleaving enzyme
BDNF	Brain derived neurotrophic growth factor
BiEP	biotinylated epoxide
[Ca ²⁺] _i	calcium concentration (intracellular)
Cal1	calpain 1
Cal2	calpain 2
CaMKII	Ca ²⁺ /calmodulin-dependent protein kinases II
CathB	cathepsin B
Cdk5	cyclin-dependent kinase 5 (cell division protein kinase 5)
cGMP	cyclic guanosine monophosphate
CREB	cyclic adenosine monophosphate response element binding protein
DTNB	(5,5'-dithiobis-2-nitrobenzoic acid [Ellmans Reagent])
GSH	glutathione
GSK-3 β	glycogen synthase kinase 3 beta
IP	intraperitoneal
LTP	long term potentiation
MAPK	mitogen-activated protein kinases
MTD	maximum tolerated dose
NFT	neurofibrillary tangle
NO	nitric oxide

ABBREVIATIONS (continued)

NO _x	NO species (NO [•] , NO ⁻ , NO ⁺ , HNO)
OGD	oxygen glucose deprivation
PBS	phosphate buffer solution
PD	pharmacodynamics
PK	pharmacokinetics
PKA	protein kinase A
RAWM	radial arm water maze
sGC	soluble guanylyl cyclase
WT	wild-type

SUMMARY

Alzheimer's disease (AD) is a progressive neurodegenerative disorder that threatens to reach epidemic proportions in the near future. The fastest growing population demographic is citizens over the age of 65, and the number one risk factor for developing AD is age. Approximately 50 % of individuals over the age of 85 suffer from some form of dementia and the financial burden created by treating and caring for these individuals reached \$172 billion last year in the United States alone. The prevalence and cost of AD promises to rise with the transitioning of the baby boomer generation into retirement and old age. Current AD therapies provide temporary symptomatic relief, but eventually become ineffective due to the presence of significant neurodegeneration. The steps we take in drug discovery research over the next 15 years will be vitally important to thwart the oncoming AD epidemic.

Several lines of evidence indicate that hyperactivation of a cytosolic calcium-dependent cysteine protease, calpain, is fundamentally involved in AD pathology and neurodegeneration. Calpain is hyperactivated in the brains of human AD patients, and its endogenous inhibitor, calpastatin, is found in significantly low abundance. Under physiological conditions, calpain is involved in numerous signaling cascades, most of which involve regulation of protein kinases. Additionally, calpain plays a key role in regulating cytoskeletal dynamics, especially those in synapses. Under pathological conditions, calpain carries out unregulated proteolysis, leading to neurodegeneration and cognition impairment. Inhibition of calpain restores synaptic function and memory deficits in transgenic murine AD models. Hence, calpain has been the subject of increased attention as a drug target for AD over the past 20 years.

SUMMARY (continued)

E-64, a thiophilic epoxide incorporating natural product, is a potent inhibitor of calpain and most other cysteine proteases. E-64 was identified as being capable of restoring synaptic plasticity and reversing cognition deficits in murine AD models, and calpain inhibition was hypothesized as being chiefly responsible for these effects. However, E-64 is a non-selective cysteine protease inhibitor, and suffers from detrimental structural features as a CNS drug candidate. A library of epoxide incorporating peptidomimetics was synthesized, including three successive generations designed to: increase potency, gain selectivity, and improve drugability. Examination of previously reported inhibitor-bound x-ray structures and computational modeling studies gave insight into ligand design and a speculative binding motif. With the knowledge that the lead compound possessed promising efficacy, competition experiments were employed to understand the potency and selectivity of novel analogs relative to E-64. As a result of the lead optimization effort, novel inhibitors were generated with better potency, increased selectivity, and more desirable physiochemical properties than E-64.

Selected epoxide peptidomimetics were tested for efficacy using *in vivo* behavioral models in APP/PS1 transgenic AD mice and *ex vivo* experiments of synaptic plasticity. The novel E-64 analogs were found to reverse cognition impairment following short term and long term administration to APP/PS1 mice in conditional fear and spatial memory paradigms. Preliminary pharmacokinetic studies yielded predictable PK profiles and MTD's were determined for selected inhibitors. Our epoxide peptidomimetics have negligible toxicity in mice in the form of lethality or malaise following chronic administration at the MTD with no observable gross organ abnormalities. The efficacy and safety of these novel calpain

SUMMARY (continued)

inhibitors supports further evaluation of their PK/PD profile as preclinical candidates for AD in preparation for filing an IND application.

Furoxans (1, 2, 5 oxadiazole-N-oxides) are thiol-dependent NO mimetics that have been the focus of intensive medicinal chemistry efforts over the past 30 years. Furoxans have been reported to display numerous interesting biological activities including: anti-infective properties, anti-parasitic effects, and toxicity as anti-cancer. Efforts to develop furoxans for these activities have focused on highly reactive furoxans, which rapidly react with biological thiols, thereby producing large amounts of NO and the cytotoxic effects associated with high cellular NO concentrations. However, the inherent reactivity of the furoxan ring is influenced by the nature of its substitution, and hence, may be attenuated to produce agents that give lower fluxes of NO. At physiological concentrations, NO possesses a variety of neuroprotective and procognitive effects. The enhancement of the NO/sGC/CREB signaling cascade may provide an appropriate approach to treat neurodegenerative disorders, specifically AD. To the best of our knowledge, there are no previous reports attempting to attenuate furoxan reactivity via ring substitution, nor are there any reports of targeting furoxans to the CNS.

A library of furoxan incorporating peptidomimetics was designed to judge the potential of modulating furoxan ring reactivity by substituting its adjacent aryl-system. Novel furoxans were analyzed for NO₂⁻ release and depletion of thiol in the presence of excess cysteine. The reaction products were monitored/identified by HPLC-MS. Substitution of the conjugated aryl system significantly impacted furoxan reactivity. Interestingly, reduced reaction rates of with thiol did not necessarily correspond with the propensity for NO release. Most of the

SUMMARY (continued)

furoxans were found to be neuroprotective in primary neurons following OGD, while a few were found to be toxic. The neuroprotective properties were ameliorated in the presence of a sGC inhibitor, ODQ, supporting a mechanistic role of the NO/cGMP/CREB signaling pathway. This mechanism was further supported by the ability of one furoxan to restore synaptic function in hippocampal slices co-perfused with oligomeric A β , an activity commonly observed in molecules that stimulate the NO/cGMP/CREB pathway. The discovery of novel neuroprotective and procognitive activities of attenuated furoxans supports further study as potential AD therapeutics.

In this work, we evaluated two approaches utilizing thiophilic peptidomimetics for potential use as AD therapeutics. Epoxide incorporating molecules were found to be safe and effective *in vivo* and calpain inhibition is hypothesized as being a primary mechanism responsible for cognition enhancement. The novel approach of designing attenuated furoxans as thiophilic peptidomimetics for the CNS also gave promising results, as some furoxans were found to be neuroprotective and procognitive. The common feature of these distinct molecular classes is their impact on phosphorylation of the memory-related transcription factor CREB. Epoxide based calpain inhibitors and attenuated furoxans are exciting prospects in AD drug discovery and further preclinical investigation of both chemical classes is warranted.

CHAPTER 1. CALPAIN AS A THERAPEUTIC TARGET FOR ALZHEIMERS DISEASE

1. Introduction

1.1 Alzheimer Disease: An Approaching Epidemic

Alzheimer's disease (AD) is a progressive neurodegenerative disorder that threatens to reach epidemic proportions in the coming years. At the beginning of the 20th century, the average life expectancy was approximately 47.3 years.(Jellinger 2006) Today, thanks largely in part to advances in medical science, nutrition, and basic sanitation; the average life expectancy in the United States and Western Europe is approximately 77.9 years. We are witnessing a remarkable event in human history; the population explosion of the past 50 years has resulted in an upheaval of the age distribution profile of the global population. The fastest growing population demographic in developed nations is citizens over the age of 65. By 2025, the number of people in Europe and the United States aged 80–90 years is expected to double, reaching 153 million.(Carol J. Farran 2011) 33 % of the entire population will be older than 65, and about 25 % will be over the age of 80. This becomes a source of growing concern with consideration that the number one risk factor for developing AD is age. Currently, 1 out of every 3 people over the age of 75 shows signs of dementia, while a staggering 50 % of individuals over the age of 85 suffer from some form of dementia. Given these statistics, it is abundantly clear that without intervention, AD will reach epidemic proportions in the next 50 years.

There are currently 35.4 million individuals who suffer from dementia, and the global prevalence is on pace to double every 20 years (to 65 million by 2030, and 115 million by 2050). While the notion of loved ones, and potentially ourselves, ultimately yielding to the symptoms of

dementia is certainly frightening, the imminent economic impact is truly horrific. Simply put, the financial burden created by caring for individuals who provide no productivity and require disproportionate resources to maintain, will become an overwhelming hardship in the future. The direct costs required to care for AD patients in the United States is expected to rise from the 2010 annual expenditure of \$172 billion, to at least \$1 trillion by 2050. Current therapies for AD provide minimal symptomatic relief, and there is no apparent cure on the verge of clinical impact and regulatory approval. The average time to translate a drug from the benchside to bedside is at least 15 years. The steps we take in preclinical medicinal chemistry research to develop new approaches for AD therapy over the next 10 years becomes vitally important in our hope to combat the looming epidemic.

1.2 Brief History of AD

AD is the most prevalent form of dementia in the elderly population and is only definitively diagnosed by the presence of A β plaques and neurofibrillary tangles upon post-mortem autopsy. Dementia is a general term to describe a decline in mental ability significant enough to interfere with activities of daily living.(McDowell 2001) In general, age is the number one risk factor for AD. However, ~5 % of AD cases are familial resulting in early disease onset and progression due to genetic predisposition. A representative example of early onset AD is represented by Auguste D, a 51 year old German woman who was admitted to a Frankfurt hospital in 1901. She presented with several debilitating symptoms, including: reduced comprehension and memory, aphasia, disorientation, unpredictable behavior, paranoia, auditory hallucinations, and pronounced psychosocial impairment.(Maurer, Volk et al. 1997) Once admitted, Auguste D was examined by a German psychiatrist, Alois Alzheimer, who continued to follow Auguste D's case until her death 5 years later in April 1906. Alzheimer then carried out a detailed autopsy utilizing

recently refined biomedical tools in a hope to “help psychiatry through the microscope.” He went on to describe Auguste D’s unusual neuropathological features in a lecture in 1906 and in press in 1911 (Figure 2).(Alzheimer 1911)

Figure 1. 1st characterization of AD

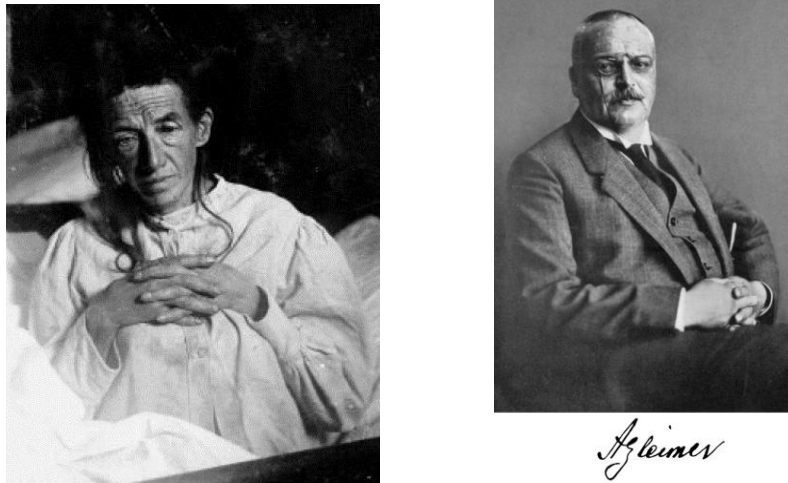


Fig. 1. Left: Photograph of Auguste D (circa 1902). Right: Photograph of Alois Alzheimer (1864-1915).(Blennow, de Leon et al.)

Figure 2. NFT’s and senile plaques

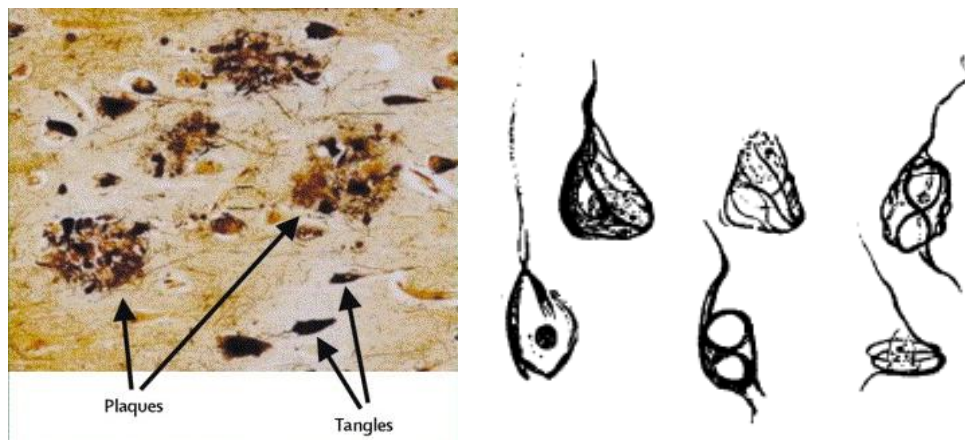


Fig.2. Left: Plaques and tangles observed by silver staining of the cerebral cortex of AD patient brain.(Blennow, de Leon et al.) Right: Depiction of plaques and tangles as reported by Alzheimer in 1911.

1.2 Pathophysiology

AD destroys neurons in the cortex and limbic structures of the CNS, particularly areas responsible for learning, memory, reasoning and behavior (i.e. the basal forebrain, amygdale, hippocampus and the cerebral cortex).(Jellinger 2006) AD disease pathology is characterized by the two pathological hallmarks first described by Alzheimer over 100 years ago, neurofibrillary tangles (NFT's) and senile plaques (Figure 2). Although NFT's and senile plaques are present in normal aged brains, their prevalence is dramatically increased in AD patients, particularly in areas associated with cognition and memory.(Blennow, de Leon et al.) These protein aggregates disrupt synaptic transmission and cytoskeletal trafficking, resulting in neurodegeneration and impaired cognition.

1.2.1 Neurofibrillary Tangles (NFT's)

Neurofibrillary tangles are dense bundles of neurofilament fragments primarily comprised of a hyperphosphorylated cytoskeletal protein, tau.(Khachaturian 1985) Under normal physiological conditions, tau is responsible for cytoskeletal dynamics, and plays a key role in the stabilizing microtubules.(K.S 1990) Tau hyperphosphorylation may lead to the formation of paired helical filaments, which further aggregate to form NFTs. NFTs disrupt the ability of neurons to perform fundamental cytoskeletal remodeling and intracellular trafficking which results in reduced synaptic plasticity leading to neurodegeneration. The presence of hyperphosphorylated tau leading to NFT formation in AD is not completely understood. Kinases involved in the phosphorylation state of tau have been studied extensively. Evidence exists to support the presence of upregulated activity of several cytoskeletal regulating protein kinases, specifically GSK-3 β , Cdk5, CaMKII and MAP-2.(Michel 1993; Lund, McKenna et al. 2001)

However, whether protein kinase dysregulation is a causative or resulting hallmark of AD pathology has yet to be discovered.

1.2.2 Senile plaques

Proteolytic degradation of APP may result in the formation of a 37-43 AA proteolytic degradation product, beta-amyloid ($A\beta$), which is the chief constituent of senile plaque protein deposits. APP is primarily a substrate for two competing enzymes, α -secretase and β -secretase, which cleave APP to give extracellular $sAPP\alpha$ and $sAPP\beta$ signaling fragments, as well as C83 and C99 intramembrane amino acid fragments, respectively (Figure 3). The C99 intramembrane peptide may be processed further by γ -secretase, leading to the formation of $A\beta$ peptide fragments, typically $A\beta_{37}$, $A\beta_{38}$, $A\beta_{39}$, $A\beta_{40}$, $A\beta_{41}$, $A\beta_{42}$, and $A\beta_{43}$. Of these resulting peptide fragments, $A\beta_{42}$ is particularly prone to aggregation and is highly neurotoxic. The native physiological role of APP and its resulting proteolytic products is not well understood. Recently, $A\beta_{42}$ was suggested to be essential to learning in memory at sub-pathological concentrations.(Puzzo, Privitera et al.)

$A\beta$ has been the focus of unparalleled attention in understanding the disease progression and pathology of AD following the creation of the “Amyloid Hypothesis.” The “Amyloid Hypothesis” was originally presented by Dennis Selkoe in a plenary lecture at the 5th International Conference on AD in 1996.

The Amyloid Hypothesis for AD: “Alzheimer’s disease is a clinicopathological syndrome in which different gene defects can lead—directly or indirectly—to altered APP expression or proteolytic processing or to changes in $A\beta$ stability or aggregation. These result in a chronic imbalance between $A\beta$ production and clearance. Gradual

accumulation of aggregated A β initiates a complex, multistep cascade that includes gliosis, inflammatory changes, neuritic/synaptic change, tangles and transmitter loss.”

This hypothesis served as the starting point for numerous attempts to develop pathological interventions through small molecule modulators/inhibitors of β -secretase, and γ -secretase, as well as agents to discourage A β aggregation or promote A β clearance. Over the past 15 years, the development of β -secretase and γ -secretase inhibitors was considered the most promising therapeutic strategy for AD. However, an inadequate understanding of the native physiological roles of β -secretase, γ -secretase, and A β has resulted in molecules that have failed to gain regulatory approval.

Figure 3. APP proteolytic degradation by secretases

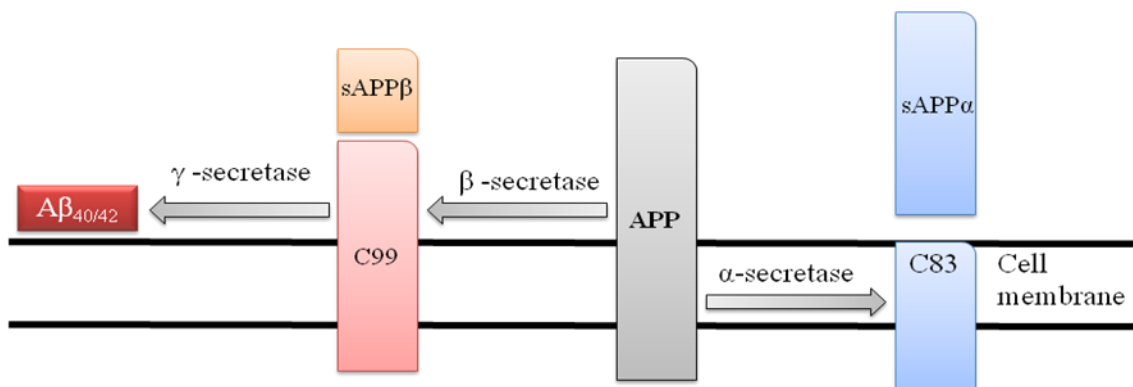


Fig.3. APP processing by α -secretase or β -secretase results the formation of APP breakdown product. γ -secretase processing of the C99 peptide results in the formation of multiple A β species, of which A β_{42} is highly toxic, and proposed to be the most significant causative factor in AD.

1.2.3 Current clinical approaches

Current therapeutic agents provide symptomatic relief using pharmacological intervention. Unfortunately, these agents have no impact on the progression of the disease and become ineffective with time. AD results in neurodegeneration and cell death in regions of the brain responsible for learning, memory, and behavioral processes. The concept of the “cholinergic hypothesis for AD” was developed in the 1980s, and proposes that a loss in cholinergic function in the CNS is responsible for cognition impairment in AD. (Krall, Sramek et al. 1999; Terry and Buccafusco 2003) Based on this hypothesis, cholinesterase inhibitors were designed to prevent the breakdown of acetylcholine, resulting in increased levels of acetylcholine at the synaptic cleft. Cholinesterase inhibitors were found to have efficacy in the form of symptomatic relief in mild cognitively impaired patients. Four of the five currently approved drugs for AD therapy are cholinesterase inhibitors (tacrine, rivastigmine, galantamine, donepezil). (Wilkinson, Francis et al. 2004) Cholinesterase inhibitors are generally safe, but peripheral cholinergic effects often lead to nausea, vomiting, loss of appetite, upset stomach, slowed heart rate and increased gastric motility.

The only non-cholinesterase inhibitor approved drug for use in AD patients is memantine. (Robinson and Keating 2006) Memantine acts through a glutamatergic pathway as a noncompetitive NMDA receptor antagonist, resulting in a reduction in glutamate release and reduced potential for glutamate induced excitotoxicity in hypersensitive neurons. Memantine and/or cholinesterase inhibitors have the ability to temporarily relieve the symptoms of mild cognition impairment; but these therapies have little discernible impact on disease progression, and eventually become completely ineffective in the presence of overwhelming neuronal cell death.

1.3 Calpain as a Therapeutic Target for AD

1.3.1 The Calpain System

Calpains are a class of ubiquitously expressed calcium-dependent cysteine proteases that regulate various intracellular signaling cascades and are fundamentally involved in regulating protein kinases that are responsible for cytoskeletal dynamics and remodeling. (Goll, Thompson et al. 2003) Calpains act through proteolytic processing, rather than proteolytic digestion, to influence the activity and structure of substrates. Dozens of calpain substrates have been characterized and reviewed in detail. (K.K. Wang 1999; Goll, Thompson et al. 2003; Wu and Lynch 2006)

Calpain was first described as early as 1964 and was eventually characterized as a calcium-activated neutral protease, designated CANP. (Guroff 1964; Meyer, Fischer et al. 1964; Huston and Krebs 1968) Examination of the cDNA cloned catalytic subunit of calpain led to its designation as a chimeric enzyme, containing the structural motifs of a cysteine protease and a calmodulin-like Ca^{2+} binding module. (Ohno, Emori et al. 1984) The name “calpain” was eventually adopted, and is derived from its chimeric features of a calmodulin like Ca^{2+} binding motif, and its position within the papain superfamily of CA clan cysteine proteases (ie. **cal**modulin + **papain** = **calpain**). (Suzuki 1991)

The majority of calpains in mammalian systems are known as “typical” calpains, ten of which have been fully characterized. Two calpains are ubiquitously expressed, Calpain 1 (μ -Calpain, Cal1), and Calpain 2 (m-Calpain, Cal2), named for the amount of $[\text{Ca}^{2+}]_i$ required for activation under *in vitro* conditions, ~3-50 μM and 400-800 μM , respectively (TABLE I). Although Cal1 and Cal2 are ubiquitously expressed, their relative levels of expression vary significantly depending tissue and cell type. Unlike Cal1 and Cal2, other typical calpains are not

ubiquitously expressed, but are distributed in a tissue specific manner. For example, calpain 3, known as p94, is only found skeletal muscle and is the 3rd most highly expressed calpain isoform. Calpain 3 hyperactivation is responsible for limb-girdle muscular dystrophy type 2A, and has been suggested to be responsible for Duchenne-type muscular dystrophy.(Richard, Broux et al. 1995) A brief examination of other tissue specific calpain isoforms is given in TABLE I, and have been reviewed previously in the literature.(Goll, Thompson et al. 2003)

Biochemical examination has led to a wealth of information concerning isoform sequence homology and calcium binding domain of calpain isoforms. Typical calpains share a common small regulatory subunit (28 kDa) and possess a distinct large catalytic subunit (80-100 kDa), with unique thresholds of calcium induced activation. The large catalytic subunit contains four domains (Figure 4), including: domain I, which masks the active-site cysteine residue and is proteolytically cleaved by autocatalysis upon Ca^{2+} induced activation; domain II, which is responsible for protease activity; domain III, which contains a C2-like Ca^{2+} binding module; and domain IV, a 5-EF hand Ca^{2+} binding domain. Cal1 and Cal2 isoforms possess 60 % amino acid sequence homology within their entire large catalytic subunit, while domain II, containing the active-site cysteine residue, is highly conserved among several cysteine proteases. This creates a major obstacle in designing small molecules as selective calpain inhibitors. The conserved small subunit is composed of two domains: domain V, a glycine rich hydrophobic domain for enzyme-phospholipid interactions; and domain IV, a 5-EF hand Ca^{2+} binding domain. Similar to domain I, a portion of the N-terminus of domain V is also cleaved during catalytic activation.

TABLE I
MAIN MEMBERS OF “THE CALPAIN SYSTEM” IN HUMANS^a

Member Type	Subunit Size (large, small)	[Ca ²⁺] for Half Maximal Activity	Additional Information
Calpain 1 (μ-Calpain)	80, 28 kDa	3-50 μM	highly expressed at synapses
Calpain 2 (m-Calpain)	80, 28 kDa	400-800 μM	
Calpastatin (Endogenous inhibitor)	Variable (46-87 kDa)	Requires Ca ²⁺ bound calpain for inhibition	found in low abundance in AD brain(Higuchi, Iwata et al.)
Calpain 3 (p94)	94, 30 kDa	10-100 μM	skeletal muscle(Richard, Broux et al. 1995)
Lp82	94, 30 kDa	10-100 μM	lens, retina(Ma, Hata et al. 1999)
Calpain 8 (nCL-2) Calpain 9 (nCL-4)	80, 30 kDa	50-500 μM	stomach(Hata, Abe et al.)

^a List of extensively characterized calpain isoforms in humans. Cal1 and Cal2 are ubiquitously expressed, whereas other isoforms are tissue specific. Typical tissue specific calpains with modest expression include p94, Lp82, and nCL-3. At least 10 mammalian calpain variants have been identified in the human genome. Aside from the isoforms listed above, the functional significance of other isoforms is not completely understood due to relatively low levels of expression in humans.

Figure 4. Schematic of Cal1 and Cal2 structure motifs

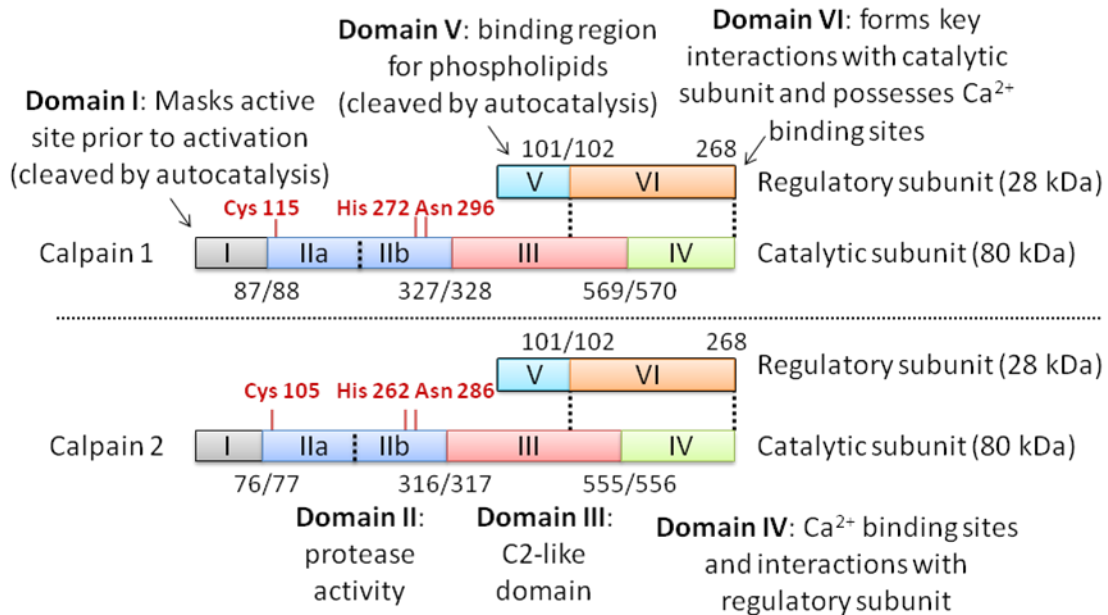
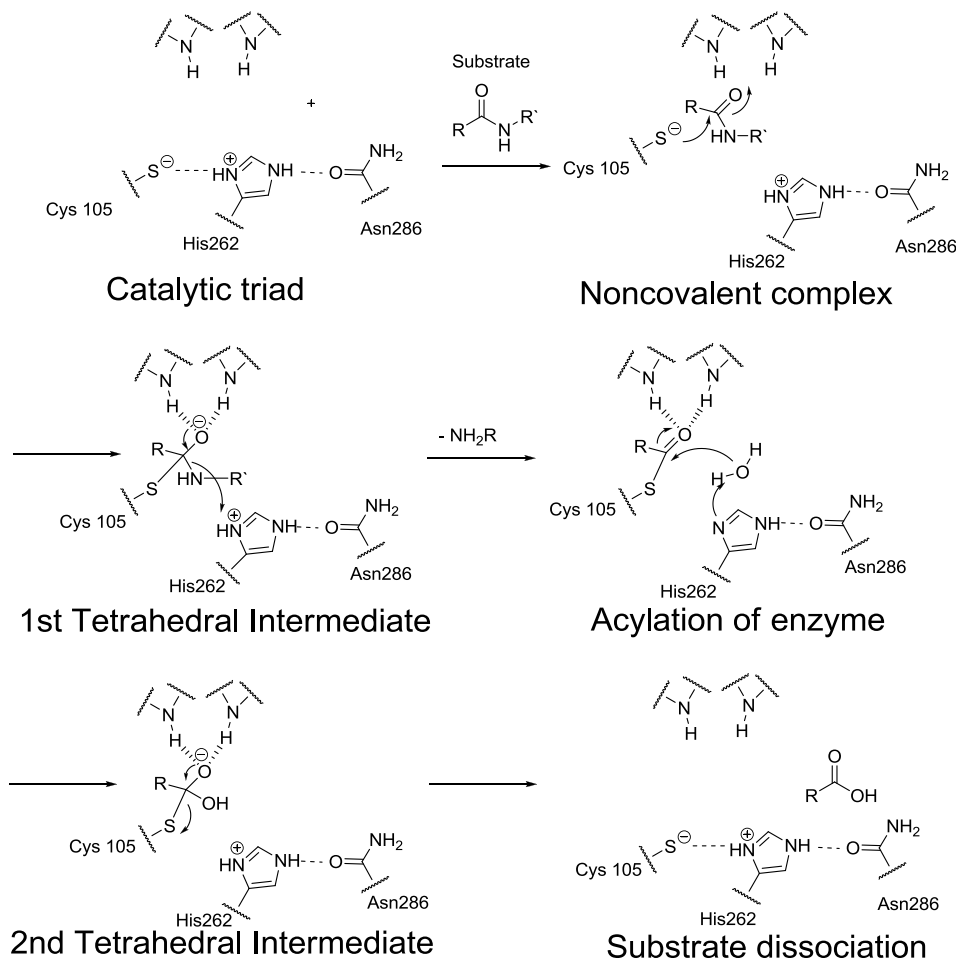


Fig.4. Cal1 and Cal2 possess a large catalytic subunit containing 4 domains and a small regulatory subunit of 2 domains. Domain I is responsible for shielding the active-site cysteine residue from premature proteolysis prior to Ca^{2+} -induced activation. Domain II, containing the active site cysteine residue, carries out proteolytic activity following activation. Domain III is a C2-like calcium binding domain. Domain IV and domain VI create essential interactions between the large and small subunits. Domain V is a hydrophobic glycine rich domain proposed to function as the binding site for phospholipids to modulate the threshold of Ca^{2+} activation.

Scheme 1. Chemical mechanism of calpain proteolytic activity ^a



^a The Cal1 active site has a catalytic triad containing Cys105, His262, and Asn286.

Subsequent to thiophilic attack by the active site cysteine, backbone amides stabilize a tetrahedral intermediate, leading to acylation of the active site cysteine. His262 then activates a H₂O molecule towards nucleophilic attack of the acylated thioester, and formation of a second tetrahedral intermediate. Breakdown of the second tetrahedral intermediate results in dissociation of the C-terminus of the cleaved peptide fragment, and regeneration of the catalytic triad.

The chemical mechanism of calpain proteolytic activity was elucidated over two decades ago, and is consistent with the proteolytic mechanism of other cysteine proteases (Scheme 1). The amino acid sequence of the active site cysteine containing peptide fragment was first identified from protein digest of incubations using radiolabelled iodoacetamide with calpain 1 isolated from chickens. Subsequent studies employing active site mutagenesis characterized the calpain catalytic triad; containing Cys105, His262, and Asn286. Since then, numerous x-ray structures have supported these findings.(Moldoveanu, Hosfield et al. 2002; Moldoveanu, Campbell et al. 2004; Cuerrier, Moldoveanu et al. 2005; Cuerrier, Moldoveanu et al. 2006; Hanna, Campbell et al. 2008; Qian, Cuerrier et al. 2008) Calpain proteolysis is initiated by thiophilic attack of a substrate with formation of a tetrahedral intermediate, followed by acylation of the active site cysteine, nucleophilic attack by an activated H₂O molecule, formation of a second tetrahedral intermediate, and dissociation of the cleaved peptide fragments. (Suzuki, Hayashi et al. 1983; Arthur, Gauthier et al. 1995)

Calpain activity is directly regulated by an endogenous peptidyl inhibitor, calpastatin. Calpains exist in the cytosol as pro-enzymes in their “inactive” form, and become proteolytically activated via an autocatalytic mechanism involving cleavage of domain I in the presence of sufficient [Ca²⁺]_i.(Moldoveanu, Hosfield et al. 2002) Calpastatin is a peptidyl calpain specific inhibitor and only inhibits catalytically active Ca²⁺-bound calpain.(Hanna, Campbell et al. 2008) Recently, a x-ray structure of calpastatin bound calpain revealed that calpastatin inhibition takes advantage of binding to several lower affinity sites present only in the calcium-bound enzyme, resulting in specific inhibition of Ca²⁺-bound calpain. (Hanna, Campbell et al. 2008) Unfortunately, the ability of calpastatin to harness the cumulative effects of many low affinity binding interactions requires a peptidyl structure large enough to produce a specific tight

binding inhibitor gives little insight into the design of selective high affinity small molecule inhibitors.

Calpain plays an important role in regulating cytoskeletal dynamics and intracellular Ca^{2+} signaling.(Huang and Wang 2001) Calpains regulate several protein kinases that effect cytoskeletal remodeling and stabilization. Hence, they generally play an active role in processes involving cell mobility and cell cycle progression. Under physiological conditions, transient and localized Ca^{2+} fluxes from extracellular or intracellular sources results in activation of local calpain populations. This leads to regulatory activity of cytoskeletal dynamics and intracellular Ca^{2+} signaling.

Although Cal1 and Cal2 are ubiquitously expressed in mammalian cells, their expression and function is highly variable depending on locale.(Nakamura, Imahori et al. 1988) For instance, both Cal1 and Cal2 are highly expressed in the cell body of neurons, while postsynaptic density studies have indicated Cal1 is the prominent isoform in axonal and dendritic processes.(Simonson, Baudry et al. 1985) Just as Cal1 has high axonal/dendritic expression, the Cal2 isoform is the predominant isoform in glial cells. Additionally, mRNA analysis in adult rat brains indicated that Cal1 and calpastatin have similar expression patterns in all neurons, but have significantly lower expression in glia.(Goto, Iwamoto et al. 1994)

The abundance of Cal1 in synapses and dendrites supports the integral involvement of calpains in regulating synaptic cytoskeletal remodeling in response to localized $[\text{Ca}^{2+}]_i$ transients.(K.K. Wang 1999; Huang and Wang 2001; Di Rosa, Odrijin et al. 2002) Calpain plays a key role in modulating synaptic plasticity.(Lynch and Baudry 1987; Lynch, Muller et al. 1988) Studies examining the differential rate of calpain proteolytic processing of post-synaptic

cytoskeletal protein components concluded that spectrin is the component most susceptible to proteolysis, followed by tubulin, CaMKII, and MAP-2, while no degradation of actin was observed.(Dosemeci and Reese 1995) Location-specific calpain activation and spectrin proteolysis is proposed to facilitate reorganization of post synaptic densities and contribute to synaptic plasticity.

Figure 5. Schematic of calpains involvement in AD related pathologic pathways

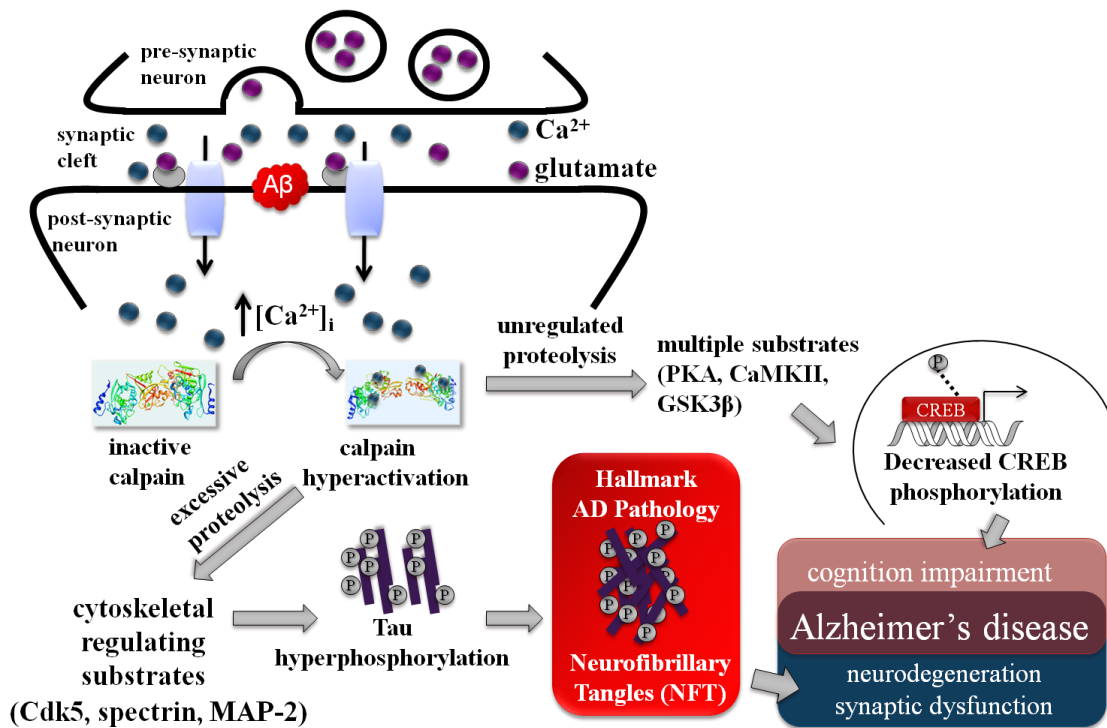


Fig.5. In response to A β or other neurotoxic insults, post-synaptic neurons become hypersensitized to glutamate, resulting in temporary spikes in $[Ca^{2+}]_i$. Elevated levels of $[Ca^{2+}]_i$ causes widespread calpain activation and unregulated proteolysis. Calpain is intimately involved in cytoskeletal dynamics. Excessive proteolysis of cytoskeletal regulating protein kinases leads to tau hyperphosphorylation, the formation of paired helical filaments, and eventually NFTs. NFTs are found in abundance in the brains of AD patients, and significantly disrupt intracellular protein trafficking and synaptic plasticity. Excess calpain activation may also lead to poor regulation of intracellular protein kinases involved in Ca^{2+} signaling (i.e. PKA, CaMKII, GSK-3B) leading to decreased CREB phosphorylation and cognition impairment.

Pathological conditions may result in hyperactivation of calpain, leading to unregulated proteolysis and neurodegeneration.(Di Rosa, Odrijin et al. 2002) As discussed above, Ca^{2+} signaling pathways physiological activation of localized calpain populations leads to highly specific, and is tightly regulated by calpastatin. However, excessive levels of $[\text{Ca}^{2+}]_i$ may result in widespread calpain activation. Proteolysis is an irreversible process, and unregulated calpain proteolytic activity results in permanent pathological changes leading to neurodegeneration. The physiological threshold of $[\text{Ca}^{2+}]_i$ levels required for widespread calpain activation, or hyperactivated calpain, is unknown due to the exceptionally high levels of Ca^{2+} needed to produce reliable calpain activity *in vitro*, which do not correspond to realistic cellular Ca^{2+} concentrations, *vide supra*.

Calpain hyperactivation is fundamentally involved in the pathology of AD (Figure 5). Calpain carries out direct proteolytic actions and modulatory effects on several protein kinases involved in tau phosphorylation/dephosphorylation, as well as playing a key role in regulating cytoskeleton dynamics, especially those present in synapses.(Donkor 2000; Di Rosa, Odrijin et al. 2002; Goll, Thompson et al. 2003) (Shea, Beermann et al. 1994; Shea, Cressman et al. 1995; Shea, Prabhakar et al. 1997; Tsuji, Shimohama et al. 1998; Town, Zolton et al. 2002; Veeranna, Kaji et al. 2004; Wu and Lynch 2006) As mentioned earlier, calpain activation results in decreased phosphorylation of CREB, leading to cognition impairment and reduced synaptic plasticity. Cal1, the primary calpain isoform found in the synapse, is abnormally activated in the brains of AD patients, and calpastatin is found in significantly low amounts.(Saito, Elce et al. 1993; Tsuji, Shimohama et al. 1998)

Calpain activation in AD transgenic mice results in APP processing and increased levels of A β deposition. Recently, transgenic mice containing the A β overproducing APP/PS1 mutations were crossed with calpastatin overexpressing mice to give triple transgenic APP/PS1/CAPN

hybrids.(Liang, Duan et al.) APP/PS1/CAPN mice lacked A β deposits and displayed markedly decreased BACE1 expression levels compared to APP/PS1 transgenic control mice. Since calpastatin is a specific inhibitor of calpain, calpain activity is now hypothesized as being fundamentally involved in A β pathology.

Calpain inhibitors show promising neuroprotective and cognition enhancing properties in murine models of neurodegeneration and AD. Inhibition by a calpain selective inhibitor, **PD150606**, rescues synaptic function in the form of LTP following ischemic.(Farkas, Tantos et al. 2004) Calpain inhibition has also been shown to restore A β -induced synaptic deficits, and prevents A β -induced behavioral dysfunction in rats.(Granic, Nyakas et al.) Evidence supports the ability of calpain inhibition to restore synaptic function and increase neuronal plasticity via increasing phosphorylation of the memory-related transcription factor, CREB.(Silva, Kogan et al. 1998; Farkas, Tantos et al. 2004; Trinchese, Fa et al. 2008)Overexpression of calpastatin demonstrated the key role of calpain in excitotoxicity-induced cytoskeletal degeneration, and direct blockade of calpain proteolysis has been shown to rescue neurons from glutamate excitotoxicity.(Higuchi, Tomioka et al. 2005)(Rami, Ferger et al. 1997) Taken as a whole, these observations strongly support the development of calpain inhibitors for therapeutic intervention in situations of neurodegeneration, specifically AD.(Lynn, Robert et al. 1988; Saito, Elce et al. 1993; Rao, Mohan et al. 2008)

1.3.2 A Brief Review of Calpain Inhibitors in the Literature

The potential advantages of developing selective calpain inhibitors are indicated in several disease states and have been the source of intensive research over the past few decades. In general, calpain inhibitors can be split into two broad categories; peptidyl and non-peptide incorporating molecules. Non-peptide inhibitors act as noncompetitive, allosteric modulators of

calpain. Conversely, peptidyl inhibitors contain a peptidomimetic portion and a reactive electrophile for active site modification. Numerous active site directed peptidomimetics have been developed using a wide range of reactive electrophiles (Figure 7). These reactive groups, or warheads, inhibit calpain by either reversible or irreversible modification of the active site cysteine. Active site directed agents have received the most attention. Hence, reports of active site directed inhibitors are more prevalent than that of allosteric modulators in the literature. Both circumstances are reviewed briefly below.

Inhibitors targeting the calcium binding sites of calpain display potent and selective activity against calpain, but are structurally unfavorable as drug candidates. Calpain possesses a unique Ca^{2+} binding domain that is not present in other cysteine proteases. Therefore, a class of non-active site targeted calpain inhibitors could gain selectivity through unique interactions with the calcium-binding domains of calpain. The prominent effort to develop non-active site calpain inhibitors came courtesy of Kevin Wang's group in the Parke-Davis research faction of Warner Lambert, now Pfizer, in the 1990's. The screening of >150,000 compounds led to the identification of α -mercaptoacrylic acid derivatives as highly selective calpain inhibitors (Figure 6).(Wang, Nath et al. 1996; Wang, Posner et al. 1996) Selectivity was assayed by inhibition kinetic studies for calpain, cathepsin B (CathB), papain, and other related cysteine protease. **PD150606** was found to be neuroprotective against oxygen glucose deprivation (OGD) in neuronal cell culture and protective against AMPA induced toxicity to Purkinje cells. Unfortunately, the α -mercaptoacrylic acid functionality has poor metabolic stability, and is unsuitable as a drug candidate. Prior to the creation **PD15606**, calpastatin was the only known calpain selective inhibitor. Calpastatin does not readily cross cell membranes, hence, the discovery of **PD15606** as a cell-permeable selective calpain inhibitor has been fundamental in improving our understanding of calpain related chemical biology over the past fifteen years.

Figure 6. Non-active site directed inhibitors

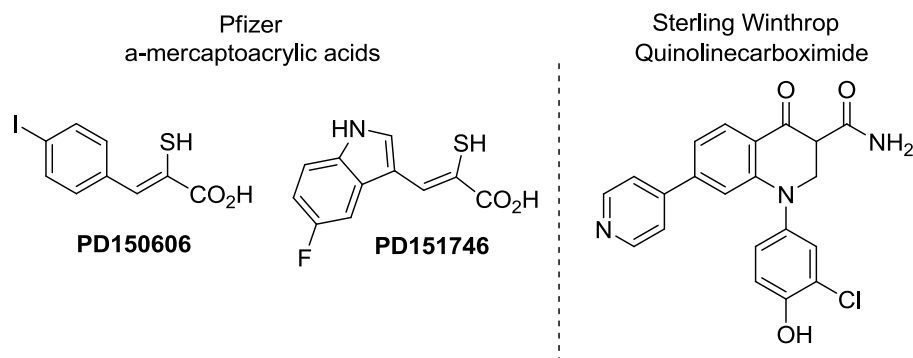


Fig. 6. **PD150606** and **PD151746** were shown to be highly selective by disrupting the interaction at Ca^{2+} binding sites of calpain. X-ray structures of **PD150606** with porcine Cal1 supported binding of **PD150606** to domain IV of Cal1. Quinoline carboximides were developed by Sterling Winthrop, and possessed modest activity for calpain.

Figure 7. Examples of cysteine reactive “warheads”

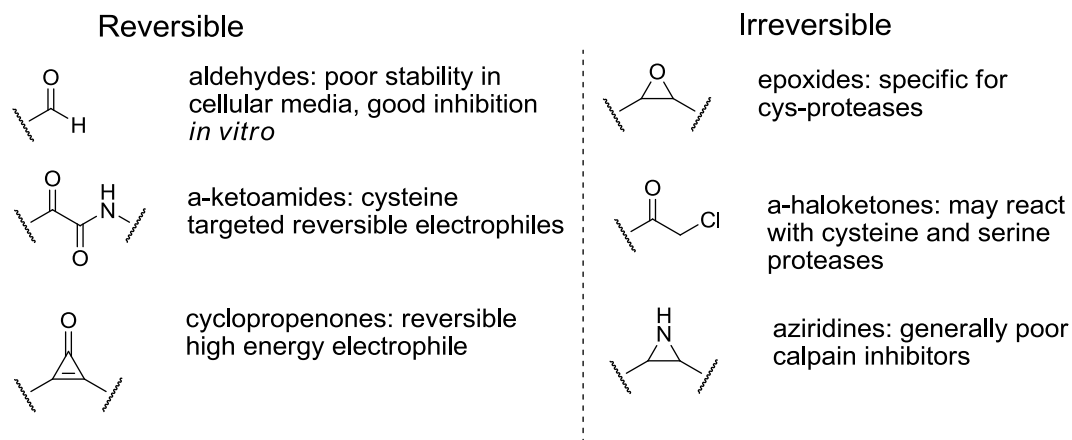


Fig.7. Electrophilic warheads carry out inhibition via reversible or irreversible modification of the active site cysteine. Reversible warheads include aldehydes, α-ketoamides, and cyclopropanones(Li, Chen et al. 2007); examples of irreversible warheads are epoxides, α-haloketones, and aziridines.

Figure 8. Aldehyde incorporating peptidomimetic calpain inhibitors

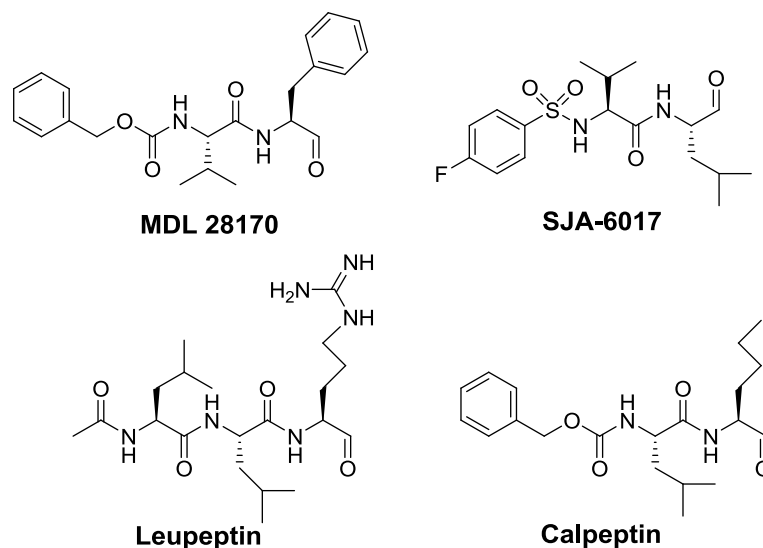


Fig.8. Aldehyde based inhibitors often display potent calpain inhibition. However, their inherent reactivity results in low selectivity and poor metabolic stability.

Figure 9. α -ketoamide incorporating peptidomimetic calpain inhibitors

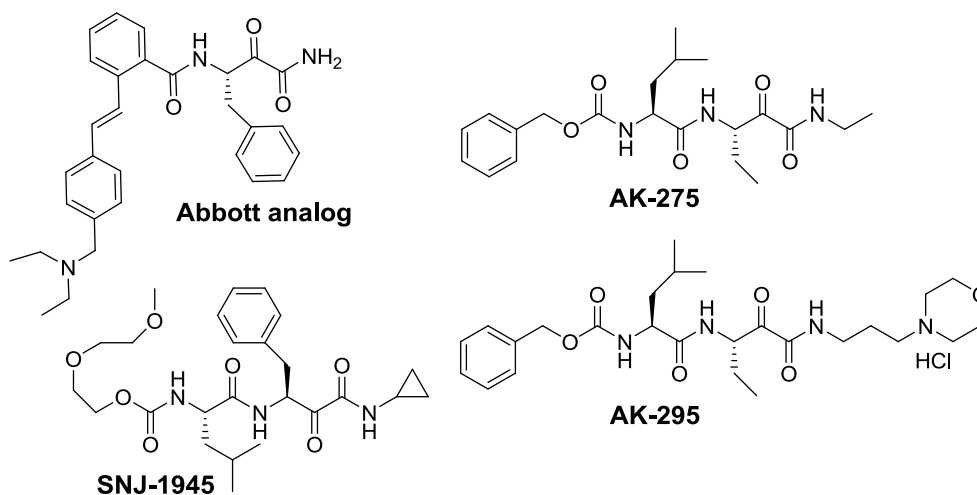


Fig.9. α -ketoamide incorporating inhibitors have been the most extensively reported inhibitors in the literature. Separate reports on each of these compounds cite significant neuroprotective effects in various murine and rat models of stroke and neurodegeneration.

The development of non-active site directed allosteric calpain inhibitors has received much attention, but yielded limited success. Most efforts to develop allosteric modulators were carried out by the pharmaceutical industry, making detailed information somewhat difficult to attain. Quinoline carboximides were developed by Sterling Winthrop, patented in 1997, and showed modest calpain inhibition *in vitro* ($IC_{50} = 2 \mu M$). (Graybill, Dolle et al. 1995) Quinoline carboximides were not seen to competitively inhibit calpain, leading to their designation as allosteric calpain inhibitors. Abbott Labs reported the HIV drug, ritanovir, as being a non-competitive calpain inhibitor. (Wan and DePetrillo 2002; Ghibelli, Mengoni et al. 2003) However, more recent reports have disputed these findings. (Cuerrier, Nie et al. 2005)

Electrophilic, carbonyl-containing warheads have been used extensively as reversible calpain inhibitors. Peptidomimetic aldehydes were first developed as highly reactive electrophiles for calpain inhibition, and led to the identification of several high affinity inhibitors, including leupeptin, calpeptin, **MDL-28170**, and **SJA-6017** (Figure 8). Unfortunately, the peptidyl aldehydes were found to have poor stability in biological environments, leading to the design of hemiacetal, hydrazone, and α -ketoamide analogs as aldehyde prodrugs. (Schultz, Varma-Nelson et al. 1989; Shujaath 1991; Nakamura, Miyashita et al. 2003; Shirasaki, Miyashita et al. 2006; Shirasaki, Nakamura et al. 2006)

The development of α -ketoamide warheads resulted in molecules with beneficial activity against neurodegeneration *in vivo* using murine models of stroke (Figure 9). While aldehyde inhibitors possessed poor activity *in vivo*, several corresponding α -ketoamide analogs have demonstrated protective effects using *in vivo* paradigms. For example, a peptidyl α -ketoamide inhibitor, **AK-275**, and its water soluble analog, **AK-295**, have shown significant protective effects against ischemic neurodegeneration in a murine stroke model. (Bartus, Baker et al. 1994; Bartus, Hayward et al. 1994; Bartus, Elliott et al. 1995) Separately, a benzoylalanine-derived α -

ketoamide demonstrated bioavailability and *in vivo* efficacy with a 41 % decrease in neuronal loss in the presence of traumatic brain injury in a fluid percussion model in rats.(Lubisch and Moller 2002) Additionally, the α -ketoamide **SNJ-1945** was found to protect neuronal loss in cerebral ischemia induced damage in mice, and later x-ray structure of **SNJ-1945** bound to porcine Cal1 was resolved.(Cuerrier, Moldoveanu et al. 2006; Koumura, Nonaka et al. 2008; Ma, Tochigi et al. 2009)

A natural product, **E-64**, L-trans-epoxysuccinyl-leucylamido(4-guanidino)butane, was one of the first cysteine protease inhibitors identified which exploits the electrophilicity of small ring heterocycles, utilizing an epoxide for active site modification (Figure 10).(Sugita, Ishiura et al. 1980; Parkes, Kembhavi et al. 1985) **E-64** was first isolated from cultures of *Aspergillus japonicas* in 1978, and is the prototypical epoxide incorporating protease inhibitor.(K. Hanada 1978) While being non-reactive towards other protease superfamilies (i.e. aspartic, serine, ect.), **E-64** serves as a high affinity, non-selective, irreversible cysteine protease inhibitor.(K. Hanada 1978; Barrett, Kembhavi et al. 1982) The epoxide ring has been shown to be extremely important to this class of molecules, as alkene and aziridine containing analogs possessed weak inhibitory activity (Figure 10).(Parkes, Kembhavi et al. 1985; Schirmeister 1999) A survey of the RCSB protein databank yields eleven instances of x-ray crystal structures of eukaryotic enzymes bound by **E-64**, including: rat calpain 1 catalytic domain (Cal1_{cat}), human cathepsin K, papain, and several other papain like cysteine proteases.(Mary E. McGrath 1997; Matsumoto, Mizoue et al. 1999; Moldoveanu, Campbell et al. 2004)

An **E-64** analog, **E-64d**, advanced to phase III clinical trials in the 1980's for the treatment of muscular dystrophy. This work took the fairly straightforward approach of replacing the guanidino functionality of **E-64** with an isoamyl moiety to create **E-64c**.(Barrett, Kembhavi et al.

1982) **E-64c** showed potent non-selective cysteine protease activity *in vitro*, but negligible *in vivo* efficacy, leading to the creation of its prodrug, **E-64d** (a.k.a. EST or loxistatin), which displayed negligible protease inhibition *in vitro*, but promising *in vivo* efficacy.(M. Tamai 1986; Masaharu Tamai 1987) **E-64d** was developed in Japan for the treatment of muscular dystrophy; but, the clinical trial was discontinued during phase III, citing a lack of efficacy for the prescribed indication.(Miyahara 1985; Satoyashi 1992; Scrip 1992) It is noteworthy that despite evidence of species-specific hepatic toxicity in rats,(Fukushima, Arai et al. 1990) **E-64d** is well tolerated in humans.

1.3.3 Potential of Epoxide Peptidomimetic Calpain Inhibitors in AD Therapy

Recently, epoxide peptidomimetic cysteine protease inhibitors have demonstrated several promising features as potential therapeutics for AD therapy. **E-64** was reported as being capable of restoring synaptic transmission in the form of LTP in hippocampal slices from APP/PS1 mice.(Trinchese, Fa et al. 2008) The established link between calpain inhibition leading to increased CREB phosphorylation and improved synaptic plasticity supports the hypothesis that restoration of LTP is the result of calpain inhibition by **E-64**. In the same report, promising results were established in the ability of **E-64** to improve cognition deficits in spatial-working and associative fear memory in behavioral models of AD using APP/PS1 mice. These outcomes support calpain inhibition by epoxide-based peptidomimetics as a rational target for pathological intervention in AD and make a selective high affinity calpain inhibitor highly desirable.

Separate reports have shown a renewed interest in the epoxide peptidomimetic studied for muscular dystrophy in the 1980's, **E-64d**, as a potential treatment for AD. **E-64d** is reported to decrease BACE1 expression, APP processing, and A β deposition in AD transgenic mouse models,(Hook, Kindy et al. 2007) and has been recently entered phase I clinical trials for

AD.(Hook 2006; Hook, Hook et al. 2007; Hook, Kindy et al. 2008) These efforts illustrate the potential for the development of epoxide-based peptidomimetics for pathological intervention in AD, using **E-64** as a lead compound to develop selective calpain inhibitors.

Figure 10. Epoxide containing peptidomimetic calpain inhibitors

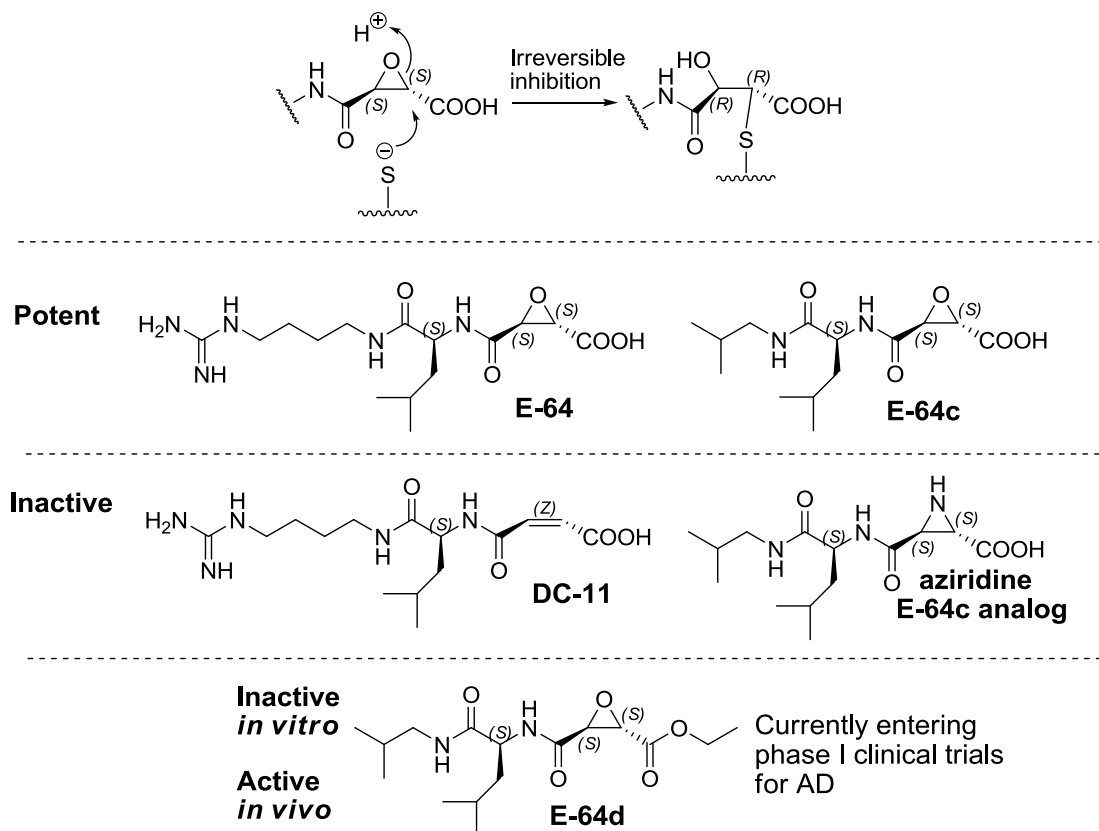


Fig.10. Epoxysuccinate containing peptidomimetics carry out irreversible calpain inhibition via covalent modification of the active site cysteine. Examination of dozens of **E-64** analogs led to the conclusion that the epoxide is required for calpain inhibition, as **DC-11** and an aziridine containing analog possess negligible activity. The isoamyl **E-64** analog, **E-64c**, displayed potent activity *in vitro*, but negligible activity *in vivo*. **E-64d**, a prodrug ester of **E-64c**, was found to give poor calpain inhibition *in vitro*, but the ability to restore righting reflex in dystrophic hamster.

Ample attempts to develop epoxide peptidomimetic cysteine protease inhibitors have been cataloged previously.(Otto and Schirmeister 1997; Donkor 2000) These reports provide a wealth of information towards understanding the SAR for inhibition of cysteine proteases. In the past, development has focused on modifying two key structural features: 1) an electrophilic warhead capable of reversible or irreversible modification of the active site cysteine and 2) a peptidomimetic portion to reproduce the interactions made by naturally occurring protein substrates. The demonstrated efficacy of **E-64** and related compounds supports maintaining the epoxide moiety in lead development. Hence, optimization focused on the peptidomimetic scaffold.

Before detailed analysis of the SAR of epoxide cysteine protease inhibitors, it is important to briefly review the structural nomenclature of cysteine protease substrates and inhibitors (Figure 11). Protease substrate nomenclature recognizes the amino acid residues extending from the N-terminal side of the scissile bond as “unprimed” residues, designated P1, P2, P3, etc. The respective substrate binding sites of the unprimed residues of these residues are known as the S1 site, site S2, and so on. Conversely, the primed residues on the C-terminal side are designate P1', P2', P3', and so on. A similar designation is used for inhibitor nomenclature (See Figure 11).

Epoxide peptidomimetics have been successfully developed to impart potency and selectivity for various cysteine proteases. CA clan cysteine proteases have fairly similar unprimed substrate binding pockets and significantly different primed binding site features.(Otto and Schirmeister 1997) The presence of a similar unprimed binding region results in a common preference of hydrophobic residues at the S2 subsite (ie. Leu, Ile, Val, Phe, Tyr).(Greenbaum, Medzihradszky et al. 2000; Greenbaum, Arnold et al. 2002) Previous attempts to develop bispeptidyl or “chimeric” molecules capable of interacting at the primed and unprimed regions found that the structural requirements for exploiting both the S and S' subsites are not additive.(Schaschke,

Assfalg-Machleidt et al. 1997) From this, the authors suggested that *S,S* epoxide derivatives conform preferentially into the unprimed pocket whereas binding into the primed subsites is favored by compounds with the *R,R* configuration. **E-64** and related *S,S* epoxide with large hydrophobic residues at the P2 position have shown poor selectivity in the past.

Using a bispeptidyl scaffold containing a *R,R* epoxide was found to be a suitable strategy to develop cathepsin selective inhibitors. The Leu-Pro containing compounds **CA-074**, and **NS-134** are both reported to be selective for CathB, and the bispeptidyl **CLIK** derivative has shown selectivity for CathL (Figure 12). *R,R* bispeptidyl derivatives show promising potency and selectivity for cathepsin and are generally poor calpain inhibitors. Separately, the *R,R* epoxide **NCO-700** showed promising anti-cancer activity against human breast and prostate tumor cell lines, although this activity appears to be through a mechanism independent of cysteine protease inhibition.(Shibata, Yamamoto et al. 1997; Eilon, Gu et al. 2000)

The development of selective epoxide peptidomimetic calpain inhibitors has been largely neglected in the past. For the most part, these efforts focused on large peptide like molecules. Initially, simple **E-64** analogs were developed, converging on **E-64c** as a potent non-selective **E-64** analog. Notably, recent efforts by Peter Davies group at Queens University examined calpain specificity by screening a positional scanning peptidyl-epoxide library, and concluded that the P2 position is the most essential determinant of calpain selectivity.(Cuerrier, Moldoveanu et al. 2007) The study converged on selective analogs containing a P2 *L*-histidine (**WRH**) and a non-natural peptidomimetic analog (**WR-18**) (Figure 12). Unfortunately, these molecules possess poor drug like properties (ie. large molecular weight, several ionizable groups, clogP < -2.5). Regardless, these results give new insight into the possibility of developing selective small molecules calpain inhibitors.

Figure 11. Review of cysteine protease substrate and inhibitor nomenclature

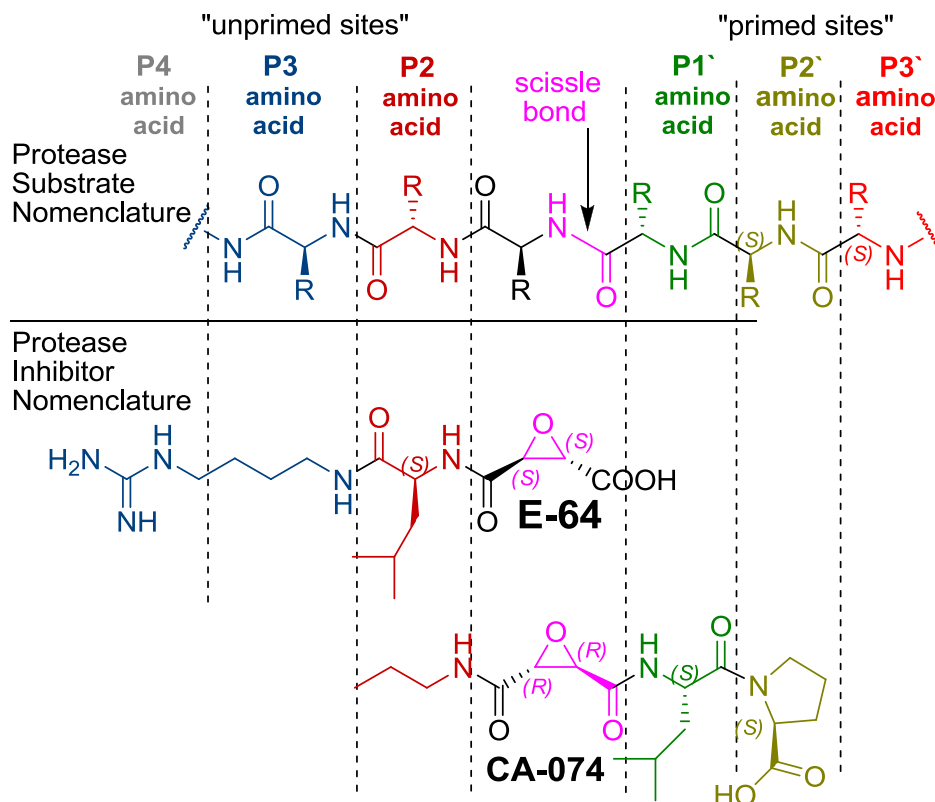


Fig.11. Amino acid residues extending from the N-terminal side of the scissile bond are denoted P1, P2, P3, etc. The unprimed residues on the C-terminal side are designate P1', P2', P3', and so on. A similar designation is used for inhibitors nomenclature, although inhibitors lack a true P1 amino acid fragment, and are named starting from P2 position. Epoxide peptidomimetics with an *S,S* epoxide (as in **E-64**), favor interactions at unprimed binding sites, whereas *R,R* epoxides (such as **CA-074**) confer interactions at the primed portion.

Figure 12. Representative examples of reported epoxide peptidomimetics

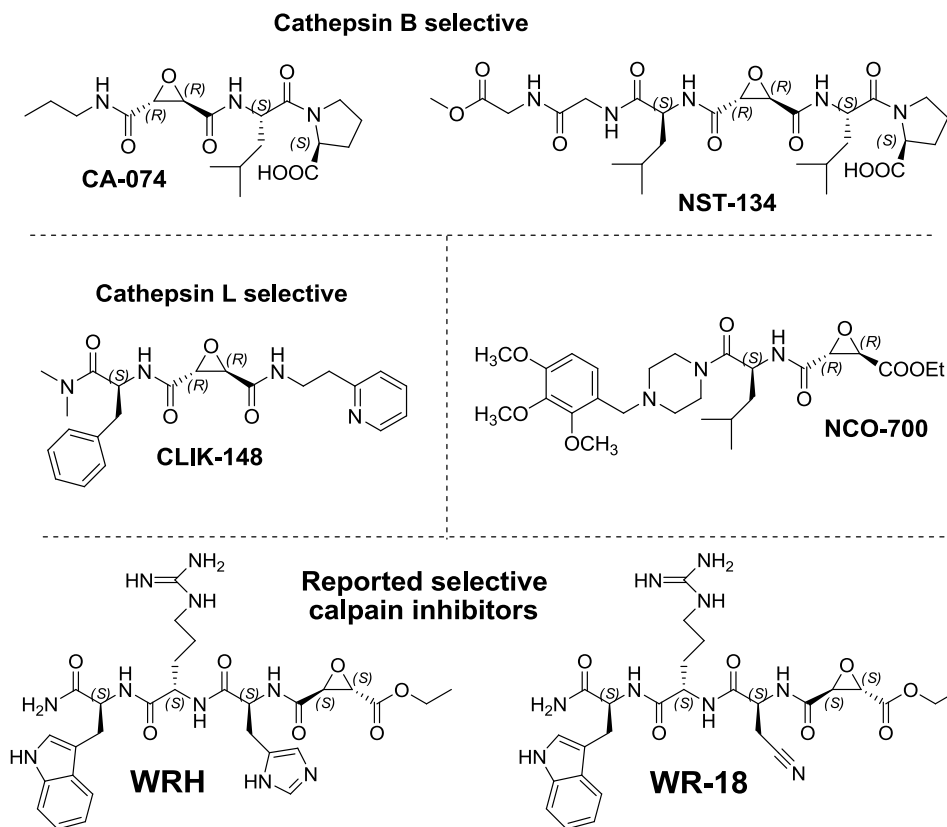


Fig.12. Peptidomimetic **E-64** analogs with *R,R* epoxide stereochemistry generally result in binding interactions at the P' site. **CA-074** and **NST-134** are reported to be highly selective for CathB, while **CLIK-148** is selective for CathL. The *R,R* epoxide ester, **NCO-700**, showed promising anti-cancer activity against human breast and prostate cancer cell lines. The exact mechanism of **NCO-700** induced apoptosis is not well understood, but did not correlate with potency of protease inhibition. **NCO-700** is well tolerated in mammals, and entered phase II clinical trials as a potential oncolytic agent. Structures of reported calpain selective epoxides of Queens University. Unfortunately, **WRH** and **WR-18** possess poor druglike properties for the CNS (ie. MW > 550, several ionizable groups, clogP < -2.5).

Figure 13. Lead optimization strategy

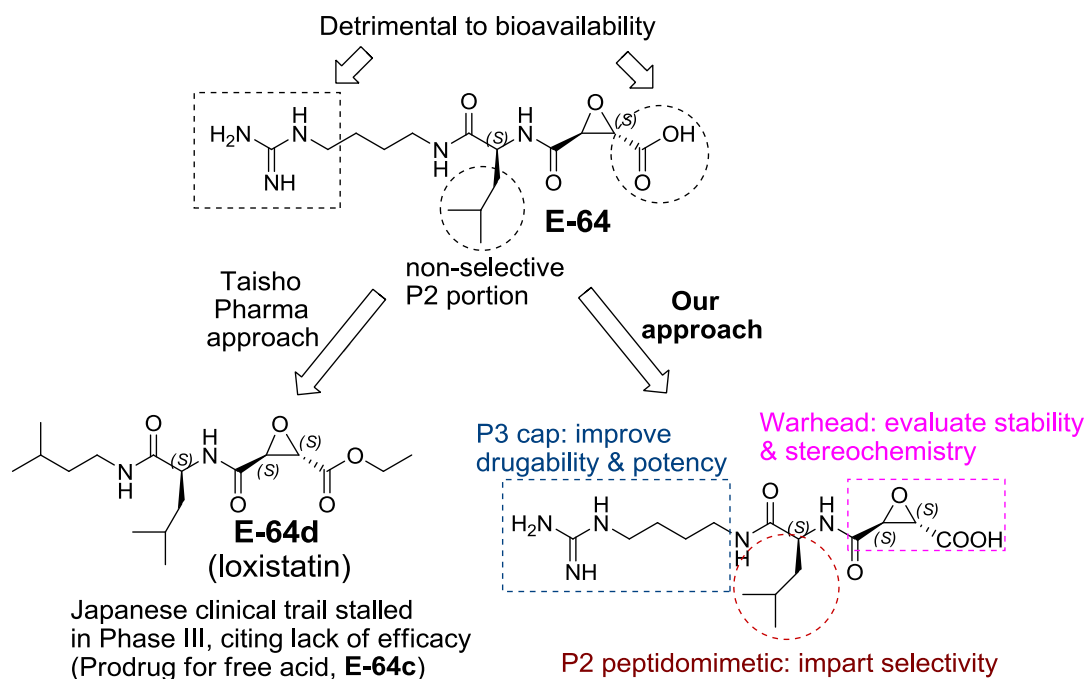


Fig.13. Early efforts to develop **E-64** analogs as cysteine protease inhibitors

converged on **E-64d**, a prodrug ester of the highly potent epoxyacid **E-64c**. Our approach focuses on evaluating and optimizing three key parts of the molecules: 1) the epoxide warhead, 2) an appropriate P3 cap group, and 3) the P2 peptidomimetic scaffold.

2. Results

2.1 Assay Development & Lead Optimization

Herein, we report a comprehensive medicinal chemistry approach to the development of epoxide peptidomimetic calpain inhibitors. The lead optimization strategy focused on modifying three structural features of the inhibitor: 1) the epoxide stereochemistry, 2) the appropriate P3 cap group to improve potency and drugability, and 3) incorporation of the appropriate P2 functionality to impart selectivity (

Figure 13). FRET substrates were employed to measure calpain inhibition and competition assays were developed to gain insight into the relative selectivity and potency of novel E-64 analogs *in vitro*. *Ex vivo* experiments measuring restoration of LTP by inhibitors upon co-perfusion with oligomeric A β in hippocampi from WT mice were used as a preliminary screen of procognitive efficacy. *In vivo* behavioral/toxicity experiments were carried out to determine functional efficacy and tolerability.

2.1.1 Evaluating Calpain Inhibition using a FRET substrate

Calpain activity was measured using human erythrocyte Cal1 in the presence of a FRET substrate. Calpain, as a Ca²⁺-dependent cysteine protease, requires a reducing environment and sufficient Ca²⁺ concentrations for *in vitro* activity, hence, an activation buffer containing CaCl₂ and a non-thiol reducing agent, TCEP, was used for Cal1 activation. Preliminary IC₅₀ values were obtained by co-incubation of varying concentrations of the appropriate inhibitor (1 nM-10 μ M) in the presence of the FRET substrate (DABCYL)TPLK-SPPSPR-(EDANS) and Cal1 with the activation buffer. Fluorescence was measured following a 20 min incubation and percent inhibition calculated by normalizing to control experiments containing no inhibitor. A peptide

inhibitor, Z-LLY-FMK, was used as a positive control, and gave potent calpain activity (0 % remaining activity in the presence of 1 nM peptidyl inhibitor after 20 min).

End point analysis using the FRET assay was capable of separating 1st generation inhibitors into three broad classes based on their observed potencies: 1) potent inhibitors ($IC_{50} = 50 \text{ nM} - 1 \text{ }\mu\text{M}$); 2) weak inhibitors ($IC_{50} = 1 - 10 \text{ }\mu\text{M}$); and 3) inactive inhibitors ($IC_{50} > 10 \text{ }\mu\text{M}$) (Figure 14). 1st generation inhibitors were designed to mimic **E-64** at the P2 position, containing a *S*-isopropyl moiety, while varying the P3 cap group to increase potency and bioavailability compared to the guanidino group of **E-64**. In some instances, the stereochemistry and substitution of the epoxide warhead itself was changed to confirm the necessity of an *S,S* epoxysuccinate warhead. Direct analogs of **E-64** with varied P3 functionalities yielded several potent inhibitors with IC_{50} values calculated to be 50-250 nM. *R,R* epoxide and epoxyester derivatives were found to have weak activity, while a phenyl-epoxide containing analog was inactive.

A more detailed concentration curve (inhibitor concentrations of 50 nM, 100 nM, 250 nM, and 500 nM) was carried out for the potent inhibitors in order to obtain a more precise measure of the respective IC_{50} values, and potentially discriminate between potent inhibitors in an effort to form a SAR (Figure 15). Unfortunately, background signal noise from the FRET substrate was found to be a limiting factor in assay sensitivity at the low levels of calpain activity observed. Calpain is known to prefer large protein substrates, rather than small peptidic ones. (Takashi 1983) Although peptidyl molecules, like the FRET substrate, are more desirable as a simplified means of monitoring calpain activity, they are ultimately poor substrates for calpain when compared to calpains natural protein/enzyme substrates. This phenomenon is a well known obstacle of measuring calpain activity *in vitro*, and has likely contributed to difficulties encountered in the development of calpain inhibitors in the past.

Several 1st generation **E-64** analogs were found to be potent calpain inhibitors (TABLE II). Most potent inhibitors were found to have approximately equipotent activity, with IC₅₀ values ~ 100 nM (\pm 20-50 nM), and one inhibitor, **5**, seemed to display improved activity compared to the other analogs tested. These results are consistent with previous reports that molecules possessing bulky hydrophobic amino acid residues at the P2 position (i.e. Leu, Ile, Phe, Val) have high affinity for Cal1.

The *S,S* epoxide stereochemistry was found to be important, as *R,R* derivatives, **6** and **8**, showed weaker activity than their *S,S* counterparts (**5** and **7**). The *S,S* epoxide stereochemistry has been proposed to be optimal based on quantum mechanics/molecular modeling (QM/MM) calculations suggesting the formation of a conserved interaction network by *S,S* epoxides enables close contact between the active site cysteine and the C2 epoxide reacting center. (Mladenovic, Ansorg et al. 2008) This hypothesis is supported by our data, and numerous other *in vitro* accounts of *S,S* epoxides being preferred as cysteine protease inhibitors. (Otto and Schirmeister 1997)

Figure 14. Structures and Inhibition curves from end point analysis using the FRET assay

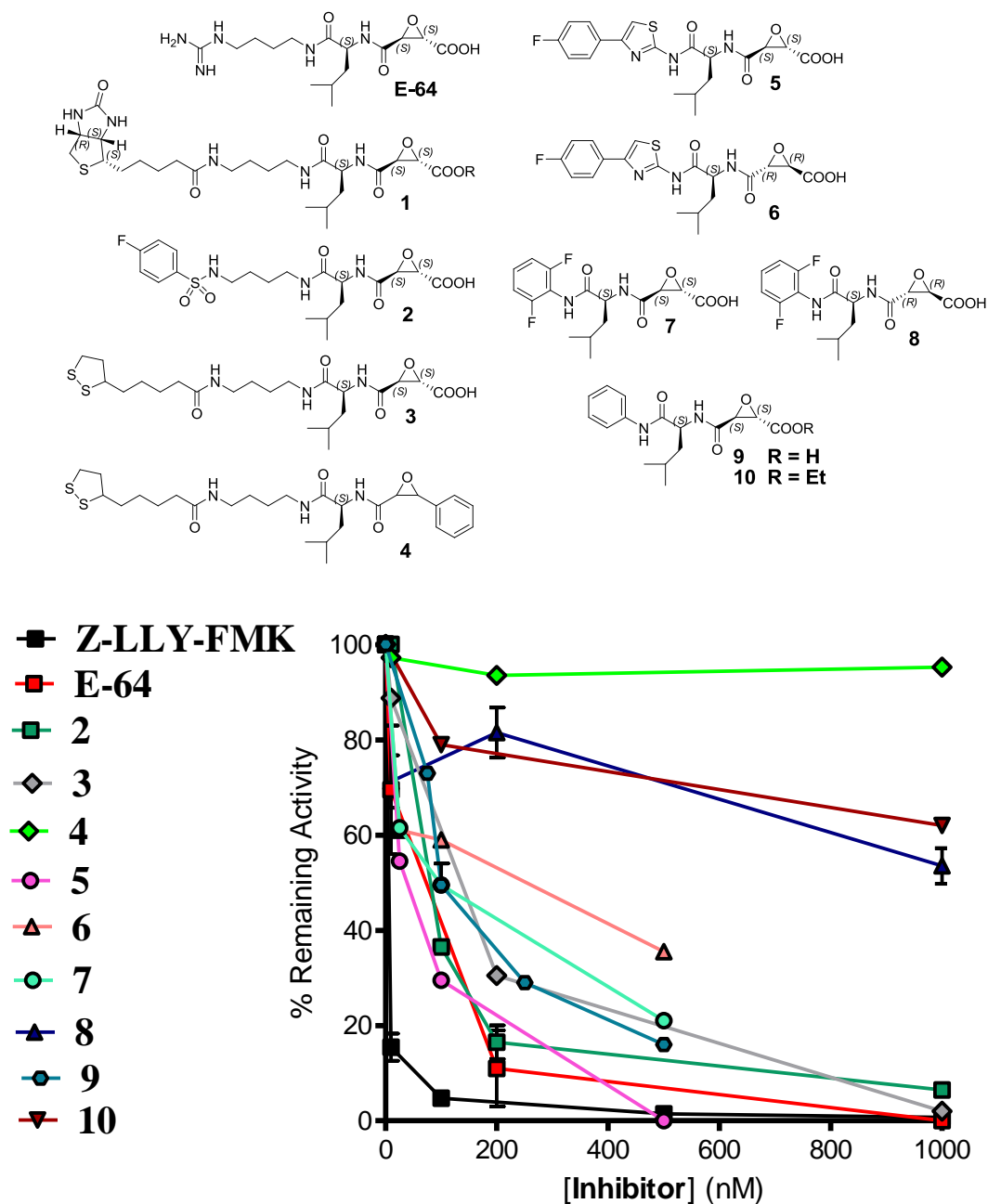


Fig.14. Structures and representative inhibition curves of 1st generation inhibitors from the FRET assay after incubation of human Cal1 with the FRET substrate in the presence of varying concentrations of inhibitors. Examination of % activity at 1 μ M demonstrates that molecules can generally be separated into three categories: potent, weak, and inactive.

Figure 15. Inhibition curves of potent inhibitors at concentration near the IC₅₀ values

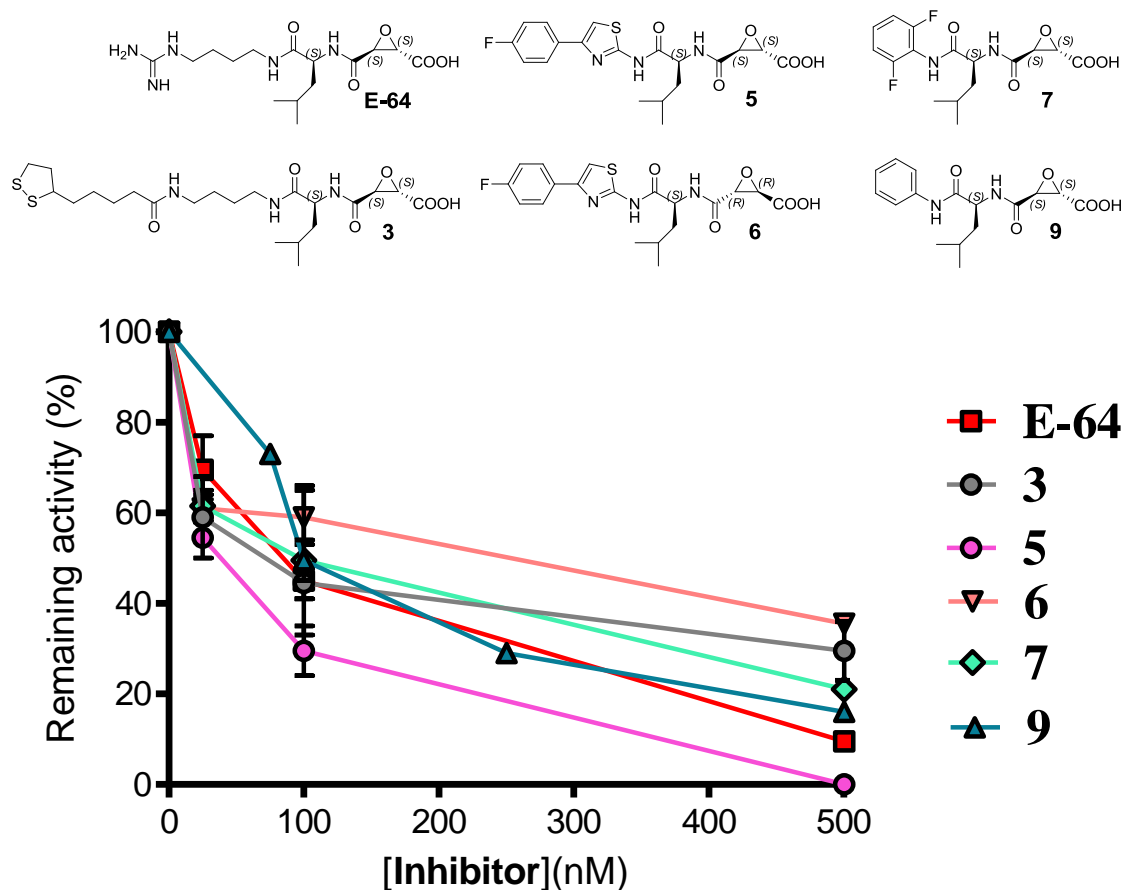
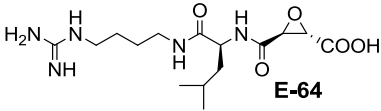
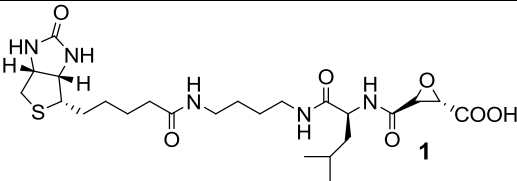
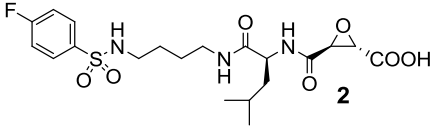
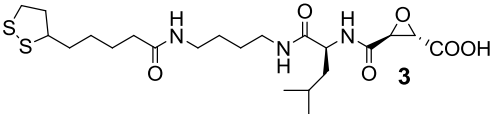
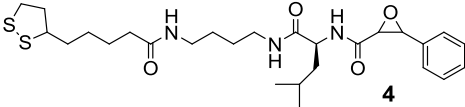
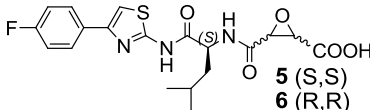
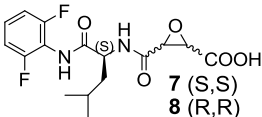
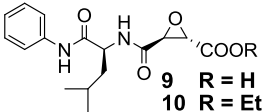


Fig.15. Detailed inhibition curves generated for potent inhibitors. Low concentrations of inhibitors (10, 100, and 500 nM) were used in an attempt to acquire more precise IC₅₀ values. The resulting inhibition curve suggested **5** as the most potent compound, although the signal to noise and standard error of the experiment failed to give a hierarchy of inhibitor potency. Inhibitor structures and their corresponding IC₅₀ values are discussed later in the lead optimization and SAR sections. Data represents the mean \pm S.D. of duplicate experiments.

TABLE II

STRUCTURES AND IC₅₀ VALUES OF 1ST GENERATION CALPAIN INHIBITORS^a

Structure (entry number)	Cal I IC ₅₀ (epoxide stereochemistry)
 E-64	100 nM (<i>S,S</i>)
 1	150 nM (<i>S,S</i>)
 2	100 nM (<i>S,S</i>)
 3	100 nM (<i>S,S</i>)
 4	> 1 μM
 5 (<i>S,S</i>) 6 (<i>R,R</i>)	5: 50 nM (<i>S,S</i>) 6: 250 nM (<i>R,R</i>)
 7 (<i>S,S</i>) 8 (<i>R,R</i>)	7: 100 nM (<i>S,S</i>) 8: > 1 μM (<i>R,R</i>)
 9 <i>R</i> = H 10 <i>R</i> = Et	9: 100 nM (<i>S,S</i>) 10: > 1 μM (<i>S,S</i>)

^a Inhibition was measured by monitoring fluorescence emission at 480 nm after 20 min incubations with varying concentration of inhibitor in the presence of the FRET substrate. Inhibition normalized to control incubations in the absence of inhibitor. Data represents the mean ± S.D. of duplicate experiments.

2.1.2 Employing LC-MS/MS in Lead Optimization of Calpain Inhibitors

An alternative technique using LC-MS/MS was pursued to complement the inhibition results of the FRET assay, and aid in designating the optimal P3 cap for incorporation into successive generations of novel calpain inhibitors. The preliminary IC₅₀ values afforded insight into the approximate activities of 1st generation inhibitors, but lacked the ability to absolutely discriminate between potent inhibitors. Calpain inhibition by epoxide peptidomimetics results in covalent modification of the active site cysteine. Proteomic analysis of calpain active site modification allows for quantitation of the modified active site cysteine. Using a competitive environment paradigm, inhibitors may be compared in one-on-one competition for calpain, allowing for a quantitative comparison of relative affinity and active site modification.

Recombinant Cal1 catalytic domain (Cal1_{cat}) is devoid of autocatalytic activity, and has emerged as a unique tool that makes assaying and evaluating calpain inhibitors more reliable. Cal1_{cat}, often called “Mini-calpain”, is composed of recombinant fragments of the proteolytic domains I and II of the full-length enzyme, and has been used as a surrogate to study calpain activity in the past.(Moldoveanu, Hosfield et al. 2002; Moldoveanu, Campbell et al. 2004; Cuerrier, Moldoveanu et al. 2005; Cuerrier, Moldoveanu et al. 2006) The recombinant proteolytic core, Cal1_{cat}, is devoid of the complications often encountered when assaying the full length protein, namely: autolysis, subunit dissociation, and protein aggregation. Additionally, recombinant Cal1_{cat} can be manufactured in-house through expression and purification from *E. coli*, making its application reliable, convenient, and cost effective.

Cal1_{cat} was employed in competition assays using a new proteomic model to explore active site modification using LC-MS/MS. The application of LC-MS/MS is particularly appropriate in lead optimization of irreversible calpain inhibitors due to the ultimate presence of a covalently

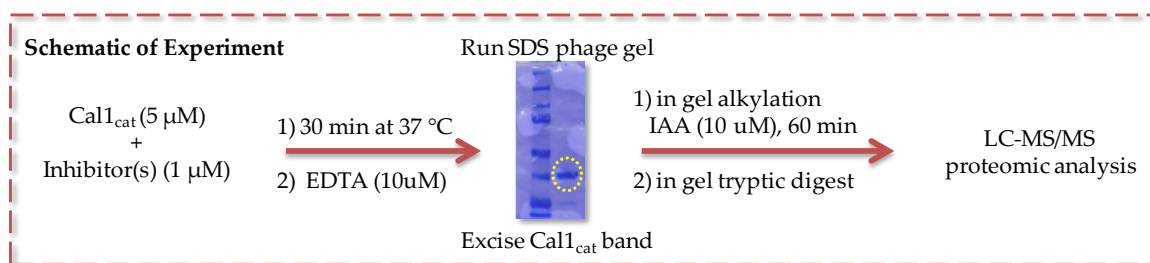
modified active site following inhibition. The experimental methodology follows the general protocols outlined in Scheme 2, and is described in the materials and methods section. Briefly, incubation of Cal1_{cat} (5 μ M) with the appropriate inhibitor(s) (1 μ M) for 30 min, followed by quenching with EDTA (10 μ M), running a SDS page, band excision, in gel alkylation with iodoacetamide (IAA) and in gel tryptic digest, and subsequent LC-MS/MS analysis affords measurements of active site modification. Proteomic analysis of the resulting tryptic digest of Cal1 or Cal1_{cat} (Figure 16), reveals a 29 amino acid (AA) peptide, containing the active site cysteine, within a relatively clean and well resolved total ion chromatogram (TIC). Both Cal1 and Cal1_{cat} gave identical 29AA active site containing peptide fragments, despite belonging to different mammalian species (*Homo sapien* vs *Rattus norvegicus*). Fortunately, this 29 AA peptide also contains 1 unmodified non-active site cysteine, which can be synthetically alkylated with IAA prior to tryptic digest to serve as an internal standard of active site modification.

One-on-one competition experiments using 1st generation inhibitors in competition with **E-64** identified compound **5** as the lone inhibitor capable of giving comparable modification to **E-64** (Figure 17,). In fact, competition experiments involving **E-64** and **5** demonstrated a higher abundance of compound **5** modified protein (40 % **E-64** modified: 60 % **5** modified, Figure 19, TABLE III). Using the IAA modified non-active site cysteine as an internal standard, incubations containing varying concentrations of **E-64** and **5** confirmed a reliable correlation between the observed EIC peak areas of the modified active site peptide versus inhibitor concentration, $R^2 = 0.968$ and $R^2 = 0.989$, respectively (Figure 18).

While several inhibitors showed comparable activity to **E-64** in the FRET assay, only compound **5** gave significant active site modification in competition with **E-64**. Although there are several plausible reasons for this phenomenon, two explanations seem most likely: 1) the

inhibitors possess different kinetic inhibition rate profiles; and/or 2) the observed differences in activity are due sequence homology differences between the two different isoforms, human erythrocyte Cal1 in the FRET study and recombinant rat Cal1_{cat} in proteomics. Epoxide peptidomimetics containing *S,S* epoxide stereochemistry have been uniformly shown to be irreversible inhibitors of calpain in the past, with inhibition mechanisms involving 2 sequential steps: the initial binding affinity, “on and off rate” (K_i), and the turnover rate inactivation (k_i). IC_{50} values observed using the FRET assay give a cumulative measurement of the K_i and k_i , because both the reversible complex and the irreversible complex inhibit FRET-substrate turnover; however, the proteomic analysis merely measures the irreversible complex. Therefore, an inhibitor with intermediate binding affinity and a high turnover rate might appear to be a better inhibitor than a molecule with high binding affinity and a low turnover rate.

Scheme 2. Methodology used to examine active site modification by LC-MS/MS ^a



^a Recombinant rat calpain 1 catalytic domain (Cal1_{cat}) (5 μM) was incubated with the appropriate inhibitor(s) (5 μM) in the presence of the activation buffer at pH 7.4 for 30 min at 37 °C. The reaction was quenched with EDTA (10 μM) and the resulting reaction mixture ran on a SDS phage gel. The Cal1_{cat} containing band was cut from the gel and submitted to in-gel alkylation with iodoacetamide (IAA) (10 μM) for 60 min, and subsequent tryptic digest. LC-MS/MS was then carried out and the resulting total ion chromatograms (TIC) and extracted ion chromatograms (EIC) were analyzed for the anticipated modified peptide fragments.

Figure 16. Resulting TIC from tryptic digest of Cal1 and Cal1_{cat}

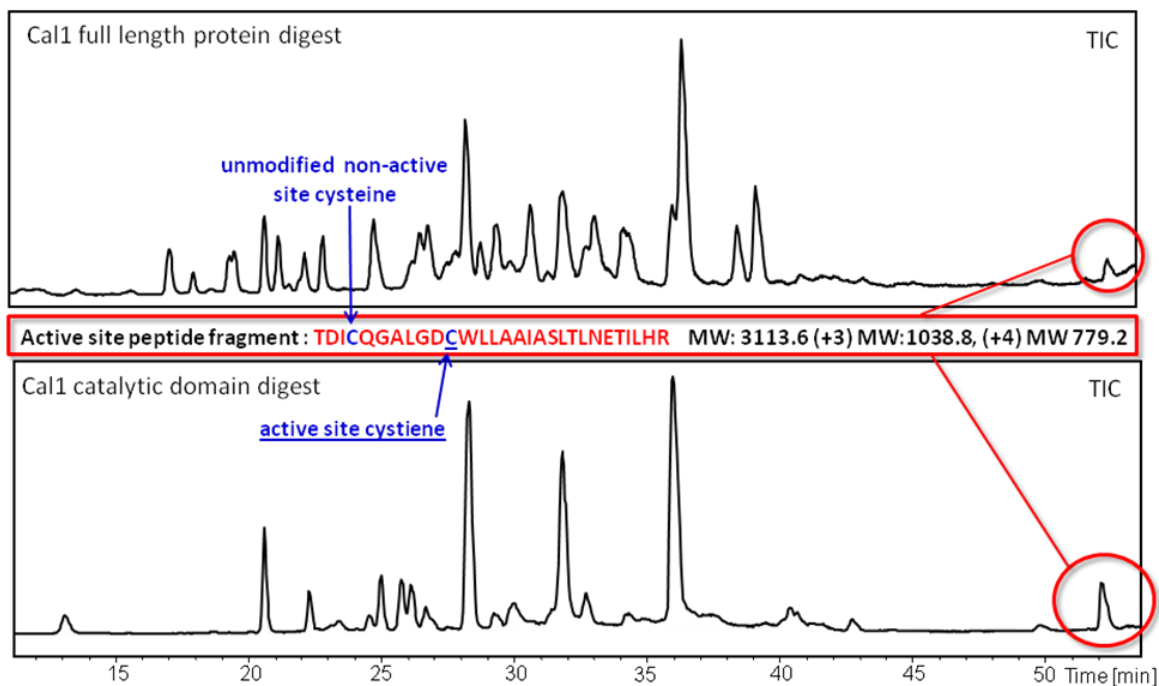


Fig.16. Total ion chromatogram (TIC) of the resulting peptide fragments from tryptic digest of IAA labeled human erythrocyte Cal1 full length protein (top) and recombinant rat Cal1 catalytic domain (bottom). The peak representing the active site peptide (circled in red) contains the active site cysteine, and one unmodified non-active site cysteine. Both enzymes afforded a 29 AA fragment found to contain the IAA modified active site cysteine. Active site peptides possessed 18 % sequence coverage for the human full length calpain 1, and 22 % coverage for the recombinant rat catalytic domain.

Figure 17. Resulting EIC for the treatment of Cal1_{cat} with **E-64** and **5**

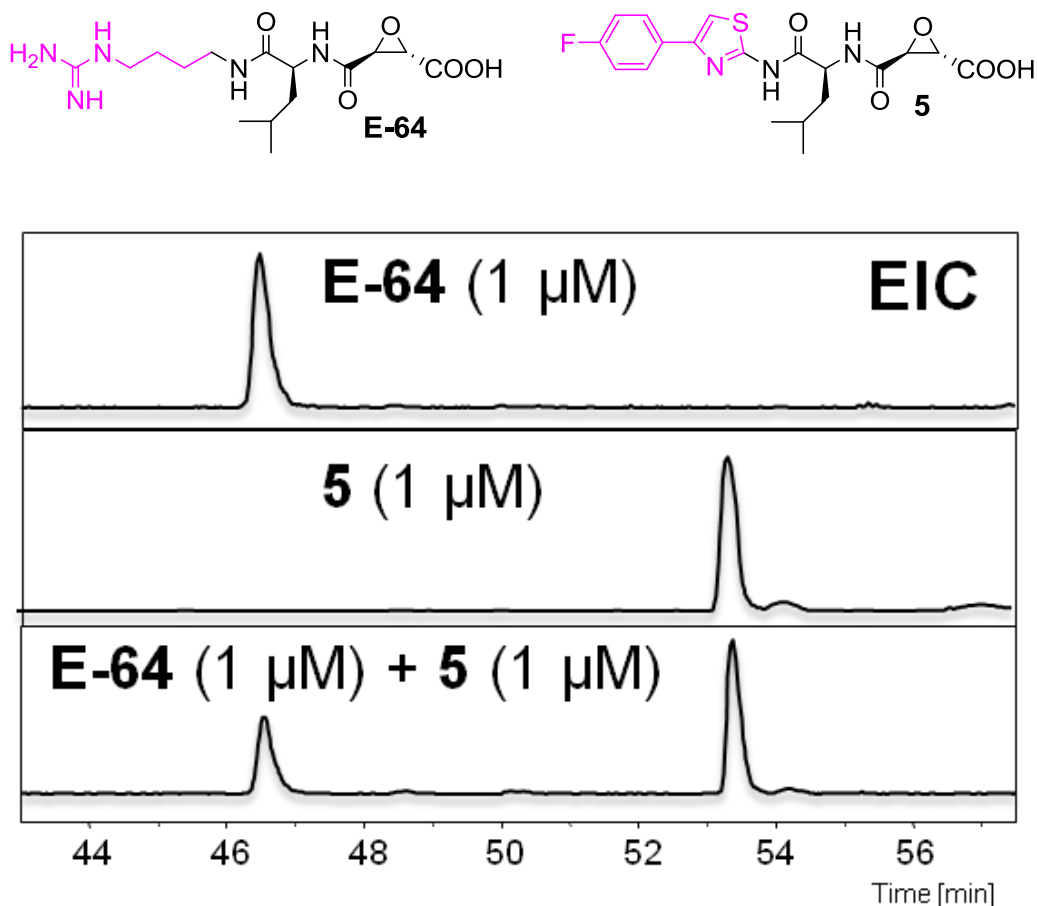


Fig.17. Recombinant rat calpain 1 catalytic domain (Cal1_{cat}) (5 μM) was incubated with the appropriate inhibitor: **E-64** (1 μM), **5** (1 μM), or both **E-64** and **5** (1 μM:1 μM), in the presence of the activation buffer at pH 7.4 for 30 min at 37 °C. The reaction was quenched with EDTA (10 μM), run on a SDS page gel, and the Cal1_{cat} containing band was excised. Subsequent in-gel alkylation with iodoacetamide (IAA) (10 μM), tryptic digest, and LC-MS/MS afforded the extracted ion chromatograms (EIC) shown. Comparison of the area under the curve of the EIC peaks demonstrates approximately 60 % of the active site peptide is modified by **5** following competition with **E-64**.

Figure 18. Calibration curve of active site modification at varying inhibitor concentration

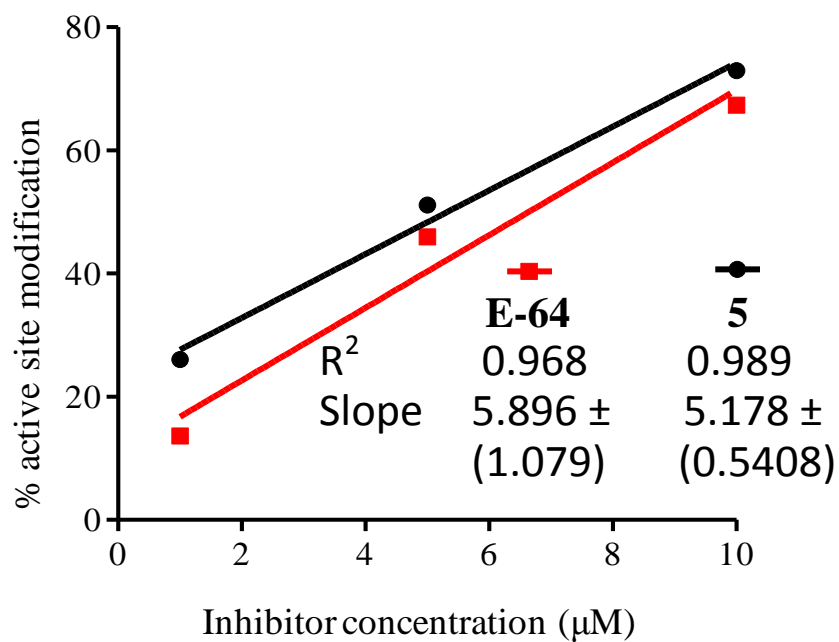


Fig.18. Correlation between the area under the curve of the extracted ion chromatograms and the concentration of inhibitor incubated with recombinant rat Ca1_{cat} . This correlation demonstrates the consistency and potential of using LC-MS as a semi-quantitative measure of active site modification by epoxide based calpain inhibitors.

Figure 19. Structures of 1st generation inhibitors examined in LC-MS/MS assay

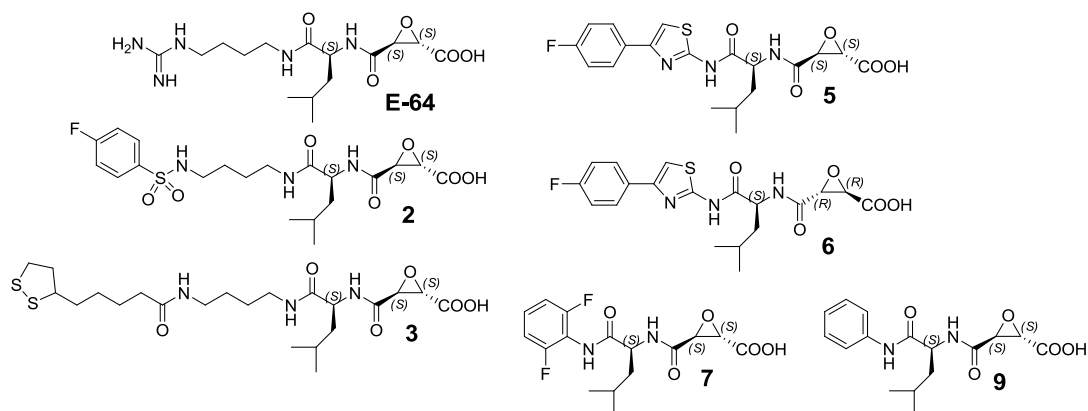


TABLE III

ACTIVE SITE MODIFICATION FOLLOWING COMPETITION WITH E-64^a

Entry	% E-64 modification	% compound modification	Cal1 IC ₅₀ (FRET assay)
2	100 %	ND	100 nM
3	98.5 %	1.5 %	100 nM
5	40.0 %	60.0 %	50 nM
6	99.6 %	0.4 %	250 nM
7	98.7 %	1.5 %	100 nM
9	95.9 %	4.1 %	100 nM

^a Percent active site modification by 1st generation inhibitors (1 μ M) in competition with **E-64** (1 μ M). IC₅₀ values calculated using linear regression of % Cal1 activity remaining after 20 min with varying concentrations of inhibitor. Compound **5** was supported as being most potent inhibitor in both assays.

The Cal1_{cat} employed to explore active site modification using LC-MS/MS may give a misleading account of calpain inhibitor potency. The emergence of a recombinant catalytic domain that is devoid of autocatalytic activity but maintains proteolytic activation in the presence of Ca²⁺ seems to be a promising tool for high throughput calpain inhibition studies. However, previous reports have indicated some drawbacks of using Cal1_{cat} to mimic full length Cal1. Specifically, Cal1_{cat} is weakly active compared to the intact full length protein. This reduced activity has been demonstrated with high affinity peptidyl substrates, and in one instance a 37.5 fold lower k_{cat} was observed for Cal1_{cat}. (Moldoveanu, Hosfield et al. 2002) A dramatically reduced k_{cat} would explain why most inhibitors gave low levels of active site modification of Cal1_{cat}, despite displaying potent activity in the FRET assay. An explanation for the exceptional ability of **E-64** and **5** to produce an increased k_{cat} is not immediately apparent. Ultimately, in-depth inhibition kinetic analysis must be pursued to answer these questions, and obtain absolute values of K_i and k_i.

Taken as a whole, these results highlight the benefits and caveats of complementing traditional enzyme inhibition measurements with modern LC-MS/MS techniques employing Cal1_{cat}, and cumulatively supported compound **5** as the most potent 1st generation calpain inhibitor. Hence, the 4-F-phenyl-thiazole moiety was designated as the superior P3 cap for incorporation into subsequent lead optimization efforts. At this point, classical medicinal chemistry dictates the generation of a library of aryl-thiazole derivatives with varying aryl substitution patterns in order to potentially achieve improved potency. However, inhibitors with increased potency often possess diminished selectivity, and there is no guarantee that an analog with improved potency will be realized. We pursued a more focused approach with the

knowledge that compound **5** was more potent and more druglike than the highly efficacious lead compound, **E-64**.

2.2 2nd generation inhibitors: gaining selectivity

In addition to calpain, inhibition of other cysteine proteases has been hypothesized to have potential in AD therapy, specifically inhibition of lysosomal cathepsins. (Yamashima, Kohda et al. 1998; Hook 2006; Pignol, Auvin et al. 2006) Moreover, concurrent inhibition of multiple cysteine proteases has been suggested as an appropriate route of therapeutic intervention in AD. (Yamashima, Kohda et al. 1998; Adamec, Mohan et al. 2000; Bendiske and Bahr 2003; Hook, Toneff et al. 2005; Hook 2006; Zhou, Scott et al. 2006; Hook, Kindy et al. 2007) Regardless of this fact, calpain hyperactivation has been confirmed to be fundamentally involved in AD pathology, *vide supra*. Selectivity towards a validated target is ultimately preferred in drug development in order to accurately understand the mechanism of action, which aids in predicting the potential for unwanted side effects and anticipating biomarker development.

Elaborations of the P2 segment were pursued to impart selectivity while maintaining the potency gained using the novel 4-F-phenyl-thiazole P3 cap. As discussed earlier, molecules containing a *L*-leucine functionality at the P2 position, as in compound **5** and **E-64**, have shown notoriously poor selectivity amongst cysteine proteases in the past. (Donkor 2000) Recently, a group at Queens University examined calpain specificity by screening a positional scanning peptidyl-epoxide library, and concluded that the P2 position is the most essential determinant of calpain selectivity. (Cuerrier, Moldoveanu et al. 2007) In this study, an array of P4-P3-P2-epoxide combinations was examined for inhibitory activity against human Cal1, Cal2, rat recombinant Cal1_{cat}, CathB, CathK, CathL, and papain. The study converged on selective analogs containing a P2 *L*-histidine (**WRH**) and a non-natural peptidomimetic analog (**WR-18**),

and an x-ray structure of recombinant rat Cal1_{cat} bound by **WR-18** was resolved. X-ray crystallography examination suggested a hydrogen bond occurring within the S2 pocket between the cyano group of **WR-18** and a highly conserved water molecule, which is present at the periphery of the S2 pocket in all Cal1/Cal2 crystal structures (Figure 20). (Cuerrier, Moldoveanu et al. 2007) The water molecule involved is stabilized by calpain backbone residues Glu-349 and Thr-210, and appears to be a fixed feature of the calpain S2 pocket. Supported by a high degree of selectivity obtained by inhibitors containing histidine moieties at the P2 position, they hypothesized that improved selectivity may be gained via incorporation of a properly positioned H-bond acceptor at the P2 site.

Design of 2nd generation molecules focused on developing inhibitors with a properly positioned H-bond acceptor at the P2 position to explore possible interactions with the conserved H₂O molecule of the S2 pocket (TABLE IV). A *L*-histidine incorporating analog of **5** was synthesized as a high priority target (**13**), along with other peptidomimetics (**11-20**), including two *N*-methyl *L*-histidine derivatives (**17** and **18**). *L*-Histidine incorporating peptidomimetics may become protonated under physiological conditions, and as a result, have shown evidence of possessing poor drugability properties in the past. The thiazole moiety has been used successfully in the past as a bioisosteric replacement of the imidazole of the histidine containing compounds. Hence, principal efforts focused on the creation of the 4-F-phenyl-thiazole containing analog, **20**. In contrast to the *L*-leucine containing 1st generation analogs, few *L*-histidine and *L*-β-alaninethiazolyl derivatives gave potent activity. As expected, analogs containing the optimal 4-F-phenyl-thiazole P3 cap group afforded the most potent compounds, **13** and **20**, with equipotent activity to **E-64** (IC₅₀ ~ 100 nM).

Figure 20. Rationalization of potential for calpain selectivity via the P2 moiety

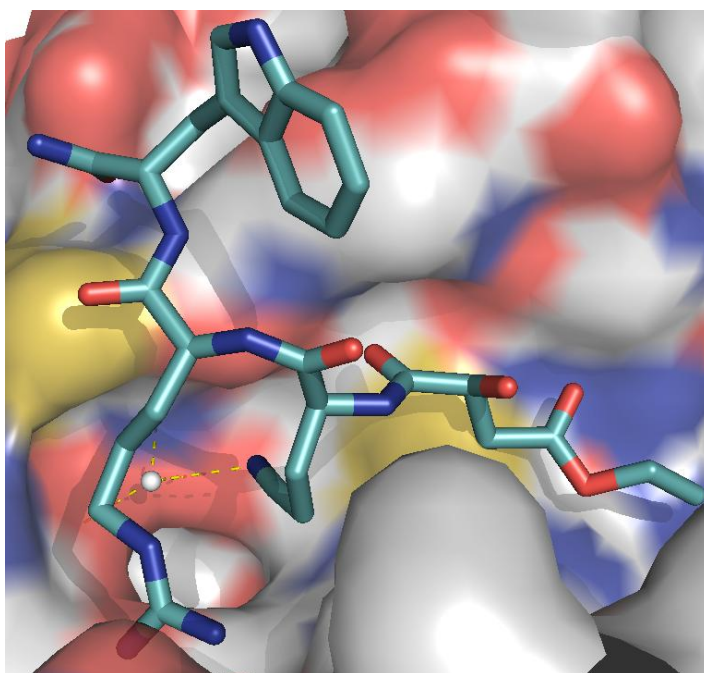
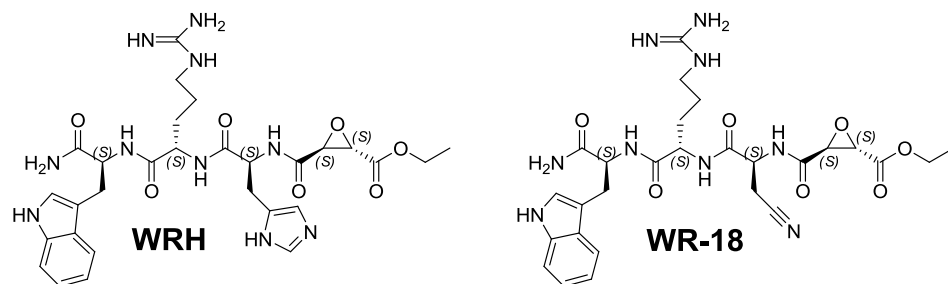
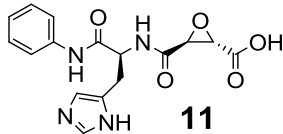
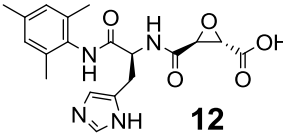
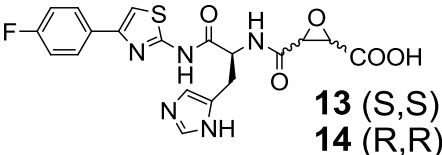
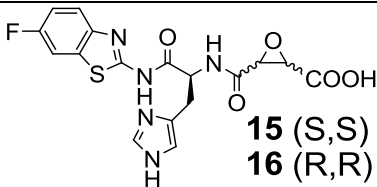
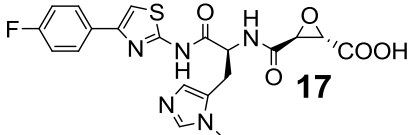
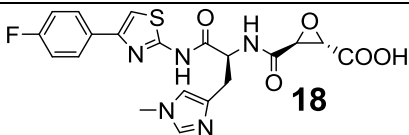
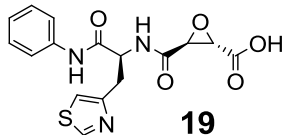
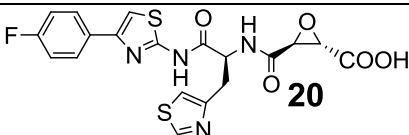


Fig.20. Top: Structures of reported calpain selective epoxides of Queens University. WRH and WR-18 were found to be selective for human Cal1 with IC₅₀ values of 437 nM and 333 nM, respectively. Bottom: x-ray structure of WR-18 bound to recombinant rat Cal1_{cat} illustrating the presence of a conserved H₂O molecule within the S2 pocket. This H₂O is a fixed feature of all calpain x-ray structures, and was hypothesized to be capable of aiding in acquiring selectivity for calpain. PyMol was used to render the x-ray structure of WR-18 and Cal1_{cat} (PDB: 2NQG).

TABLE IV
STRUCTURES AND IC₅₀ VALUES OF 2ND GENERATION CALPAIN
INHIBITORS^a

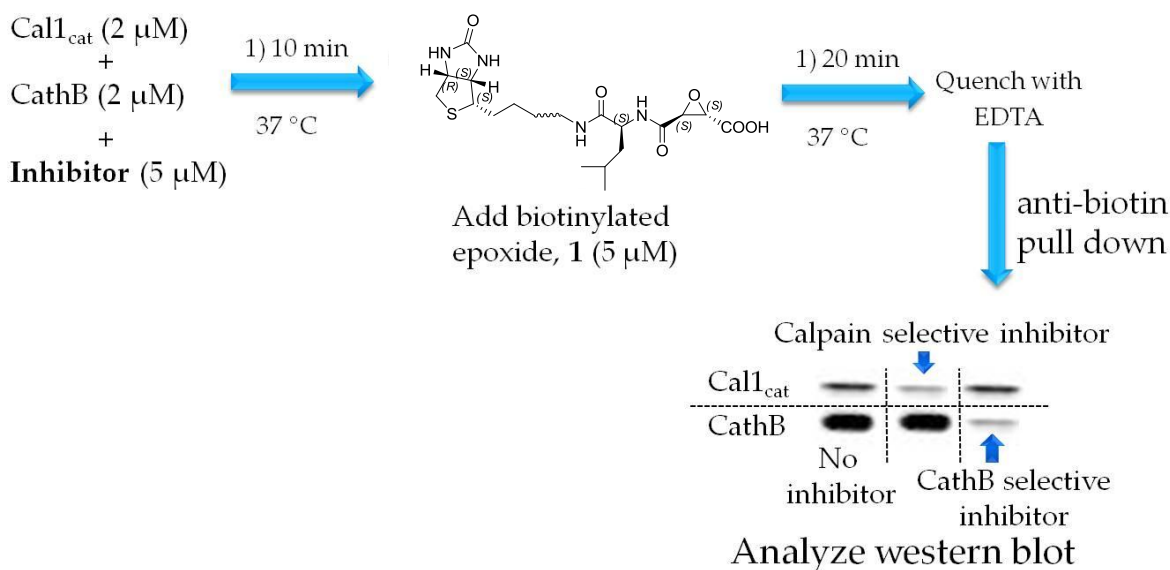
Structure (entry number)	Cal1 IC ₅₀ (epoxide stereochemistry)
 11	5 μM (<i>S,S</i>)
 12	5 μM (<i>S,S</i>)
 13 (<i>S,S</i>) 14 (<i>R,R</i>)	13: 100 nM (<i>S,S</i>) 14: > 1 μM (<i>R,R</i>)
 15 (<i>S,S</i>) 16 (<i>R,R</i>)	15: 500 nM (<i>S,S</i>) 16: > 1 μM (<i>R,R</i>)
 17	5 μM (<i>S,S</i>)
 18	225 nM (<i>S,S</i>)
 19	2.5 μM (<i>S,S</i>)
 20	100 nM (<i>S,S</i>)

^a Inhibition of human erythrocyte calpain 1 by select 1st generation calpain inhibitors. Data represents the mean ± S.D. of duplicate experiments.

Selectivity was evaluated using competition experiments employing a synthesized biotinylated epoxide (**1**) to allow visualization of protease modification by selected inhibitors in the presence of equimolar amounts of Cal1_{cat} and CathB. Compound **1** serves as a suitable probe for examining calpain selectivity for multiple reasons, including: it incorporates an epoxide warhead for irreversible modification of the active site cysteine of cysteine proteases; **1** mimics the non-selective nature of **E-64** via incorporation of a leucine residue at the P2 position; and it possesses a biotin moiety which allows for visualization of protein modification by western immunoblotting. Cal1_{cat} was again chosen as a surrogate of calpain selectivity. As described earlier, Cal1_{cat} has significantly decreased activity compared to full length Cal1. Nonetheless, Cal1_{cat} has demonstrated similar substrate specificity to the full length enzyme in the past, making it an appropriate tool for evaluating selectivity.(Moldoveanu, Hosfield et al. 2002; Moldoveanu, Campbell et al. 2004; Cuerrier, Moldoveanu et al. 2005; Cuerrier, Moldoveanu et al. 2007)

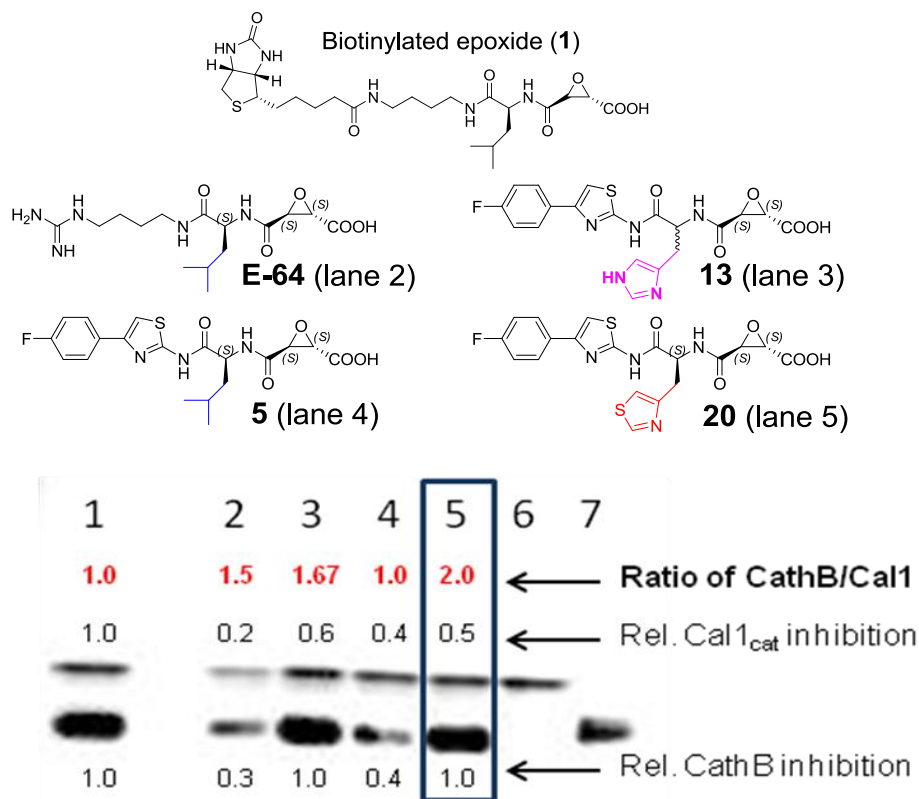
Along with **E-64**, three compounds were chosen based on potency and structural similarity for side by side comparison of selectivity using the competition assay, including: the most potent compound of the entire series (**5**), and direct analogues possessing a *L*-histidine (**13**) or a *L*- β -alaninethiazolyl (**20**) at the P2 position. This dataset (compounds **5**, **13**, and **20**) allows for an absolute determination of the impact of the P2 position on selectivity, as the rest of the molecular structure is unchanged. Cal1_{cat} (2 μ M) and CathB (2 μ M) were pre-treated with inhibitors (5 μ M) for 10 min, followed by incubation with the biotinylated epoxide, **1** (5 μ M), quenching with EDTA (10 μ M), streptavidin-HP pull down, and western blot analysis (Scheme 3).

Scheme 3. Schematic of competition assay methodology using Cal1_{cat} and CathB^a



^a The appropriate inhibitor (5 μM) was pre-incubated in a mixture containing Cal1_{cat} (2 μM), CathB (2 μM), TCEP (1 mM), and Ca²⁺ (30 μM) for 10 min at 37 °C. The biotinylated epoxide, **1** (5 μM), was then added and the mixture incubated for an additional 20 min. The reaction was quenched with EDTA (10 mM) and protein modification by **1** analyzed following streptavidin-HP pull down and western immunoblotting. The western blot shown is hypothetical, and illustrates the anticipated outcome of a high affinity selective inhibitors of Cal1_{cat} or CathB. In this paradigm, a high affinity calpain selective inhibitor would result in a western blot with weakened Cal1_{cat} band absorbance, with no change in absorbance of the CathB band. Conversely, a high affinity CathB selective inhibitor would have no effect on the Cal1_{cat} band, while decreasing the abundance of the CathB band.

Figure 21. Competition experiment examining relative Cal1_{cat} vs CathB modification ^a



Lane1- Cal1_{cat} (2 μ M) + CathB (2 μ M) + **1** (5 μ M)
 Lane2- Cal1_{cat} (2 μ M) + CathB (2 μ M) + **1** (5 μ M) + **E-64** (5 μ M)
 Lane3- Cal1_{cat} (2 μ M) + CathB (2 μ M) + **1** (5 μ M) + **13** (5 μ M)
 Lane4- Cal1_{cat} (2 μ M) + CathB (2 μ M) + **1** (5 μ M) + **5** (5 μ M)
 Lane5- Cal1_{cat} (2 μ M) + CathB (2 μ M) + **1** (5 μ M) + **20** (5 μ M)
 Lane6- Cal1_{cat} (2 μ M) + **1** (5 μ M)
 Lane7- CathB (1 μ M) + **1** (5 μ M)

Fig.21. Top: Structures of inhibitors examined. Bottom: western blotting of protein modification by a biotinylated epoxide (**1**) following preincubation of Cal1_{cat} (2 μ M), and CathB (2 μ M) with the appropriate inhibitor (5 μ M) [Lane 1, 6 and 7 (no inhibitor), Lane 2 (**E-64**), Lane 3 (**13**), Lane 4 (**5**), Lane 5 (**20**). By comparing the overall absorbance of each lane compared the control incubation (lane 1), the relative % modification by each inhibitor is calculated (shown above Cal1_{cat} band and below the CathB band). The ratio of CathB/Cal1_{cat} modification and relative “selectivity” is calculated by dividing the relative % modification of CathB by the relative % modification of Cal1_{cat}.

Relative selectivity was ascertained by comparing the intensity of each biotin-immunoreactive band versus the control (Figure 21), and is represented by the value given above the Cal1_{cat} band and below the CathB band, respectively. A selectivity ratio was calculated by dividing the relative CathB inhibition by the relative Cal1_{cat} inhibition. Consequently, in this paradigm the selectivity ratio with the largest nominal value would indicate most selective inhibitor for calpain, and conversely for CathB. As expected, **E-64** (lane 2) shows poor selectivity, binding to both Cal1_{cat} and CathB with strong affinity. Predictably, the *L*-leucine containing compound **5** (lane 4) also showed a lack of selectivity for Cal1_{cat}, with a selectivity ratio of 1.0. This finding is in agreement with literature precedence of peptidomimetics hydrophobic AA residues at the P2 position (ie. Leu, Ile, Phe, Val) displaying poor selectivity within the CA clan cysteine protease superfamily. Compounds **13** (lane 3) and **20** (lane 5) show the best selectivity, with relatively no change in intensity in CathB band, and corresponding selectivity ratios of 1.67 and 2.0, respectively. This observation supports the Queens University groups' conclusion that incorporation of a properly oriented H-bond acceptor at the P2 position may increase preference for calpain.

Papain is a promiscuous cysteine protease which displays loose substrate preferences and serves as a good pan-cysteine protease model. Inhibition rate constants (k_i/K_i) were measured for **E-64**, **5** and **20** against papain and recombinant rat Cal1_{cat} using a FRET substrate. Inhibition by **E-64** was used as a benchmark of activity and a relative selectivity index was calculated compared to **E-64** (TABLE V). Consistent with our initial IC₅₀ values using human full length Cal1, inhibition rate constants for compounds **5** and **20** with Cal1_{cat} afforded approximately equipotent activity to **E-64**. In agreement with the Cal1_{cat}/CathB competition experiments, **5** is less selective than **E-64** for calpain than papain, with nearly double the potency of **E-64** against

papain (82 % greater relative k_i/K_i than **E-64** vs papain) and a relative selectivity index of 0.52. Compound **20** on the other hand showed considerably reduced activity versus papain, with relative k_i/K_i values 49 % that of **E-64**, and a selectivity index of 2.0. These findings are consistent with reports on the non-selective nature of *L*-leucine containing cysteine protease inhibitors, and support the suggestion that a properly placed hydrogen bond acceptor at the P2 position imparts increased selectivity for calpain.

Computational docking studies are a useful tool to aid in conceptualization and visualization of molecular interactions in drug discovery, particularly when inhibitor bound x-ray crystal structures are readily available, as is the case for calpain. The use of the recent **WR-18** bound x-ray structure (PDB: 2NQG) is particularly beneficial because it illustrates the complex formed between **WR-18** and recombinant rat Cal_{1cat}, which is the same enzyme we used in our selectivity assays. Inhibitors were docked into the **WR-18** bound Cal_{1cat} x-ray structure using GOLD docking platform with the distance and angle of the epoxide reaction transition state geometry as primary constraints. Structural overlay of docking results for compounds **5**, **13**, and **20** predicts a common binding motif, with the P3 cap group extended into the solvent exposed S4-S3 region and the P2 peptidomimetic moiety situated within the S2 pocket (Figure 23). Indeed, docking results illustrate the potential of **13** and **20** possess a similar binding motif to **WR-18** and take advantage of the conserved H₂O residue by incorporating a properly positioned H-bond acceptor.

Figure 22. Examination of inhibition kinetics of selected inhibitors against Cal1_{cat} and papain

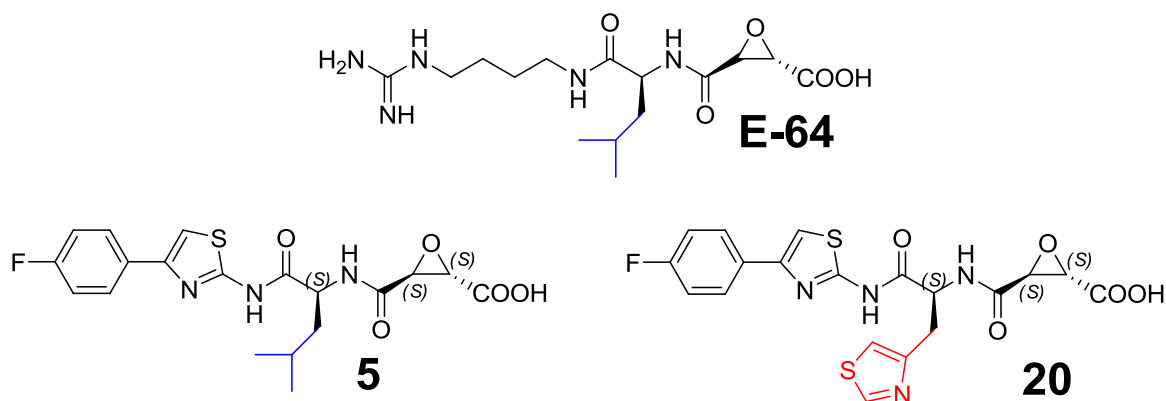


TABLE V

INHIBITION RATE CONSTANTS VERSUS CAL1 AND PAPAIN^a

Entry	Cal1k _i /K _i ^a	% of E-64 ^b	Papain k _i /K _i ^a	% of E-64 ^b	Relative Selectivity ^c
E-64	2.95e ⁰⁴ (±1.52e ⁰³)	-	5.79e ⁰⁶ (±5.23e ⁰⁵)	-	-
5	2.77e ⁰⁴ (±1.98e ⁰³)	94 %	1.05e ⁰⁷ (±4.10e ⁰⁵)	182 %	0.52
20	2.98e ⁰⁴ (±1.40e ⁰³)	101 %	2.83e ⁰⁶ (± 4.72e ⁰⁵)	49 %	2.06

^a Observed inhibition rate constants for selected inhibitors versus Cal1 and papain. ^bcalculated

% k_i/K_i relative to E-64. ^cRelative calculated selectivity (Cal1k_i/K_i papain k_i/K_i) compared to E-64. Inhibition rate constants were obtained by continuously monitoring FRET substrate turnover at varying concentrations of inhibitor (100 nM-5 uM) for 45 min.

Figure 23. Docking results illustrating predicted binding poses of novel inhibitors

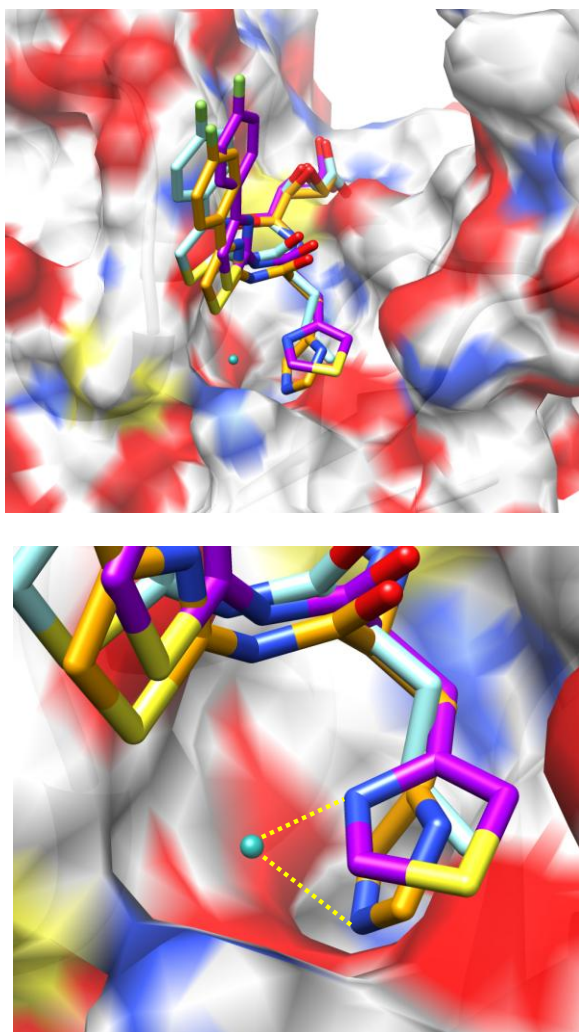


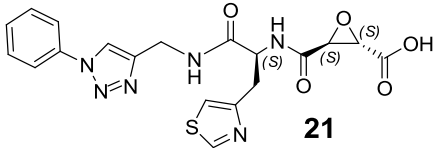
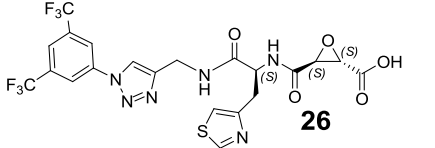
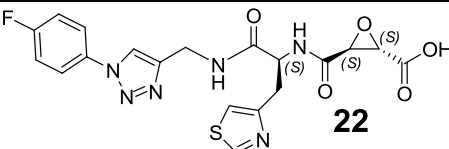
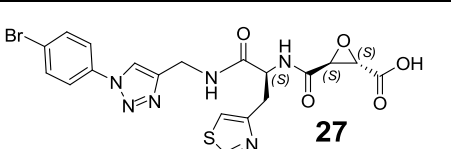
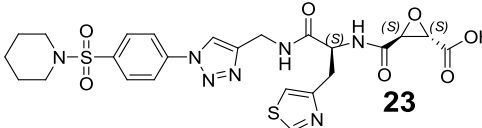
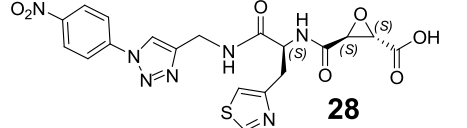
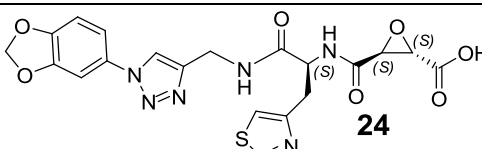
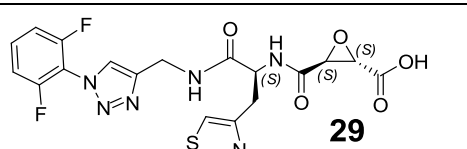
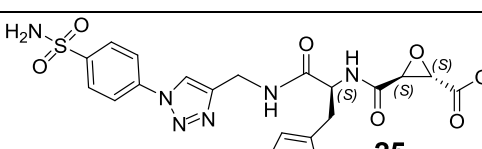
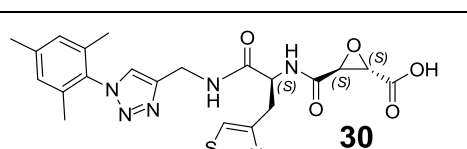
Fig.23. Selected inhibitors (compounds **5**, **13**, and **20**) were docked within the **WR-18** x-ray structure of recominant rat Cal1_{cat} [PDB: 2NQG]. Docking was carried out via GOLD docking platform using Sybyl molecular modeling software. Top: Structural overlay of putative docking poses for compounds **5**, **13**, and **20** with the [PDB: 2NQG]. Bottom: Magnified S2 pocket illustrating proposed H-bond formed between the conserved H₂O molecule and the P2 moiety. Docking poses rendered using UCSF Chimera molecular modeling software.

2.3 3rd generation inhibitors: P3 refinement and molecular diversity

With the confirmed role of the P2 position in determining selectivity, further refinement of the P3 position used computational guidance, and employed a novel click chemistry approach to rapidly generate a library of analogs of compound **20**. This P3 refinement differs from the initially avoided “classical” approach of derivatizing compound **5**, which would have required a tedious convergent synthesis approach. We hypothesized that a library of epoxide peptidomimetics could be synthesized using a divergent approach through the application of “click chemistry” methodologies. Thirty two synthetically accessible analogs of compound **20** were screened *in silico* using a combination of docking scores utilizing multiple Cal1 crystal structures and a geometric parameter associated with the transition state for covalent modification. QSAR analysis predicted analog activity based on Nsig values, and led to the rapid synthesis of ten such analogs (TABLE VI).

Compounds predicted to be poor inhibitors (**21**, **23**, **25**, and **29**) yielded relatively high IC₅₀ values, while molecules predicted to be effective inhibitors displayed potent activity for calpain (**22**, **24**, **27**, and **28**). A notable outlier was the 3,5 bistrifluoromethylphenyl derivative, **26**, which displayed poor calpain activity despite being predicted to be the most potent compound based on *in silico* screening. The ultimate goal of the work is to efficiently produce novel potent calpain inhibitors, therefore, precise IC₅₀ values were not pursued for all inhibitors to validate the computational model. Nonetheless, a tentative trend can be assigned based on the IC₅₀ values that were acquired, and a reasonable correlation is observed, although more data points would be needed to completely assess the predictive power of this model (Figure 24).

TABLE VI
3RD GENERATION INHIBITORS WITH VARYING P3 CAP GROUPS^a

Structure (Entry number)	Cal1 IC ₅₀	Structure (Entry number)	Cal1 IC ₅₀
 21	> 1 μM	 26	> 1 μM
 22	100 nM	 27	60 nM
 23	1.5 μM	 28	300 nM
 24	400 nM	 29	> 1 μM
 25	> 1 μM	 30	> 1 μM

^a Structures and representative IC₅₀ values of 3rd generation inhibitors. FRET substrate turnover was monitored after 20 min incubation with varying concentrations of the appropriate inhibitor with human Cal1.

Figure 24. Tentative correlation between Nsig values and observed IC₅₀ values

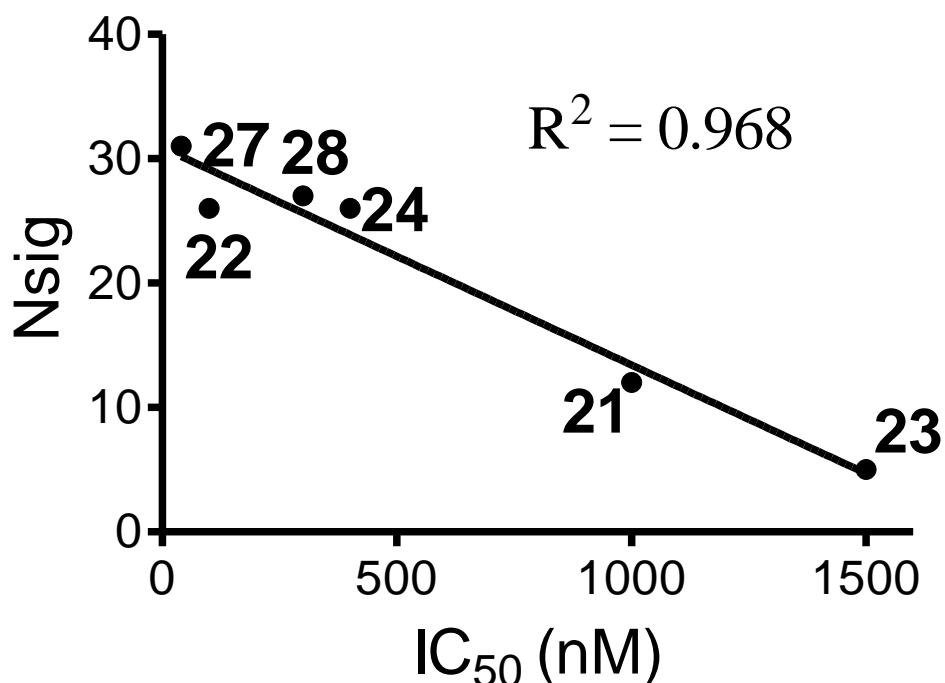


Fig.24. A tentative trend is observed based on the IC₅₀ values and the Nsig parameter from computational modeling. The Nsig value is a computational descriptors designed to correlate inhibitory activity. Generation of the Nsig parameter followed docking studies of 1st and 2nd generation inhibitors. Larger Nsig values predict smaller IC₅₀ values (ie. more potent inhibitors). A few inhibitors were excluded due to the lack of a definitive IC₅₀ value (those with IC₅₀ values > 1.0 μ M). Ultimately, more data points would be preferable to completely assess the predictive power of this model, but the observed trend is noteworthy.

2.4 *Ex vivo* and *in vivo* evaluation of efficacy and safety

Establishing safety, efficacy, and bioavailability are the chief objectives of preclinical compound evaluation during drug development. The cysteine protease inhibitor **E-64d** has been evaluated in clinical trials previously, but failed to gain regulatory approval due to lack of efficacy in the prescribed indication. Nonetheless, these trials established a clinical safety profile for epoxide based irreversible cysteine protease inhibitors. The reported lack of efficacy for muscular dystrophy does not rule out the possibility of effectiveness against other indications. This is evidenced by the renewed interest in **E-64d**, which recently entered a phase I trial in the US for AD therapy. (Tjernberg, Lilliehook et al. 1997; Hook 2006; Hook, Hook et al. 2007) Herein, we describe the *ex vivo* and *in vivo* efficacy of novel epoxide peptidomimetic calpain inhibitors, and explore their PK/toxicological properties.

LTP in the Schaffer collateral pathway of the hippocampus is a cellular model of learning and memory (for review see (Kandel 2001)), which is significantly impaired after perfusion with oligomers of A β . (Lambert, Barlow et al. 1998) A β induced inhibition of LTP is reversed by calpain inhibitors via a mechanisms shown to be involve phosphorylation of the memory related transcription factor CREB.²⁸ In addition, calpain is integrally involved in remodeling of post-synaptic protein densities and plays a key role in regulating synaptic plasticity. Functional efficacy of novel epoxide based calpain inhibitors was assessed in the LTP paradigm using either hippocampi from WT mice co-perfused with oligomeric A β .

The involvement of calpain in synaptic plasticity and long term potentiation (LTP) suggests that a correlation should exist between Cal1 IC₅₀ values and the potency of transmission rescue. Previous reports by our collaborators have demonstrated the ability of **E-64** to restore LTP in response to A β induced synaptic deficit in APP/PS1 transgenic mice. Restoration of LTP

following co-perfusion with oligomeric A β was measured at varying concentration of **E-64** (100 nM, 500 nM, 600 nM, 750 nM, and 1 μ M). The EC₅₀ of LTP restoration by **E-64** was determined to be ~650 nM (Figure 25). The concentration dependent response of synaptic rescue by **E-64** suggests the possibility of correlating *ex vivo* LTP rescue with *in vitro* calpain inhibition by testing novel inhibitors at the EC₅₀.

All novel calpain inhibitors were capable of restoring synaptic function in response to A β induced synaptic deficits. A LTP ratio was calculated in an attempt to discriminate between the LTP rescue for various inhibitors (Figure 26). The LTP ratio was calculated by normalizing to A β treated controls (Drug + A β / vehicle A β). Residual potentiation was averaged during the last 5 min of LTP following treatment with the appropriate inhibitor (650 nM). All inhibitors were capable of restoring LTP to levels equivalent to **E-64** elicited transmission rescue. Despite the ability of all inhibitors to restore LTP, no correlation was observed between Cal1 IC₅₀ and LTP restoration (Figure 27). This is likely a result of the high degree of standard error afforded by f-EPSP measurements and approximate IC₅₀ designations. Hence, LTP is not a suitable technique to evaluate functional potency of calpain inhibitors. Nonetheless, restoration of LTP serves as a valuable tool for “yes/no” answers regarding the ability of small molecules to restore synaptic transmission following A β induced deficit, and interpretation beyond this point is somewhat erroneous.

Figure 25. Determination of ED_{50} of synaptic rescue in LTP by **E-64**

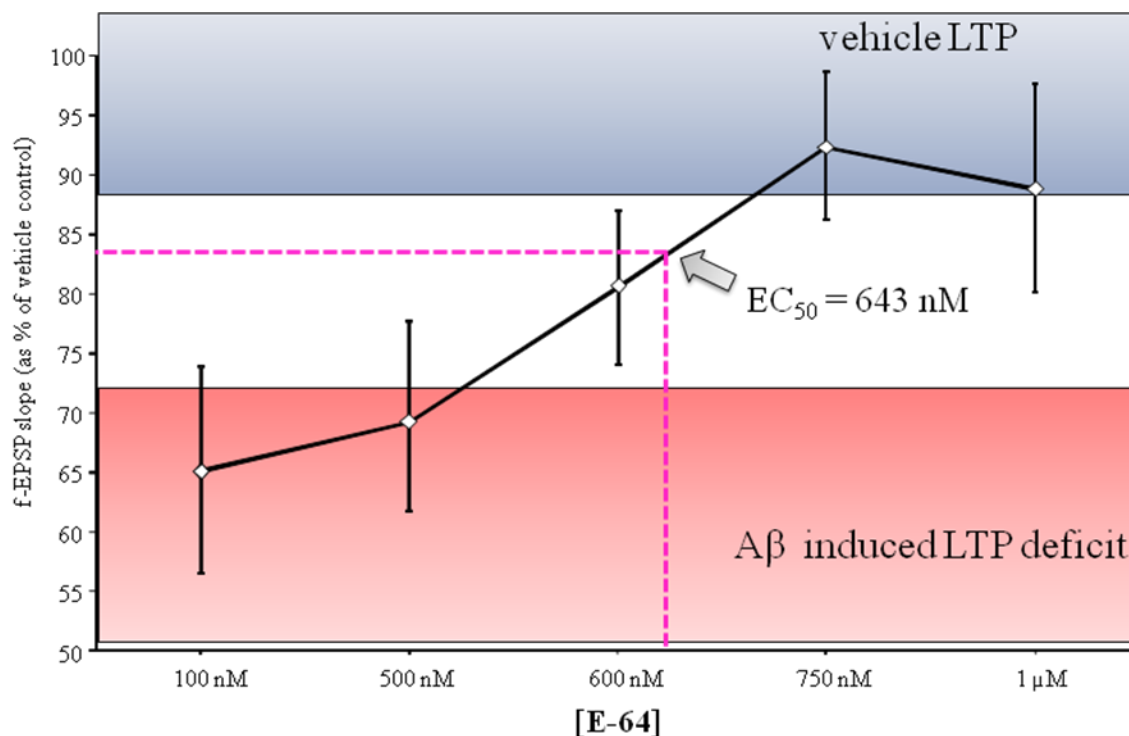


Fig.25. Long term potentiation (LTP) measures propagation of electrochemical potential (f-EPSP) from the CA3 to the CA1 region of the hippocampus. Oligomeric A β is known to impair LTP. Varying concentrations of **E-64** (100 nM, 500 nM, 600 nM, 750 nM, and 1 μ M) were examined for the ability to rescue LTP in hippocampal slices co-perfused with oligomeric A β . f-EPSP signal was normalized against f-EPSP levels of hippocampi from vehicle treated control mice. Typically, A β induced deficits in synaptic transmission results in a 30-50 % loss in f-EPSP signal. The EC_{50} for rescue of LTP by **E-64** was determined to be ~ 650 nM. This concentration was used for the screening of subsequent novel calpain inhibitors in an attempt to correlate calpain potency with restoration of synaptic function.

Figure 26. Ratio of LTP restoration by epoxide peptidomimetic calpain inhibitors

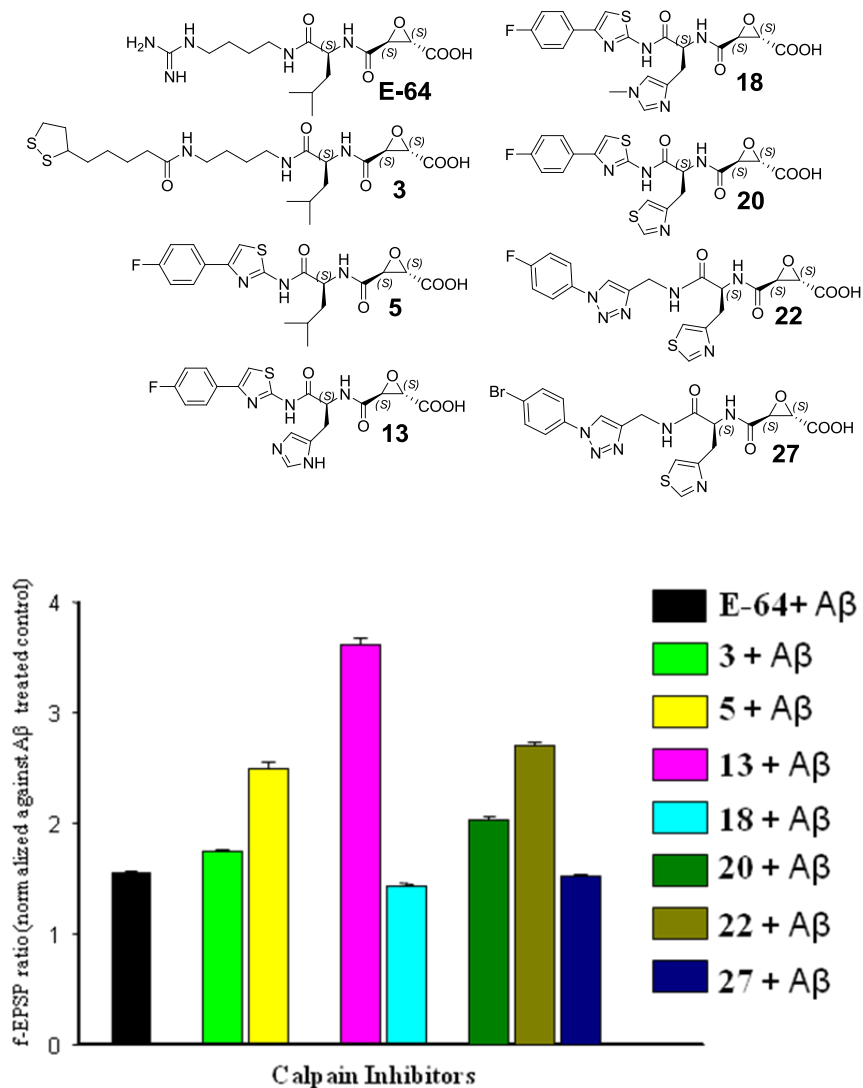


Fig.26. Top: Structures of inhibitors examined in LTP paradigm. Bottom: Restoration of LTP by epoxide peptidomimetic calpain inhibitor after co-perfusion with oligomeric Aβ. Represented as LTP ratio, normalized against Aβ treated controls (Drug + Aβ/ vehicle Aβ). Residual potentiation was averaged during the last 5 min of LTP following treatment with the appropriate inhibitor (650 nM). All inhibitors were capable of restoring LTP to levels equivalent to **E-64** elicited transmission rescue.

Figure 27. Lack of a correlation between Cal1 IC₅₀ and LTP restoration

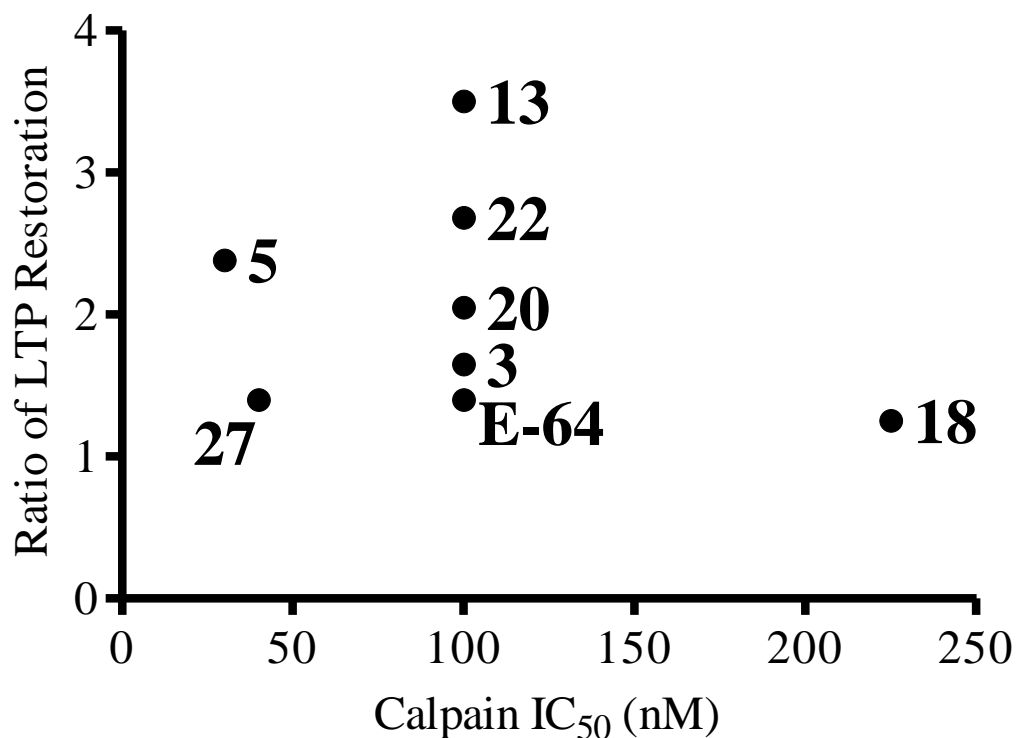


Fig.27. No correlation was observed between Cal1 IC₅₀ and ratio of LTP restoration. This is likely a result of the high degree of standard error afforded by f-EPSP measurements, natural variations of LTP, and high background signal noise in the Cal1 FRET assay used to obtain the IC₅₀ values. LTP serves as a valuable tool for “yes/no” answers regarding the ability of small molecules to restore synaptic transmission following A β induced deficit, and interpretation beyond this point is somewhat erroneous.

In vivo functional efficacy was assessed in paradigms of contextual fear memory and spatial-working memory. Restoration of LTP in hippocampal slices by our inhibitors suggested utility as procognitive agents in an *ex vivo* paradigm. Equimolar doses of **13** (7.57 mg/kg), **20** (7.86 mg/kg) and **22** (7.83 mg/kg) were administered daily via IP injections to 2 month old APP/PS1 mice for either 1 month in the short term dosing group, or 5 months in a chronic administration group. Contextual fear memory was assessed by monitoring freezing behavior in response to an electrical shock 24 h after conditioning. Spatial-working memory evaluated in the radial arm water maze (RAWM) paradigm. All three inhibitors were beneficial against the loss of contextual fear memory and reference memory in both the short term (Figure 28 and Figure 29) and chronic dosing groups (Figure 30 and Figure 31). Additionally, there was no observed toxicity in WT littermates. Similarly, the inhibitors improved the performance of APP/PS1 mice with the 2-day RAWM task without affecting the performance of WT littermates.

Calpain is a key regulator of cytoskeleton dynamics, especially those in synapses; hence, our next goal was to determine *in vivo* efficacy of our inhibitors in murine AD animals. This kind of investigation offers insight on specific calpain inhibition within the brain. Calpain cleaves spectrin at a single location between Tyr1176 and Gly1177, creating two breakdown products with molecular weights of 150 and 145 kDa.(Roberts-Lewis and Siman 1993; Nedrełow, Cianci et al. 2003) Using western blot analysis, we measured prevention of calpain-generated spectrin fragments following IP treatment for 12 d with **13** (7.57 mg/kg), **20** (7.86 mg/kg) and **22** (7.83 mg/kg), (Figure 32). The histidine containing derivative, **13**, was slightly effective at decreasing amounts of calpain dependent spectrin cleavage, while the thiazole containing **20** and **22** dramatically reduced the amount of fragments. This clearly demonstrates that epoxy acid based peptidomimetics inhibit calpain activity in the brain.

Figure 28. Contextual fear memory following 30 d treatment to 2 month old APP/PS1 mice

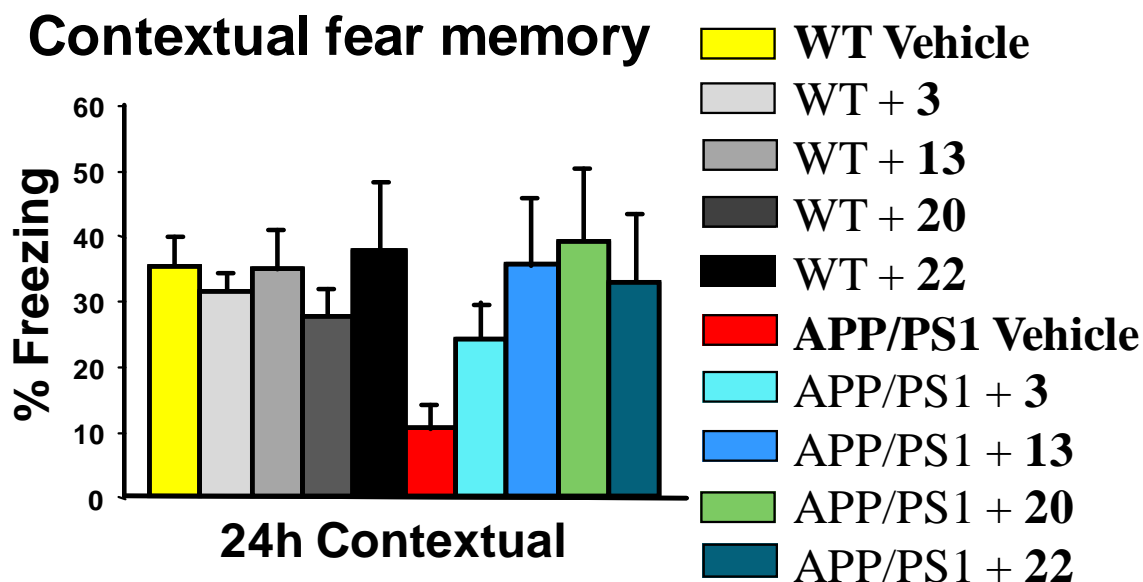


Fig. 28. Daily treatment with the appropriate calpain inhibitor (**3**, **13**, **20**, or **22**) from the age of 2 months until 3 months ameliorated the defect in contextual fear memory in APP/PS1 mice. Contextual fear memory was assessed by measuring latency period or “freezing behavior” following administration of electrical stimuli. All compounds were capable of reversing cognition defects in contextual fear memory in APP/PS1 mice.

APP/PS1-vehicle: n=15; APP/PS1-**3**: n=6; APP/PS1-**13**: n=10; WT-vehicle: n=15; WT-**3**: n=5; WT-**13**: n=8, APP/PS1-**20**: n=11; WT-**20**: n=8, APP/PS1-**22**: n=10; WT-**22**: n=8.

P<0.05 in all transgenic groups treated with compound compared to their respective vehicle-treated APP/PS1 mice.

Figure 29. Spatial-working memory following 30 d treatment to 2 month old APP/PS1 mice

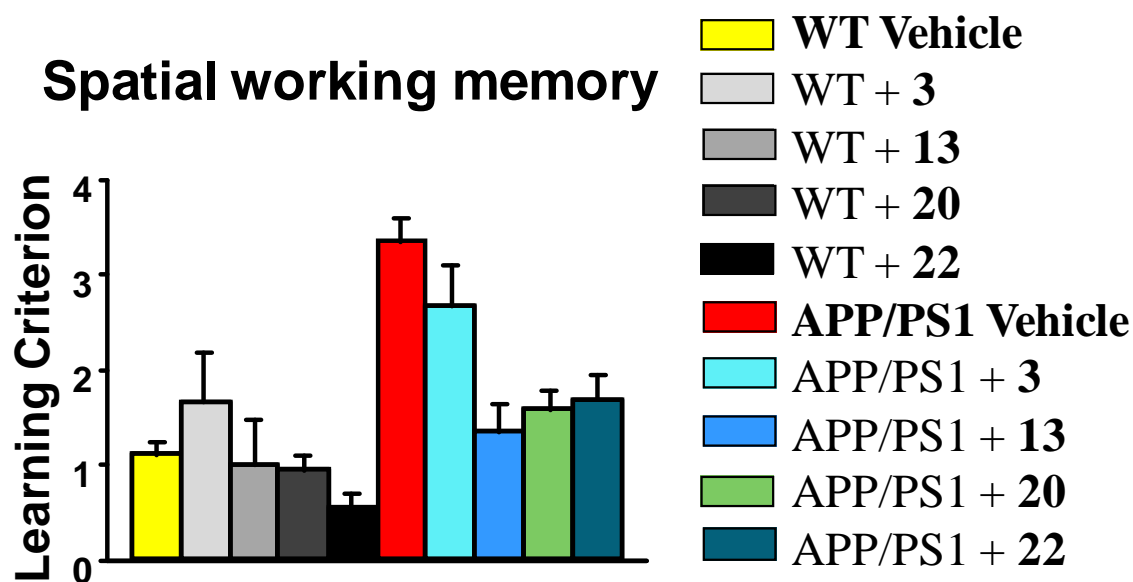


Fig. 29. Daily treatment with the appropriate calpain inhibitor (**3**, **13**, **20**, or **22**) from the age of 2 months until 3 months ameliorated the defect in contextual fear memory in APP/PS1 mice. Spatial-working memory was assessed using the radial arm water maze paradigm, and is represented number of errors made per experiment, or “learning criteria”. All compounds were capable of reversing cognition defects in spatial working memory in APP/PS1 mice. APP/PS1-vehicle: n=15; APP/PS1-**3**: n=6; APP/PS1-**13**: n=10; WT-vehicle: n=15; WT-**3**: n=5; WT-**13**: n=8, APP/PS1-**20**: n=11; WT-**20**: n=8, APP/PS1-**22**: n=10; WT-**22**: n=8. $P < 0.05$ in all transgenic groups treated with compound compared to their respective vehicle-treated APP/PS1 mice.

Figure 30. Contextual fear memory following 5 month treatment to APP/PS1 mice

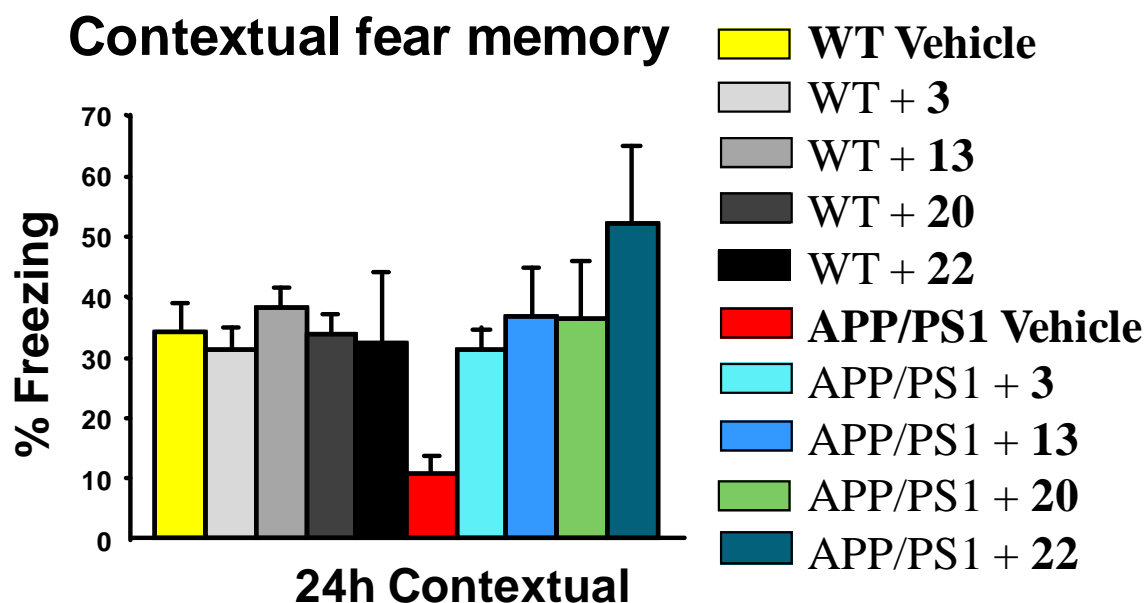


Fig. 30. Daily treatment with **3**, **13**, **20**, and **22** from the age of 2 months until 7 months ameliorated the defect in contextual fear memory (**A**) and reference memory (**B**) in APP/PS1 mice. APP/PS1-vehicle: n=17; APP/PS1-**3**: n=9; APP/PS1-**13**: n=10; WT-vehicle: n=18; WT-**3**: n=9; WT-**13**: n=9, APP/PS1-**20**: n=10; WT-**20**: n=9, APP/PS1-**22**: n=11; WT-**22**: n=9. $P < 0.05$ in all transgenic groups treated with compound compared to their respective vehicle-treated transgenics (except for **3** reference memory which was not significant).

Figure 31. Spatial-working memory following 5 month treatment to APP/PS1 mice

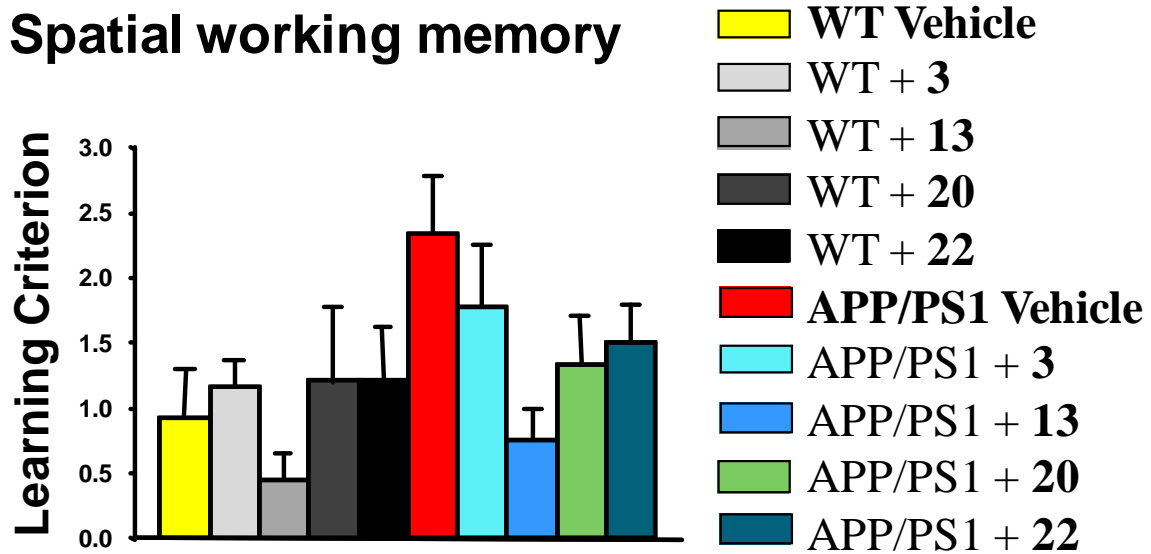


Fig. 31. Daily treatment with **3**, **13**, **20**, and **22** from the age of 2 months until 7 months ameliorated the defect in contextual fear memory (**A**) and reference memory (**B**) in APP/PS1 mice. APP/PS1-vehicle: n=17; APP/PS1-**3**: n=9; APP/PS1-**13**: n=10; WT-vehicle: n=18; WT-**3**: n=9; WT-**13**: n=9, APP/PS1-**20**: n=10; WT-**20**: n=9, APP/PS1-**22**: n=11; WT-**22**: n=9. $P < 0.05$ in all transgenic groups treated with compound compared to their respective vehicle-treated transgenics (except for **3** reference memory which was not significant).

Figure 32. Reduction in calpain dependent spectrin degradation products in the brain

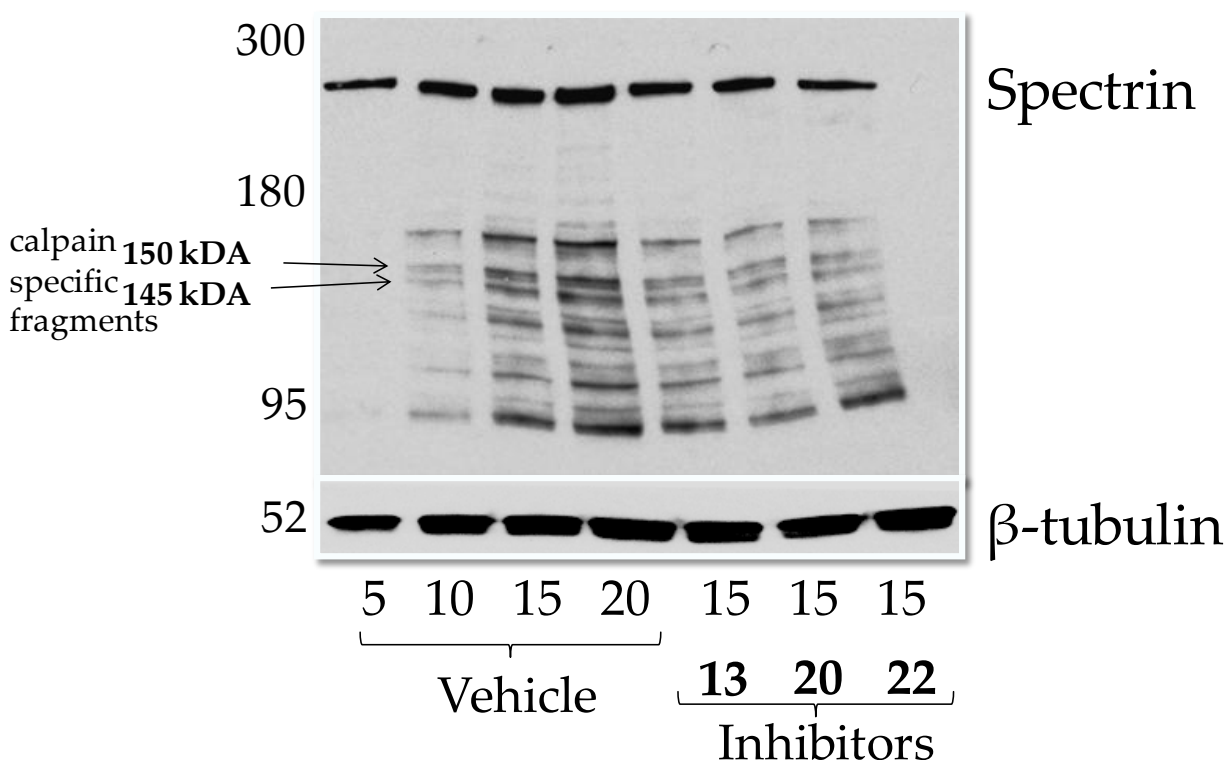


Fig.32. Western blot of spectrin proteolytic degradation products from brain homogenates of WT mice following IP treatment for 12 d with equimolar amounts of selected inhibitors: **13** (7.57 mg/kg), **20** (7.86 mg/kg) and **22** (7.83 mg/kg). Vehicle protein concentration array was generated by loading lanes with 5, 10, 15 and 20 μ g total protein. Samples from compound treated animals were loaded at 15 μ g/lane. Calpain cleaves spectrin to create two unique breakdown products with molecular weights of 150 and 145 kDa. The *L*-histidine containing derivative, **13**, was slightly effective at decreasing amounts of calpain dependent spectrin cleavage, while the thiazole containing **20** and **22** reduced the amount calpain specific cleavage fragments. This result clearly demonstrates that our epoxide peptidomimetics inhibit calpain activity in the brain.

2.5 Preliminary pharmacokinetics and toxicity assessment

To assess the PK profile, plasma concentrations of **13**, **20**, and **22** were determined by LC-MS/MS after IP administration to ICR mice (Figure 33) in the same quantities used in the *in vivo* behavioral assays [**13** (7.57 mg/kg), **20** (7.86 mg/kg) and **22** (7.83 mg/kg)]. The analysis of kinetics indicates that all three compounds **13**, **20**, and **22** are rapidly absorbed upon IP injection. The peak plasma concentration following IP administration occurred at 0.25, 0.5 and 0.125 h, respectively, the absolute bioavailabilities were 80.4 %, 87.3 % and 41.3 %, with $t_{1/2}$'s of ~0.6 h, ~1.1 h and ~0.6 h, respectively.

Initial information regarding toxicity can be gained from observations made in the behavioral assays described above using APP/PS1 mice and WT littermates. No apparent toxicity was observed at the therapeutic dose in WT littermates following short term and chronic administration in the behavioral assays. Subsequent evaluation yielded maximum tolerated doses of the three compounds being studied, and WT animals were treated with the respective MTD of each compound ([**13**, 100 mg/kg]; [**20**, 150 mg/kg]; **22**, 200 mg/kg]) for either short term or long term treatment. No compounds gave any apparent signs of toxicity in the form of lethality or malaise. Necropsy was performed on day 14, and examination criteria included weights and measurements of organs, appearance of organs (fat deposition, hemorrhage, pigment deposition or other changes, lesion, consistency), research of specific macrolesion occurrence such as abnormal growths, fibrosis, and necrosis. No gross organ abnormalities were observed for the short term or the chronically treated animal (Figure 34). In the case of **13**, some nephrotoxicity as evidenced by the clear appearance of isometrical vacuolization observed using hematoxylin/eosin staining of a kidney slice obtained from this treatment group. **20** and **22** treatment gave no such toxicity.

Figure 33. Plasma concentrations of calpain inhibitors following IP administration

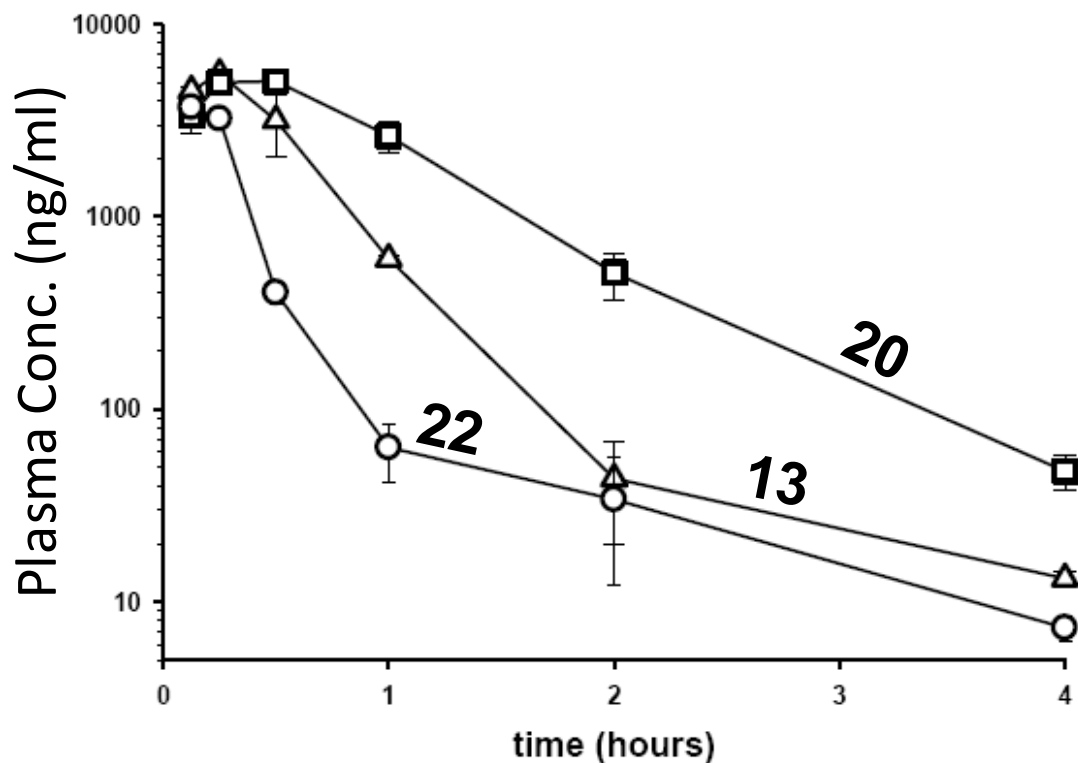


Fig.33. PK curve of plasma concentrations in ICR mice following IP injections of inhibitors in the same quantities used in the *in vivo* behavioral assays [**13** (7.57 mg/kg), **20** (7.86 mg/kg) and **22** (7.83 mg/kg)]. The peak plasma concentration following IP administration occurred at: **13**, 0.25 h; **20**, 0.5 h; and **22**, 0.125 h. The absolute bioavailabilities were: **13**, 80.4 %; **20**, 87.3 %; and **22**, 41.3 %, and the plasma half life's ($t_{1/2}$) were determined to be: 0.6 h for **13**; 1.1 h for **20**; and 0.6 h for **22**.

Figure 34. Photographic examination for signs of *in vivo* toxicity

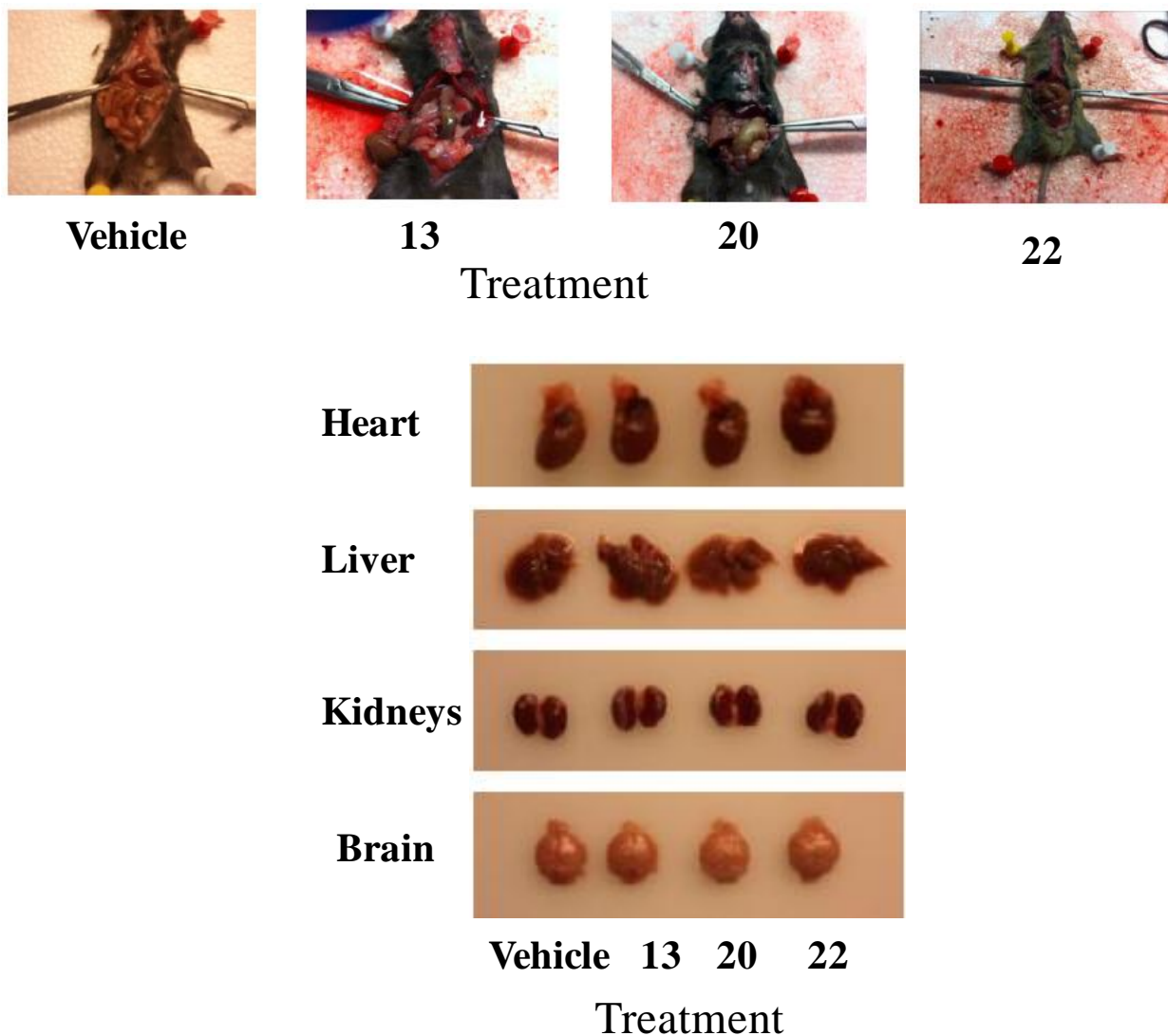


Fig.34. Top: Photographic validation of the conditions at necropsy following treatment with 15 d treatment of epoxide peptidomimetic calpain inhibitors at the respective MTD's (**13**, 100 mg/kg; **20**, 150 mg/kg, and **22**, 200 mg/kg). Bottom: Photographic evidence of no apparent gross organ abnormalities following daily treatment with the MTD of each compound for 15 d.

3. Discussion

3.1 *In Vitro* Assay Directed Drug Discovery

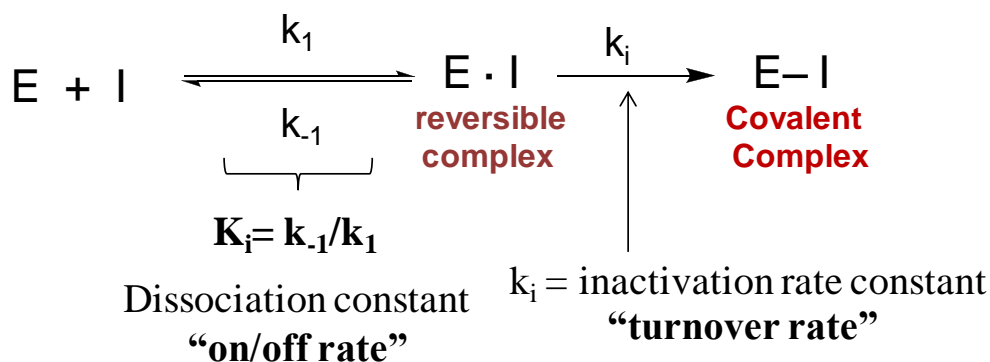
Full length Cal1 is superior to Cal1_{cat} as a means of comparing and contrasting calpain inhibitor potency. Our data certainly supports previous accounts of the significantly reduced proteolytic activity of Cal1_{cat} compared to full length Cal1. A large disparity was observed between the relative IC₅₀ values obtained using full length Cal1 and the amount of active site modification using Cal1_{cat}. Calpain catalytic activity involves a substrate induced conformational change which leads to thiophilic attack and proteolysis.(Moldoveanu, Hosfield et al. 2002) It is plausible that certain inhibitors could possess similar binding affinity for both the enzymes, while having differential capacity to induce conformation changes leading to active site modification. Although the Cal1 and Cal1_{cat} were isolated from separate mammalian species, *Homo sapien* vs *Rattus norvegicus*, we observed identical 29AA active site containing peptide fragments. X-ray structures support a common secondary structure for both Cal1 and Cal1_{cat}.(Moldoveanu, Campbell et al. 2004) The presence of supplementary domains in full length Cal1 makes substrate induced conformational changes more favorable than in its recombinant Cal1_{cat} counterpart. Hence, potent inhibitors are capable of eliciting covalent modification in Cal1, as demonstrated by the k_i values in TABLE VII. Conversely, only sufficiently tight binding inhibitors are capable of making it favorable for Cal1_{cat} to perform such changes leading to proteolytic turnover, as seen in our LC-MS results. This is further supported by comparison of inhibition rate constants of **E-64** and **20** versus Cal1 and Cal1_{cat} (TABLE VII, Figure 35). Regardless of the generally weaker activity of Cal1_{cat} compared to Cal1, the rate of inactivation (k_i) is considerably decreased (3-4 fold lower), while the K_i is less significantly impacted (~ 20 times lower). In the comparison of **E-64** and compound **20** with Cal1, the k_i/K_i

reveals approximately equipotent activity, in agreement with our initial FRET assay end point analysis. Examining the inhibition rate constants for Cal1_{cat} suggests that its inability to successfully mimic Cal1 is mostly due to relatively lower rate of inactivation. Our evidence seems to support this hypothesis, as several potent inhibitors were incapable of giving significant active site modification for Cal1_{cat}. The full length Cal1 isoform seems the most appropriate choice for trying to quantify potency of calpain inhibition.

Evaluating irreversible calpain inhibitors using end-point analysis gives little information to develop a QSAR of calpain inhibitors. Obtaining IC₅₀ values from end-point analysis of inhibition at vary concentrations of inhibitors provides a rudimentary way of determining the relative activity of irreversible inhibitors. As with all types of irreversible enzyme inhibitors, enzyme activity is highly dependent pre-incubation time and experimental methodology. This is especially significant in the case of Cal1, which shows varying degrees of autocatalytic activity, and is prone to aggregation during inhibition assay. Although Cal1_{cat} is devoid of this autocatalysis, its relatively weaker activity than full length Cal1 creates additional challenges with a significantly reduced signal to noise in the FRET assay. Ultimately, continuously monitoring calpain activity at varying concentrations of inhibitor is the ideal way to compare and contrast inhibitor potency (TABLE VII, Figure 35). This type of analysis was pursued for **E-64**, **5**, and **20** with Cal1 and papain, and resulted in calculation of inhibition rate constants. This method is somewhat time consuming and less desirable as a means of high-throughput compound screening. However, the ability to calculate 2nd order rate constants for inhibitors would give much insight into the relative impact of substituents on initial binding affinity and enzyme turnover rate. The preliminary IC₅₀ values from end-point analysis give no inference into

the relative binding affinity of inhibitor, and are essentially useless in developing a QSAR of binding prior to active site modification.

Figure 35. Determination of 2nd order rate constant k_i/K_i



Calculate K_i and k_i by: $1/k_{\text{obs}} = K_i/k_i [\text{I}] + 1/k_i$

TABLE VII

COMPARISON OF CAL1 AND CAL1CAT INHIBITION RATE CONSTANTS^a

	Full length human erythrocyte Cal1			Recombinant Cal1 _{cat}		
Compound	K_i	k_i	k_i/K_i	K_i	k_i	k_i/K_i
E64	4.0	0.12	3.0e^{+04}	21.5	6.6e^{-04}	30.6
20	2.6	0.08	3.0e^{+04}	82.2	5.1e^{-04}	6.2

^a Observed inhibition rate constants for selected inhibitors versus Cal1 and Cal1_{cat}. Inhibition rate constants were obtained by continuously monitoring FRET substrate turnover at varying concentrations of inhibitor. Inhibition curves were processed using linear regression in Graphpad Prism 5.0 software. Comparison of kinetic rate constants of Cal1 and Cal1_{cat} shows that while Cal1cat possess weaker activity than Cal1, the rate of inactivation (k_i) is significantly decreased (3 fold lower), while the K_i is only slight reduced (~ 20 times lower) in activity.

Recombinant rat Cal1_{cat} can be a valuable tool in the development of calpain inhibitors when used appropriately. As discussed above, the use of Cal1_{cat} to measure inhibitor potency is less desirable than full length Cal1, and end point analysis of inhibitory activity is certainly inappropriate. However, Cal1_{cat} does have certain advantages aside from its acknowledged feature of lacking autocatalytic activity. Our competition experiments involving incubation of inhibitors in the presence of Cal1_{cat} and CathB demonstrate perhaps an ideal application of Cal1_{cat}. In this assay, we rely on the similar specificity of Cal1_{cat} to Cal1 and its relative activity towards all inhibitors. Cal1_{cat} is unsuitable for end point analysis of calpain activity due to its inability to successfully mimic the k_i/K_i of the full length protein.

Proteomic methods may hold potential as a complementary approach to traditional enzyme inhibition assays. This approach is ideal in the pursuit of epoxide based calpain inhibitors due to: 1) the challenges presented in assaying an unstable and autocatalytic protein such as calpain; 2) the presence of a covalently modified protein after inhibition; and 3) the fortunate presence of an unmodified cysteine within the digest fragment containing the active site cysteine to allow quantification via alkylation with an internal standard. In this study, one-on-one competition assays were used to compare 1st generation compounds to the lead compound, however, the robustness of this assay was not completely utilized. Co-incubations using several inhibitors would result in the ability to screen dozens of inhibitors in a small period of time. The use of the full length protein is desirable, due to the apparent differences in inhibition rate constants and covalent modification of Cal1_{cat}. Our proteomic technique may allow for the screening of isoform selective calpain inhibitors using a competitive environment paradigm. Cal2 possesses a high degree of sequence similarity with Cal1, and it is plausible that tryptic digest of Cal2 may produce an active site fragment distinct from that of Cal1 digest. Therefore, competition assays

using equimolar amounts of Cal1 and Cal2 with inhibitors may hold the potential as a novel method for developing a Cal1/Cal2 selectivity profile without the use of expensive and time consuming inhibition kinetics studies. The significance of Cal1/Cal2 selectivity is poorly understood, and is likely to be exceedingly challenging considering the typical failures in gaining selectivity for calpains over other CA clan proteases (CathB, CathL). Nonetheless, Cal1 is the isoform localized at the synapse and is presumed to be primarily responsible for decreased CREB phosphorylation and synaptic dysfunction in AD.

3.2 SAR of Calpain Inhibitors

There are numerous examples of calpain inhibitors with IC_{50} 's in the low nM range in the literature, although few of these attempts have resulted in any reliable gain in selectivity. Notably, Donkor's group has provided a selectivity ratio for several inhibitors using inhibition rate constants to determine a cal1 vs cathB selectivity ratio. These works noted that some specificity can be acquired at the P2 position in the form of proline mimetic aldehyde and α -ketoamide incorporating inhibitors, and aggressively synthesized a larger number of compounds utilizing stereo-specific proline substituents.(Donkor, Korukonda et al. 2003)(Korukonda, Guan et al. 2006) Separately, the Davies group at Queens university speculated a hydrogen bond occurring within the S2 pocket formed between the cyano group a non-natural amino acid epoxide inhibitor and a water molecule(which is present in all calpain I-II crystal structures) at the periphery of the S2 pocket, and that new inhibitors might be designed to take advantage of this phenomena.(Cuerrier, Moldoveanu et al. 2007) Correspondingly, our results clearly demonstrate the utility of incorporating a properly placed H-bond acceptor at the P2 position, and support the hypothesis put forward by the Queens group. Previous failures in developing selectivity for calpain central around the desire to impart selectivity at the S4-S3 subsite. The

fortunate discovery of a high affinity P3 cap group allowed us to diversify the P2 position while maintaining a high degree of potency.

3.3 *In vivo* evaluation and potential in AD therapy

LTP in the hippocampus has been studied for over 20 years, and the requirement for LTP plays a distinct functional role in memory consolidation *in vivo* using murine models of learning and memory.(Morris, Anderson et al. 1986; McHugh, Blum et al. 1996) Restoration of LTP has been reported by various molecular agents, including: NO mimetics, PDE inhibitors, β -adrenergic receptor agonists, dopamine agonist, anti-estrogens, and calpain inhibitors.(Stramiello and Wagner ; Frey and Morris 1997; Lu, Kandel et al. 1999; Straube and Frey 2003; Trinchese, Fa et al. 2008; Puzzo, Staniszewski et al. 2009) Most of these agents facilitate increased phosphorylation of the memory related transcription factor, CREB, a required step in memory consolidation. All calpain inhibitors were capable of restoring LTP in hippocampi from APP/PS1 or WT hippocampi co-perfused with oligomeric A β . Correspondingly, all inhibitors tested *in vivo* were capable of reversing cognition deficits in APP/PS1 mice following short term and long term treatment regimens. While the short term treatment to 2 month old APP/PS1 mice serves as a model of mild cognition impairment, the long term treatment group serves as perhaps a better model of AD therapy encountered in the clinic. Early diagnosis of AD is difficult, and typical pharmacological intervention does not begin until the disease has progressed substantially. Our inhibitors have no impact on A β load following short term or long term administration to APP/PS1 mice (data not shown). Accordingly, the brains of 7 month old transgenic AD mice have significant A β load. The ability of our epoxide peptidomimetics to reverse cognition deficits under these circumstances is remarkable, and further supports calpain inhibition as a valuable target for future AD therapy.

The difficult diagnoses and delayed treatment schedule of AD suggests that recent approaches to modulate or inhibit β -/ γ -secretase may hold limited utility due to the presence of significant A β deposition prior to introducing therapy. Molecules capable of restoring synaptic function in the presence of significant A β deposition, such as our inhibitors, are an increasingly attractive alternative. Increased CREB phosphorylation results in amplified expression of BDNF, which nourishes neurons and promotes neurogenesis. Laferla's seminal work with neuronal stem cells clearly demonstrates the ability of BDNF to protect hippocampal neurons and halt neurodegeneration in the presence of pathological A β deposition without impacting levels of A β . (Blurton-Jones, Kitazawa et al. 2009; Morrisette, Parachikova et al. 2009) Calpain inhibition leading to increased CREB phosphorylation is proposed as being chiefly responsible for the procognitive effects of our inhibitors *in vivo*, and it is conceivable that a resulting increase in BDNF expression allows our inhibitors to maintain their cognition enhancing effects despite the high concentration of A β in 7 month old APP/PS1 transgenic mice. BDNF is involved in regulating calpain activity, as demonstrated by its participation in ERK mediated Cal2 activation at pathological $[Ca^{2+}]_i$. In addition to CREB signaling, calpain inhibitors may possess protective effects against neurodegeneration. As discussed earlier, calpain plays a key role in regulating skeletal dynamics, and calpain inhibition under pathological conditions leads to more efficient cytoskeletal remodeling and increased synaptic plasticity. Enhanced synaptic plasticity and regulated cytoskeletal dynamics could potentially explain the ability of our inhibitors to maintain cognition enhancing properties despite a large A β burden. It is plausible that the proposed neurotrophic effects of BDNF and modulated cytoskeletal dynamics are a collective feature of calpain inhibition, resulting in neuroprotection and cognition enhancement in the presence of pathological A β deposition. From a clinical point of view, the caveat to treating AD patients with cholinesterase inhibitors is that eventually the disease pathology results in substantial

neurodegeneration, to the point that relatively few neurons remain for cholinesterase inhibitors to carry out their therapeutic effect. Hence, molecules capable of restoring synaptic function while potentially protecting neurons from A β induced toxicity are promising prospects in drug discovery for AD.

Our epoxide based calpain inhibitors possessed fairly predictable PK parameters. **13**, **20** and **22** are rapidly absorbed upon IP injection. The peak plasma concentration following IP administration occurred at 0.25, 0.5 and 0.125 h, respectively, the absolute bioavailabilities were 80.4 %, 87.3 % and 41.3 %, with $t_{1/2}$'s of \sim 0.6 h, \sim 1.1 h and \sim 0.6 h, respectively. Although administration of the drugs gave in vivo behavioral effects and decreased levels of calpain dependent spectrin cleavage in the brain, the drugs themselves were not readily observed in the brain. This result has two possible explanations: 1) The molecules act peripherally, leading to calpain inhibition in the brain through some unrealized mechanism, 2) the inhibitors are covalently bound to proteins, and hence, they can not be measured by liquid-liquid extraction. The most apparent answer would involve protein bound transport of the inhibitors into the brain resulting in calpain inhibition by some undiscovered mechanism. The exact distribution and brain:plasma ratio of the inhibitors will be the focus of subsequent research efforts.

The epoxide peptidomimetics were well tolerated and produced no signs of lethality or malaise upon acute or chronic treatment. This outcome agrees with previous Phase I studies on **E-64d** that reported a good safety profile in human subjects. Following the initial Phase I study of **E-64d** single dose, the second Phase I study on **E-64d** monitored continuous administration in healthy adult male volunteers to investigate its safety and pharmacokinetics. In the first stage, 100 mg was administered 3 times a day after meals for 1 day, and in the next stage, 100 mg was administered 3 times a day after meals for 7 consecutive days. No change due to **E-64d** was found from the observation of the subjective and objective symptoms and clinical tests. **E-64d**

was detected as **E-64c** (the proposed effective form of **E-64d**) in serum and urine after oral administration. No accumulation of **E-64d** was observed after continuous administration, and approximately 30% of total **E-64d** was collected in urine. The differences in bioavailability, distribution, and metabolism between humans and mice make any in depth correlation difficult, but the general lack of toxicity in for our compounds, and the record of tolerability in **E-64d** are promising outcomes.

4. Summary

The design, synthesis and inhibitory activity of novel epoxide calpain inhibitors resulted in molecules with increased potency, selectivity, and improved bioavailability properties compared to the lead compound, **E-64**. A novel high affinity P3 cap group was realized, in the form of a 4-F-phenyl-thiazole by adapting proteomic techniques into the lead optimization platform. The hypothesis that selectivity may be attained by incorporating a properly positioned H-bond acceptor at the P2 position was supported by imidazole and thiazole containing analogs, which displayed greater selectivity for calpain than did the corresponding isopropyl containing inhibitors. A 3rd generation was designed using *in silico* screening to increase molecular diversity and potency while maintaining the selectivity gained by the P2 position of 2nd generation analogs. Selected calpain inhibitors are evaluated for *in vivo* efficacy and safety in the subsequent chapter.

All epoxide peptidomimetics selected from lead optimization were capable of restoring LTP after co-perfusion with oligomeric A β , suggesting their ability to inhibit calpain leading to increased CREB phosphorylation and synaptic plasticity. The inhibitors were also capable of reversing cognition deficits in behavioral models of spatial working memory and contextual fear memory following short and long term treatment, suggesting possible utility in situations of

moderate and severe disease progression. All inhibitors gave similar results *in vivo*, hence, **20** has emerged as the most promising preclinical candidate based on calpain selectivity, synthetic accessibility, and physiochemical properties. Ultimately, the limited preliminary PK data involving i.p. administration leaves unanswered questions regarding the potential oral drugability of these molecules, as well as their distribution and brain bioavailability profile. At this point, formulation considerations should be a primary consideration of future studies prior to the carrying out a complete PD/PK profile.

Compound **20** is a novel epoxide incorporating peptidomimetic with the capability of reversing reductions in synaptic plasticity and memory in a murine transgenic model of AD regardless of the severity of the plaque load. The synthesis of **20** is reasonably accessible, and its negligible toxicity and predictable PK characteristics contribute to its appeal. Safety is the number one concern in preclinical compound development, and **20** displayed no apparent signs of toxicity with a therapeutic index > 20. Recommendations for future studies include further validating the mechanism of action and addressing questions regarding the oral bioavailability of epoxyacid incorporating peptidomimetics.

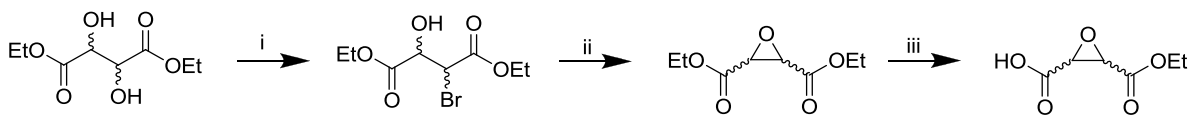
5. Materials and Methods

All chemicals and reagents were purchased from Sigma-Aldrich (St. Louis, MO), TCI America, or Fisher scientific and used as received unless stated otherwise. *Ex vivo* and *in vivo* measurement of cognition enhancement were carried out by collaborators at Columbia University (Dr. Mauro Fa`, Hong Zhang, Agnieszka Staniszewski, under the supervision of the project principal investigator, Dr. Ottavio Arancio). Protocols and methods are briefly described below, and have been amended from versions supplied by collaborators.

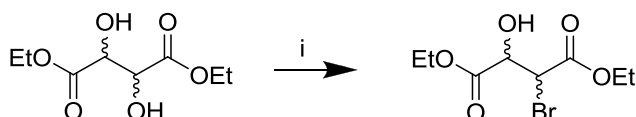
5.1 Synthesis

All synthesized compounds were fully characterized by ^1H NMR, and ^{13}C NMR. The structures of all novel final compounds were supported using in house HRMS. All compounds submitted for biological testing were confirmed to be > 95 % pure by preparative HPLC. Full synthetic, and in *In vivo* evaluation, particularly for determining maximum tolerated dose, required the synthesis of compound on a gram-scale. Synthetic approach and general reaction procedures are outlined and briefly described below. Consult Appendix A for full experimental details.

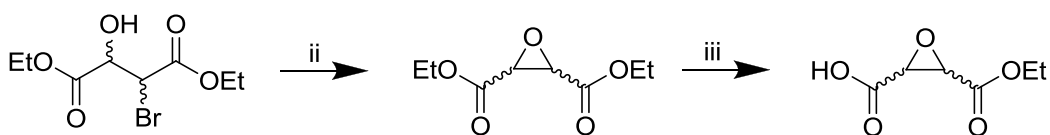
Scheme 4. Stereo-specific synthesis of the epoxide monoester



i) HBr (33 %) in acetic acid, r.t, 12 h, then acetyl chloride, reflux, 12 h, 75-80 %; ii) DBU, Et₂O, 0 °C, 12 h, 70-80 %; iii) ethanolic KOH, 0 °C, 6 h, 75-85 %.

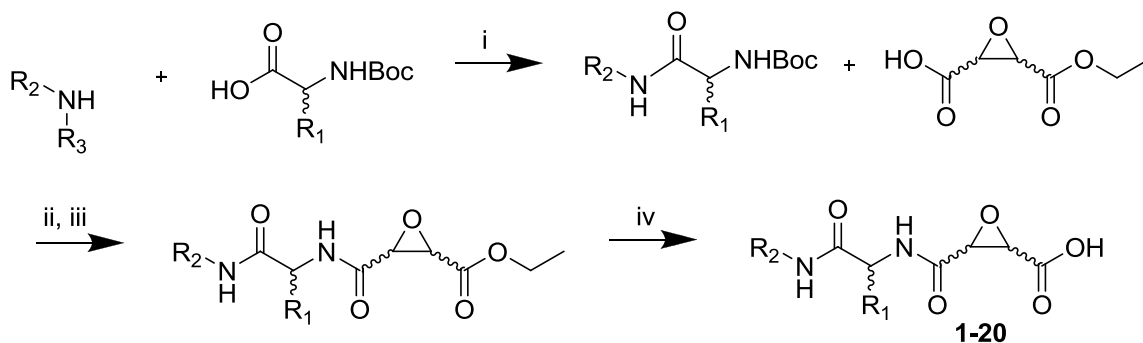


The epoxide warhead was synthesized from either *D*-DET or *L*-DET in three steps to give the stereospecific synthesis of the *S,S* and *R,R*, respectively. (Seiki Saito 1996) The initial reaction step follows the synthesis of stereospecific epoxides via vicinal bromohydrins from vicinal diols described previously, involving monoacetylation of the diol, cyclization to a 1,3-dioxolan-2-ylum ion, and capture of this intermediate by bromide ion to yield the epoxide mono-acids after work-up and distillation. (Golding, Hall et al. 1973; Schmidt, Talbiersky et al. 1980)

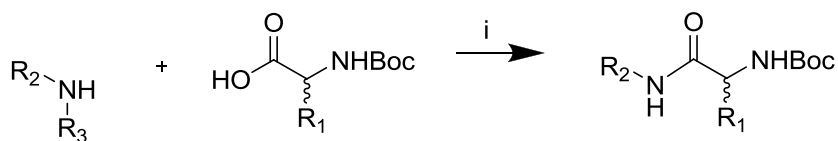


Ring closure with the non-nucleophilic base, DBU, at 0 °C affords the epoxide diethylester, Mono-saponification of the epoxide diethyl ester using one equivalent of ethanolic KOH at 0 °C yields the epoxide monoacid in high yield (~80 %).

Scheme 5. Peptide coupling and hydrolysis reactions to afford the desired peptidomimetics



i) EDCI, HOBT, DMF, 0 °C, 25-75 %; ii) TFA, CH₂Cl₂, 0 °C; then iii) EDCI, HOBT, DIPEA, DMF, 0 °C, 25-75 %; iv) LiOH, THF/MeOH/H₂O, 0 °C, 30-85 %.

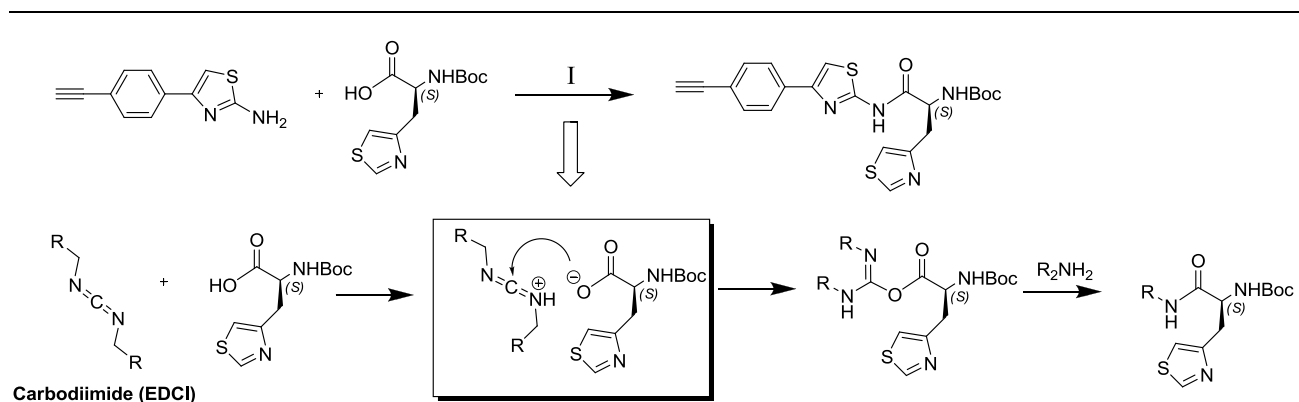


i) EDCI, HOBT, DMF, 0 °C, 25-75 %

Generalized peptide coupling procedures dictate activation Boc-protected amino acids using CDI or EDCI, in a polar aprotic solvent, DMF or CH₂Cl₂, followed by addition of the appropriate amine in the presence of a tertiary base, DIPEA or TEA, to yield the peptidomimetic scaffolds. Utilization of HOBT is necessary, as *L*-histidine incorporating peptidomimetics racemize upon coupling with the corresponding aryl-amines to give an enantiomeric mixture, which is easily diagnosed following conversion to a diastereomeric mixture upon coupling to the stereospecific epoxy-acid.

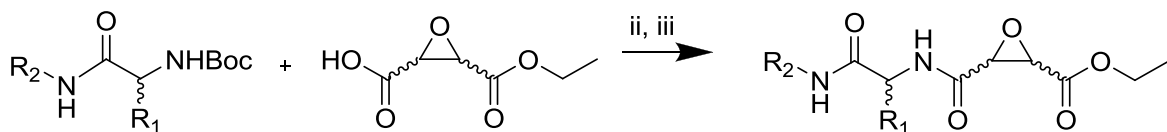
Optimal conditions for the preliminary coupling in Scheme 5 involved activation of the R₂-carboxylic acid in DMF with EDCI and HOBT at 0 °C; followed by the addition the free R₃-amine. The conventional use of a tertiary base was noticed to significantly decrease reaction yields. In the case of one analog, reactions carried out in the absence of a tertiary base gave significantly higher yields (TABLE VIII). Given the mechanism involved in activation by EDCI, we hypothesize the presence of a base limits the ability of the acid to form an ion pair with the activating carbodiimide, resulting in decreased formation of the key O-acylisourea intermediate.

TABLE VIII
EFFECT OF DIPEA ON INITIAL PEPTIDE COUPLING REACTION ^a



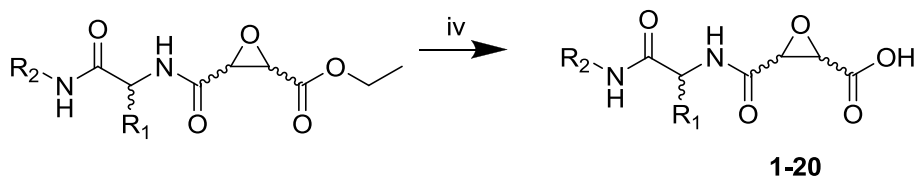
Reaction	EDCI	HOBT	DIPEA	Isolated Yield ^b
I-a	1.1 eq	1.1 eq	2.5 eq	28 %
I-b	1.1 eq	1.1 eq	1.1 eq	30 %
I-c	1.1 eq	1.1 eq	-	79 %

^a Hypothesized explanation of observed increase in yield in the absence of base. Carboxylate activation performed in minimal DMF at 0 °C. ^b Isolated yield based on quantity obtained following flash chromatography.



ii) TFA, CH₂Cl₂, 0 °C; then iii) EDCI, HOBT, DIPEA, DMF, 0 °C, 25-75 %;

The Boc-protected peptidomimetic scaffold was deprotected with TFA. Then standard coupling procedures were used employing EDCI and HOBT in the presence of the appropriate epoxyacid. Contrary to the initial peptide coupling, the most favorable conditions for coupling the epoxide require the vigilant addition of only one equivalent of base, with no product formed in the absence of DIPEA (TABLE IX).



iv) LiOH, THF/MeOH/H₂O, 0 °C, 30-85 %.

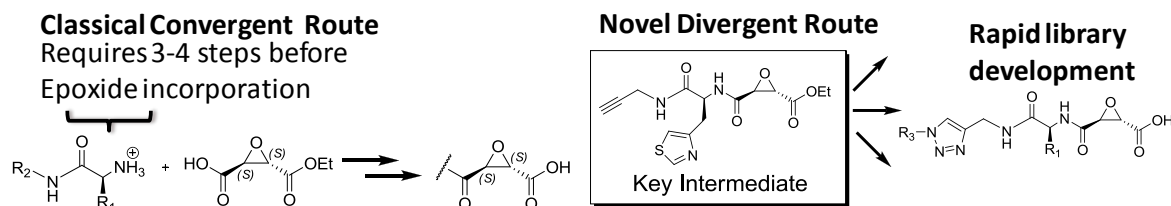
Based catalyzed saponification with LiOH at 0 °C afforded the desired peptidomimetic epoxides.

TABLE IX
EFFECT OF DIPEA ON INITIAL PEPTIDE COUPLING^a

Reaction	EDCI	HOBT	DIPEA	Isolated Yield ^b
II-a	1.1 eq	1.1 eq	2.5 eq	28 %
II-b	1.1 eq	1.1 eq	1.0 eq	52 %
II-c	1.1 eq	1.1 eq	-	No reaction

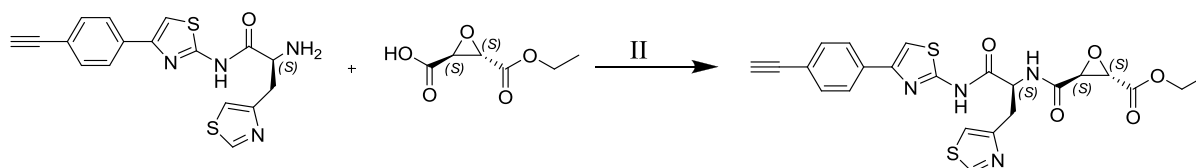
^a Carboxylate activation performed in minimal DMF at 0 °C. ^b Isolated yield based on quantity obtained following flash chromatography.

Scheme 6. Divergent synthetic route utilizing click chemistry



A major limitation to the synthesis of epoxide based inhibitors is the perceived tendency of the epoxide warhead to undergo nucleophilic attack. Hence, convergent synthesis is utilized and the epoxide is incorporated in the final synthetic step.

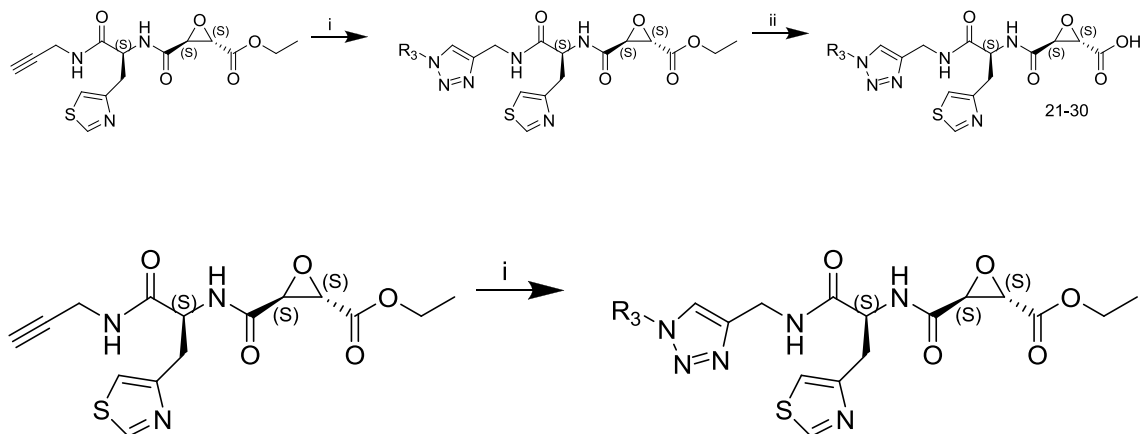
TABLE X
EFFECT OF DIPEA ON EPOXIDE ESTER COUPLING REACTION ^a



Reaction	EDCI	HOBt	DIPEA	Isolated Yield ^b
II-a	1.1eq	1.1 eq	2.5 eq	28 %
II-b	1.1 eq	1.1 eq	1.0 eq	52 %
II-c	1.1 eq	1.1 eq	-	No reaction

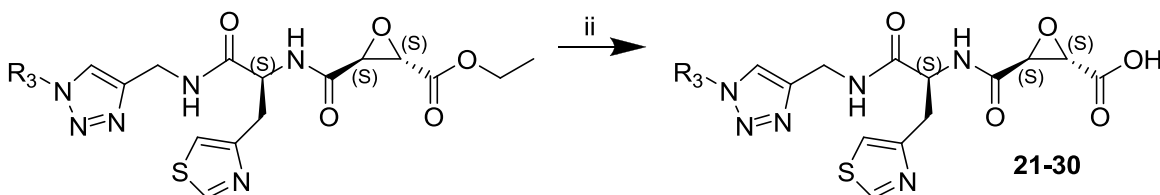
^a Carboxylate activation performed in minimal DMF at 0 °C. ^b Isolated yield based on quantity obtained following flash chromatography.

Scheme 7. Novel synthesis of the triazole incorporating epoxide peptidomimetics



i) R_3-N_3 , $CuSO_4$, NaAsc, TBTA, $H_2O/t-BuOH/EtOH$ (2:1:1), r.t., 12 h, 90-100 %.

The key alkynyl intermediate was functionalized with varying aryl-azides using a Cu [II] catalyzed Huisgen addition, with the aid of TBTA to give the corresponding triazole-aryl incorporating epoxide in nearly quantitative yield. Due to the large disparity in solubility properties of the products compared to the starting reagents, in some instance, the triazole incorporating epoxide esters precipitate out of solution upon creation, allowing simple filtration purification.



ii) LiOH, THF/MeOH/ H_2O , $0^\circ C$, 95-100 %.

Subsequent ester hydrolysis afforded the corresponding carboxylic acids (**21-30**).

TABLE XI
STRUCTURE DESIGNATIONS OF SCHEME 5 ANALOGS

Entry	R1	R2	Stereo
1	L-Leucine	D-Biotin-NH-(CH ₂) ₄ -NH ₂	<i>S,S,S</i>
2	L-Leucine	4-F-Phenyl-SO ₂ -NH-(CH ₂) ₄ -NH ₂	<i>S,S,S</i>
3	L-Leucine	Lipoyl-NH-(CH ₂) ₄ -NH ₂	<i>S,S,S</i>
5	L-Leucine	4-(4-Fluorophenyl)thiazol-2-amine	<i>S,S,S</i>
6	L-Leucine	4-(4-Fluorophenyl)thiazol-2-amine	<i>S,R,R</i>
7	L-Leucine	2,6 difluorophenyl	<i>S,S,S</i>
8	L-Leucine	2,6 difluorophenyl	<i>S,R,R</i>
9	L-Leucine	Phenyl	<i>S,S,S</i>
11	L-Histidine	Phenyl	<i>S,S,S</i>
12	L-Histidine	1,3,5 trimethylaniline	<i>S,S,S</i>
13	L-Histidine	4-(4-Fluorophenyl)thiazol-2-amine	<i>S/R,S, S</i>
14	L-Histidine	4-(4-Fluorophenyl)thiazol-2-amine	<i>S/R,R, R</i>
15	L-Histidine	6-fluorobenzo[d]thiazol-2-amine	<i>S/R,S, S</i>
16	L-Histidine	6-fluorobenzo[d]thiazol-2-amine	<i>S/R,R, R</i>
17	L-His(2-Me)-OH	4-(4-Fluorophenyl)thiazol-2-amine	<i>S,S,S</i>
18	L-His(4-Me)-OH	4-(4-Fluorophenyl)thiazol-2-amine	<i>S,S,S</i>
19	L-Ala(4-thiazoyl)-OH	Phenyl	<i>S,S,S</i>
20	L-Ala(4-thiazoyl)-OH	4-(4-Fluorophenyl)thiazol-2-amine	<i>S,S,S</i>

TABLE XII
STRUCTURE DESIGNATIONS OF SCHEME 7 ANALOGS

Compound	R3
21	Phenyl
22	4-fluorophenyl
23	4-phenylsulfonylpiperidine
24	1,3-methylenedioxyphenyl
25	4-phenylsulfonylamide
26	3,5-trifluoromethylphenyl
27	4-bromophenyl
28	4-nitrophenyl
29	2,6 fluorophenyl
30	1,3,5 trimethylphenyl

5.2 FRET assay of calpain inhibition

The Calbiochem InnoZyme activity kit is used for measuring the inhibition effect inhibitors on human erythrocyte calpain 1 activity. A calpain FRET substrate, (DABCYL)-TPLKSPPPSPR-(EDANS), was used to detect the activity of Cal1. 20 μ M of the FRET substrate, 10 nM of native Cal1, and 20 μ M TCEP (reducing agent) were added to the reaction mixture containing assay buffer (Tris (10 mM), NaCl (100 mM), pH 7.4). Cal1 was activated by the addition of 10 μ M calcium. Cleavage of the scissile bond amide bond, K-S, releases the fluorophore (EDANS) from the internal quenching molecule (DABCYL), resulting in an increase in fluorescence measured at 320 nm excitation and 480 nm emission wave lengths for

30 min. Each inhibitor (10 nM, 100 nM, 1 μ M, and 10 μ M) was added to the reaction mixture to detect inhibition of Cal1 and reduction in fluorescence was measured by 96 well-plate reader. Approximate IC₅₀ values of each compound were generated using linear regression within graphpad prism software.

5.3 LC-MS/MS approach

The Cal1_{cat} (5 μ M) was incubated with E64 (5 μ M) for 20 min. The reaction was quenched with EDTA (10 μ M) and reaction mixture ran on a SDS phage gel. The Cal1_{cat} containing band was cut from the gel and submitted to in-gel alkylation with IAA (~100 mM) for 60 min, and subsequent tryptic digest. LC-MS/MS was then analyzed for TIC and EIC of anticipated modified peptide fragments.

5.4 Calpain vs cathepsin B: preference assay

The appropriate inhibitor (5uM) was pre-incubated in a mixture containing Cal1_{cat} (2 μ M), CathB (2 μ M), TCEP (1 mM), and Ca²⁺ (30 μ M) for 10 min at 37 °C. BiEP (5 μ M) was then added and the mixture incubated an additional 10 min. The reaction was quenched with EDTA (10 μ M) and samples were ran using 4-16% SDS PAGE gel, subsequently transferred to PVDF membrane and visualized by Pierce ECL (Enhanced chemiluminescent)western blotting substrate. Intensity of each blot was calculated using densitometry software. Relative inhibition of each enzyme was calculated with respect to without inhibitor of that enzyme. Inhibitor preference to Calpain with respect to Cathepsin B, was calculated by dividing relative calpain inhibition with relative Cathepsin B inhibition of that particular inhibitor.

5.5 LTP

Hippocampal slices from 2 month old APP/PS1 mice or wild type mice were maintained in an interface chamber at 29 °C for 90 min prior to recording. Slices were perfused with saline solution (124.0 mM NaCl, 4.4 mM KCl, 1.0 mM Na₂HPO₄, 25.0 mM NaHCO₃, 2.0 mM CaCl₂, 2.0 mM MgSO₄, and 10 mM glucose) continuously bubbled with 95% O₂ and 5% CO₂. The fEPSPs were recorded from the CA1 region of the hippocampus by placement of both the stimulating and the recording electrodes in the CA1 stratum radiatum. LTP was recorded following a 15 min baseline in which individual fEPSP were recorded every min at an intensity that evokes a response ~35 % of the maximum evoked response. Calpain inhibitors (1 μM) with or without oligomeric Aβ (650 nM [the calculated ED₅₀ of E-64 in LTP) were perfused for 20 min prior to LTP induction.

5.6 Calpain dependent spectrin cleavage in brain homogenates

Calpain dependent spectrin cleavage results in the formation of a specific 150 kDa and 145 kDa proteolytic degradation product. Wild type mice were treated with equimolar amounts of **13** (7.57 mg/kg), **20** (7.86 mg/kg) and **22** (7.83 mg/kg) via IP injection every day for 12 d. The mice were then sacrificed and brain homogenates analyzed for spectrin proteolytic degradation by western blotting.

5.7 Cognition Enhancement

Contextual fear memory and the 2-day RAWM test were carried out to assess *in vivo* efficacy in APP/PS1 mice and WT littermates. Mice were treated daily (i.p) with equimolar amounts of **13** (7.57 mg/kg), **20** (7.86 mg/kg) and **22** (7.83 mg/kg) to 2 month old APP/PS1 mice for 30 d in

a short term treatment group, and from 2 months until 7 months of age in the chronic treatment group.

5.8 Pharmacokinetics

13, **20**, and **22** were submitted to a CRO for PK studies. WT mice were treated with equimolar amounts of **13** (7.57 mg/kg), **20** (7.86 mg/kg), and **22** (7.83 mg/kg), and plasma concentrations measured at 15 min, 30 min, 1 h, 2 h, & 4 h.

5.9 Acute Toxicity

Maximum tolerated dose (MTD) was computed as the maximum administered dose that did not produce any toxic effect in terms of malaise or death. Toxicity was assessed by monitoring changes in food/liquid intake, weight change, locomotion, exploratory behavior, and mortality during the first 24 h with continuous monitoring for the first 4 h, and for 14 d after the compounds administration. Necropsy was performed on day 14, and examination criteria included weights and measurements of organs, appearance of organs (fat deposition, hemorrhage, pigment deposition or other changes, lesion, consistency), research of specific macrolesion occurrence such as abnormal growths, fibrosis, necrosis.

5.10 Chronic Toxicity

WT animals were treated with the respective MTD daily for 15 d for each drug or vehicle. Body weight, fluid/food intake, and sign of behavioral distress were continuously monitored over the course of the treatment. At the end of the chronic treatment, animals were sacrificed and necropsy was carried out. Necropsy was performed on day 14, and examination criteria included weights and measurements of organs, appearance of organs (fat deposition, hemorrhage, pigment

deposition or other changes, lesion, consistency), research of specific macrolesion occurrence such as abnormal growths, fibrosis, necrosis.

CHAPTER 2. EPOXIDE PRODRUGS: DISCOVERY OF AN UNREPORTED MECHANISM OF PRODRUG BREAKDOWN

1. Introduction

The most common prodrug moiety in marketed drugs is esterified carboxylate groups.(Beaumont, Webster et al. 2003) Typical ester prodrugs include simple aliphatic groups (ie. methyl, ethyl), as well as bulky constituents (*t*-butyl, *i*-propyl) to discourage ester hydrolysis and metabolism via steric hindrance. Simple ethyl ester prodrugs have also been employed in multiple clinically utilized therapeutics (ie. Oseltamivir (Tamiflu[®]), Imidapril, Spirapril, etc.).(Song and White 2002) Generally, ethyl ester moieties are sufficient stable to act as an efficient prodrug approach for masking carboxylic acids. In fact, ACE inhibitor prodrug ethyl esters tend to be stable to hydrolysis in human blood and require the action of hepatic or intestinal esterases to liberate the daughter drug entity.(Jurima-Romet, Huang et al. 1991; Sun, Cipriano et al. 1994)

E-64c, an isoamyl amine containing **E-64** analog, demonstrated potent non-selective cysteine protease inhibition *in vitro*, and the capacity to improve righting ability upon IP injection to dystrophic chickens. **E-64c** also impeded the progression of necrotic changes in muscular dystrophic hamsters following administration with an osmotic minipump.(Hudecki, Pollina et al. 1981)(Jasmin and Proschek 1984) Unfortunately, **E-64c** possessed negligible *in vivo* effects when administered orally, presumably due to low absorbability through the intestine. **E-64d**, the ethyl ester prodrug of **E-64c**, was shown to have poor *in vitro* protease inhibition, but good *in vivo* activity (Figure 36). **E-64d** was proposed to rapidly hydrolyze *in vivo* to **E-64c** (< 5 min), which then presumably carries out cysteine protease inhibition.(M. Tamai 1986)

Figure 36. Prodrug ester approach for epoxysuccinate containing peptidomimetics

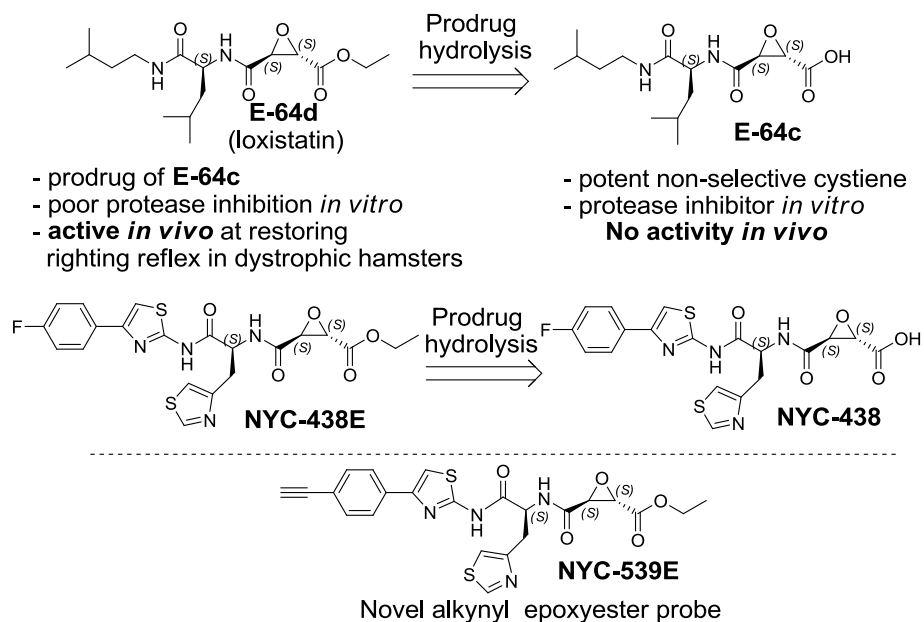


Fig.36. Ethyl ester prodrugs have been used for epoxysuccinate containing protease inhibitors in the past. **E-64c** was found to be a potent cysteine protease inhibitor *in vitro*, but gave negligible protease inhibition *in vivo*. The ethyl ester prodrug of **E-64c**, designated **E-64d** (later named loxistatin), was active *in vivo* at restoring righting reflex in dystrophic hamsters after administration oral administration. Our novel calpain inhibitor, **NYC-438** (designated compound **20** in chapter 1), was found to be capable of restoring cognition deficits in behavioral experiments following short term and long term IP administration to APP/PS1 transgenic AD mice. The epoxysuccinate functionality of **NYC-438** will likely hinder GI absorbability upon oral administration. Hence, **NYC-438E**, the prodrug ethyl ester of **NYC-438** was created. The novel alkynyl epoxide **NYC-539E** was designed for target validation *in vivo*, and was examined for stability alongside **NYC-438E**.

The development of epoxide peptidomimetic calpain inhibitors in our lab has led to the identification of **NYC-438** (designated compound **20** in Chapter 1) as possessing several desirable properties for further drug development: 1) ability to decrease levels of calpain dependent spectrin cleavage following *in vivo* administration; 2) capacity to reverse cognition deficits in behavioral assays using APP/PS1 mice following short or long term treatment; 3) the ability to restore synaptic plasticity in hippocampal slices co-perfused with oligomeric A β ; and 4) a MTD = 150 mg/kg with negligible toxicity and no gross organ abnormalities upon chronic treatment. These promising *in vivo* effects were observed following IP administration, and it is foreseeable that **NYC-438** could potentially possess the same oral bioavailability problems encountered in the case of **E-64c**.

In an effort to address the perceived oral bioavailability problems of **NYC-438**, an ethyl ester prodrug was created, **NYC-438E**. Preliminary evaluation of **NYC-438E** stability and reactivity are discussed below. Reactivity analysis with glutathione (GSH) led to the discovery of an unanticipated reaction profile, and follow-up studies examining **E-64d** showed a similar unreported prodrug breakdown pathway. The discovery of an overlooked reaction profile of epoxide ethyl esters creates challenges in prodrug development of **NYC-438** and questions regarding the mechanism of action and biological targets of the clinical candidate **E-64d**.

2. Results

2.1 Prodrug Aqueous Stability

A synthetic precursor of the promising preclinical candidate **NYC-438** is an ethyl ester, **NYC-438E**, which directly emulates the approach previously used with **E-64c**. **NYC-438E** is a synthetic precursor of **NYC-438**, which adds to its appeal for use in preliminary prodrug stability

studies. The aqueous stability of **NYC-438E** and **NYC-438** was studied at a range of biologically relevant pH's. Incubation of **NYC-438E** (5 μ M) in phosphate buffer (PB) (50 mM, varying pH[6.4, 7.4, 8.4]) showed evident signs of base catalyzed hydrolysis of the prodrug to give the intact drug entity **NYC-438** (Figure 37), with an apparent $t_{1/2} \sim 7$ h in PBS (pH 7.4) at 25 °C. Follow-up studies with **E-64d** and **NYC-438** employing a temperature controlled HPLC gave $t_{1/2}$'s from 2-4 h at 37 °C in PB at pH 7.4 (Figure 38, Figure 39).

The observed rate of prodrug hydrolysis is in agreement with literature reports on the stability of ethyl esters. Simple alkyl esters, particularly ethyl esters, are generally stable over the pH range of approximately pH 4 to pH 8.(Bundgaard and Larsen 1980; Nielsen and Bundgaard 1987) In accordance with the chemical stability of simple alkyl esters, in some cases the *in vivo* bioconversion rate is sufficiently slow that the primary prodrug breakdown mechanism is esterase mediated. Indeed, in the case of penicillin class of antibiotics, simple alkyl and aryl esters are not hydrolyzed *in vivo*, and required the introduction of double esters to increase the conversion rate.(Bundgaard and Hansen 1981) The observed rate of ester hydrolysis suggests that ethyl esters may be suitable as prodrug candidates for epoxide acids. However, as we will see, an unanticipated competing mechanism of epoxide ester reactivity in the presence of biological thiols produces an undesirable prodrug reactivity profile.

Figure 37. Effect of pH on prodrug ester saponification in PB (50 mM) at 25 °C

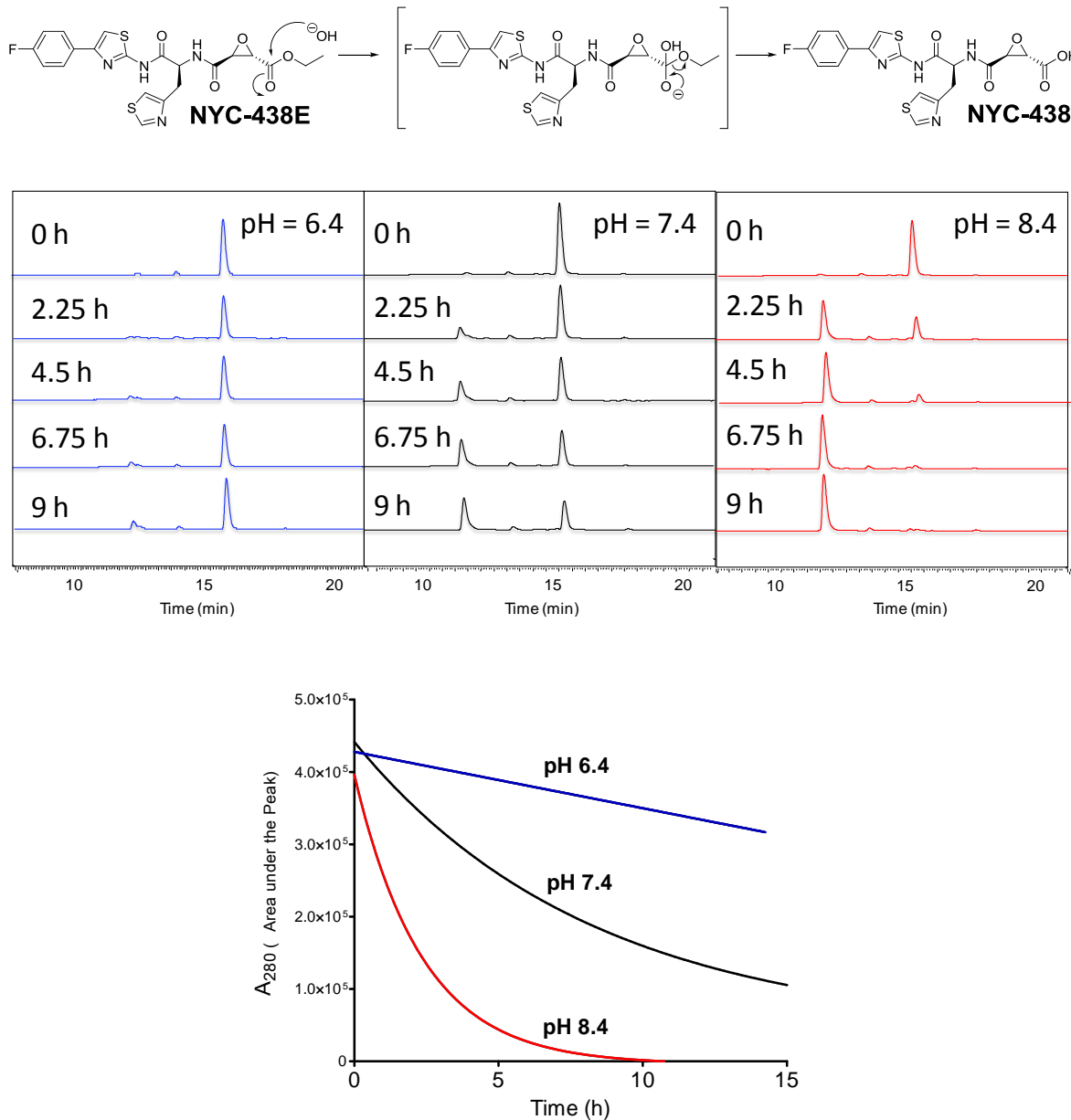


Fig.37. Top: Mechanism of base catalyzed ester saponification. Middle: HPLC chromatograms of **NYC-438E** (25 μM) in PB (50 mM, at varying pH [6.4, 7.4, or 8.4]) at 25 °C, analyzed by HPLC-UV at regular intervals. Bottom: a one phase exponential decay curve was generated based upon percent starting material remaining according to integration of the starting material signal peak area ($\lambda = 280 \text{ nm}$).

Figure 38. NYC-438E ester saponification in phosphate buffer (50 mM, pH 7.4) at 37 °C

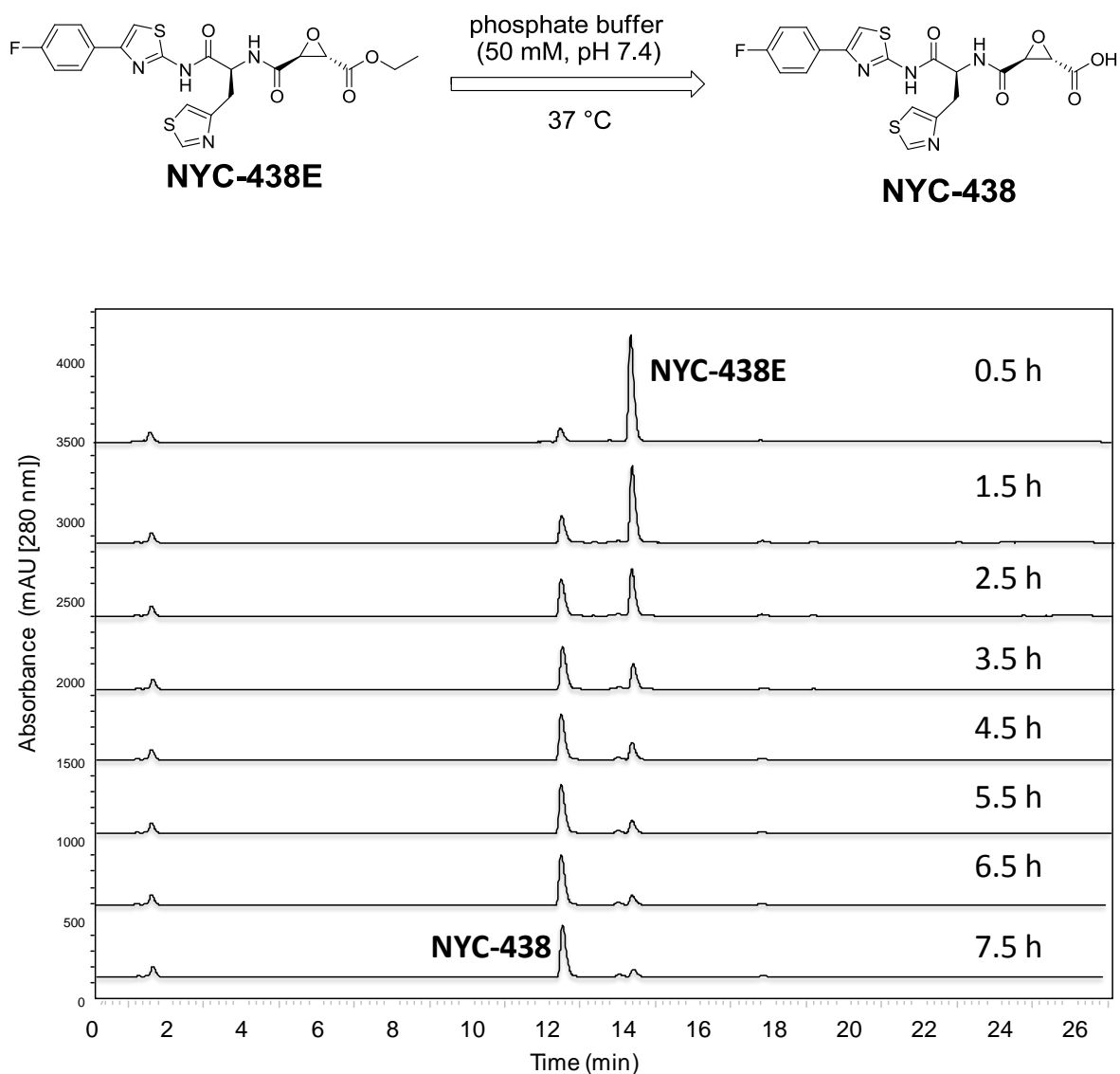


Fig.38. NYC-438E (25 μ M) was dissolved in PB (pH 7.4, 50 mM) at 37 °C. The solution was analyzed by HPLC-UV at 1 h intervals. % starting material remaining was determined by integration of the peak area signal at (λ = 280 nm).

Figure 39. E-64d ester saponification in phosphate buffer (50 mM, pH 7.4) at 37 °C

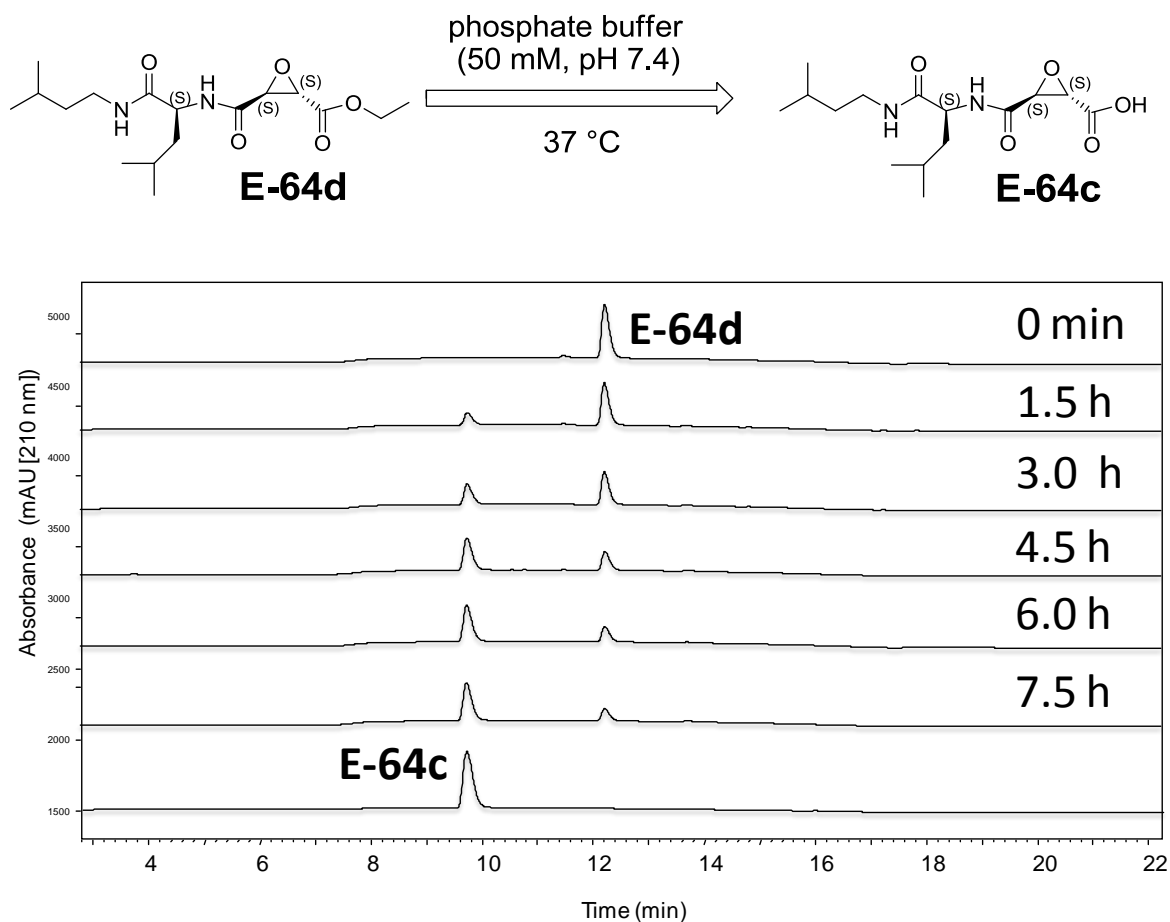


Fig.39. E-64d (250 μ M) was dissolved in PB (pH 7.4, 50 mM) at 37 °C. The solution was analyzed by HPLC-UV at 1.5 h intervals. % starting material remaining was determined by integration of the peak area signal at (λ = 210 nm).

2.2 Prodrug reactivity with GSH: competing breakdown pathways

Previous studies have indicated GSH and cysteine conjugation as being major *in vivo* pathways of **E-64d** metabolism and excretion.(Fukushima, Arai et al. 1989) Therefore, we examined the parent drugs or prodrugs after incubation in PBS at 25 °C in the presence or absence of excess glutathione.

The relative abundance of reaction products were calculated by measuring the area under the peak of the corresponding HPLC-UV chromatogram, and the identity of reaction products was carried out by LC-MS/MS analysis. Control experiments using the desired epoxyacid clinical candidates (**NYC-438**, **NYC-539**, and **E-64c**) showed negligible reactivity (> 99 % remaining after 24 h) towards hydrolysis in PBS or reaction with excess GSH. This result is in agreement with previous observations showing minimal conjugation of **E-64c** with GSH *in vitro*.(Fukushima, Arai et al. 1989) In contrast, the epoxide esters (**NYC-438E**, **NYC-539E**, and **E-64d**) readily reacted with excess GSH (5 mM), $t_{1/2} \sim 1$ h in PB (50 mM, pH 7.4) at 37 °C (Figure 41, Figure 43, and Figure 45). Intriguingly, the reactions products seem to be the result of two competing prodrug breakdown pathways (Figure 42, Figure 44, and Figure 46). One pathway (denoted pathway A) involves the rapid modification of the epoxide ester (**E**) via thiophilic attack of the epoxide ring to give the ester-glutathione conjugate, **E-SG**. Subsequent hydrolysis of the **E-SG** conjugate yields the acid-glutathione adduct (**A-SG**). Conversely, pathway B involves classical base catalyzed ester hydrolysis leading to the formation of the desired epoxyacid calpain inhibitor, **A**. As mentioned above, the epoxyacid incorporating molecules show negligible reactivity toward GSH. Hence, the acid-glutathione conjugate (**A-SG**) is mainly the result of ester saponification from the **E-SG** species. The presence of two competing pathways for epoxide ester prodrug breakdown is a new finding, the consequence of which is discussed below.

Figure 40. Analysis of the reaction between epoxide prodrug esters and GSH

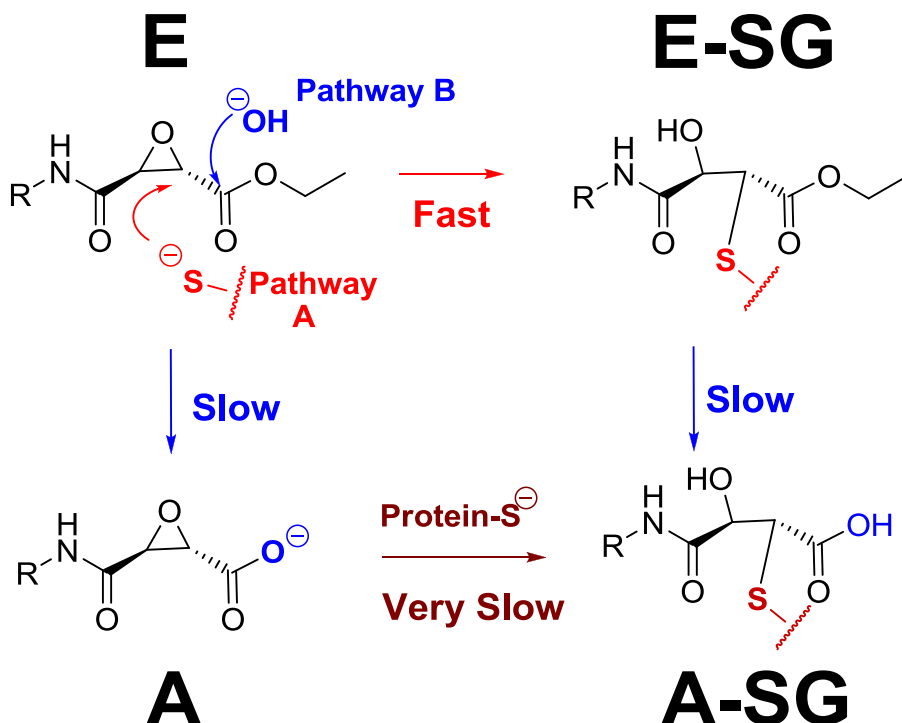


Fig.40. Illustration of the competing prodrug breakdown profiles of epoxide esters with thiols. Reaction of the appropriate epoxide ester prodrug with GSH (5 mM) in PB (50 mM, pH 7.4) gives reaction products shown above (Figure 41, Figure 43, and Figure 45). Pathway A involves rapid modification of the epoxide ester (**E**) via thiophilic attack of the epoxide ring to give the epoxide glutathione conjugate, **E-SG**. Subsequent hydrolysis of the **E-SG** conjugate yields the acid glutathione adduct (**A-SG**). Pathway B involves base catalyzed ester hydrolysis leading to the formation of the desired epoxyacid calpain inhibitor, **A**. The **A** species represent the potent calpain inhibitors previously studied, and possesses negligible reactivity towards thiols, as seen in the very slow rate of reaction with GSH. **A-SG** may form through either pathways, but is mostly formed from ester hydrolysis of **E-SG**.

Figure 41. HPLC time course of the products from reaction of **NYC-438E** and GSH

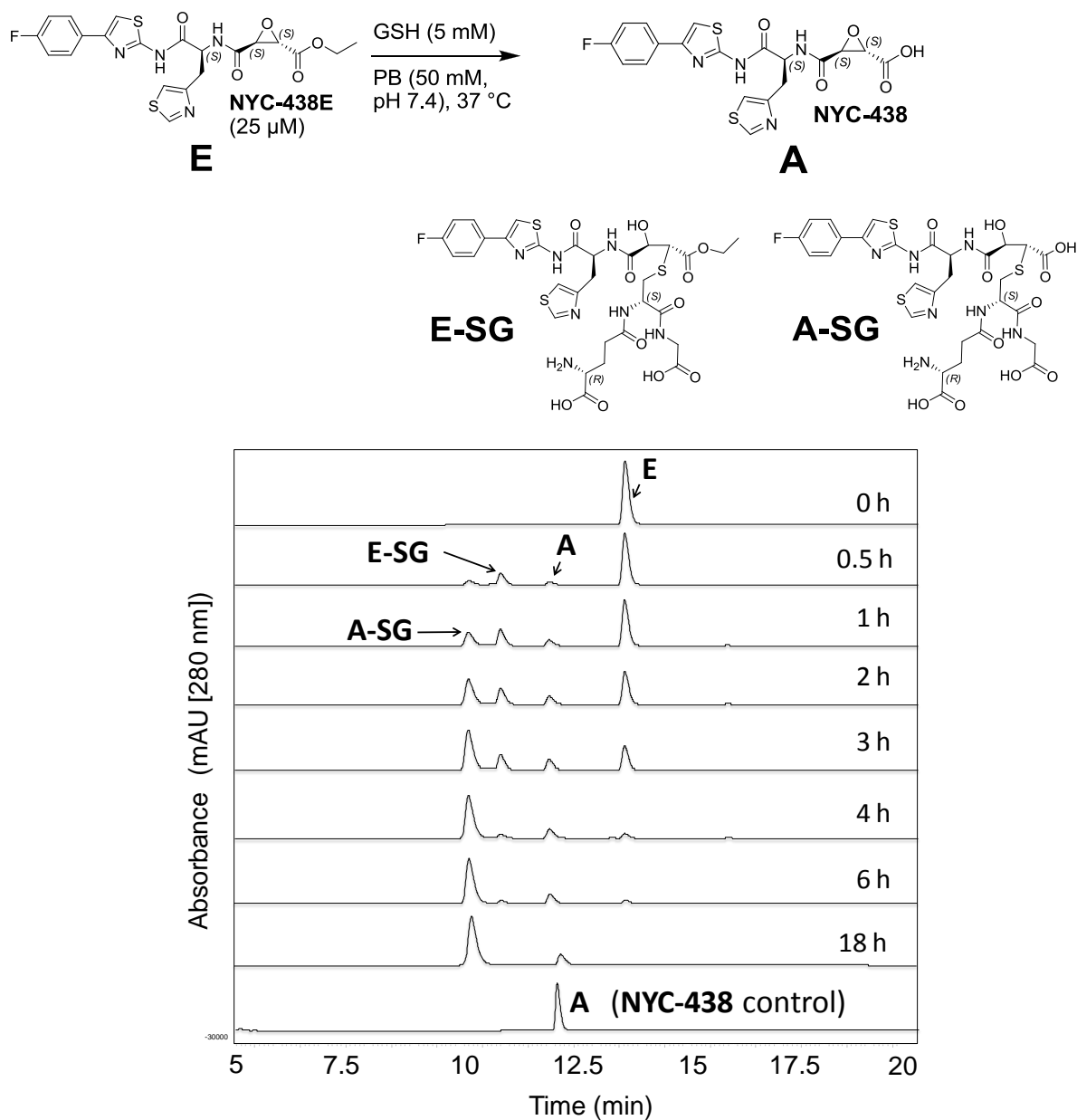


Fig.41. Structures and HPLC chromatograms from the incubation of **NYC-438E** (25 μ M) with GSH (5 mM) in PB (50 mM, pH 7.4) at 37 °C. Product structures were assigned using LC-MS/MS analysis of the reaction. Initially, the epoxide ester (**E**) primarily reacts with GSH to give the ester-GSH adduct (**E-SG**). Ester hydrolysis of **E** and/or **E-SG** leads to the formation of the epoxyacid-glutathione conjugate (**A-SG**) and the desired prodrug breakdown product **A** (**NYC-438**), respectively.

Figure 42. Graphic representation of reaction products of **NYC-438E** with GSH

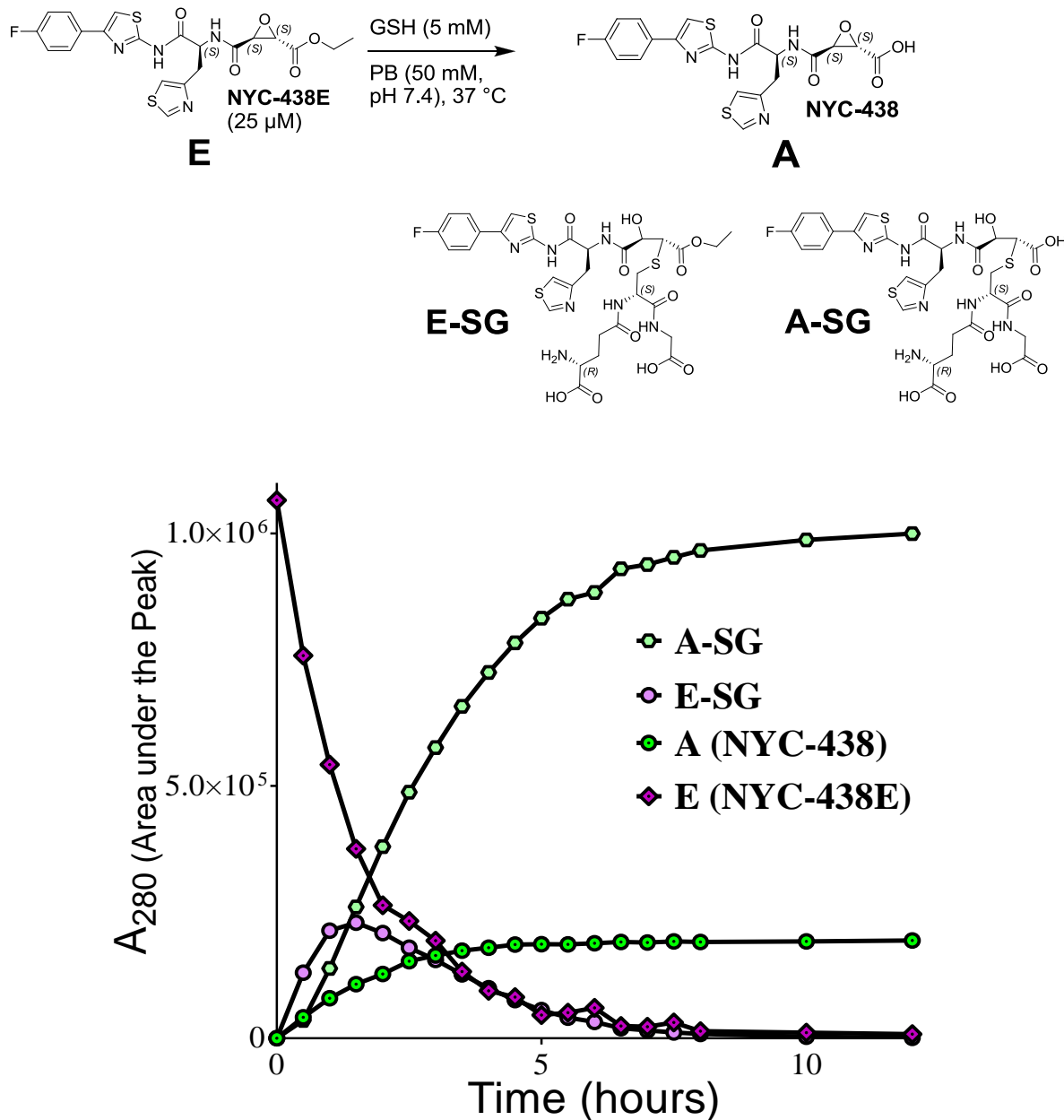


Fig.42. Graphical representation of the reaction product profile after incubation of **NYC-438E** (25 μ M) with GSH (5 mM) in PB (50 mM, pH 7.4) at 37 °C, monitored by HPLC-UV. Initially, **E-SG** formation is the pathway most responsible for prodrug breakdown. The desired breakdown of **NYC-438E** (**E**) to **NYC-438** (**A**) is only a minor prodrug breakdown pathway.

Figure 43. HPLC time course of the products from reaction of **NYC-539E** and GSH

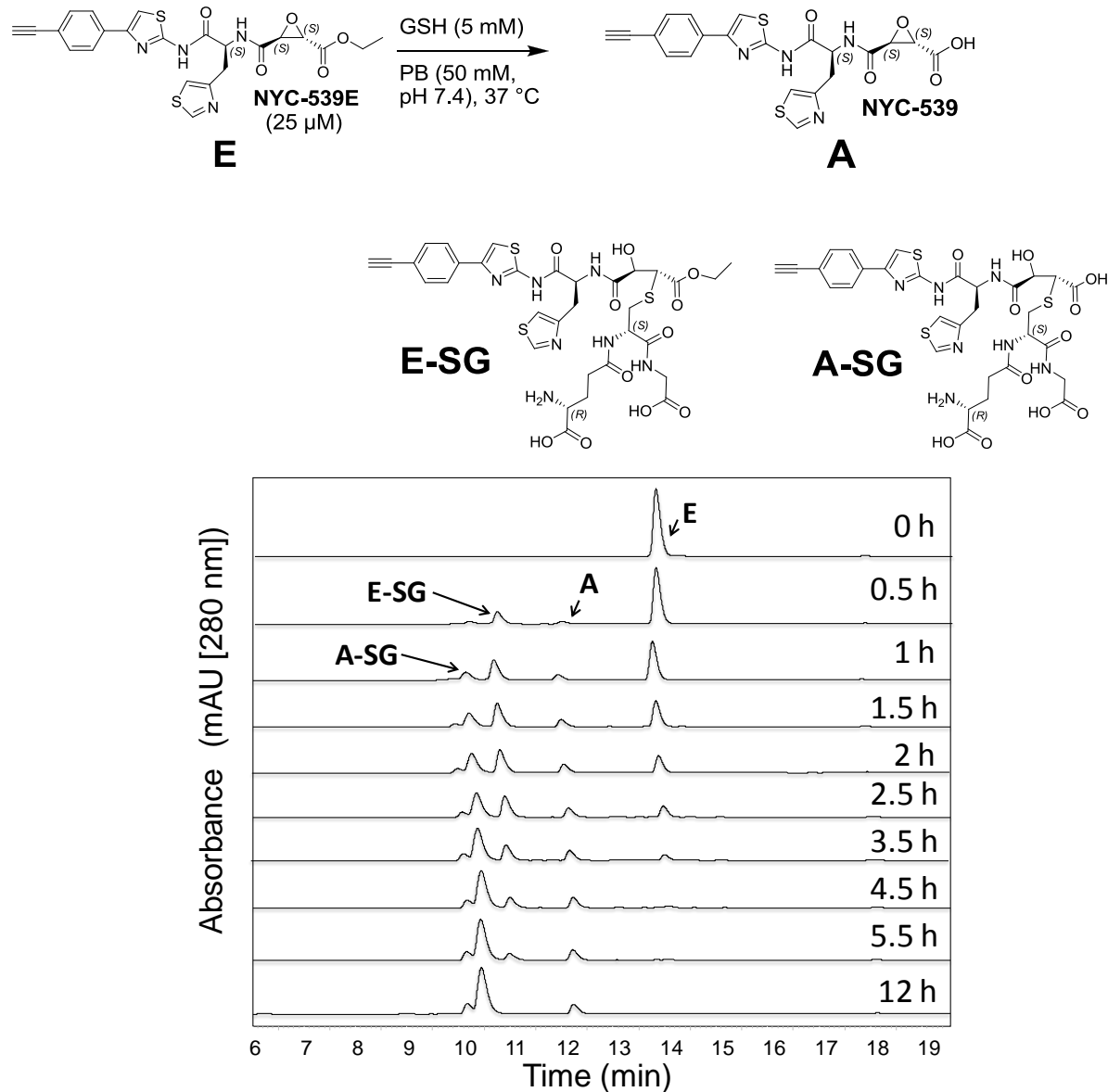


Fig.43. HPLC chromatogram of aliquots from the incubation of **NYC-539E** (25 μ M) with GSH (5 mM) in PB (50 mM, pH 7.4) at 37 $^{\circ}$ C. The structures were assigned using LC-MS/MS analysis of reaction products. Initially, the epoxide ester (**E**) primarily reacts with GSH to give the ester-GSH adduct (**E-SG**). Ester hydrolysis of **E** and/or **E-SG** leads to the formation of the epoxyacid-glutathione conjugate (**A-SG**) and the desire acid prodrug breakdown product (**A**, **NYC-539**), respectively.

Figure 44. Graphic representation of reaction products of **NYC-539E** with GSH

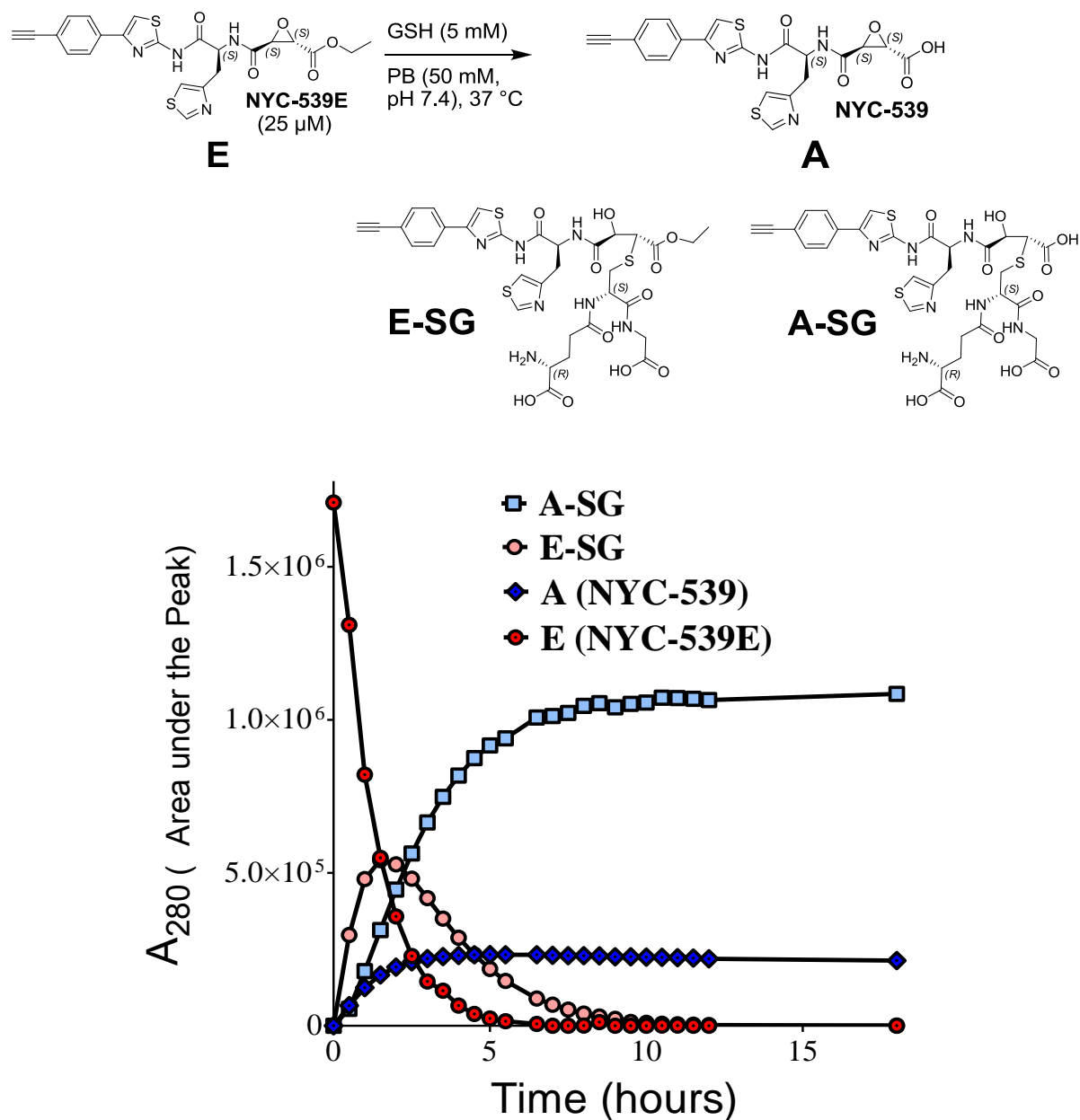


Fig.44. Graphical representation of the reaction product profile after incubation of **NYC-539E** (25 μ M) with GSH (5 mM) in PB (50 mM, pH 7.4) at 37 $^{\circ}$ C, monitored by HPLC-UV. Initially, **E-SG** formation is the pathway most responsible for prodrug breakdown. The desired breakdown of **NYC-539E** (**E**) to **NYC-539** (**A**) is only a minor prodrug breakdown pathway.

Figure 45. HPLC time course of the products from reaction of **E-64d** and GSH

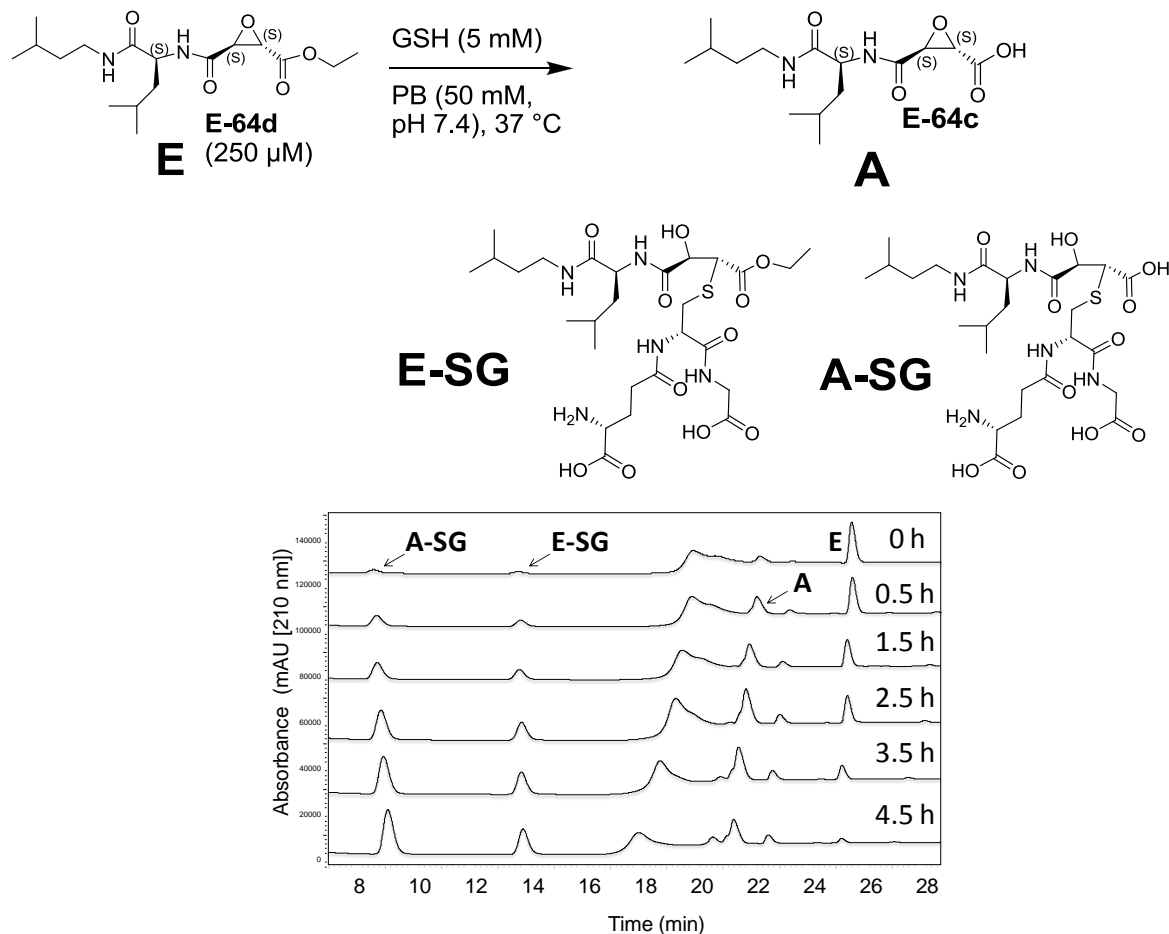


Fig.45. HPLC chromatogram of aliquots from the incubation of **E-64d** (250 μ M) with GSH (5 mM) in PB (50 mM, pH 7.4) at 37 $^{\circ}$ C. The structures were assigned using LC-MS/MS analysis of reaction products. **E-64d** demonstrated a slightly different reaction profile compared to the other epoxide esters. The acid glutathione conjugate (**A-SG**) was the major product pathway from the beginning of the reaction. The ester glutathione conjugate (**E-SG**) was the 2nd most abundant product. Unlike our novel calpain inhibitors (**NYC-438** and **NYC-539**), **E-64d** lacks a conjugated π -system, hence, it has poor UV absorbance. As a result, experiments used an increased quantity of prodrug ester (250 μ M) and monitored products at 210 nm. Monitoring absorbance at 210 nm also results in a baseline drift in the chromatogram between 18-20 min.

Figure 46. Graphic representation of reaction products of **E-64d** with GSH

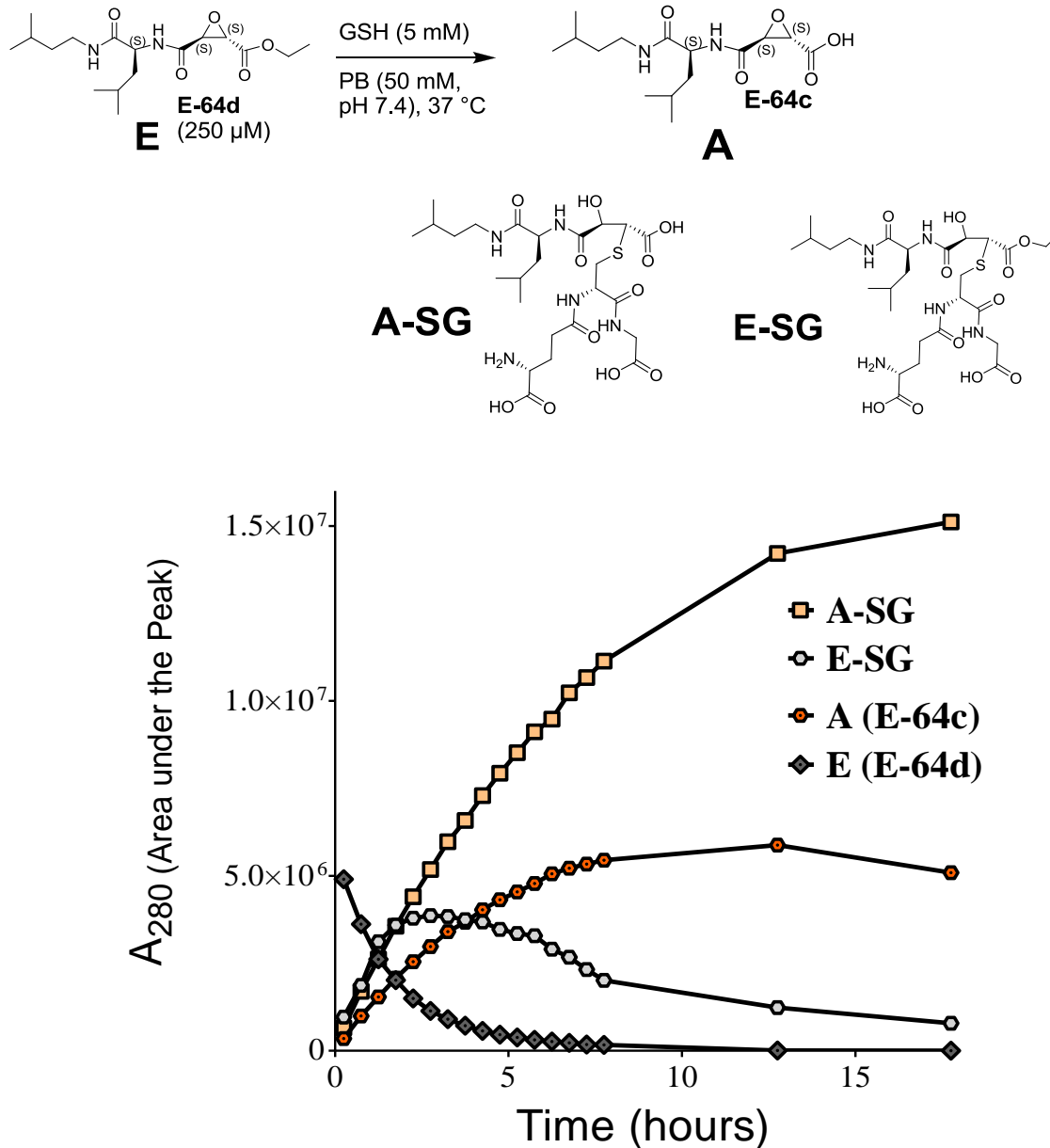


Fig.46. Graphical representation of the reaction product profile after incubation of **E-64d** (250 μ M) with GSH (5 mM) in PB (50 mM, pH 7.4) at 37 $^{\circ}$ C, monitored by HPLC-UV. In general, **E-64d** has a similar reaction profile with GSH as the other epoxide esters tested. One notable difference is the rate of formation of the acid-conjugate (**A-SG**) and the ester conjugate (**E-SG**) seems to be equal until the **E-64d** starting material is completely consumed. In contrast, **E-SG** formation was more rapid in the NYC ester reactions.

3. Discussion

3.1 Impact on NYC-438 prodrug development

Our results create major concerns regarding the use of ethyl esters as prodrugs for epoxyacid peptidomimetics. Previous studies examining the clinical AD candidate **E-64d** proposed rapid hydrolysis *in vivo* to the its active form, **E-64c**. In light of these result, typical prodrug strategies would suggest incorporation or a *t*-butyl or *i*-propyl ester to hamper the rate of ester hydrolysis. However, while this strategy may indeed slow ester saponification by steric influence, it is less likely to have a profound impact of epoxide ring thiophilicity compared to the ethyl ester. The reactivity of the epoxide ring in the prodrug molecules suggests that modulation of electronic effects may be a more appropriate strategy in designing prodrugs for epoxyacids. In this context, the notion of deactivated esters (i.e. *p*-methoxybenzene esters), deactivated thioesters, or even activated amide containing prodrugs are of interest. The synthesis of such prodrugs may prove challenging, as their formation requires nucleophilic attack adjacent to a reactive electrophile.

The observation of the parent epoxyacid drugs being highly stable against thiophilic attack by GSH, suggests that they could hold potential as selective reactive electrophiles. An early concern of developing peptidomimetics incorporating a reactive group was the potential for non-specific reactions with reactive biological thiols. However, the epoxyacid functionality appears to be quite stable in the presence of excess GSH at 37 °C. The epoxyacid calpain inhibitors are quite reactive towards Cal1 (see chapter 1), therefore, the relatively non-reactive nature of epoxyacids towards biological thiols creates the possibility of these molecules to be highly specific as calpain reactive peptidomimetics. Unfortunately, developing an appropriate prodrug strategy may be challenging due to the unexpected reactivity of the epoxy ester prodrugs. An

ideal prodrug strategy is demonstrated in Figure 47, and includes shifting the prodrug breakdown pathway toward saponification and away from the rapid formation of thiol adducts.

Figure 47. The ideal prodrug scenario for epoxyacids

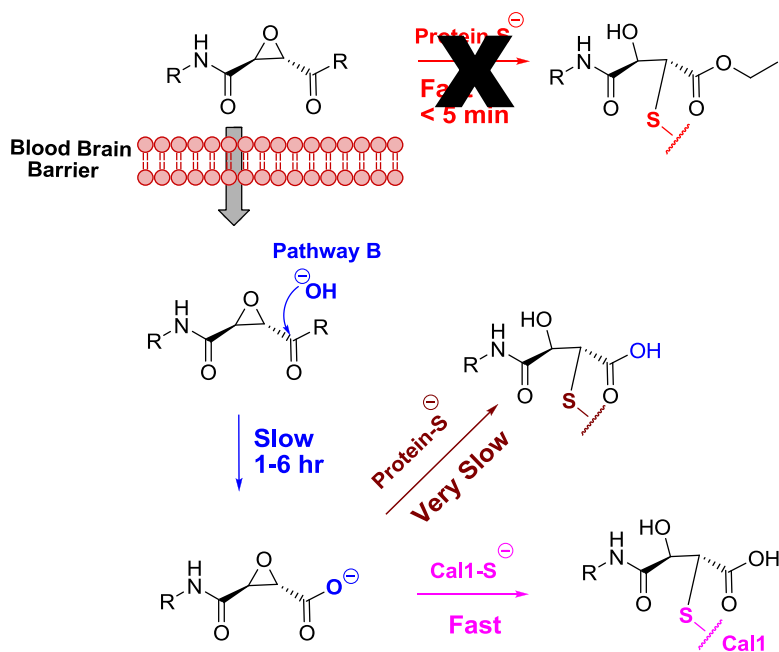


Fig.47. Depiction of the ideal prodrug strategy for CNS targeted epoxide peptidomimetic calpain inhibitors. The reactivity of the epoxide ethyl ester towards GSH suggests that modulation of electronic effects may be an appropriate strategy in designing prodrugs for epoxyacids. A successful prodrug strategy would shift the prodrug breakdown equilibrium away from the rapid epoxide modification seen in the case of epoxide esters. The ideal prodrug R group would hydrolyze slowly to give the desired epoxide acid calpain inhibitor and preferable aid in crossing the BBB. In this context, deactivated thioesters, deactivated esters (i.e. *p*-methoxybenzene esters), or activated amide containing prodrugs are of interest.

3.2 Implications on mechanism of action of clinical candidate E-64d

The observed rapid breakdown of epoxide esters in the presence of GSH is in agreement with reports of **E-64d** levels being undetectable < 5 min after *in vivo* administration of a substantial quantity of **E-64d** (100 mg/kg). Interestingly, the formation of **E-SG** adducts has not been reported, probably due to errors in experimental design in previous studies; specifically, 1) the inappropriate assumptions of a one way linear pathway leading to **A-SG** formation, and 2) the absence of modern technology which resulted in an inability to isolate and identify one of the three major isolated *in vivo* metabolites previously.(Fukushima, Arai et al. 1989) Here we make the discovery of an overlooked dominating pathway of epoxide ester prodrug breakdown is through thiophilic attack of the epoxide rather than ester hydrolysis. This suggests that the absence of detectable **E-64d** levels *in vivo* is likely due to rapid protein modification, rather than the presumed conversion to the desired parent carboxylate. Accordingly, *in vivo* activity of the epoxide ester is likely due to off target protein modification, and is unlikely due to direct inhibition of cysteine proteases as previously suggested. This result also may explain the observed lack of efficacy of **E-64d** in phase III clinical trials. At any rate, it is interesting that molecules displaying such high rates of thiol modification are reported to be safe and well tolerated in man. Further experiments employing the novel alkynyl epoxyester probe, **NYC-539E**, may aid in answering some of these questions. *In vitro* or *in vivo* treatment with **NYC-539E** followed by *in situ* couplings with a biotin-azide should allow for visualization of protein modification by western blot, or perhaps identification of modified proteins by LC-MS following tryptic digest.

4. Conclusions

In an effort to duplicate the reported successful prodrug approach of **E-64d**, we evaluated the synthetic precursor ethyl ester of **NYC-438**, **NYC-438E**. Reactivity analysis of **NYC-438E** with GSH led to the discovery of an unanticipated reaction profile, and follow-up studies examining **E-64d** showed a similar unreported prodrug breakdown pathway. Prodrug ester breakdown seems to include two competing pathways: 1) the classical ester saponification pathway, and 2) a dominate thiol modification pathway involving epoxide ring opening. These competing pathways have been overlooked in the past, likely because they both ultimately result in the same epoxyacid modified thiol adducts. The discovery of this unexpected reaction profile creates challenges in prodrug development for **NYC-438**, but also suggests opportunities in selectively targeting calpain. Off-target modification of the parent epoxyacid drug candidate was negligible. The result also creates major questions concerning the biological targets of the clinical candidate **E-64d**. Further studies using the novel alkynyl probe **NYC-539E** should aide in identification of which proteins react most readily with epoxide ethyl esters *in vivo*.

5. Materials and Methods

5.1 Materials

All chemicals and reagents were purchased from Sigma-Aldrich (St. Louis, MO) and used as received unless stated otherwise.

5.2 Synthesis

Epoxide ester prodrugs were fully characterized by ^1H NMR, ^{13}C NMR, and the structures supported using in house HRMS. Compounds were confirmed to be > 95 % pure by analytical HPLC. Full synthetic methodologies are described in detail within Appendix A, and

characterization spectra given in Appendix B. E-64d was purchased from Sigma-Aldrich, and hydrolyzed to give E-64c reference sample.

5.3 HPLC analysis of stability/reactivity

Prodrug stability and reactivity were determined by HPLC-MS/MS. Reaction progress and kinetics was monitored using HPLC, and structures assigned using LC-MS/MS. Typical experiments involved incubation of the prodrug/drug [**NYC-438E** and **NYC-539E** (100 μ M), or **E-64d** (250 μ M)] in PBS (pH 6.4; 7.4; or 8.4) with excess glutathione (5 mM), and the reaction progress monitored by HPLC-UV absorbance.

CHAPTER 3. DEVELOPMENT OF ATTENUATED FUROXANS AS NOVEL NEUROPROTECTIVE AND PROCOGNITIVE THIOPHILIC NO-MIMETICS

1. Introduction

The wide range of biological activity of compounds containing a furoxan (1, 2, 5-oxadiazole-*N*-oxide) or benzofuroxan heterocycle has been known for decades. (Stuart 1975; Ghosh, Ternai et al. 1981; Cerecetto and Gonzalez 2007) Although thermally stable and stable towards a range of acid-base conditions, furoxans are thiophilic electrophiles. (Medana, Ermondi et al. 1994) This reactivity may underlie observed biological activity; for example, the nitrobenzofuroxans were described as “thiol-neutralizing agents” in early work on the anti-leukemic properties of benzofuroxans and benzofurazans. (Ghosh and Whitehouse 1968; Whitehouse and Ghosh 1968) However, the most commonly accepted mechanism underlying furoxan activity involves thiol-dependent NO release. (Ferioli, Fazzini et al. 1993) In recent years, the furoxan moiety has been the subject of increased attention, pioneered by Gasco and others, owing to a plethora of interesting biological activities observed against a diverse range of targets. (Boschi, Di Stilo et al. 1997; Boiani, Cerecetto et al. 2001; Boschi, Tron et al. 2003; Cena, Lolli et al. 2003; Sorba, Galli et al. 2003; Cena, Boschi et al. 2004; Tosco, Bertinaria et al. 2005; Velazquez, Rao et al. 2005; Buonsanti, Bertinaria et al. 2007; Buonsanti, Bertinaria et al. 2007; Boiani, Aguirre et al. 2008; Chegaev, Cena et al. 2009)

Despite ample attempts to develop furoxans as NO mimetics, no efforts have pursued the possibility of neuroprotective furoxans for the CNS. The majority of attempts to develop furoxans have focused on highly reactive furoxans that produce large fluxes of NO, thereby eliciting the cytotoxic effects associated with NO at high concentrations. Indeed, while NO

possesses cytotoxic effects at high concentrations, low levels of NO are potentially protective, particularly in the CNS.(Thatcher, Nicolescu et al. 2004) This is not surprising, as most furoxans share the limitation of being highly reactive and cytotoxic. However, whilst the furoxan ring possesses inherent reactivity toward thiols, the identity and pattern of furoxan substitution can potentially dictate the reactivity and propensity for NO release, and therefore may be manipulated to produce furoxans with attenuated reactivity, which may hold potential as neuroprotective agents.

NO signaling via the second messenger molecule, cGMP, is essential for normal brain function.(Thatcher, Bennett et al. 2006) NO stimulates cGMP production through the activation of NO-sensitive soluble guanylyl cyclase (sGC or NO-GC), which in turn leads to activation of the memory-related transcription factor, cyclic-AMP response element binding protein (CREB).(Haley, Wilcox et al. 1992; Zhuo, Hu et al. 1994; Lu, Kandel et al. 1999; Bon and Garthwaite 2003) Moreover, evidence indicates that NO may act directly in presynaptic neurons.(Arancio, Kiebler et al. 1996) At physiological concentrations, NO possesses a variety of neuroprotective and procognitive effects via a combination of cGMP-dependent and independent pathways, the latter including S-nitrosation of the active site cysteine of caspase-3 inhibiting execution of apoptotic cell death. (Mohr, Zech et al. 1997)While physiological concentrations of NO are essential for neuronal function, high concentrations of NO may lead to cell death. Therefore, an ideal neuroprotective and procognitive NO mimetic would possess the ability to produce a lower flux of NO over a sustained period of time. In this context, a furoxan with attenuated reactivity, as a thiol-dependent, non-spontaneous NO donor is of interest (Scheme 8). To date, limited attempts have been made to modulate furoxan reactivity, and no reports have appeared on therapeutic applications in the CNS.

Enhancement of NO/sGC signaling may provide a novel approach to the treatment of Alzheimer's disease (AD) and other neurodegenerative disorders, through neuroprotective and procognitive actions. (Lipton, Choi et al. 1993; Smith, Dringenberg et al. 2000; Reynolds, Bennett et al. 2002; Thatcher, Nicolescu et al. 2004; Puzzo, Vitolo et al. 2005; Thatcher 2005) Brain derived neurotrophic growth factor (BDNF), a downstream target of CREB, nourishes neurons, resulting in increased neurogenesis and enhanced synaptic plasticity. (Vitolo, Sant'Angelo et al. 2002; Blurton-Jones, Kitazawa et al. 2009; Puzzo, Staniszewski et al. 2009) BDNF impairment has been demonstrated in the AD brain, and A β , the major component of amyloid plaques, has been shown to inhibit NO/sGC/CREB signaling, leading to synaptic impairment. (Peng, Wu et al. 2005) The importance of NO signaling in modulating synaptic plasticity and its correlation to enhanced learning and memory, as well as the neuroprotective effects of NO, support the development of NO mimetics for the treatment of neurodegeneration and AD. (Puzzo, Vitolo et al. 2005; Puzzo, Staniszewski et al. 2009)

Scheme 8. Potential mechanisms of furoxan bioactivation and neuroprotection^a



^a Attenuated furoxans may elicit neuroprotection by two potential mechanisms. At physiological concentrations, NO possesses a variety of neuroprotective and procognitive effects via a combination of cGMP-dependent and independent pathways. S-nitrosation of pro-apoptotic caspases results in inhibition of apoptotic cell death in primary neurons. NO stimulates cGMP production through the activation of soluble guanylyl cyclase, sGC, which in turn leads to activation of the memory-related transcription factor, cyclic-AMP response element binding protein (CREB). CREB phosphorylation is essential for synaptic plasticity and memory consolidation. Molecules that activate the sGC/cGMP/CREB signaling pathway are able to restore synaptic function in the form of LTP. While physiological concentrations of NO are essential for neuronal function, high concentrations of NO may lead to cell death. Therefore, an ideal neuroprotective and procognitive NO mimetic would possess the ability to produce a controlled flux of NO of a long period.

2. Results

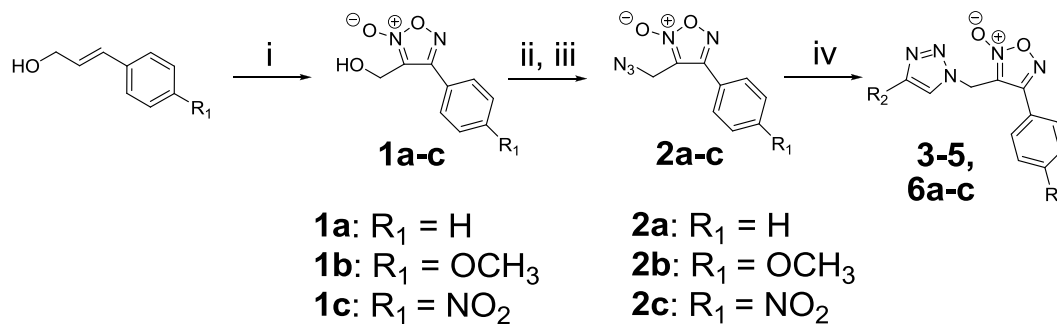
2.1 Design and Synthesis

Furoxan reactivity is presumed to be most sensitive to changes in direct substitution of the furoxan ring and its conjugated systems. Contrary to modifications made in substitution of the conjugated aryl system, a methylene linker was maintained opposite to the aryl system in order to minimize potential effects on reactivity by derivatization at this end of the molecule. Recent evidence has shown the utility of non-selective cysteine protease inhibitors for neurodegenerative diseases,(Hook, Kindy et al. 2007; Trinchese, Fa et al. 2008) and it was speculated that a peptidomimetic thiophilic furoxan may hold the distinct potential to inhibit cysteine proteases, such as calpain, by direct reaction with active site cysteines. Peptidomimetic scaffolds were therefore designed in an effort to impart a protease recognition unit, while having negligible impact on the reactivity of the furoxan ring itself, and allowing a divergent synthetic approach; although ultimately the furoxans were poor cysteine protease inhibitors (data not shown).

The initial synthetic strategy, to produce a variety of furoxans using divergent synthesis, started from the aryl furoxan alcohols (**1a-c**) (Scheme 9). Furoxans incorporating classical electron donating (*p*-OCH₃, **1b**) and electron withdrawing (*p*-NO₂, **1c**) groups were designed to examine the effect of modifying furoxan ring reactivity via manipulations of electronic properties of the conjugated aryl system. The 4-arylfuroxan-3-methanol compounds were prepared by cyclization of the corresponding arylcinnamyl alcohols by the action of sodium nitrite in acetic acid to yield the corresponding 4-arylfuroxan-2N-oxide alcohols. The alcohols were then activated using tosyl chloride to allow conversion to the 4-arylfuroxan-2N-oxide azides (**2a-c**) using NaN₃ in DMF at 60 °C. Terminal alkynes were synthesized using standard

peptide coupling procedures (see Appendix A for full experimental details) and then reacted with **2a-c** through a 2,3-dipolar cycloaddition to yield the corresponding furoxan-triazole containing derivatives **3-5**, as well as a subset of analogues containing *p*-substituted arenes (**6a-c**). The peptidomimetic oxadiazole-2N-oxides (**6a-c**) were then tautomerized in boiling toluene to afford **7a-c**. The tautomerization is performed in boiling toluene (120 °C) for 3-7 d, and although the percent conversion varied according to aryl-substitution, the reactions are distinctly clean, with no apparent breakdown products of the peptidomimetic or furoxan functionalities visible on TLC. **2a** and **2b** were also converted to their corresponding amines (**8a** & **8b**) via a Staudinger reduction followed by DMAP catalyzed coupling to a peptidomimetic synthon to give **9a** & **9b** (Scheme 10). The furazan analogue **10** was produced by treatment of **9a** with a combination of activated zinc and ammonium formate at reflux. (Balicki, Cybulski et al. 2003) The furoxans were found to be stable to acidic and basic reaction work-ups, and silica-gel chromatography during the course of synthesis. The presence of signals at ~ 108 and 115 Hz on ¹³C NMR spectra, corresponding to the C3 and C4 carbons of the furoxan ring were typically used to designate the 1,2,5 oxadiazole-2N-oxide configuration. X-ray analysis of one derivative, **6c**, confirmed the presence of the 1,2,5 oxadiazole-2N-oxide ring, and resolved the stereochemistry of the peptidomimetic *L*-valine as being the natural *S*-isomer used in the initial peptidomimetic synthesis (Figure 48).

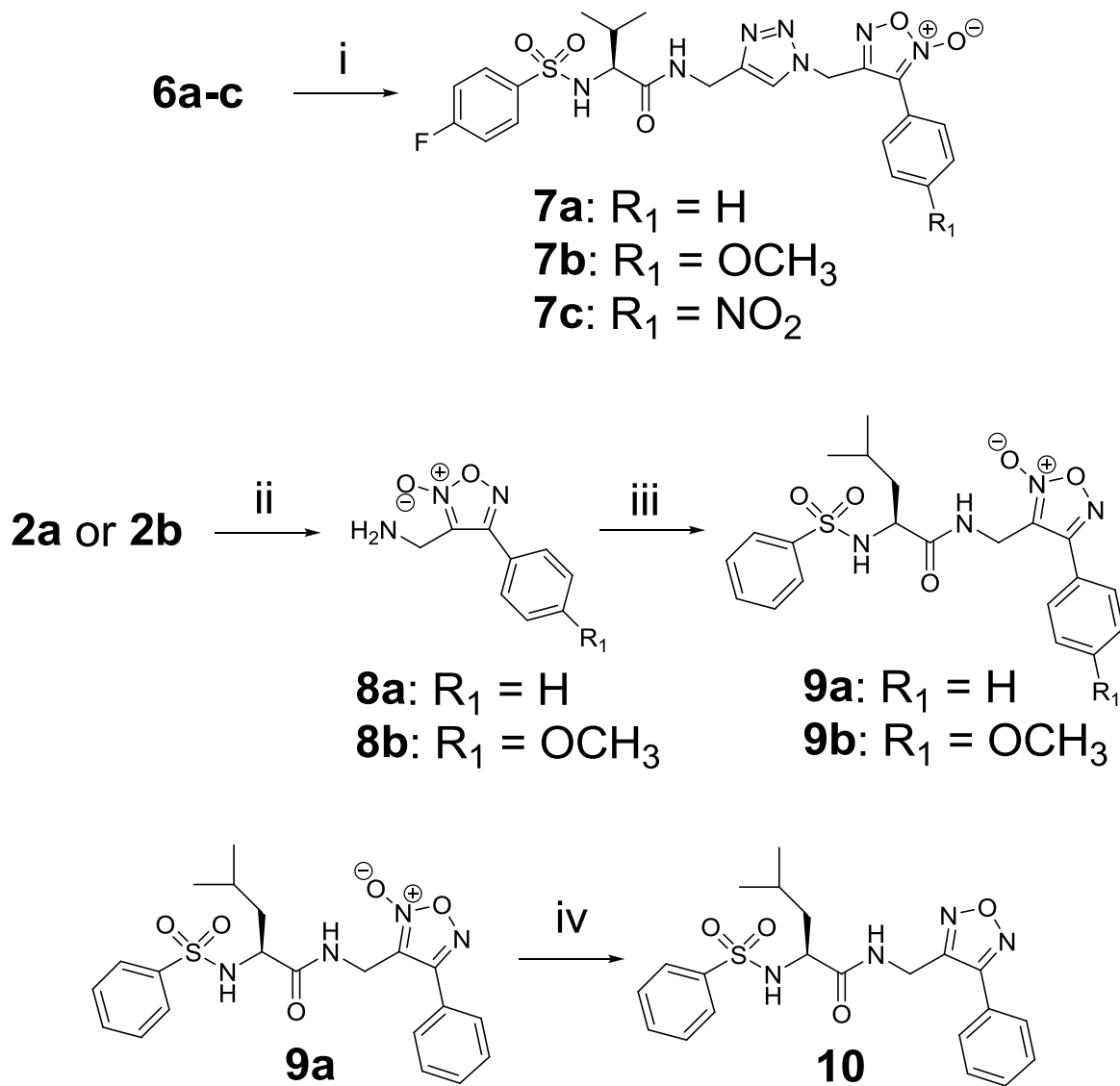
Scheme 9. Synthesis of furoxan-triazole incorporating peptidomimetics ^a



Entry	R ₁	R ₂
3	-H	
4	-OCH ₃	
5	-OCH ₃	
6a	-H	
6b	-OCH ₃	
6c	-NO ₂	

^aReagents and Conditions: i) NaNO₂, acetic acid, < 20 °C; ii) TsCl, TEA, CH₂Cl₂, 0 °C; iii) NaN₃, DMF, 60 °C; iv) CuI, DIPEA, toluene, with phenylacetylene for **3**; 2,8-Dimethyl-5-(prop-2-ynyl)-2,3,4,5-tetrahydro-1H-pyrido[4,3-b]indole for **5**; (S)-2-(4-Fluorophenylsulfonamido)-3-methyl-N-(prop-2-ynyl)butanamide for **6a-c**; or CuSO₄, sodium ascorbate, 3-ethynylaniline, *t*-BuOH/EtOH/H₂O for **4**.

Scheme 10. Synthesis of furoxan peptidomimetics continued ^a



^aReagents and Conditions: i) toluene, 120 °C, 3 d; ii) P(Ph₃), 35 % NH₄OH, DMF, r.t.; iii) EDCI, DMAP, (S)-4-Methyl-2-(phenylsulfonamido)pentanoic acid, CH₂Cl₂, 0 °C; iv) **9a**, Zn, ammonium formate, MeOH, 60 °C.

Figure 48. X-ray structure of the *p*-NO₂ containing furoxan triazole peptidomimetic **6c**

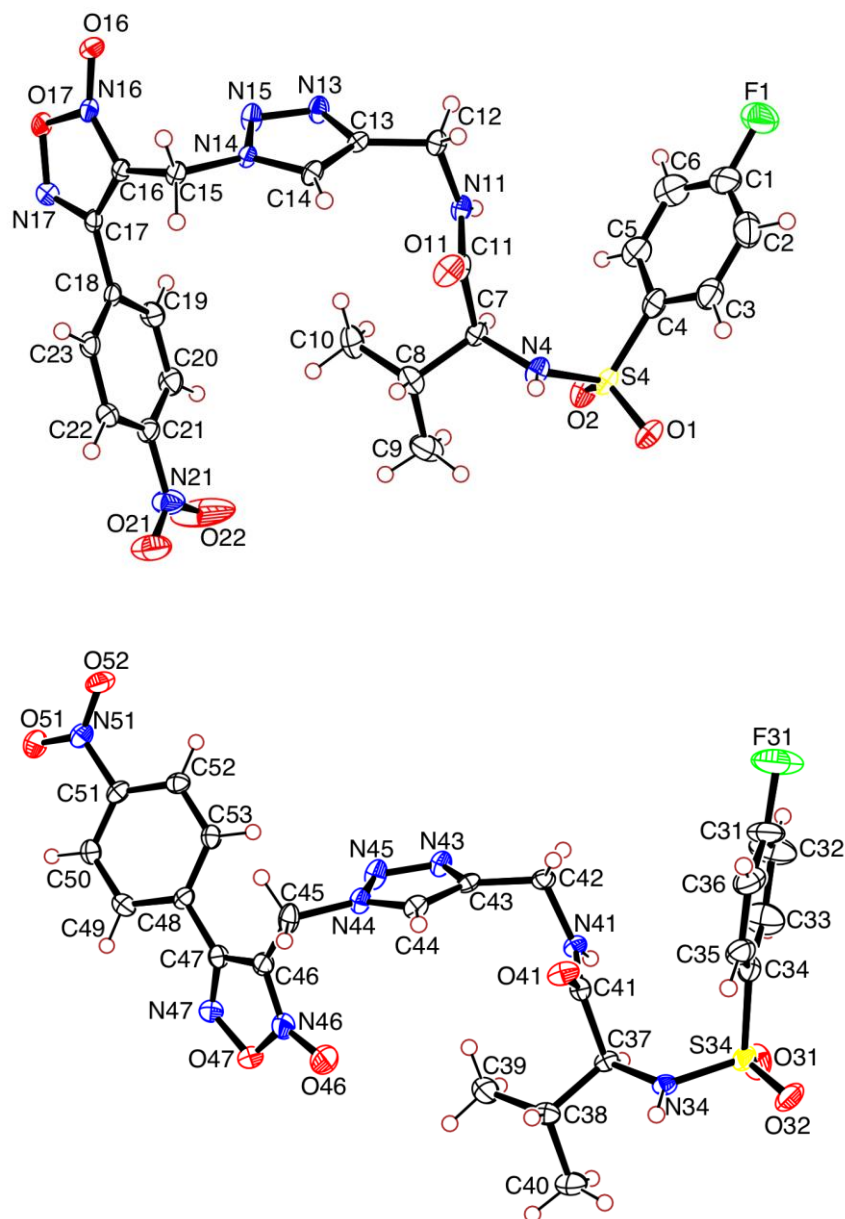


Fig.48. The presence of signals at ~ 108 and 115 Hz on ¹³C NMR spectra, corresponding to the C3 and C4 carbons of the furoxan ring were typically used to designate the 1, 2, 5 oxadiazole-2N-oxide configuration. X-ray analysis of one derivative, **6c**, confirmed the presence of the 1, 2, 5 oxadiazole-2N-oxide ring.

2.2 Furoxan Reactivity

Attenuating the reactivity of the furoxan ring through structural modifications is of paramount importance in NO-mimetic design. The majority of benzofuroxans are not expected to release NO on the basis of a study by Medana and co-workers separately measuring NO_2^- , N_2O , and NO. (Medana, Di Stilo et al. 1999) In contrast, the formation of both NO and nitrosothiols from furoxans has been postulated from attack of thiolate anion; the furoxan impramidil was reported to yield nitrite, nitrate, and a *bis*-oxime containing product. (Feelisch, Schönafinger et al. 1992; Medana, Ermondi et al. 1994; Medana, Ermondi et al. 1994; Sako, Oda et al. 1998) The exact mechanism of furoxan degradation leading to NO bioactivity has not been defined and is beyond the scope of the present work. A putative mechanism is shown in Scheme 11 for reaction of the furoxan **9a** with cysteine. In this mechanism: 1) formation of a keto-oxime **E** necessarily requires loss of a nitrogen oxide (NO_x); 2) thiol may be regenerated after initial ring-opening, resulting in **C**; and 3) initial ring-opening may result in thiol oxidation to form a disulfide, producing **B**. *Therefore, in the reaction of furoxan with thiol, the consumption of thiol is not intrinsically correlated with release of NO_x .*

Support for the mechanism shown in Scheme 11 was gained from study of the reaction of furoxan **9a** at physiological pH and temperature in the presence of excess cysteine. After 2 h reaction, products were identified by HPLC-MS/MS; the parent and daughter ions of the major product were compatible with the *bis*-oxime hydrate **D**. The product corresponding to the keto-oxime, **E** (or its enol tautomer) and loss of NO_x constituted 11 % of the reaction mixture. A compound corresponding to a cysteine-containing product (**A**) was observed, but constituted < 1 % of products from integration of the UV absorbance chromatogram.

The rate of reaction with cysteine was observed to be lower for **6a-c** than that of **9a** based upon the % of starting material remaining: **9a**, 11 %; **6a**, 68 %; **6b**, 75 %; **6c**, 14 % (Figure 49).

The greater thiophilicity of **9a** is compatible with intramolecular stabilization of the developing negative charge in intermediate **V**, which has previously been reported to accelerate furoxan breakdown. More importantly, the predicted modulation of reactivity by substitution of the phenyl ring, with electron-donating (**6b**) or electron-withdrawing (**6c**) substituents, was validated by the data. Thus, analysis of the reaction products from **6a-c** demonstrated that structural modification modulates overall furoxan reactivity, and the potential of developing furoxans as attenuated NO mimetics.

The comparable reaction of cysteine (5 mM) at pH 7.4 (PBS, 50 mM) and 37 °C was studied with **6a-c**. **6a** yielded three main reaction products, and putative structures have been assigned based on the observed m/z values (Figure 50). Approximately 72 % of **6a** remained after 2 h, and no cysteine adduct was observed. Two distinct peaks were observed with the same m/z for **E**, which is presumably in equilibrium as keto-oxime/nitroso-enol isomers. One of the major products is proposed to be the keto-oxime containing, **E** (~8-12 %), and the likely end product NO_x release.

The relatively high and complex reactivity of **6c** compared to the other furoxans studied is easily noticed upon examination of the reaction profiles by HPLC-MS/MS (Figure 51). **6c** gave some products that were not seen for any of the other derivatives studied, namely products **I** & **II**. **I** (~ 5 %) corresponds to a product likely resulting from the peptidomimetic triazole **I** acting as a stable leaving group. **II** represents a hydroxylamine containing molecule which represents ~55 % of total products, presumably formed as the result of a highly energetic intermediate that results in the breaking apart of the furoxan ring itself. **I** and **II** are speculated to be responsible for the large amounts of NO_2^- observed from **6c** in the griess assay. The NO_x releasing product (**E**) only represents approximately 13 % of the entire reaction products. In the manuscript, **6c** was omitted from the correlation of NO_2^- versus neuroprotection due to the

atypical NO_2^- production observed; however, if considering the relative amount of **E** as indicative of NO_x release, **6c** would fit adequately into our correlation for NO_x and neuroprotection. These findings signify the complex and high reactivity of **6c**, and support our hypothesis that in this circumstance, NO_2^- generation does not correlate with biologically relevant NO_x produced. **6c** gave some products that were not seen for any of the other derivatives studied, namely products **I** & **II**. **I** (~ 5 %) corresponds to a product likely resulting from the peptidomimetic triazole **I** acting as a stable leaving group. **II** represents a hydroxylamine containing molecule which represents ~55 % of total products, presumably formed as the result of a highly energetic intermediate that results in the breaking apart of the furoxan ring itself.

Figure 49. Observed trend in furoxan reactivity

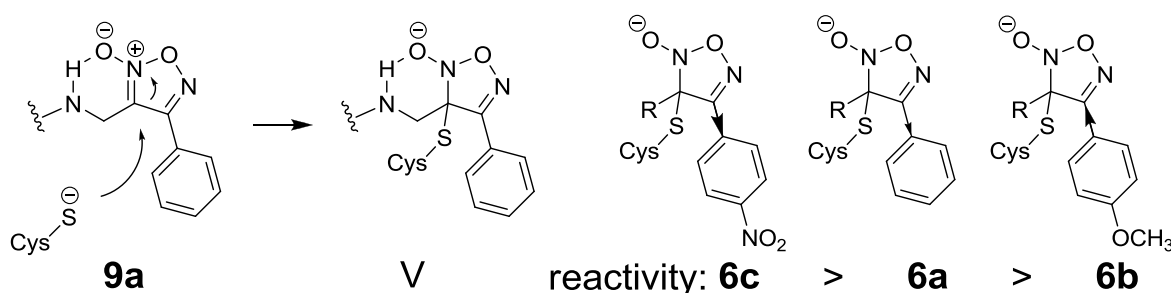
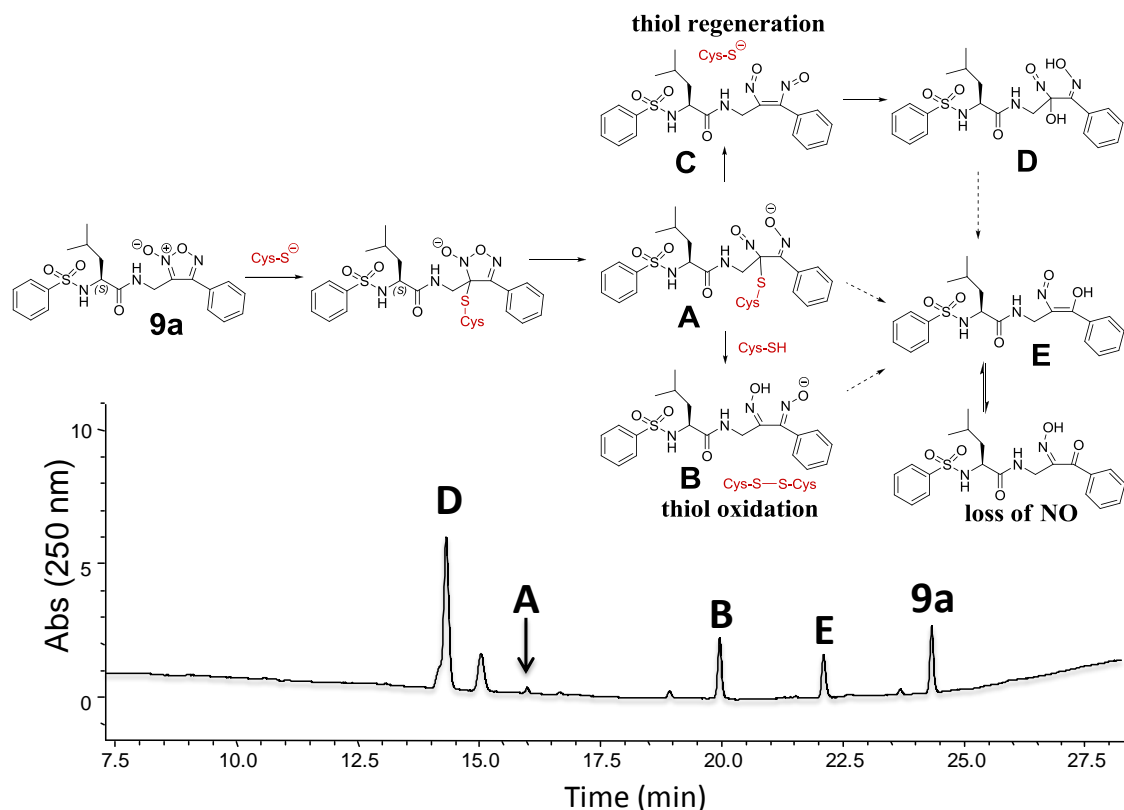


Fig.49. Trend in reactivity based on % remaining parent furoxan (75 μM) after 2 h incubation with excess cysteine (5.0 mM) in PBS (50 mM, pH 7.4) at 37 °C. Analyzed by HPLC-UV ($\lambda = 250\text{nm}$). Although **9a** gave low levels of NO_2^- production in the griess assay, it also gave the least amount of remaining starting material after 2 h with excess cysteine. This observation is supported by previous accounts of furoxans with that ability to stabilize the developing charge of the N-oxide ring possessing increased reactivity.

Scheme 11. Putative mechanism describing products observed from the reaction of the furoxan **9a** with cysteine ^a



^a Putative mechanism describing reaction proposed structures of products observed using UV absorbance chromatogram at 250 nm for **9a** (75 μ M) in the presence of excess cysteine (5 mM) in PBS (50 mM, pH 7.4) at 37 $^{\circ}$ C for 2 h. This reaction products include: 1) the thiol containing adduct, **A**, which is observable by EIC analysis but represents <1 % of the total products based on HPLC-UV peak area; 2) the thiol oxidation product **B**; 3) the reduced ring-opened product **C**; 4) the formation of a keto-oxime **E** necessarily requires loss of a nitrogen oxide (NO_x); 2) thiol may be regenerated after initial ring-opening, resulting in **C**; and 3) initial ring-opening may result. 4) the major *bis*-oxime hydrate **D**; and 5) the keto-oxime, **E** (or its enol tautomer) and loss of NO_x constituted 11 % of the reaction mixture. The relative abundance of each product was measured as: **A** (< 1 %), **B** (14 %); **D** (58 %); **E** (11 %); **9a** remaining (11 %). One peak at \sim 15.0 min was not identified due to poor ionization.

Figure 50. Chromatogram of products from reaction between the furoxan **6a** and cysteine

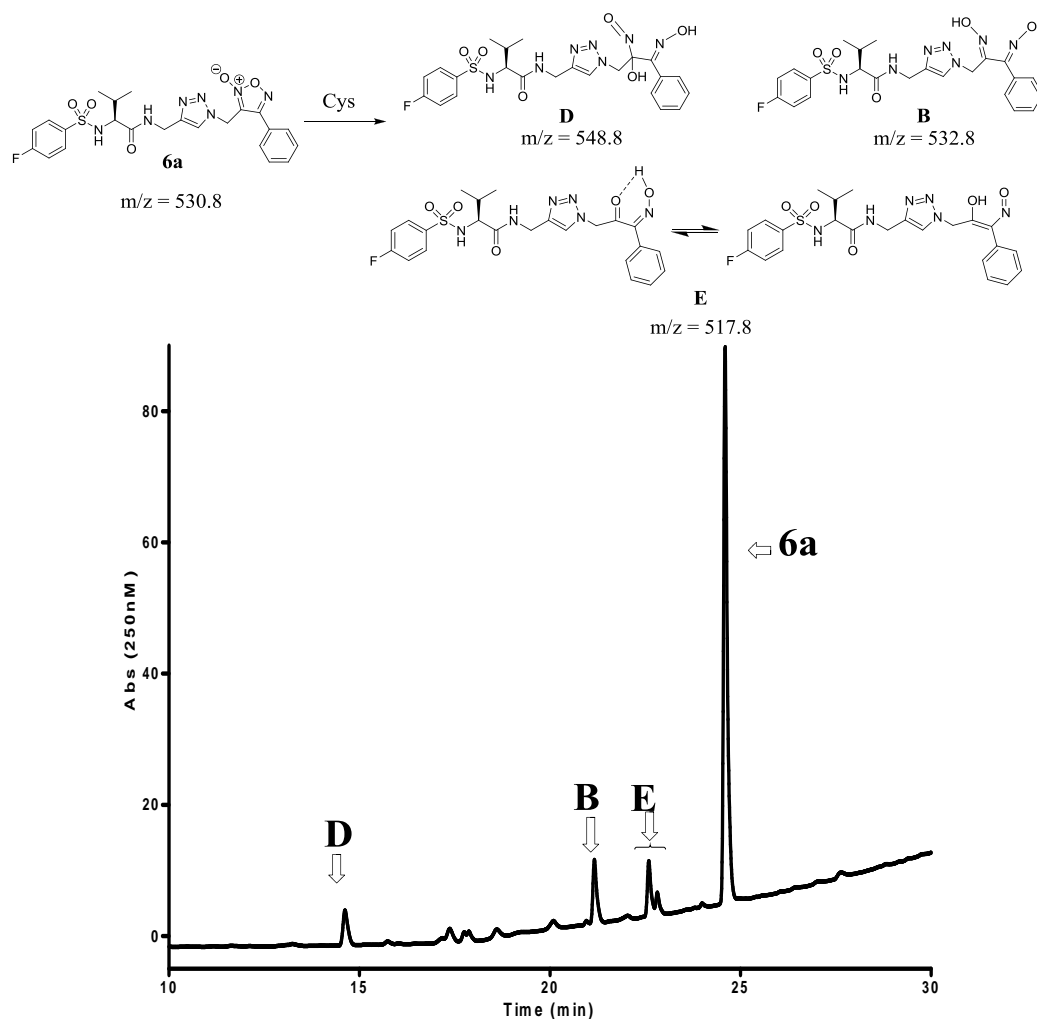


Fig.50. HPLC-UV ($\lambda = 250\text{nm}$) chromatogram of the reaction between **6a** (75 μM) with L-cysteine (2.5 mM) in phosphate buffer (50 mM, pH 7.4) at 37 °C for 2 h. Reaction product structures were proposed based on LC-MS/MS analysis. The reaction products include: 1) thiol oxidation product **B**; the *bis*-oxime hydrate **D**; and the keto-oxime, **E** (or its enol tautomer) and loss of NO_x constituted 11 % of the reaction mixture. The relative abundance of each product was measured as: **B** (10 %); **D** (7 %); **E** (11 %); **6a** remaining (73 %).

Figure 51. Chromatogram of products from the reaction of the furoxan **6c** and cysteine

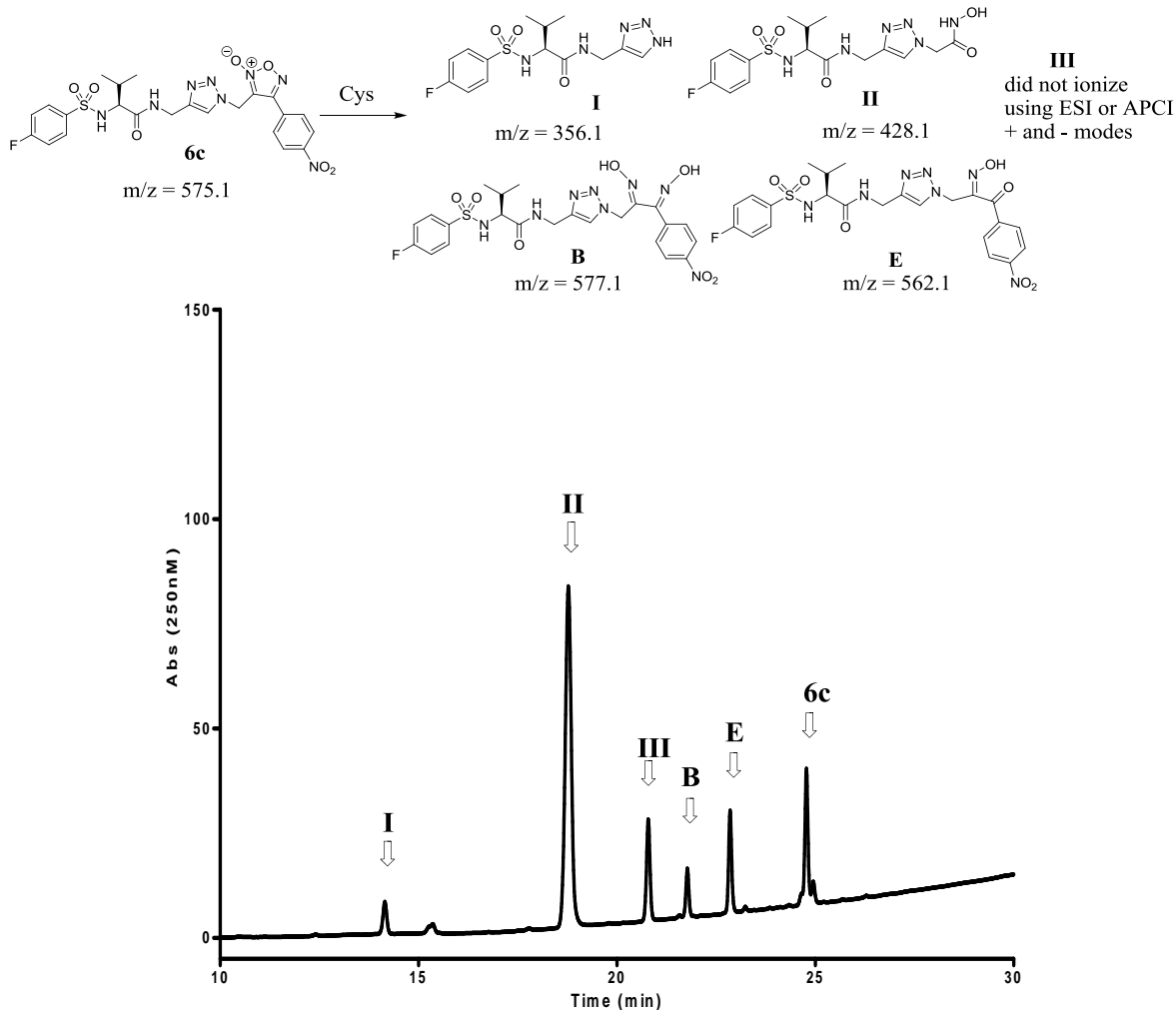


Fig.51. HPLC-UV ($\lambda = 250\text{nm}$) chromatogram of the reaction between **6c** (75 μM) with L-cysteine (2.5 mM) in phosphate buffer (50 mM, pH 7.4) at 37 °C for 2 h. Reaction product structures were proposed based on LC-MS/MS analysis. **6c** gave the most complex reactivity, including the hydroxylamine (**II**) which is speculated as being responsible for the high levels of NO_2^- observed in the greiss assay. The keto-oxime, **E**, accounted for ~ 13% of the total reaction products.

The tautomeric analogs (**7a-c**) have diminished reactivity compared to **6a-c**, and only yield the keto-oxime product proposed to be responsible for NO_x production. Reactions were carried out in a similar manner to those described for **6a-c** in the presence of excess cysteine. Intriguingly, in addition to the tautomeric furoxans **7a-c** possessing markedly reduced reactivity compared to the related furoxans **6a-c**, the only reaction product observed was that of the keto-oxime species, **E**. Comparison of the most reactive furoxan of the entire series, **6c**, with its N-oxide tautomer, **7c**, clearly demonstrates the drastic change in reactivity (Figure 52). Product **E** from the reaction of **6c** and **7c** possesses the same m/z values, similar fragmentation products and identical retention times (Figure 53). A similar observation was made in the comparison of **6a** and **7a** (Figure 54, Figure 55). As described above, the furoxan **6c** gives several reaction products, however, **7c** gives only one product.

For comparison, the reaction product profile of an extensively studied α -cyano-furoxan, 3-cyano-4-phenyl-1,2,5-oxadiazole 2-oxide (**11**), was analyzed under similar conditions. Previous studies of α -cyano-furoxans as anti-cancer agents also included observations of cytotoxicity.(Boiani, Cerecetto et al. 2001) We observed **11** to be highly reactive, with no starting furoxan remaining after 30 min in the presence of excess cysteine (Figure 56). A mechanism of NO release from **11** has been proposed previously, and the major product observed in our incubations corresponded to the oxazole containing cysteine adduct identified by Gasco et al., previously by NMR. Compound **11** is much more reactive than our most reactive furoxan, **6c**. The α -cyano functionality adjacent to the furoxan ring of **11** is electron withdrawing and is clearly responsible for the accelerated reactivity. The neighboring effect by the α -cyano group results in a different reaction product profiles, higher reactivity, and potentially a different mechanism leading to NO_x generation than is seen in our furoxan series.

Figure 52. Comparison of reaction products from **6c** and **7c** with cysteine

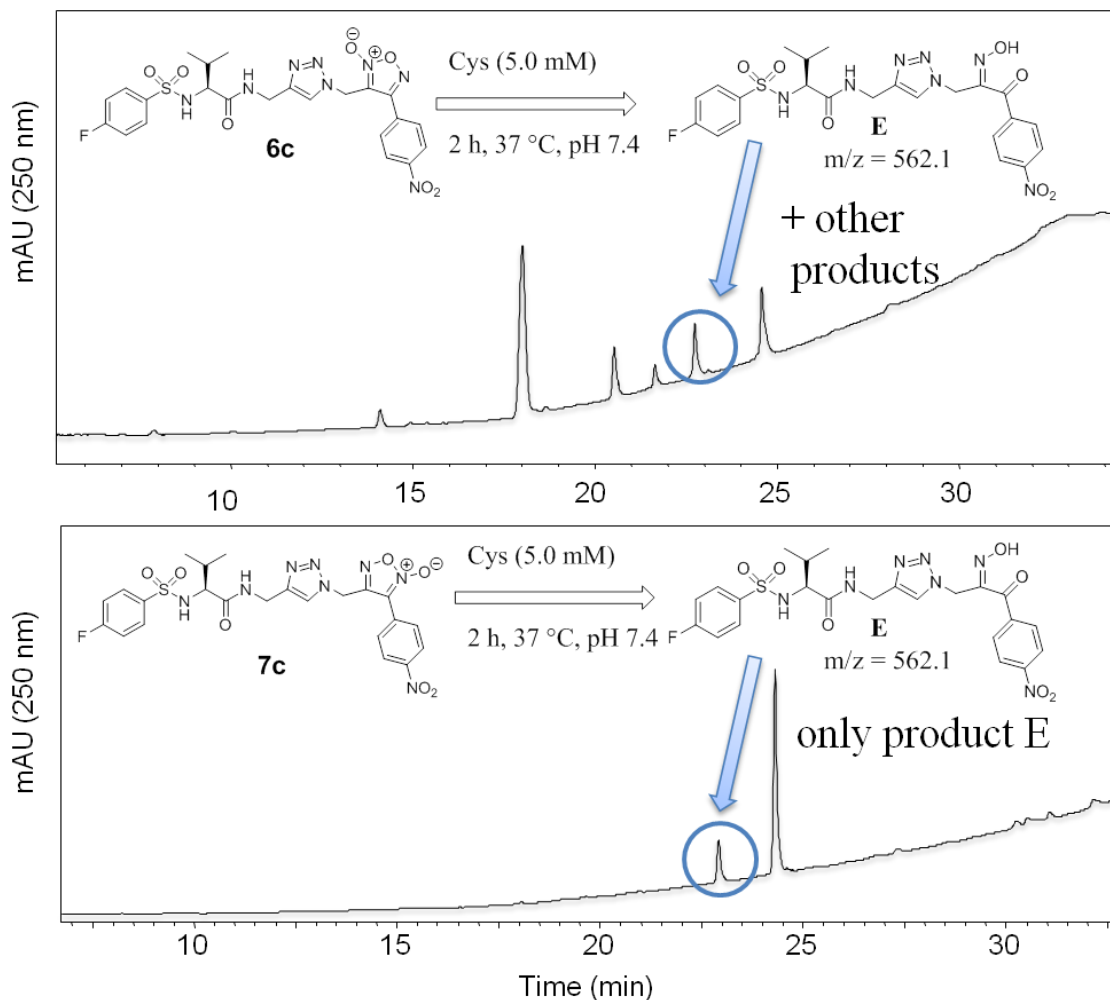


Fig.52. Comparison of the HPLC-UV ($\lambda = 250\text{nm}$) chromatogram of the reaction between **6c** and **7c** (75 μM) with L-cysteine (2.5 mM) in phosphate buffer (50 mM, pH 7.4) at 37 °C for 2 h. Putative structures assigned by LC-MS/MS analysis. While **6c** gave the most complex reactivity, including ~ 13 % of the keto-oxime containing product, **E**, the tautomeric **7c** showed diminished reactivity, and only gave the keto-oxime product.

Figure 53. Mass spectrum of proposed keto-oxime product from **6c** and **7c**

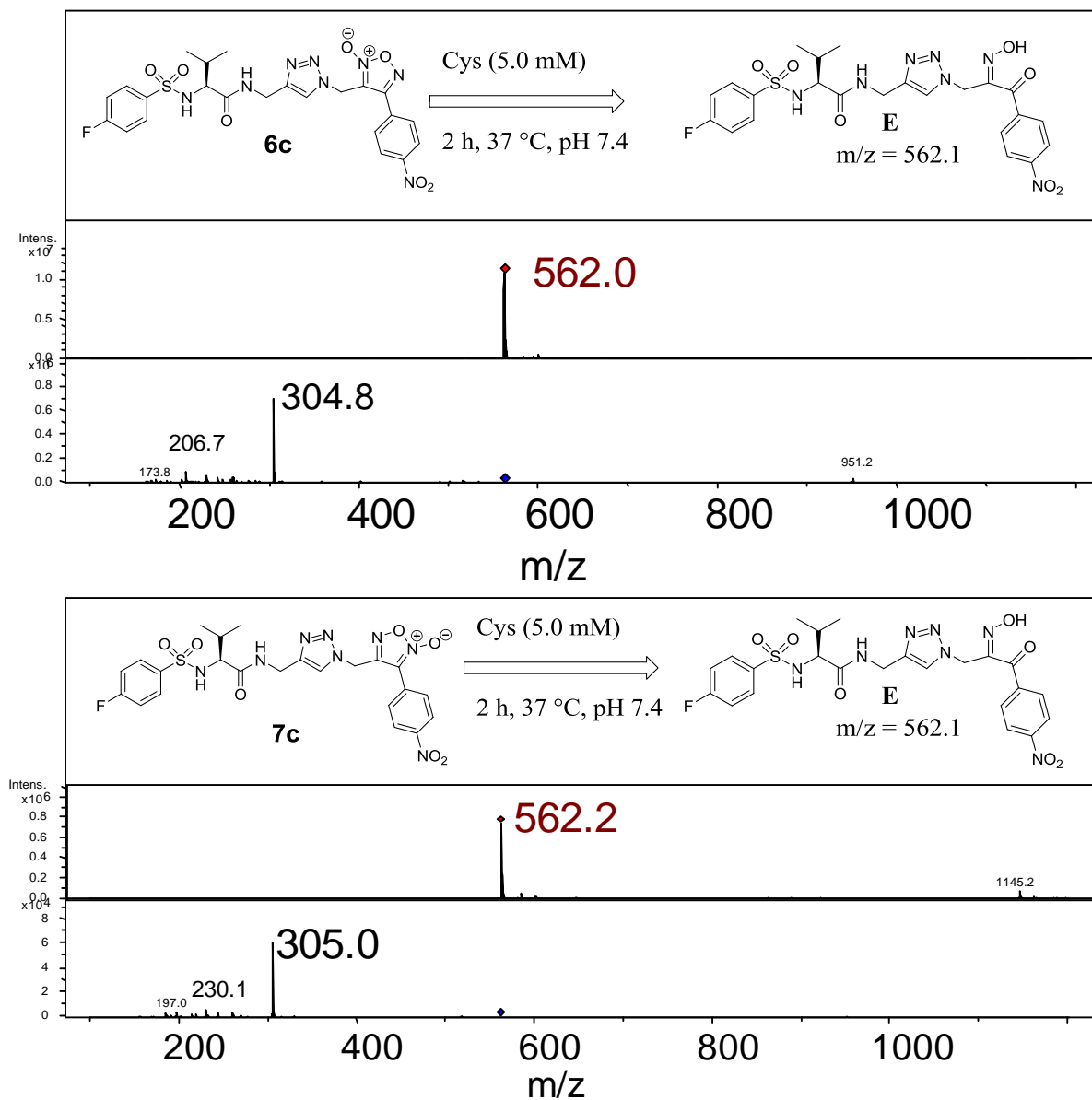


Fig.53. Mass spectrum illustrating the observed m/z values of the keto-oxime product from the reaction of **6c** (top) or **7c** (bottom) with cysteine (ESI (+) mode). Both products have approximately the same m/z value, major fragmentation ion, and retention times.

Figure 54. Comparison of reaction products from **6a** and **7a** with cysteine

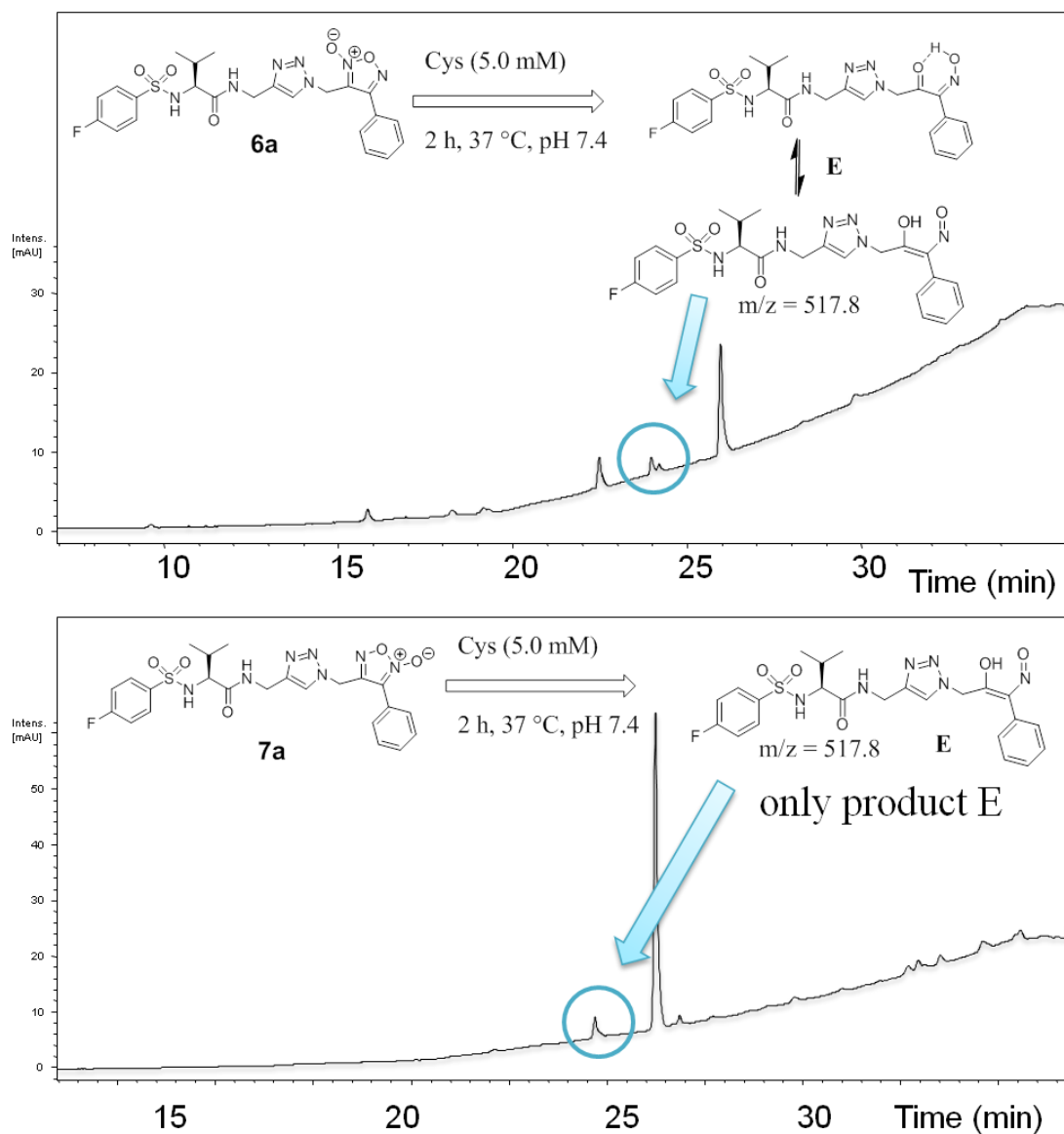


Fig.54. Comparison of the HPLC-UV ($\lambda = 250\text{nm}$) chromatogram of the reaction between **6a** or **7a** (75 μM) with L-cysteine (5.0 mM) in phosphate buffer (50 mM, pH 7.4) at 37 °C for 2 h. Putative structures assigned by LC-MS/MS analysis. **6a** was the only furoxan to appear to give two peaks that correspond to the NOx release product (**E**). **7a** gave only one product as the keto-oxime **E**, but not in tautomeric equilibrium as proposed for **E** from **6a**.

Figure 55. Mass spectrum of proposed keto-oxime product from **6a** and **7a**

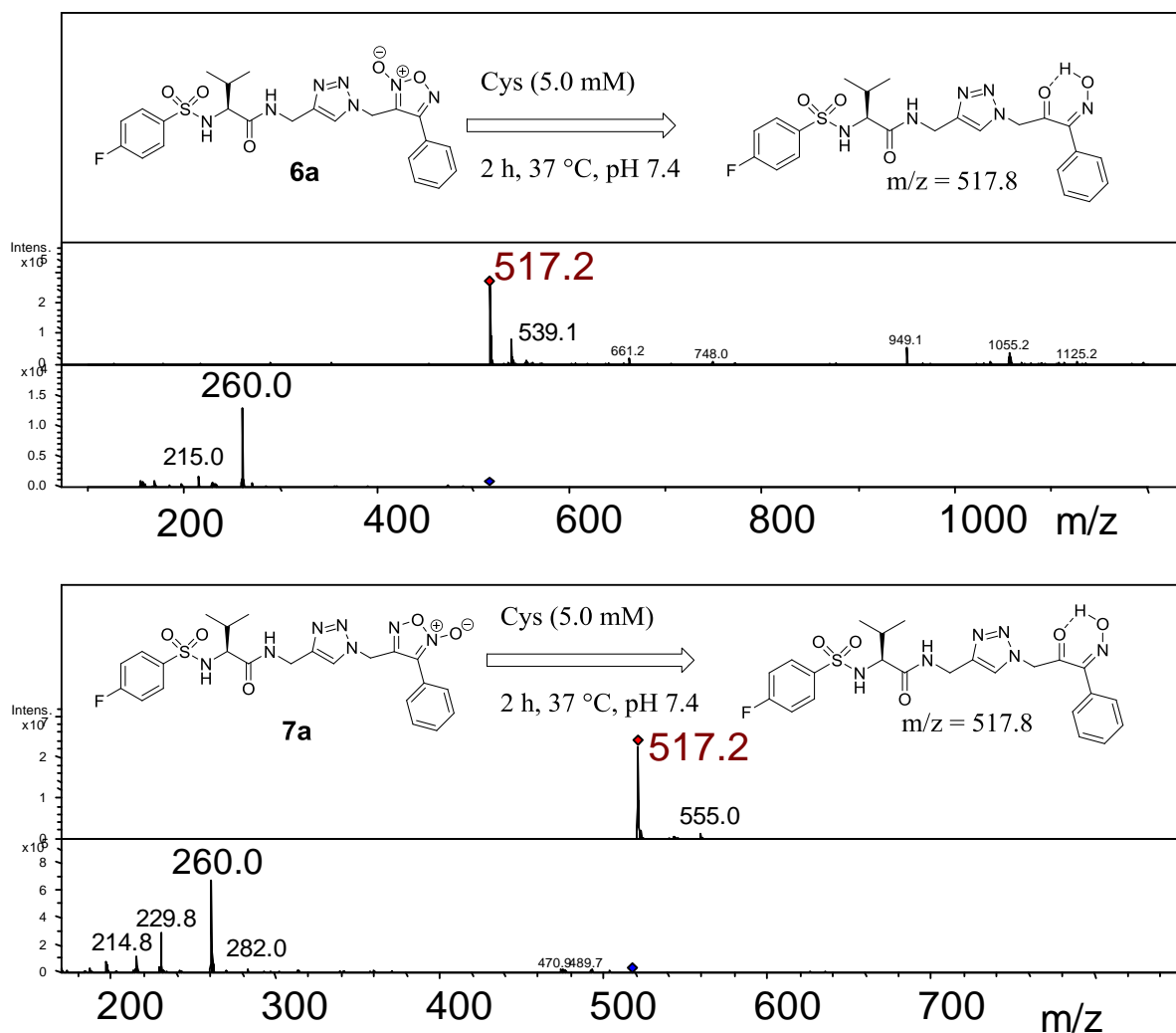


Fig.55. Mass spectrum illustrating the observed m/z values of the keto-oxime product from the reaction of **6a** (top) or **7a** (bottom) with cysteine (ESI (+) mode). Both products have approximately the same m/z value, major fragmentation ion, and retention times. Although the identical m/z supports a shared mechanism of NO_x generation, product **E** from **6a** exists as tautomers, while product **E** from **7a** gives only one peak. Both tautomeric peaks for the **E** product observed for **6a** gave identical m/z values.

Figure 56. Chromatogram of products from reaction between the furoxan **11** and cysteine

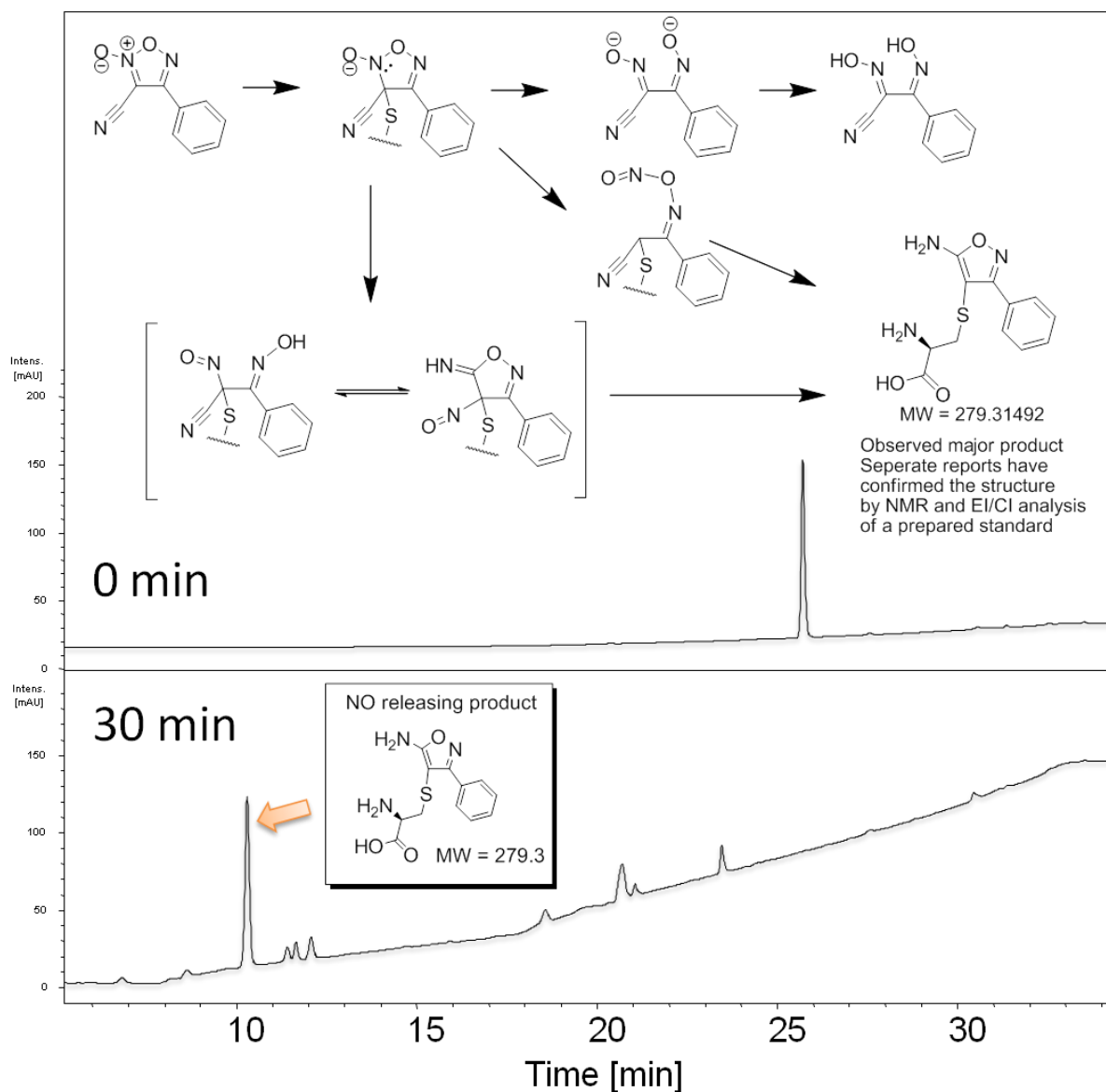


Fig.56. Top: Proposed mechanism by Gasco et al., to explain the formation of the oxazole thiol adduct. The chromatograms show **11** prior to cysteine addition (time = 0 min) and the resulting reaction products after 30 min with excess cysteine. **11** completely reacts after 30 min, and the m/z of the major product corresponds to the oxazole product previously reported for **11**. The furoxan **11** is much more reactive than even our most reactive furoxan, **6c**.

To gain further mechanistic understanding about the formation and existence of the keto-oxime product (**E**), we performed isotope labeling studies utilizing H_2^{18}O . Incubations were carried out similarly to those used for mechanistic analysis, with the implementation of H_2^{18}O . **6c** or **7c** (150 μM) were incubated in equal volumes of PBS (50 μM , pH 7.4)/ H_2O or H_2^{18}O in the presence of excess cysteine (5 mM) at 37 °C for 2 h. Reaction aliquots were analyzed by HPLC-MS/MS. Control experiments containing the naturally abundant ^{16}O afforded the aforementioned keto-oxime product, **E**, with a $[\text{M}+\text{H}^+]$ of 562.2 m/z (Figure 57, Figure 58). Interestingly, we observed implementation of ^{18}O into the product corresponding to **E**, with a mass of 564.2 m/z . The ratio of ^{16}O : ^{18}O incorporated in **E** was proportional to the relative amounts of PBS/ H_2O or H_2^{18}O , approximately 1:1. These results clearly demonstrate that the -OH in **E** originates from H_2O , and not from molecular O_2 , or a complex and unlikely rearrangement of the parent N-Oxide moiety itself. Despite the distinctive differences in the reactivity of **6c** and **7c**, the incorporation of ^{18}O into **E** is equivalent in both instances, suggesting a common mechanistic pathway leading to the formation of the keto-oxime product, and correspondingly, NO_x related biological activity. This is in agreement with the hypothesis of a shared mechanistic pathway leading to the NO_x release previously discussed for the initial comparison of **6c** and **7c** reactivity.

Figure 57. Mass spectrum demonstrating incorporation of ^{18}O into keto-oxime product of **6c**

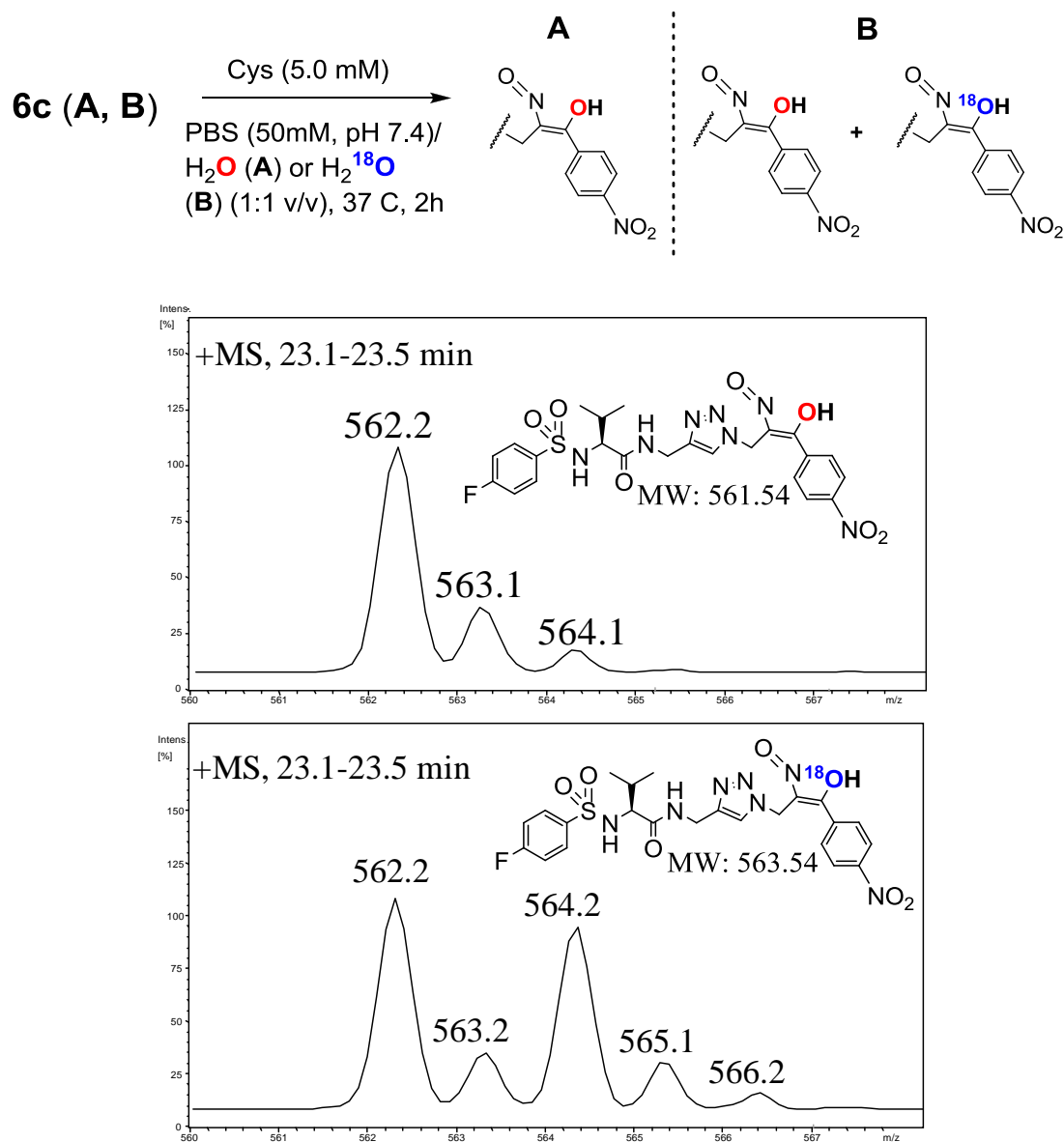


Fig.57. Mass spectrum demonstrating incorporation of ^{18}O into **E** generated from the reaction of **6c** with cysteine (ESI (+) mode). **6c** (150 μM) incubated with cysteine in PBS (50 μM , pH 7.4)/ H_2O (**A**) or H_2^{18}O (**B**) (1:1 [v/v]) for 2 h at 37 $^\circ\text{C}$. ^{18}O was incorporated at approximately the same ratio as the $\text{H}_2\text{O}/\text{H}_2^{18}\text{O}$ used in the incubation.

Figure 58. Mass spectrum demonstrating incorporation of ^{18}O into keto-oxime product of **7c**

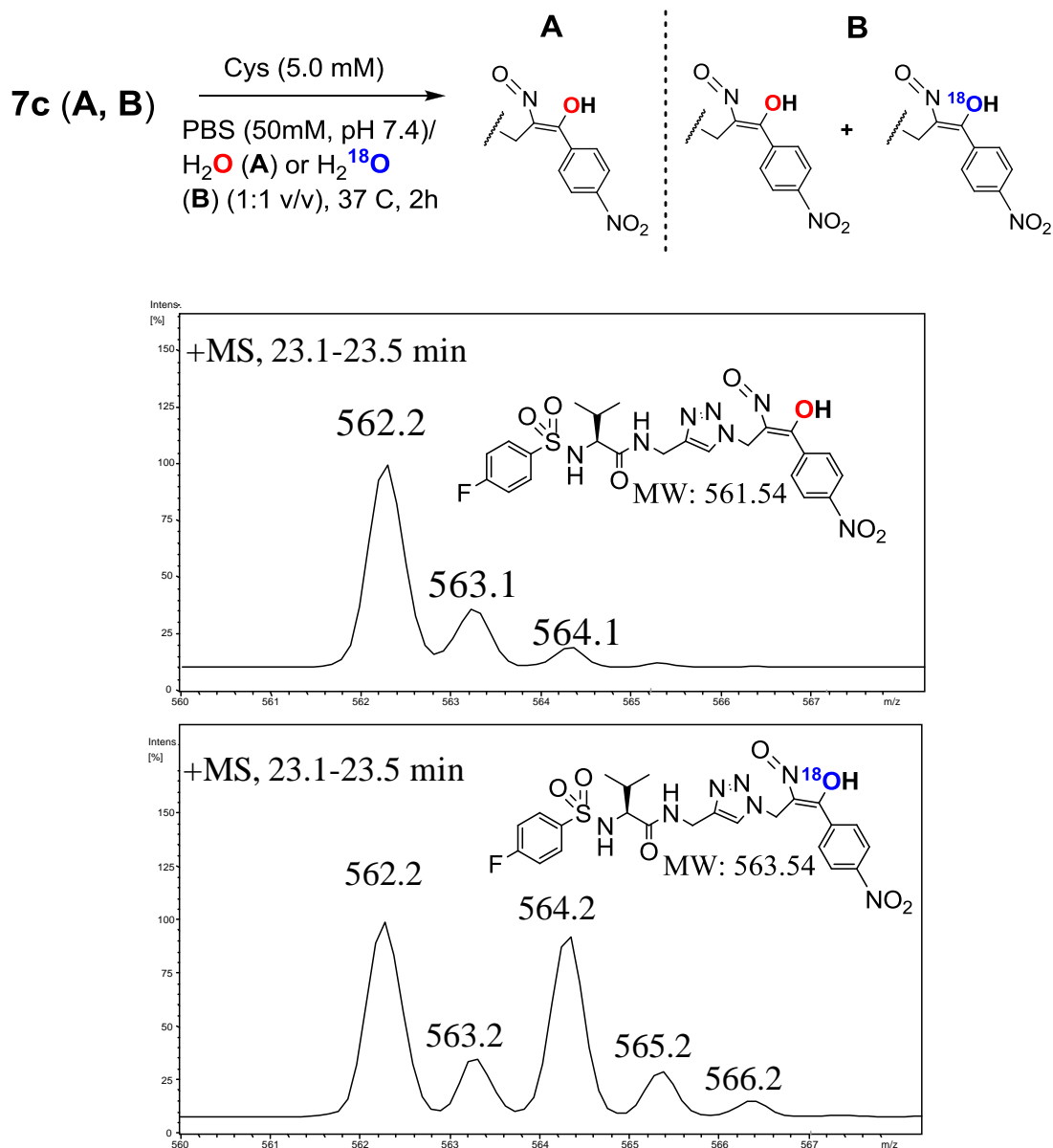


Fig.58. Mass spectrum demonstrating incorporation of ^{18}O into **E** generated from the reaction of **7c** with cysteine (ESI (+) mode). **7c** (150 μM) incubated with cysteine in PBS (50 μM , pH 7.4)/ H_2O (**A**) or H_2^{18}O (**B**) (1:1 [v/v]) for 2 h at 37 °C.

2.3 NO₂⁻ production

The analysis of the reaction of **9a** with cysteine identified reaction products expected for thiol regeneration, thiol oxidation, and loss of NO_x (Scheme 11). It has been reported previously that formation of inorganic nitrite, as a measure of NO_x release, in the presence of excess cysteine (5 mM), showed reasonable correlation with vascular tissue relaxation for a series of furoxans. (Ferioli, Folco et al. 1995) In a similar fashion, the Griess assay for NO₂⁻ was used to analyze reactions of furoxans (250 μM) with cysteine (2.5 mM) in a 1:1 solution of CH₃CN: PBS (50 mM, pH 7.4) at 37 °C after 24 h. Additional kinetic examination of NO₂⁻ production was carried out and the rate of NO₂⁻ production corresponds with quantitative NO₂⁻ production, which plateaus after 24 h. In agreement with the reported stability of furoxans in aqueous media, control incubations performed under identical conditions in the absence of cysteine gave no measurable NO_x production (data not shown). The furoxans studied yielded between 2-80 % mol equivalents of NO₂⁻ over the reaction time studied (TABLE XIII). The oxadiazole-2N-oxides **6a-c** yielded considerably more NO₂⁻ than the tautomeric **7a-c**. The *p*-OCH₃ substituted furoxans (**4**, **5**, and **6b**) also gave much larger amounts of NO₂⁻ compared to both the tautomeric, **7a-c**, and the methylenamine containing **9a-b**. For comparison, the bioactivation of a well studied α-cyano-furoxan, 3-cyano-4-phenyl-1,2,5-oxadiazole 2-oxide (**11**), was analyzed under similar conditions. A recent extensive study of furoxans as anti-parasitic agents, converged on **11** and other α-cyano-furoxans as drug candidates. (Rai, Sayed et al. 2009) Previous studies of α-cyano-furoxans as anti-cancer agents also included observations of cytotoxicity. (Boiani, Cerecetto et al. 2001) As might be expected if higher concentrations of NO_x lead to toxicity, **11** generated large amounts of NO₂⁻ on reaction with cysteine. Again as anticipated, the furazan **10** provided a negative control for NO₂⁻ release.

TABLE XIII**NO₂⁻ PRODUCTION FROM FUROXANS AFTER 24 H WITH EXCESS CYSTEINE^a**

Entry	NO ₂ ⁻ production (μM) ^a	NO ₂ ⁻ production as % (mol/mol) ^b
2a	9.2 (±0.1)	18.4 %
2b	5.1 (±0.1)	10.4 %
2c	14.8 (±0.8)	29.6 %
3	40.1 (±0.8)	80.2 %
4	6.3 (±0.1)	12.6 %
5	9.7 (±0.1)	19.4 %
6a	6.8 (±0.1)	13.6 %
6b	3.9 (±0.7)	7.8 %
6c	21.8 (±0.5)	43.6 %
7a	1.0 (±0.4)	2.0 %
7b	1.8 (±0.1)	3.5 %
7c	1.3 (±0.1)	2.5 %
9a	1.2 (±0.2)	2.4 %
9b	0.5 (±0.1)	1.0 %
10	0.0 (±0.1)	0 %
11	29.1 (±0.3)	58.2 %

^a Time course of nitrite production upon incubation of cysteine (2.5 mM) with the appropriate furoxan (250 μM) at 37 °C in PBS (50 mM, pH 7.4). Aliquots were analyzed at (1, 2, 4, 8, 12, 18, and 24 h). Observed rate constants calculated using linear regression analysis of 1-18 h time points.

2.4 Thiol oxidation

NO-mediated *S*-nitrosation of active site cysteines is an important step in the regulation of several proteins involved in cytoskeletal remodeling and cellular apoptosis. (Melino, Bernassola et al. 1997; Ascenzi, Salvati et al. 2001; Ascenzi, Bocedi et al. 2004) Moreover, *S*-nitrosation may potentially result in NO facilitated cysteine oxidation, leading to mixed disulfide formation. As discussed earlier, thiol-induced breakdown of furoxans may lead to thiol oxidation, thiol regeneration, or thiol alkylation (Scheme 11). DTNB (5,5'-dithiobis-2-nitrobenzoic acid or Ellmans Reagent) was used to quantify free, reduced cysteine after incubation of selected furoxans (250 μ M) with cysteine (2.5 mM). In normoxic solution, air oxidation of cysteine in the absence of furoxan leads to complete loss of reduced thiol within 12 h (Figure 59). Accordingly, a high degree of background cysteine oxidation was observed upon incubation of cysteine with selected furoxans over 4 h, necessitating the need for a more intricate experiment to examine the reaction of furoxans with cysteine.

To obtain a more quantitative measure of furoxan-mediated cysteine consumption, oxygen was depleted by bubbling with O₂-free N₂ in sealed reaction vials, followed by assay of free cysteine after reaction for 2 h (TABLE XIV). A plot of cysteine consumption versus NO₂⁻ production showed no correlation (Figure 60). Of the substituted-phenyl furoxans, **6c** gave the highest amounts of NO_x release, but the lowest cysteine consumption, confirming the disconnection between thiol consumption and NO_x release from furoxans, which is predicted by the mechanism shown in Scheme 11.

Figure 59. Depletion of reduced cysteine in the presence of furoxans

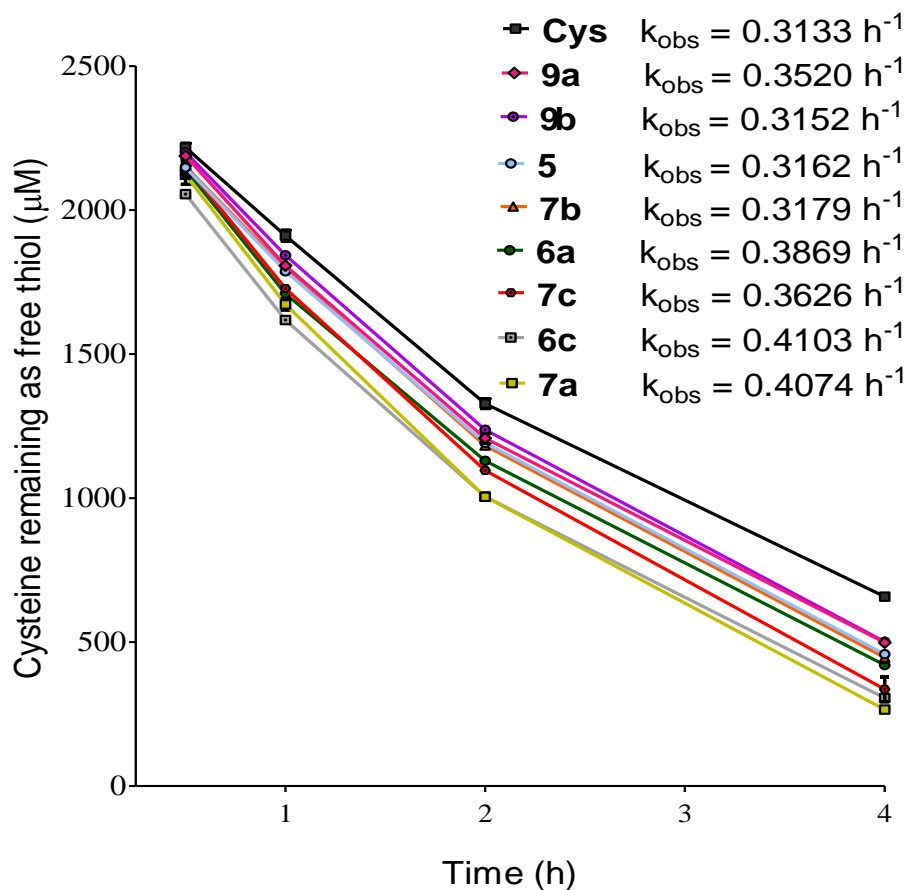


Fig.59. Cysteine remaining as free thiol upon incubation of cysteine (2500 μM) with the appropriate furoxan (250 μM) for 4 h under normoxic conditions at 37 $^{\circ}\text{C}$ in PBS (50 mM, pH 7.4)/ CH_3CN (1:1), with 1 mM EDTA. Reduced cysteine quantified using UV absorbance following treatment with DTNB solution.

TABLE XIV
CYSTEINE REMAINING AFTER 2 H INCUBATION WITH FUROXANS UNDER
HYPOXYIC CONDITIONS^a

Entry	Cys as free thiol (mM) ^a	Cys depletion as % (mol/mol) ^b
-	2267.2 (\pm 153.7)	-
4	1788.8 (\pm 18.7)	21.1 %
5	1410.1 (\pm 23.8)	37.8 %
6a	1790.8 (\pm 38.6)	21.0 %
6b	1830.4 (\pm 16.6)	19.2 %
6c	1995.2 (\pm 26.1)	12.0 %
7a	1724.4 (\pm 26.1)	23.9 %
7b	1507.2 (\pm 29.5)	33.5 %
7c	1620.4 (\pm 26.6)	28.5 %
9a	1812.1 (\pm 33.4)	20.1 %
9b	1724.4 (\pm 59.0)	23.9 %
10	1742.8 (\pm 23.3)	23.1 %

^aFree cysteine remaining in incubations containing furoxans (250 μ M) and cysteine (2.5 mM) after 2 h under hypoxic conditions at 37 °C in PBS (50 mM, pH 7.4)/ CH₃CN (1:1), with EDTA (1 mM). ^bCysteine depletion relative to the control, represented as percent cysteine depletion mol/mol.

Figure 60. Correlation between cysteine depletion and NO_2^- production

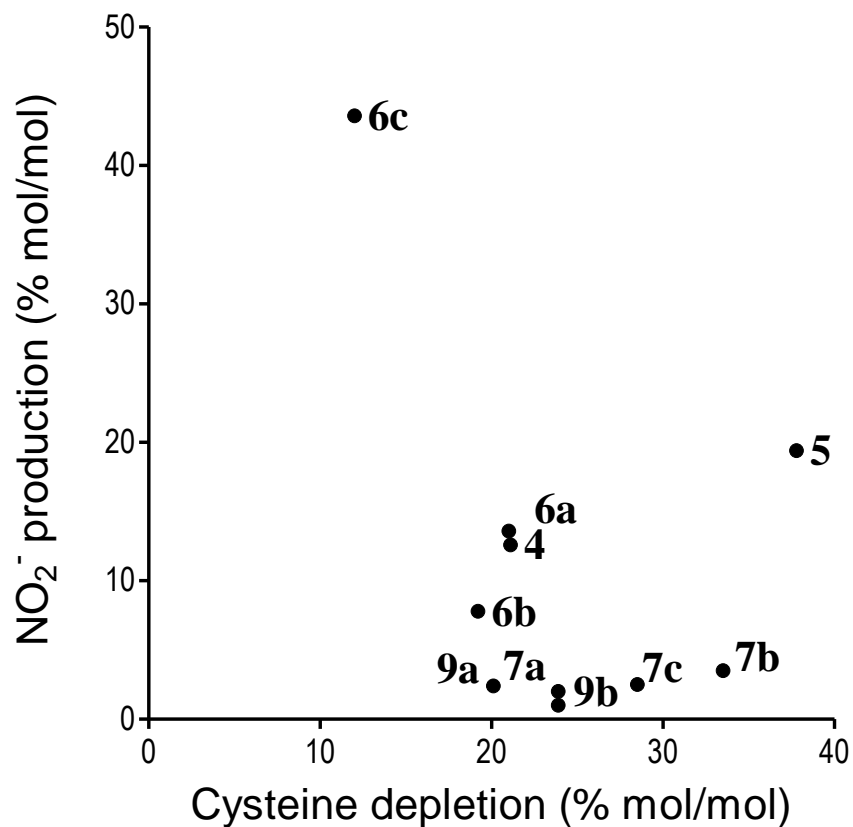


Fig.60. No correlation exists between NO_2^- production and cysteine depletion by selected furoxans. Cysteine remaining as free thiol upon incubation of cysteine (2.5 mM) with the appropriate furoxan (250 μM) for 4 h under normoxic conditions at 37 °C in PBS (50 mM, pH 7.4)/ CH_3CN (1:1), with 1 mM EDTA. Reduced cysteine quantified using UV absorbance following treatment with DTNB solution.

2.5 Neuroprotection

Neuroprotection was evaluated by 3-(4,5-dimethylthiazol-2-yl)2,5-diphenyl-tetrazolium bromide (MTT) assay of cell viability in primary rat neuronal cell cultures subjected to oxygen glucose deprivation (OGD). (Loo, Rillema et al. 1998) OGD provides a cellular model of ischemia and reperfusion injury leading to apoptotic cell death, providing a model for excitotoxic loss of neurons in neurodegenerative diseases such as ischemic stroke and AD. (Goldberg, Strasser et al. 1997) Neurons were subjected to OGD for 2 h, followed by reoxygenation and replacement with nutrient rich media containing furoxans (50 μ M) or vehicle control. After 24 h incubation, considerable neuroprotective activity was seen for several compounds (Figure 61); including the **6a-c** and **7a-c** subsets, which of NO_x generation are capable of eliciting a biological response. **3** was not tested for neuroprotection due to limitations in aqueous solubility. Interestingly, while the majority of compounds showed significant neuroprotective activity, a few furoxans showed toxicity, including the azide family (**2a-c**) that elicited a ~60-75 % loss of viability compared to the DMSO vehicle control, and the carbazole derivative, **5**, which resulted in total cell death, and reduced the MTT response to baseline (data not shown). Furthermore, the furazan analog, **10**, was also observed to be toxic. Since furazans are thiophilic, but cannot release NO_x, this would again support a mechanism of neuroprotection via NO_x production, rather than other mechanisms dependent on oxidation or alkylation of active site protein thiols, such as those of cysteine proteases (i.e. calpain, cathepsin B, or apoptotic caspases).

A trend between NO₂⁻ release and neuroprotection was tentatively identified (Figure 62). This correlation is in agreement with the concept that low levels of NO are essential for normal neuronal physiological activity, whereas high concentrations of NO can lead to cellular apoptosis and cell death. Notable outliers from this tentative correlation (**5**, **6c**) require special

considerations: 1) compounds may possess cytotoxic or neuroprotective activity through pathways other than NO signaling, and this seems to be the case for highly toxic **5**; 2) Although NO_2^- production by furoxans has been reported to correlate with biological NO signaling, in some instances NO_2^- may not give an accurate portrayal of biologically relevant NO_x production. This fact is accurately depicted by **6c**, which would be expected to be highly toxic according to its abundant NO_2^- generation, but is actually neuroprotective. **6c** possesses uncommonly high reactivity compared to the other furoxans tested, leading to an atypical reaction product profile; including a hydroxylamine containing product not seen for other furoxan studied, and is most likely responsible for the copious NO_2^- production of **6c** (Figure 51).

Further support of the involvement of the NO/sGC pathway was achieved following a second series of neuroprotection experiments utilizing ODQ, a potent and selective sGC inhibitor. Following the protocol above, after OGD primary neurons were incubated with **9a** (50 μM) and/or ODQ (10 μM). Blockade of cGMP formation by ODQ completely abolished the neuroprotective activity observed for **9a** alone, while treatment with ODQ in control groups showed no significant impact on cell survival or toxicity (Figure 63). These findings strongly support the involvement of a cGMP-dependent neuroprotective mechanism driven by NO_x production from an attenuated furoxan core and are consistent with data below from *ex vivo* LTP experiments.

Figure 61. Neuroprotection by furoxans in primary neurons following OGD

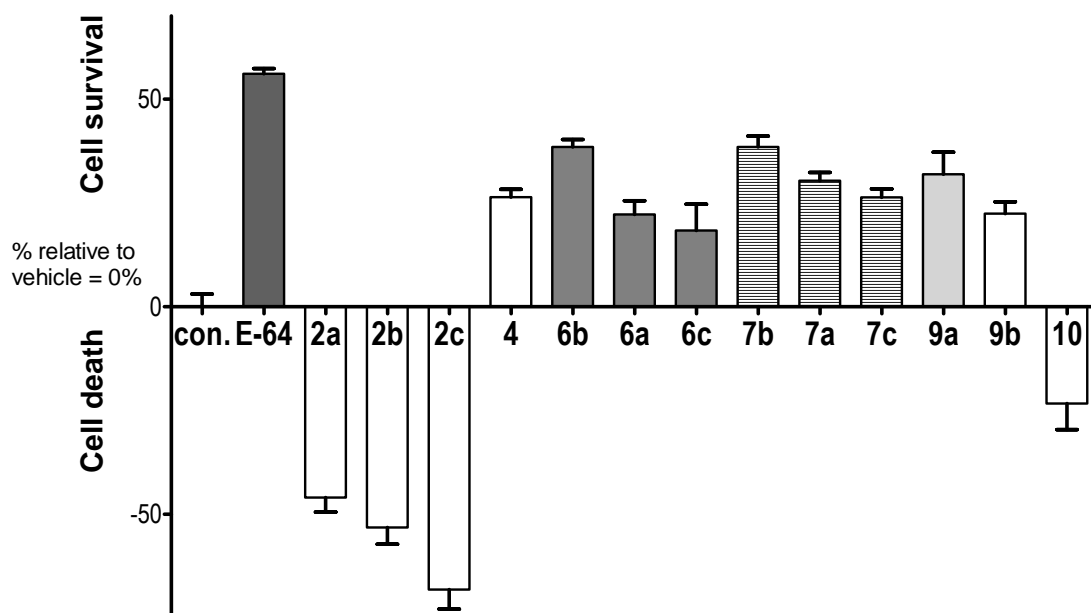


Fig.61. The effect of selected furoxans on cell survival in primary rat cortical neurons.

Primary neurons were placed in a hypoxic chamber with oxygen free media for 2 h. The cell media was replaced with nutrient rich media at atmospheric O₂ levels, and treated with the appropriate compound (50 μ M) for 24 h following. Cell viability was measured using the MTT assay of mitochondrial function. Values represent survival as % of the DMSO treated control from MTT assay (for each experiment n = 6, error is represented as mean + SEM).

Figure 62. Tentative correlation between NO_2^- production and neuroprotection

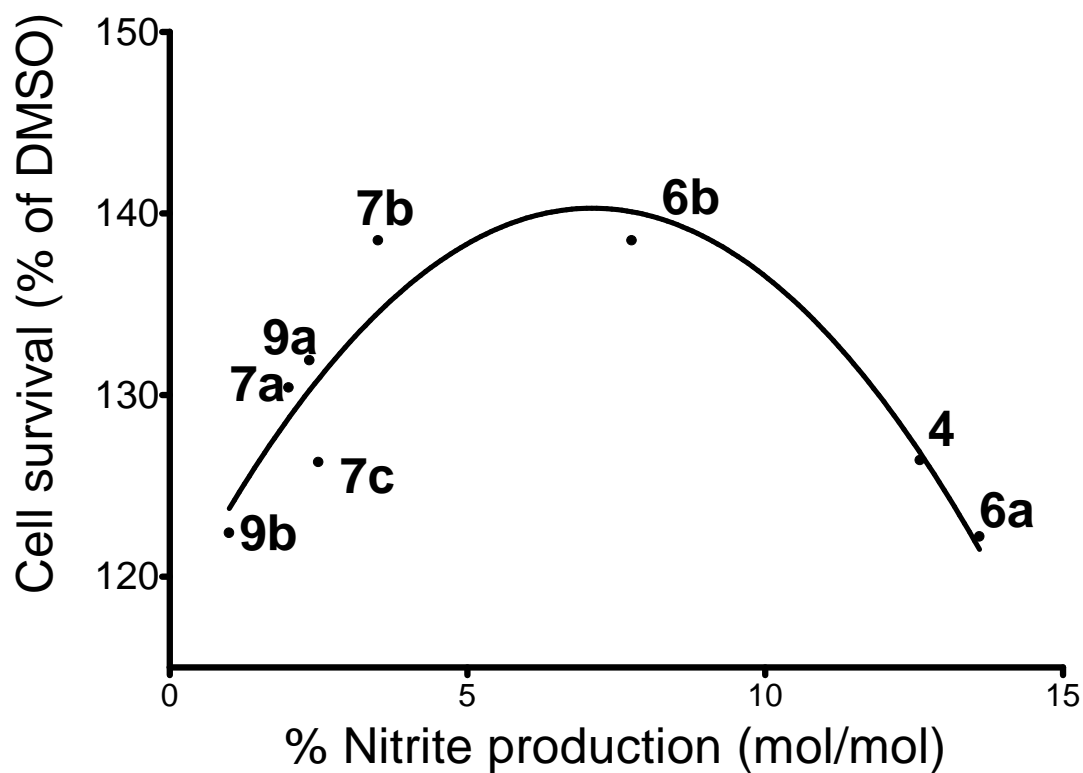


Fig.62. A tentative correlation is observed between NO_2^- production (% mol/mol) and cell survival (% of control). The ability of ODQ to abolish neuroprotective activity suggests a NO_x related mechanism of action. The tentative correlation between NO_2^- production and % survival is supported by the common observed disparity in the neuroprotective effects of NO at low concentrations, and the cytotoxic effects of NO at high concentrations.

Figure 63. Neuroprotection by furoxans in the presence of ODQ

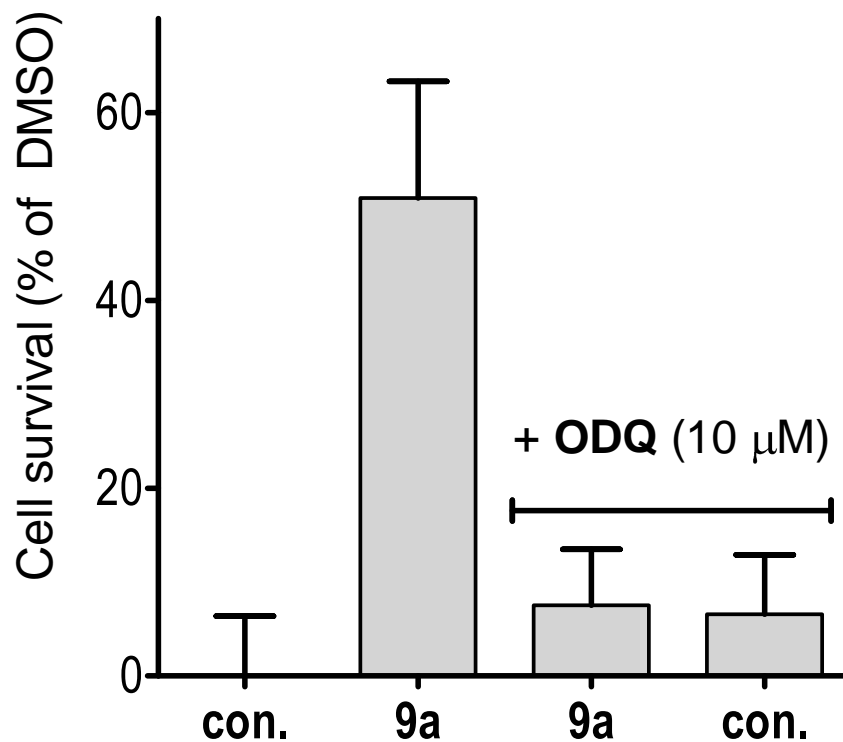


Fig.63. Primary neurons were placed in a hypoxic chamber with oxygen free media for 2 h. The cell media was replaced with nutrient rich media at atmospheric O₂ levels, and treated with the furoxan **9a** (50 μM), **9a** (50 μM) + ODQ (10 μM), and ODQ (10 μM) treated control. Values represent survival as % of DMSO treated control from MTT assay. Cell viability was measured using the MTT assay of mitochondrial function. Values represent survival as % of the DMSO treated control from MTT assay (for each experiment n = 6, error is represented as mean + SEM).

2.6 Restoration of Synaptic Function

LTP in the Schaffer collateral pathway of the hippocampus is a cellular model of learning and memory (for review see (Kandel 2001)), which is significantly impaired after perfusion with oligomers of A β .(Lambert, Barlow et al. 1998) A β induced inhibition of LTP is reversed by diazeniumdiolate NO-donors via a mechanism shown to be mediated by the NO/sGC signaling pathway.²⁸ CREB is essential for memory consolidation and NO has been shown to increase its phosphorylation by activating a number of diverse kinases through cGMP production.(Arancio, Kiebler et al. 1996) The peptidomimetic furoxan 9a was selected for the study of LTP restoration in hippocampal slices on the basis of: 1) an excellent neuroprotection (Figure 61); 2) the confirmed involvement of the NO/sGC pathway in 9a (Figure 63); and 3) desirable physiochemical properties for CNS compared to the other furoxan analogs studied (MW < 450, clogP = 2.9). It was hypothesized that 9a should possess the ability to restore synaptic function in hippocampal slices co-perfused with oligomeric A β .

In accordance with previous data and the hypothesis that NO_x release from furoxans is able to restore brain function, 9a was found to completely abrogate A β induced synaptic deficits in LTP; synaptic response to LTP induction was restored to levels matching those of untreated wild-type controls (Figure 64). This novel bioactivity of furoxans implicate the NO/sGC/CREB pathway as being activated in hippocampal slices, *in simile* with other NO-donors and further supports development of furoxans as therapeutics in dementia and neurodegeneration. These novel activities of furoxans are likely through stimulation of the NO/cGMP/CREB cascade, due to the loss of neuroprotective effects upon co-administration of ODQ. As a result, we conclude that S-nitrosation of pro-apoptotic caspases by furoxans likely has negligible impact on cell viability, although this was not directly measured. As mentioned early for calpain

Figure 64. LTP restoration by the furoxan **9a** following co-perfusion with oligomeric A β

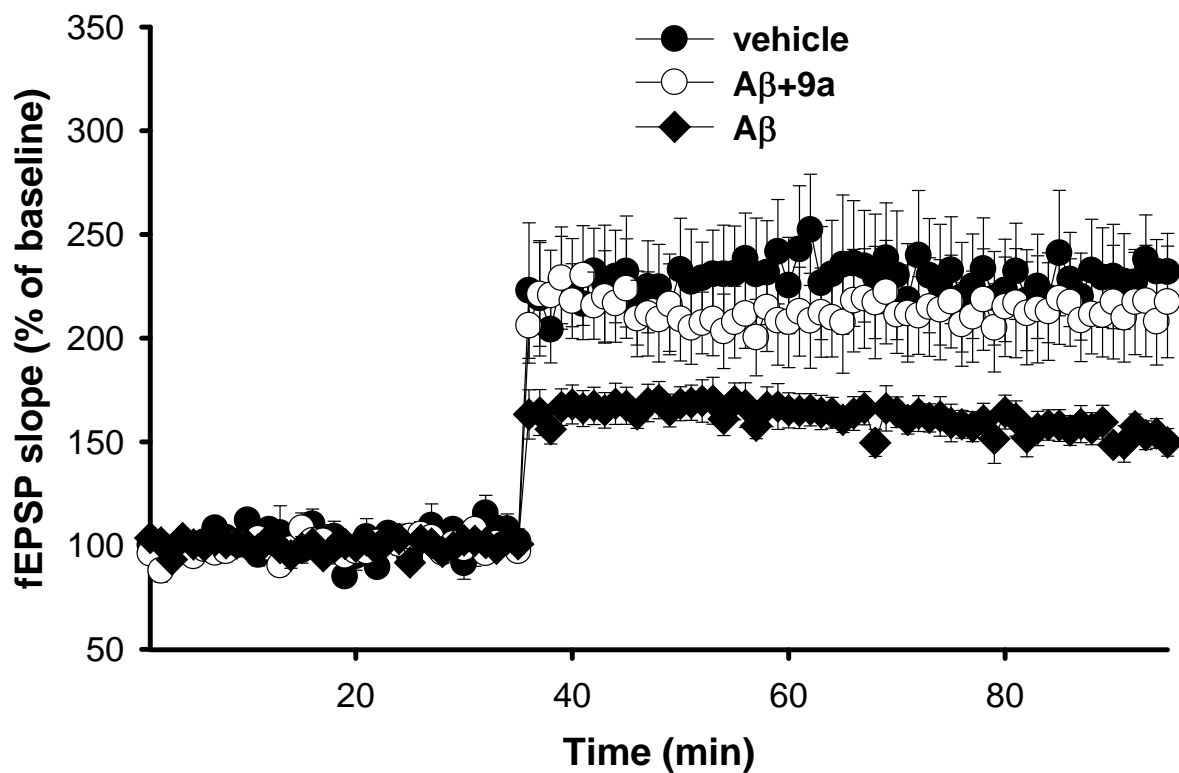


Fig.64. Restoration of long term potentiation by **9a** (1 μ M) in hippocampal slices perfused with oligomeric A β (200 nM) [for each experiment n = 7]. **9a** was able to restore synaptic transmission deficits caused by A β .

inhibitors, molecules that are capable of restoring synaptic function through CREB phosphorylation, such as furoxans, create an attractive pathway for AD therapy. Amplified BDNF expression by NO-mimetics has been validated in the past, and procognitive agents capable of increasing BDNF through CREB phosphorylation hold distinct potential as non-A β targeted therapeutic approaches.

This study yielded proof of concept results for the potential of attenuated furoxans as procognitive and neuroprotective agents. The physiochemical properties of the peptidomimetics employed are likely detrimental to brain bioavailability. A second round of compound optimization focusing on attenuated (*p*-OCH₃-Aryl) furoxans with varying adjacent cap groups to impart advantageous physiochemical properties is preferable prior to *in vivo* safety, efficacy, and PK studies.

3. Discussion

3.1 Correlating NO_x release and Neuroprotection

A tentative correlation was assigned between NO_x release versus the observed neuroprotection. Based on this correlation, the furoxan **6c** would have been speculated to be highly toxic. However, **6c** was found to have moderate neuroprotective activity. The instance of **6c** was considered to be an outlier for the correlation of neuroprotection and NO₂⁻ production based on its uncommonly high reactivity leading to an atypical reaction product profile. The furoxan N-oxide tautomer of **6c**, **7c**, was much less reactive than **6c**, and yielded only the keto-oxime product, **E**, proposed to be responsible for NO_x production. **7c** was found to be neuroprotective, suggesting that product **E** is likely responsible for biologically relevant NO_x production. The incorporation of ¹⁸O from H₂¹⁸O into the **E** species of **6c** and **7c**, along with

comparable m/z fragmentation patterns and retention times supports a shared chemical mechanism leading to the creation of the keto-oxime **E**. Therefore, it is likely that the relative production of **E** from **6c** may correlate with neuroprotective activity. **6c** gave some products that were not seen for any of the other derivatives studied, namely a hydroxylamine containing molecule which represents ~55 % of total products, which is presumably the end product of a mechanism that results in copious NO_2^- production. For example, adding the relative molar amount of **E** produced by **6c** (~ 13 %) into the neuroprotection vs NO_2^- (mol/mol) prediction seems to fit the correlation (Figure 65). Future studies might consider trying to correlate the rate of formation of the NO_x release product as a better predictor of neuroprotection than NO_2^- .

Figure 65. Correlation of NO_2^- production and neuroprotection including **6c** NO_x product

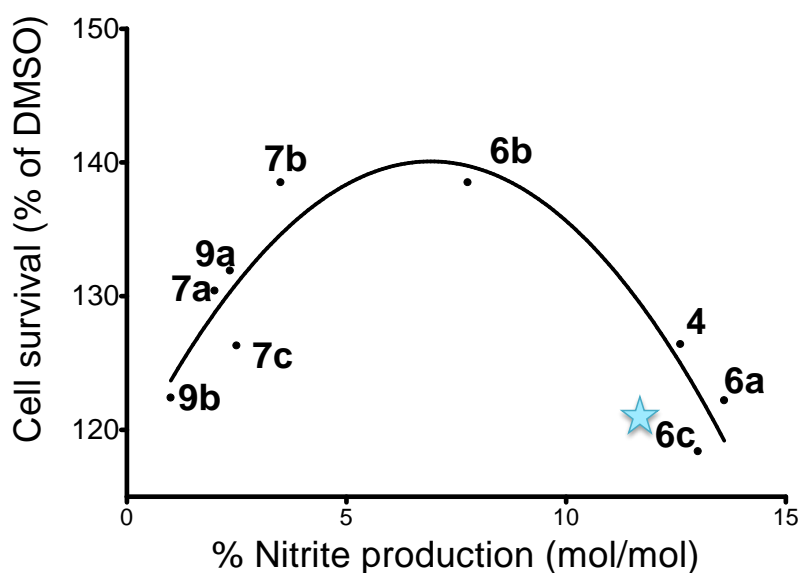


Fig.65. A tentative correlation is observed between NO_2^- production (% mol/mol) and cell survival (% of control). NO_2^- is represented as mol/mol. Reactivity analysis demonstrated that **6c** give approximately 13 % of the keto-oxime product, **E**, which is proposed to be responsible for biologically relevant NO_x production. Incorporation of the relative amount of product **E** from **6c** maintains the correlation.

3.2 Potential of Attenuated Furoxans as Novel Neuroprotective Agents

Furoxans have been the subject of intensive research efforts over the past 20 years due to a range of biological activities; however, most of these attempts focus on utilizing the cytotoxic effects of large concentrations of NO. An attenuated furoxan holds unrealized potential as a potential neuroprotective agent. Here, we demonstrate that modulation of furoxan ring reactivity is attainable through simple substitutions of the conjugated aryl-system of phenyl furoxans. Although furoxans possess inherent reactivity towards thiols, the magnitude of reactivity and propensity of NO release can clearly be modulate by appropriate substitution. Furoxans were found to be neuroprotective in a cellular model of ischemia using primary

4. Conclusions

The NO-mimetic furoxan ring was incorporated into a series of peptidomimetic scaffolds; one novel approach used click chemistry to demonstrate the potential for synthetic elaboration of this novel peptidomimetic drug class. It was postulated that substitution of the furoxan ring would lead to modulation of reactivity towards thiol-mediated bioactivation; and further, that attenuation of reactivity would unmask the cytoprotective properties of NO. This was deemed important, since cytotoxicity has been associated with the higher fluxes of NO deriving from known furoxan anti-infective agents. Attenuation of reactivity and propensity for NO release was indeed accomplished by appropriate substitution of the furoxan ring itself. Neuroprotection by furoxans in primary rat neurons subjected to ischemia-reperfusion injury correlated with NO_2^- production, but did not correlate with reduction of free thiol. Neuroprotection was abolished by co-incubation with the sGC inhibitor, ODQ, implicating the involvement of the NO/sGC cascade. One furoxan, **9a**, was observed to restore LTP following an $\text{A}\beta$ -induced synaptic deficit in mouse hippocampal slices, compatible with the known capacity of NO/sGC/CREB activation

to restore LTP. As a whole, these findings strongly suggest activation of the NO/sGC/CREB cascade as the primary mechanism of furoxan elicited neuroprotection and synaptic function restoration. Future efforts to develop attenuated furoxans for the CNS should focus on developing substitution patterns that decrease the thiophilicity of the furoxan ring itself. The work represents the first description of furoxans as neuroprotective and procognitive agents with potential application in stroke and AD.

5. Materials and Methods

5.1 Materials

All chemicals and reagents were purchased from Sigma-Aldrich (St. Louis, MO), or Fisher Scientific unless stated otherwise.

5.2 Synthesis

All synthesized compounds were fully characterized by ^1H NMR, and ^{13}C NMR. The structures of all novel final compounds were supported using in house HRMS. All compounds submitted for biological testing were confirmed to be > 95 % pure by preparative HPLC. Full synthetic methodologies are described in detail within Appendix A, and characterization spectra given in Appendix B.

5.3 Crystallography

The furoxan (**6c**) was chosen for crystallographic examination. Molecular formula:

$\text{C}_{23}\text{H}_{23}\text{FN}_8\text{O}_7\text{S}$, formula weight: 574.1418, crystal system: Orthorhombic, $\text{P2}_1\text{2}_1\text{2}_1$ (#19) with unit cell dimensions: $a = 11.334$ (1) Å $b = 21.427$ (2) Å, $c = 21.643$ (1) Å, Volume = 5256.1 (6) Å³; Z , calculated density = 8, 1.452 Mg/m³, Absorption coefficient = 0.190 mm⁻¹. A colorless

needle, with dimensions $2 \times 2 \times 40 \mu\text{m}$, was selected for data collection. The crystal was cooled to 100 K and aligned in the x-ray beam at sector 22 (SER-CAT) on the ID beamline at the Advanced Photon Source at Argonne National Lab. Data collection was carried out at a wavelength of 0.80 \AA using 5° rotations and exposure time of 1 sec, and collected with a MAR 300 mm CCD detector. 72 images were indexed and integrated using XDS, and averaged over mmm symmetry. The structure was solved using SHELX-97, and refined using WinGX and SHELXL; ORTEP was used to generate the molecular figures. Hydrogen atoms were added to the model in idealized positions. The final model gave agreement factors (R indices) of $R1 = 0.0407$, $wR2 = 0.1030$. We observed two independent molecules in the asymmetric unit, confirming the presence of the oxadiazole-2N-oxide structure within the structures.

5.4 Reactivity Analysis

The appropriate furoxan ($75 \mu\text{M}$) was incubated with L-cysteine (5 mM) in PBS (50 mM , pH 7.4) at 37°C for 2 h. The products were then separated and analyzed by HPLC-MS/MS. Peak integration from UV absorbance spectra gives the estimated relative abundance of each reaction product, and is correlated with the TIC chromatogram to identify peaks by MS/MS analysis.

5.5 Griess Assay

The parent furoxan ($250 \mu\text{M}$) was dissolved in PBS (50 mM , pH 7.4)/ CH_3CN (1:1); L-cysteine ($2500 \mu\text{M}$) was added and the mixture incubated at 37°C for 24 h. Aliquots (taken at 1, 2, 4, 8, 12, 18 & 24 h) were incubated for 10 min with griess reagent A (1.0 % sulfanilamide, 5.0 % H_3PO_4 in dH_2O)/ griess reagent B (0.1 % (N-1-naphthyl)ethylenediamine dihydrochloride in dH_2O). UV absorbance at 530 nm was measured using a Dynex MRX II microplate

spectrophotometer and calibrated using a standard curve constructed with NaNO_2 to yield nitrite concentration.

5.6 Cysteine Reactivity

The parent furoxan (250 μM) was dissolved in a solution of PBS (50 mM, pH 7.4, over Chelex 100)/ CH_3CN (1:1) containing EDTA (1 %); and the mixture purged with N_2 for 10 min; L-cysteine (2500 μM) was added and the mixture purged with N_2 for an additional 5 min followed by incubation at 37 °C for 2 h. Aliquots were mixed with DTNB (750 μM , in PBS 50 mM, pH 7.0) for 5 min. UV absorbance of DTNB mixture was measured at 412 nm using a Dynex MRX II microplate spectrophotometer and calibrated using a standard curve constructed using L-cysteine in the presence of DTNB to yield total reduced cysteine concentration.

Cited Literature

- Adamec, E., P. S. Mohan, et al. (2000). "Up-regulation of the lysosomal system in experimental models of neuronal injury: implications for Alzheimer's disease." Neuroscience **100**(3): 663-75.
- Alzheimer, A. (1911). "über eigenartige Krankheitsfälle des späteren Alters." Zeitschrift für die gesamte Neurologie und Psychiatrie **4**(1): 356-385.
- Arancio, O., M. Kiebler, et al. (1996). "Nitric oxide acts directly in the presynaptic neuron to produce long-term potentiation in cultured hippocampal neurons." Cell **87**(6): 1025-35.
- Arancio, O., M. Kiebler, et al. (1996). "Nitric Oxide Acts Directly in the Presynaptic Neuron to Produce Long-Term Potentiation in Cultured Hippocampal Neurons." Cell **87**(6): 1025-1035.
- Arthur, J. S. C., S. Gauthier, et al. (1995). "Active site residues in m-calpain: identification by site-directed mutagenesis." FEBS Letters **368**(3): 397-400.
- Ascenzi, P., A. Bocedi, et al. (2004). "Inactivation of parasite cysteine proteinases by the NO-donor 4-(phenylsulfonyl)-3-((2-(dimethylamino)ethyl)thio)-furoxan oxalate." Biochim Biophys Acta **1703**(1): 69-77.
- Ascenzi, P., L. Salvati, et al. (2001). "Inhibition of cysteine protease activity by NO-donors." Curr Protein Pept Sci **2**(2): 137-53.
- Balicki, R., M. Cybulski, et al. (2003). "An Efficient Deoxygenation of Heteroaromatic N-Oxides Using Zinc Dust/Ammonium Formate Reagent System." Synthetic Communications: An International Journal for Rapid Communication of Synthetic Organic Chemistry **33**(23): 4137 - 4141.
- Barrett, A. J., A. A. Kembhavi, et al. (1982). "L-trans-Epoxy succinyl-leucylamido(4-guanidino)butane (E-64) and its analogues as inhibitors of cysteine proteinases including cathepsins B, H and L." Biochem J **201**(1): 189-198.
- Bartus, R. T., K. L. Baker, et al. (1994). "Postischemic Administration of AK275, a Calpain Inhibitor, Provides Substantial Protection Against Focal Ischemic Brain Damage." J Cereb Blood Flow Metab **14**(4): 537-544.
- Bartus, R. T., P. J. Elliott, et al. (1995). "Calpain as a novel target for treating acute neurodegenerative disorders." Neurol Res **17**(4): 249-58.
- Bartus, R. T., N. J. Hayward, et al. (1994). "Calpain inhibitor AK295 protects neurons from focal brain ischemia. Effects of postocclusion intra-arterial administration." Stroke **25**(11): 2265-70.
- Beaumont, K., R. Webster, et al. (2003). "Design of Ester Prodrugs to Enhance Oral Absorption of Poorly Permeable Compounds: Challenges to the Discovery Scientist." Current Drug Metabolism **4**(6): 461-485.
- Bendiske, J. and B. A. Bahr (2003). "Lysosomal activation is a compensatory response against protein accumulation and associated synaptopathogenesis--an approach for slowing Alzheimer disease?" J Neuropathol Exp Neurol **62**(5): 451-63.
- Blennow, K., M. J. de Leon, et al. "Alzheimer's disease." The Lancet **368**(9533): 387-403.
- Blurton-Jones, M., M. Kitazawa, et al. (2009). "Neural stem cells improve cognition via BDNF in a transgenic model of Alzheimer disease." Proc Natl Acad Sci **106**(32): 13594-13599.
- Boiani, L., G. Aguirre, et al. (2008). "Furoxan-, alkyl nitrate-derivatives and related compounds as anti-trypanosomatid agents: mechanism of action studies." Bioorg Med Chem **16**(17): 7900-7.

Cited Literature (continued)

- Boiani, M., H. Cerecetto, et al. (2001). "1,2,5-Oxadiazole N-oxide derivatives as potential anti-cancer agents: synthesis and biological evaluation. Part IV." Eur J Med Chem **36**(10): 771-82.
- Boiani, M., H. Cerecetto, et al. (2001). "1,2,5-Oxadiazole N-oxide derivatives as potential anti-cancer agents: synthesis and biological evaluation. Part IV." Eur J Med Chem **36**(10): 771-782.
- Bon, C. L. and J. Garthwaite (2003). "On the role of nitric oxide in hippocampal long-term potentiation." J Neurosci **23**(5): 1941-8.
- Boschi, D., A. Di Stilo, et al. (1997). "Studies on agents with mixed NO-dependent vasodilating and beta-blocking activities." Pharm Res **14**(12): 1750-8.
- Boschi, D., G. C. Tron, et al. (2003). "New potential uroselective NO-donor α 1-antagonists." J Med Chem **46**(17): 3762-5.
- Bundgaard, H. and J. Hansen (1981). "Nucleophilic phosphate-catalyzed degradation of penicillins: demonstration of a penicilloyl phosphate intermediate and transformation of ampicillin to a piperazinedione." International Journal of Pharmaceutics **9**(4): 273-283.
- Bundgaard, H. and C. Larsen (1980). "Pro-drugs as drug delivery systems XVII. Esters of 4-hydroxybutyric acids as potential pro-drug types for β -lactones." International Journal of Pharmaceutics **7**(2): 169-176.
- Buonsanti, M. F., M. Bertinaria, et al. (2007). "Nitric Oxide Donor beta 2-Agonists: Furoxan Derivatives Containing the Fenoterol Moiety and Related Furazans." J Med Chem **50**(20): 5003-5011.
- Buonsanti, M. F., M. Bertinaria, et al. (2007). "Nitric oxide donor beta2-agonists: furoxan derivatives containing the fenoterol moiety and related furazans." J Med Chem **50**(20): 5003-11.
- Carol J. Farran, B. D. J., Tricia J. Johnson, Ken P. Scholz, and Jennifer Weuve (2011). "2011 Alzheimer's Disease Facts and Figures."
- Cena, C., D. Boschi, et al. (2004). "Development of a new class of potential antiatherosclerosis agents: NO-donor antioxidants." Bioorg Med Chem Lett **14**(24): 5971-4.
- Cena, C., M. L. Lolli, et al. (2003). "Antiinflammatory, gastrosparring, and antiplatelet properties of new NO-donor esters of aspirin." J Med Chem **46**(5): 747-54.
- Cerecetto, H. and M. Gonzalez (2007). "Benzofuroxan and furoxan. Chemistry and biology." Topics in Heterocyclic Chemistry **10**(Bioactive Heterocycles IV): 265-308.
- Chegaev, K., C. Cena, et al. (2009). "Edaravone Derivatives Containing NO-Donor Functions." J Med Chem **52**(2): 574-578.
- Cuerrier, D., T. Moldoveanu, et al. (2007). "Development of Calpain-specific Inactivators by Screening of Positional Scanning Epoxide Libraries." J Biol Chem **282**(13): 9600-9611.
- Cuerrier, D., T. Moldoveanu, et al. (2005). "Determination of Peptide Substrate Specificity for β -Calpain by a Peptide Library-based Approach." J Biol Chem **280**(49): 40632-40641.
- Cuerrier, D., T. Moldoveanu, et al. (2006). "Calpain inhibition by alpha-ketoamide and cyclic hemiacetal inhibitors revealed by X-ray crystallography." Biochemistry **45**(24): 7446-52.
- Cuerrier, D., Z. Nie, et al. (2005). "Ritonavir does not inhibit calpain in vitro." Biochem Biophys Res Commun **327**(1): 208-11.
- Di Rosa, G., T. Odrijin, et al. (2002). "Calpain inhibitors: a treatment for Alzheimer's disease." J Mol Neurosci **19**(1-2): 135-41.

Cited Literature (continued)

- Donkor, I. O. (2000). "A survey of Calpain Inhibitors." Current Medicinal Chemistry **7**(12): 1171.
- Donkor, I. O., R. Korukonda, et al. (2003). "Peptidyl aldehyde inhibitors of calpain incorporating P2-proline mimetics." Bio Org Med Chem Lett **13**(5): 783-784.
- Dosemeci, A. and T. S. Reese (1995). "Effect of calpain on the composition and structure of postsynaptic densities." Synapse **20**(1): 91-97.
- Eilon, G. F., J. Gu, et al. (2000). "Tumor apoptosis induced by epoxide-containing piperazines, a new class of anti-cancer agents." Cancer Chemotherapy and Pharmacology **45**(3): 183-191.
- Farkas, B., A. Tantos, et al. (2004). "Ischemia-induced increase in long-term potentiation is warded off by specific calpain inhibitor PD150606." Brain Res **1024**(1-2): 150-8.
- Feelisch, M., K. Schönafingeri, et al. (1992). "Thiol-mediated generation of nitric oxide accounts for the vasodilator action of furoxans." Biochem Pharmacol **44**(6): 1149-1157.
- Feroli, R., A. Fazzini, et al. (1993). "No-mimetic furoxans: arylsulphonylfuroxans and related compounds." Pharmacol Res **28**(3): 203-12.
- Feroli, R., G. C. Folco, et al. (1995). "A new class of furoxan derivatives as NO donors: mechanism of action and biological activity." Br J Pharmacol **114**(4): 816-20.
- Frey, U. and R. G. M. Morris (1997). "Synaptic tagging and long-term potentiation." Nature **385**(6616): 533-536.
- Fukushima, K., M. Arai, et al. (1990). "An epoxysuccinic acid derivative(loxistatin)-induced hepatic injury in rats and hamsters." Toxicology and Applied Pharmacology **105**(1): 1-12.
- Fukushima, K., M. Arai, et al. (1989). "Identification of Glutathione Conjugate Formed from Loxistatin in Rats." Xenobiotica **19**(5): 521-529.
- Ghibelli, L., F. Mengoni, et al. (2003). "Anti-apoptotic effect of HIV protease inhibitors via direct inhibition of calpain." Biochem Pharmacol **66**(8): 1505-12.
- Ghosh, P., B. Ternai, et al. (1981). "Benzofurazans and benzofuroxans: biochemical and pharmacological properties." Med Res Rev **1**(2): 159-87.
- Ghosh, P. B. and M. W. Whitehouse (1968). "Potential antileukemic and immunosuppressive drugs. Preparation and in vitro pharmacological activity of some benzo-2,1,3-oxadiazoles (benzofurazans) and their N-oxides (benzofuroxans)." J Med Chem **11**(2): 305-11.
- Goldberg, M. P., U. Strasser, et al. (1997). "Techniques for assessing neuroprotective drugs in vitro." Int Rev Neurobiol **40**: 69-93.
- Golding, B. T., D. R. Hall, et al. (1973). "Reaction between vicinal diols and hydrogen bromide in acetic acid; synthesis of chiral propylene oxide." Journal of the Chemical Society, Perkin Transactions **1**.
- Goll, D. E., V. F. Thompson, et al. (2003). "The Calpain System." Physiological Reviews **83**(3): 731-801.
- Goto, K., T. Iwamoto, et al. (1994). "Localization of mRNAs for calpain and calpastatin in the adult rat brain by in situ hybridization histochemistry." Molecular Brain Research **23**(1-2): 40-46.
- Granic, I., C. Nyakas, et al. "Calpain inhibition prevents amyloid- β -induced neurodegeneration and associated behavioral dysfunction in rats." Neuropharmacology **59**(4-5): 334-342.

Cited Literature (continued)

- Graybill, T. L., R. E. Dolle, et al. (1995). "Inhibition of human erythrocyte Calpain I by novel quinolinecarboxamides." Bioorganic & Medicinal Chemistry Letters **5**(4): 387-92.
- Greenbaum, D., K. F. Medzihradszky, et al. (2000). "Epoxide electrophiles as activity-dependent cysteine protease profiling and discovery tools." Chem Biol **7**(8): 569-81.
- Greenbaum, D. C., W. D. Arnold, et al. (2002). "Small Molecule Affinity Fingerprinting: a Tool for Enzyme Family Subclassification, Target Identification, and Inhibitor Design." Chemistry & Biology **9**(10): 1085-1094.
- Guroff, G. (1964). "A Neutral, Calcium-activated Proteinase from the Soluble Fraction of Rat Brain." J Biol Chem **239**(1): 149-155.
- Haley, J. E., G. L. Wilcox, et al. (1992). "The role of nitric oxide in hippocampal long-term potentiation." Neuron **8**(2): 211-6.
- Hanna, R. A., R. L. Campbell, et al. (2008). "Calcium-bound structure of calpain and its mechanism of inhibition by calpastatin." Nature **456**(7220): 409-412.
- Hata, S., M. Abe, et al. "Calpain 8/nCL-2 and Calpain 9/nCL-4 Constitute an Active Protease Complex, G-Calpain, Involved in Gastric Mucosal Defense." PLoS Genet **6**(7): e1001040.
- Higuchi, M., N. Iwata, et al. "Mechanistic involvement of the calpain-calpastatin system in Alzheimer neuropathology." The FASEB Journal.
- Higuchi, M., M. Tomioka, et al. (2005). "Distinct Mechanistic Roles of Calpain and Caspase Activation in Neurodegeneration as Revealed in Mice Overexpressing Their Specific Inhibitors." J Biol Chem **280**(15): 15229-15237.
- Hook, G., V. Y. Hook, et al. (2007). "Cysteine protease inhibitors reduce brain beta-amyloid and beta-secretase activity in vivo and are potential Alzheimer's disease therapeutics." Biol Chem **388**(9): 979-83.
- Hook, V., M. Kindy, et al. (2007). "Cysteine protease inhibitors effectively reduce in vivo levels of brain beta-amyloid related to Alzheimer's disease." Biol Chem **388**(2): 247-52.
- Hook, V., T. Toneff, et al. (2005). "Inhibition of cathepsin B reduces beta-amyloid production in regulated secretory vesicles of neuronal chromaffin cells: evidence for cathepsin B as a candidate beta-secretase of Alzheimer's disease." Biol Chem **386**(9): 931-40.
- Hook, V. Y., M. Kindy, et al. (2008). "Inhibitors of cathepsin B improve memory and reduce beta-amyloid in transgenic Alzheimer disease mice expressing the wild-type, but not the Swedish mutant, beta-secretase site of the amyloid precursor protein." J Biol Chem **283**(12): 7745-53.
- Hook, V. Y. H. (2006). "Neuroproteases in Peptide Neurotransmission and Neurodegenerative Diseases: Applications to Drug Discovery Research." BioDrugs **20**(2): 105.
- Huang, Y. and K. K. W. Wang (2001). "The calpain family and human disease." Trends in Molecular Medicine **7**(8): 355-362.
- Hudecki, M. S., C. M. Pollina, et al. (1981). "In Vivo Effects of Protease Inhibitors on Chickens with Hereditary Muscular Dystrophy." J Clin Inv **67**(4): 969-974.
- Huston, R. B. and E. G. Krebs (1968). "Activation of skeletal muscle phosphorylase kinase by calcium ions. II. Identification of the kinase activating factor as a proteolytic enzyme." Biochemistry **7**(6): 2116-2122.

Cited Literature (continued)

- Jasmin, G. t. and L. Proschek (1984). "Calcium and myocardial cell injury. An appraisal in the cardiomyopathic hamster." Canadian Journal of Physiology and Pharmacology **62**(7): 891-898.
- Jellinger, K. A. (2006). "Alzheimer 100 – highlights in the history of Alzheimer research." Journal of Neural Transmission **113**(11): 1603-1623.
- Jurima-Romet, M., H. S. Huang, et al. (1991). "Enalapril cytotoxicity in primary cultures of rat hepatocytes. II. Role of glutathione." Toxicology Letters **58**(3): 269-277.
- K. Hanada, M. T., M. Yamagishi, S. Ohmura, J. Sawada and I. Tanaka (1978). "Isolation and Characterization of E-64, a New Thiol Protease Inhibitor." Agricultural and Biological Chemistry **Vol.42** (3): 523-528.
- K.K. Wang, P. Y. (1999). "Calpain: Pharmacology and Toxicology of Calcium-Dependent Protease." Philadelphia, PA: Taylor & Francis.
- K.S, K. (1990). "Tau protein and Alzheimer's disease." Current Opinion in Cell Biology **2**(1): 101-104.
- Kandel, E. R. (2001). "The molecular biology of memory storage: a dialogue between genes and synapses." Science **294**(5544): 1030-8.
- Khachaturian, Z. S. (1985). "Diagnosis of Alzheimer's Disease." Arch Neurol **42**(11): 1097-1105.
- Korukonda, R., N. Guan, et al. (2006). "Synthesis, Calpain Inhibitory Activity, and Cytotoxicity of P2-Substituted Proline and Thiaproline Peptidyl Aldehydes and Peptidyl α-Ketoamides." J. Med. Chem. **49**(17): 5282-5290.
- Koumura, A., Y. Nonaka, et al. (2008). "A novel calpain inhibitor, ((1S)-1((((1S)-1-benzyl-3-cyclopropylamino-2,3-di-oxopropyl)amino)carbonyl)-3-methylbutyl) carbamic acid 5-methoxy-3-oxapentyl ester, protects neuronal cells from cerebral ischemia-induced damage in mice." Neuroscience **157**(2): 309-318.
- Krall, W. J., J. J. Sramek, et al. (1999). "Cholinesterase inhibitors: a therapeutic strategy for Alzheimer disease." The Annals of Pharmacotherapy **33**(4): 441-450.
- Lambert, M. P., A. K. Barlow, et al. (1998). "Diffusible, nonfibrillar ligands derived from Abeta1-42 are potent central nervous system neurotoxins." Proc Natl Acad Sci U S A **95**(11): 6448-53.
- Li, X., H. Chen, et al. (2007). "BDA-410: a novel synthetic calpain inhibitor active against blood stage malaria." Mol Biochem Parasitol **155**(1): 26-32.
- Liang, B., B. Y. Duan, et al. "Calpain activation promotes bace1 expression, APP processing, and amyloid plaque formation in a transgenic mouse model of Alzheimer disease." J Biol Chem.
- Lipton, S. A., Y. B. Choi, et al. (1993). "A redox-based mechanism for the neuroprotective and neurodestructive effects of nitric oxide and related nitroso-compounds." Nature **364**(6438): 626-32.
- Loo, D. T., J. R. Rillema, et al. (1998). Chapter 14 Measurement of Cell Death. Methods in Cell Biology, Academic Press. **Volume 57**: 251-264.
- Lu, Y. F., E. R. Kandel, et al. (1999). "Nitric oxide signaling contributes to late-phase LTP and CREB phosphorylation in the hippocampus." J Neurosci **19**(23): 10250-61.
- Lubisch, W. and A. Moller (2002). "Discovery of phenyl alanine derived ketoamides carrying benzoyl residues as novel calpain inhibitors." Bioorg Med Chem Lett **12**(10): 1335-8.

Cited Literature (continued)

- Lund, E. T., R. McKenna, et al. (2001). "Characterization of the in vitro phosphorylation of human tau by tau protein kinase II (cdk5/p20) using mass spectrometry." J Neurochem **76**(4): 1221-1232.
- Lynch, G. and M. Baudry (1987). "Brain spectrin, calpain and long-term changes in synaptic efficacy." Brain Res Bull **18**(6): 809-815.
- Lynch, G., D. Muller, et al. (1988). "Long-term potentiation: Persisting problems and recent results." Brain Res Bull **21**(3): 363-372.
- Lynn, S. P., S. Robert, et al. (1988). "The ultrastructural localization of calcium-activated protease α -calpain in rat brain." Synapse **2**(1): 79-88.
- M. Tamai, K. M., S. Omura, I. Koyama, Y. Ozawa and K. Hanada (1986). "In vitro and in vivo inhibition of cysteine proteases by EST, a new analog of E-64." J. Pharmacobiodyn. **9**: 672-677.
- Ma, H., I. Hata, et al. (1999). "Lp82 is the Dominant Form of Calpain in Young Mouse Lens." Experimental Eye Research **68**(4): 447-456.
- Ma, H., A. Tochigi, et al. (2009). "Calpain inhibitor SNJ-1945 attenuates events prior to angiogenesis in cultured human retinal endothelial cells." J Ocul Pharmacol Ther **25**(5): 409-14.
- Mary E. McGrath, J. L. K., Michael G. Barnes & Dieter Brömme (1997). "Crystal structure of human cathepsin K complexed with a potent inhibitor." Nature Structural Biology **4**: 105-109.
- Masaharu Tamai, S. O., Masaaki Kimura, Kazunori Hanada, Hideo Sugita (1987). "Prolongation of Life Span of Dystrophic Hamster by Cysteine Proteinase Inhibitor, Loxistatin (EST) " Journal of Pharmacobio-Dynamics **10**(11): 678-681.
- Matsumoto, K., K. Mizoue, et al. (1999). "Structural basis of inhibition of cysteine proteases by E-64 and its derivatives." Biopolymers **51**(1): 99-107.
- Maurer, K., S. Volk, et al. (1997). "Auguste D and Alzheimer's disease." The Lancet **349**(9064): 1546-1549.
- McDowell, I. (2001). "Alzheimer's disease: insights from epidemiology." Aging (Milano) **13**(3): 143-62.
- McHugh, T. J., K. I. Blum, et al. (1996). "Impaired Hippocampal Representation of Space in CA1-Specific NMDAR1 Knockout Mice." Cell **87**(7): 1339-1349.
- Medana, C., A. Di Stilo, et al. (1999). "NO donor and biological properties of different benzofuroxans." Pharm Res **16**(6): 956-60.
- Medana, C., G. Ermondi, et al. (1994). "Furoxans as nitric oxide donors. 4-Phenyl-3-furoxan carbonitrile: thiol-mediated nitric oxide release and biological evaluation." J Med Chem **37**(25): 4412-6.
- Melino, G., F. Bernassola, et al. (1997). "S-nitrosylation regulates apoptosis." Nature **388**(6641): 432-433.
- Meyer, W. L., E. H. Fischer, et al. (1964). "Activation of Skeletal Muscle Phosphorylase b Kinase by Ca^{2+} ." Biochemistry **3**(8): 1033-1039.
- Michel, G. (1993). "Tau protein and the neurofibrillary pathology of Alzheimer's disease." Trends in Neurosciences **16**(11): 460-465.

Cited Literature (continued)

- Miyahara, T., Shimojo, S., Toyohara, K., Imai, T., Miyajima, M., Honda, H., Kamegai, M., Ohzeki, M., and Kokatsu, J. (1985). "Phase I study of EST, a new thiol protease inhibitor—the 2nd report safety and pharmacokinetics in continuous administration." Rinsho Yakuri **16**: 537-546.
- Mladenovic, M., K. Ansorg, et al. (2008). "Atomistic Insights into the Inhibition of Cysteine Proteases: First QM/MM Calculations Clarifying the Stereoselectivity of Epoxide-Based Inhibitors." J Phys Chem B **112**(37): 11798-11808.
- Mohr, S., B. Zech, et al. (1997). "Inhibition of caspase-3 by S-nitrosation and oxidation caused by nitric oxide." Biochem Biophys Res Commun **238**(2): 387-91.
- Moldoveanu, T., R. L. Campbell, et al. (2004). "Crystal Structures of Calpain-E64 and -Leupeptin Inhibitor Complexes Reveal Mobile Loops Gating the Active Site." J Mol Biol **343**(5): 1313-1326.
- Moldoveanu, T., C. M. Hosfield, et al. (2002). "A Ca²⁺ Switch Aligns the Active Site of Calpain." Cell **108**(5): 649-660.
- Morris, R. G. M., E. Anderson, et al. (1986). "Selective impairment of learning and blockade of long-term potentiation by an N-methyl-D-aspartate receptor antagonist, AP5." Nature **319**(6056): 774-776.
- Morrisette, D. A., A. Parachikova, et al. (2009). "Relevance of transgenic mouse models to human Alzheimer disease." J Biol Chem **284**(10): 6033-7.
- Nakamura, M., K. Imahori, et al. (1988). "Tissue distribution of an endogenous inhibitor of calcium-activated neutral protease and age-related changes in its activity in rats." Comparative Biochemistry and Physiology Part B: Comparative Biochemistry **89**(2): 381-384.
- Nakamura, M., H. Miyashita, et al. (2003). "Novel 6-hydroxy-3-morpholinones as cornea permeable calpain inhibitors." Bioorg Med Chem **11**(24): 5449-60.
- Nedrelov, J. H., C. D. Cianci, et al. (2003). "c-Src Binds β -II Spectrin's Src Homology 3 (SH3) Domain and Blocks Calpain Susceptibility by Phosphorylating Tyr1176." J Biol Chem **278**(9): 7735-7741.
- Nielsen, N. M. r. and H. Bundgaard (1987). "Prodrugs as drug delivery systems. 68. Chemical and plasma-catalyzed hydrolysis of various esters of benzoic acid: a reference system for designing prodrug esters of carboxylic acid agents." International Journal of Pharmaceutics **39**(1-2): 75-85.
- Ohno, S., Y. Emori, et al. (1984). "Evolutionary origin of a calcium-dependent protease by fusion of genes for a thiol protease and a calcium-binding protein?" Nature **312**(5994): 566-570.
- Otto, H. H. and T. Schirmeister (1997). "Cysteine Proteases and Their Inhibitors." Chem Rev **97**(1): 133-172.
- Parkes, C., A. A. Kembhavi, et al. (1985). "Calpain inhibition by peptide epoxides." Biochem J **230**(2): 509-516.
- Peng, S., J. Wu, et al. (2005). "Precursor form of brain-derived neurotrophic factor and mature brain-derived neurotrophic factor are decreased in the pre-clinical stages of Alzheimer's disease." J Neurochem **93**(6): 1412-21.

Cited Literature (continued)

- Pignol, B., S. Auvin, et al. (2006). "Calpain inhibitors and antioxidants act synergistically to prevent cell necrosis: effects of the novel dual inhibitors (cysteine protease inhibitor and antioxidant) BN 82204 and its pro-drug BN 82270." J Neurochem **98**(4): 1217-1228.
- Puzzo, D., L. Privitera, et al. "Endogenous amyloid- β is necessary for hippocampal synaptic plasticity and memory." Annals of Neurology **69**(5): 819-830.
- Puzzo, D., A. Staniszewski, et al. (2009). "Phosphodiesterase 5 inhibition improves synaptic function, memory, and amyloid-beta load in an Alzheimer's disease mouse model." J Neurosci **29**(25): 8075-86.
- Puzzo, D., O. Vitolo, et al. (2005). "Amyloid-beta peptide inhibits activation of the nitric oxide/cGMP/cAMP-responsive element-binding protein pathway during hippocampal synaptic plasticity." J Neurosci **25**(29): 6887-97.
- Qian, J., D. Cuerrier, et al. (2008). "Cocrystal structures of primed side-extending alpha-ketoamide inhibitors reveal novel calpain-inhibitor aromatic interactions." J Med Chem **51**(17): 5264-70.
- Rai, G., A. A. Sayed, et al. (2009). "Structure mechanism insights and the role of nitric oxide donation guide the development of oxadiazole-2-oxides as therapeutic agents against schistosomiasis." J Med Chem **52**(20): 6474-83.
- Rami, A., D. Ferger, et al. (1997). "Blockade of calpain proteolytic activity rescues neurons from glutamate excitotoxicity." Neurosci Res **27**(1): 93-97.
- Rao, M. V., P. S. Mohan, et al. (2008). "Marked Calpastatin (CAST) Depletion in Alzheimer's Disease Accelerates Cytoskeleton Disruption and Neurodegeneration: Neuroprotection by CAST Overexpression." J Neurosci **28**(47): 12241-12254.
- Reynolds, J. N., B. M. Bennett, et al. (2002). "Neuroprotection against ischemic brain injury conferred by a novel nitrate ester." Bioorg Med Chem Lett **12**(20): 2863-6.
- Richard, I., O. Broux, et al. (1995). "Mutations in the proteolytic enzyme calpain 3 cause limb-girdle muscular dystrophy type 2A." Cell **81**(1): 27-40.
- Roberts-Lewis, J. M. and R. Siman (1993). "Spectrin Proteolysis in the Hippocampus: A Biochemical Marker for Neuronal Injury and Neuroprotection." Annals of the New York Academy of Sciences **679**(1): 78-86.
- Robinson, D. M. and G. M. Keating (2006). "Memantine: A Review of its Use in Alzheimer's Disease." Drugs **66**(11): 1515-1534.
- Saito, K., J. S. Elce, et al. (1993). "Widespread activation of calcium-activated neutral proteinase (calpain) in the brain in Alzheimer disease: a potential molecular basis for neuronal degeneration." Proceedings of the National Academy of Sciences of the United States of America **90**(7): 2628-2632.
- Sako, M., S. Oda, et al. (1998). Journal of Organic Chemistry **63**: 6947.
- Satoyoshi, E. (1992). "Therapeutic trials on progressive muscular dystrophy." Intern. Med. **31**: 841-846.
- Schaschke, N., I. Assfalg-Machleidt, et al. (1997). "E-64 analogues as inhibitors of cathepsin B. On the role of the absolute configuration of the epoxysuccinyl group." Bio Med Chem **5**(9): 1789-1797.

Cited Literature (continued)

- Schirmeister, T. (1999). "New Peptidic Cysteine Protease Inhibitors Derived from the Electrophilic $\hat{I}\pm$ -Amino Acid Aziridine-2,3-dicarboxylic Acid." J Med Chem **42**(4): 560-572.
- Schmidt, U., J. Talbiersky, et al. (1980). "Synthese monosubstituierter (S)-Oxirane von hoher optischer Reinheit." Angewandte Chemie **92**(3): 201-202.
- Schultz, R. M., P. Varma-Nelson, et al. (1989). "Active and inactive forms of the transition-state analog protease inhibitor leupeptin: explanation of the observed slow binding of leupeptin to cathepsin B and papain." J Biol Chem **264**(3): 1497-507.
- Scrip (1992). **1765**(11).
- Seiki Saito, K. K., Toshio Moriwake (1996). "Diethyl (2S,3R)-2-(N-tert-butoxycarbonyl)amino-3-hydroxysuccinate." Organic Syntheses **73**: 184.
- Shea, T. B., M. L. Beermann, et al. (1994). "Degradation of protein kinase C alpha and its free catalytic subunit, protein kinase M, in intact human neuroblastoma cells and under cell-free conditions. Evidence that PKM is degraded by mM calpain-mediated proteolysis at a faster rate than PKC." FEBS Lett **350**(2-3): 223-9.
- Shea, T. B., C. M. Cressman, et al. (1995). "Enhancement of neurite outgrowth following calpain inhibition is mediated by protein kinase C." J Neurochem **65**(2): 517-27.
- Shea, T. B., S. Prabhakar, et al. (1997). "Beta-amyloid and ionophore A23187 evoke tau hyperphosphorylation by distinct intracellular pathways: differential involvement of the calpain/protein kinase C system." J Neurosci Res **49**(6): 759-68.
- Shibata, T., F. Yamamoto, et al. (1997). "Effects of Protease Inhibitors on Postischemic Recovery of the Heart." Cardiovascular Drugs and Therapy **11**(4): 547-556.
- Shirasaki, Y., H. Miyashita, et al. (2006). "Exploration of orally available calpain inhibitors. Dipeptidyl a-ketoamide derivatives containing pyridine moiety." Bioorg & Med Chem **14**(16): 5691-5698.
- Shirasaki, Y., M. Nakamura, et al. (2006). "Exploration of orally available calpain inhibitors 2: peptidyl hemiacetal derivatives." J Med Chem **49**(13): 3926-32.
- Shujaath, M. (1991). "Cell-penetrating inhibitors of calpain." Trends in Biochemical Sciences **16**(0): 150-153.
- Silva, A. J., J. H. Kogan, et al. (1998). "CREB AND MEMORY." Annual Review of Neuroscience **21**(1): 127.
- Simonson, L., M. Baudry, et al. (1985). "Regional distribution of soluble calcium activated proteinase activity in neonatal and adult rat brain." Brain Research **327**(1â€“2): 153-159.
- Smith, S., H. C. Dringenberg, et al. (2000). "A novel nitrate ester reverses the cognitive impairment caused by scopolamine in the Morris water maze." Neuroreport **11**(17): 3883-6.
- Song, J. C. and C. M. White (2002). "Clinical Pharmacokinetics and Selective Pharmacodynamics of New Angiotensin Converting Enzyme Inhibitors: An Update." Clinical Pharmacokinetics **41**(3): 207-224.
- Sorba, G., U. Galli, et al. (2003). "A new furoxan NO-donor rabeprazole derivative and related compounds." Chembiochem **4**(9): 899-903.
- Stramiello, M. and J. J. Wagner "Cocaine enhancement of long-term potentiation in the CA1 region of rat hippocampus: Lamina-specific mechanisms of action." Synapse **64**(8): 644-648.

Cited Literature (continued)

- Straube, T. and J. U. Frey (2003). "Involvement of β_2 -adrenergic receptors in protein synthesis-dependent late long-term potentiation (LTP) in the dentate gyrus of freely moving rats: the critical role of the LTP induction strength." Neuroscience **119**(2): 473-479.
- Stuart, K. L. (1975). "Furazans." Heterocycles **3**(8): 651-90.
- Sugita, H., S. Ishiura, et al. (1980). "Inhibition of Epoxide Derivatives on Chicken Calcium-Activated Neutral Protease (CANP) In Vitro and In Vivo." J Biochem **87**(1): 339-341.
- Sun, J., A. Cipriano, et al. (1994). "Pharmacokinetic interaction study between benazepril and amlodipine in healthy subjects." Eur J Clin Pharmacol **47**(3): 285-289.
- Suzuki, K. (1991). "Nomenclature of calcium dependent proteinase." Biomedica biochimica acta **50**(4-6): 483-4.
- Suzuki, K., H. Hayashi, et al. (1983). "Amino acid sequence around the active site cysteine residue of calcium-activated neutral protease (CANP)." FEBS Letters **152**(1): 67-70.
- Takashi, M. (1983). "Calpain and calpastatin." Trends in Biochemical Sciences **8**(5): 167-169.
- Terry, A. V. and J. J. Buccafusco (2003). "The Cholinergic Hypothesis of Age and Alzheimer's Disease-Related Cognitive Deficits: Recent Challenges and Their Implications for Novel Drug Development." Journal of Pharmacology and Experimental Therapeutics **306**(3): 821-827.
- Thatcher, G. R. J. (2005). "An introduction to NO-related therapeutic agents." Curr Top Med Chem **5**(7): 597-601.
- Thatcher, G. R. J., B. M. Bennett, et al. (2006). "NO chimeras as therapeutic agents in Alzheimer's disease." Curr Alzheimer Res **3**(3): 237-45.
- Thatcher, G. R. J., A. C. Nicolescu, et al. (2004). "Nitrates and NO release: Contemporary aspects in biological and medicinal chemistry." Free Radic Biol Med **37**(8): 1122-1143.
- Tjernberg, L. O., C. Lilliehook, et al. (1997). "Controlling amyloid beta-peptide fibril formation with protease-stable ligands." J Biol Chem **272**(19): 12601-5.
- Tosco, P., M. Bertinaria, et al. (2005). "Furoxan analogues of the histamine H3-receptor antagonist imoproxifan and related furazan derivatives." Bioorg Med Chem **13**(15): 4750-9.
- Town, T., J. Zolton, et al. (2002). "p35/Cdk5 pathway mediates soluble amyloid-beta peptide-induced tau phosphorylation in vitro." J Neurosci Res **69**(3): 362-72.
- Trinchese, F., M. Fa, et al. (2008). "Inhibition of calpains improves memory and synaptic transmission in a mouse model of Alzheimer disease." J Clin Invest **118**(8): 2796-807.
- Tsuji, T., S. Shimohama, et al. (1998). "m-Calpain (calcium-activated neutral proteinase) in Alzheimer's disease brains." Neurosci Lett **248**(2): 109-112.
- Veeranna, T. Kaji, et al. (2004). "Calpain mediates calcium-induced activation of the erk1,2 MAPK pathway and cytoskeletal phosphorylation in neurons: relevance to Alzheimer's disease." Am J Pathol **165**(3): 795-805.
- Velazquez, C., P. N. Rao, et al. (2005). "Synthesis and biological evaluation of 3,4-diphenyl-1,2,5-oxadiazole-2-oxides and 3,4-diphenyl-1,2,5-oxadiazoles as potential hybrid COX-2 inhibitor/nitric oxide donor agents." Bioorg Med Chem **13**(8): 2749-57.
- Vitolo, O. V., A. Sant'Angelo, et al. (2002). "Amyloid beta -peptide inhibition of the PKA/CREB pathway and long-term potentiation: reversibility by drugs that enhance cAMP signaling." Proc Natl Acad Sci U S A **99**(20): 13217-21.

Cited Literature (continued)

- Wan, W. and P. B. DePetrillo (2002). "Ritonavir inhibition of calcium-activated neutral proteases." Biochem Pharmacol **63**(8): 1481-4.
- Wang, K. K., R. Nath, et al. (1996). "An alpha-mercaptoacrylic acid derivative is a selective nonpeptide cell-permeable calpain inhibitor and is neuroprotective." Proc Natl Acad Sci U S A **93**(13): 6687-92.
- Wang, K. K., A. Posner, et al. (1996). "Alpha-mercaptoacrylic acid derivatives as novel selective calpain inhibitors." Adv Exp Med Biol **389**: 95-101.
- Whitehouse, M. W. and P. B. Ghosh (1968). "4-nitrobenzofurazans and 4-nitrobenzofuroxans: a new class of thiol-neutralising agents and potent inhibitors of nucleic acid synthesis in leucocytes." Biochem Pharmacol **17**(1): 158-61.
- Wilkinson, D. G., P. T. Francis, et al. (2004). "Cholinesterase Inhibitors Used in the Treatment of Alzheimer's Disease: The Relationship Between Pharmacological Effects and Clinical Efficacy." Drugs & Aging **21**(7): 453-478.
- Wu, H. Y. and D. R. Lynch (2006). "Calpain and synaptic function." Mol Neurobiol **33**(3): 215-36.
- Yamashima, T., Y. Kohda, et al. (1998). "Inhibition of ischaemic hippocampal neuronal death in primates with cathepsin B inhibitor CA-074: a novel strategy for neuroprotection based on 'calpain-cathepsin hypothesis'." Eur J Neurosci **10**(5): 1723-33.
- Zhou, W., S. A. Scott, et al. (2006). "Cathepsin D-mediated proteolysis of apolipoprotein E: possible role in Alzheimer's disease." Neuroscience **143**(3): 689-701.
- Zhuo, M., Y. Hu, et al. (1994). "Role of guanylyl cyclase and cGMP-dependent protein kinase in long-term potentiation." Nature **368**(6472): 635-9.

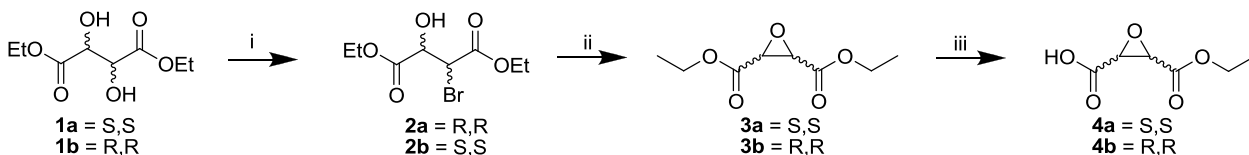
APPENDIX A. EXPERIMENTAL PROCEDURES AND CHARACTERIZATION

Important Note: Please refer to compound numbering designations from the tables and schemes within the appendix. The experimental portion has been pooled from published and submitted manuscripts. Hence, numbering within the body of the thesis document does not necessarily correlate with that of the experimental procedures. *All compounds are clearly designated by number, structure, and chemical name within the experimental and characterization appendices.*

General Methods: Unless stated otherwise, all reactions were carried out under an atmosphere of dry argon in oven-dried glassware. Indicated reaction temperatures refer to those of the reaction bath, while room temperature (rt) is noted as 25 °C. Dichloromethane (CH_2Cl_2) was distilled over CaH_2 , and THF distilled over Na(s) . All other solvents were of anhydrous quality purchased from Aldrich Chemical Co. and used as received. Pure reaction products were typically dried under high vacuum in the presence of phosphorus pentoxide. Commercially available starting materials and reagents were purchased from Aldrich, TCI and Fisher Scientific and were used as received unless specified otherwise. Analytical thin layer chromatography (TLC) was performed with (5 x 20 cm, 60 Å, 250 µm). Visualization was accomplished using a 254 nm UV lamp. ^1H and ^{13}C NMR spectra were recorded on either a Bruker Avance 400 MHz spectrometer or Bruker DPX 400 MHz spectrophotometer. Chemical shifts are reported in ppm with the solvent resonance as internal standard ($[\text{CDCl}_3$ 7.27 ppm, 77.23 ppm] $[\text{DMSO}-d_6$ 2.5 ppm, 39.51 ppm] and $[\text{MeOD}d_4$ 4.78, 49.0] for ^1H , ^{13}C respectively). Data are reported as follows: chemical shift, multiplicity (s = singlet, d = doublet, dd = doublet of doublet, t = triplet, q = quartet, br = broad, m = multiplet, abq = ab quartet), number of protons, and coupling constants. Low-resolution mass spectra (LRMS) were acquired on an Agilent 6300 Ion-Trap

LC/MS. High resolution mass spectral data was collected in-house using a Shimadzu QTOF 6500. All compounds submitted for biological testing were found to be > 95 % pure by analytical HPLC. Purity and/or low resolution mass spectral (ESI or APCI) analysis was measured using an Advantage ARMOR C18; 5 μ M; 150 x 4.6 mm analytical column, on either a Shimadzu UFLC (Instrument 1) or Agilent 1100 Series HPLC in tandem with an Agilent 6310 Ion Trap LC/MS (Instrument 2). HPLC Method: Solvents: 0.05 % FA in CH₃CN (Solvent A); 0.05 % FA in 9:1 mixture of H₂O and MeOH (Solvent B); Flow rate 1.0 mL/min; Gradient: t = 0 min, 10 % B; t = 5 min, 30 % B; t = 15 min, 70 % B; t = 30 min, 90 % B; t = 35 min, 50% B, t = 38, 10% B; stop time 45 min.

Scheme 1



Reagents: i) HBr (33 %) in acetic acid, r.t, 12 h, then acetyl chloride, reflux, 12 h, 75-80 %; ii) DBU, Et₂O, 0 °C, 12 h, 70-80 %; iii) Ethanolic KOH, 0 °C, 6 h, 75-85 %.

General procedure for large scale production of the bromohydrin (2a & 2b). HBr (33 % in acetic acid, 175 ml, 970 mmol) was added dropwise to D-DET (50 g, 242 mmol) at 0 °C over 1 h, and the reaction allowed to warm to r.t. and stirred for 12 h. The reaction mixture was then poured into ice (~500 g), and the resulting aqueous layer extracted with Et₂O (4 x 200 ml). The combined organic extracts were then washed with dH₂O (2 x 300 ml), brine (2 x 200 ml), dried over Na₂SO₄ and concentrated under reduced pressure. The resulting pale yellow oil was dissolved in anhydrous EtOH (300 mL) and acetyl chloride (8 ml, 242 mmol) was added dropwise. The solution was heated under gentle reflux for 7 h, cooled to r.t., and concentrated under reduced pressure to give

yellow oil. The crude product was purified by under reduced pressure by fractional vacuum distillation to afford the desired bromohydrins as clear colorless oils (**2a**, 54.0 g, 99.1 %; **2b**, 51.2 g, 94.0 %).

(2R,3R)-diethyl 2-bromo-3-hydroxysuccinate (2a). ^1H NMR (CDCl_3 , 400 MHz): δ 4.73-4.72 (d, 1H, 4.0 Hz); 4.69-4.68 (bt, 1H); 4.34-4.24 (m, 4H); 3.43-3.41 (d, 1H, $J = 7.2$ Hz); 1.35-1.31 (t, 6H, $J = 14.4$ Hz). ^{13}C NMR (CDCl_3 , 100 MHz): 170.27, 166.62, 72.51, 62.84, 62.62, 47.70, 14.03, 13.92.

(2S,3S)-diethyl 2-bromo-3-hydroxysuccinate (2b). ^1H NMR (CDCl_3 , 400 MHz): δ 4.73-4.72 (d, 1H, 4.0 Hz); 4.69-4.68 (bt, 1H); 4.34-4.24 (m, 4H); 3.43-3.41 (d, 1H, $J = 7.2$ Hz); 1.35-1.31 (t, 6H, $J = 14.4$ Hz). ^{13}C NMR (CDCl_3 , 100 MHz): 170.27, 166.62, 72.51, 62.84, 62.62, 47.70, 14.03, 13.92.

(2S,3S)-diethyl oxirane-2,3-dicarboxylate (3a). **2a** (38.1 g, 142 mmol) was dissolved in anhydrous Et_2O (100 ml) and DBU (32.3 g, 212.4 mmol, in Et_2O [50 ml]) was added dropwise at 0 °C for 1 h. The reaction was allowed to warm to r.t. and stirred for an additional 4 h. Reaction was quenched with cold 1N HCl to pH ~5. The resulting aqueous layer was extracted with Et_2O (3 x 150 ml). The combined organic extracts were washed with brine (2 x 100 ml), dried over Na_2SO_4 , and concentrated to give the pure product as faintly yellow oil (21.5 g, 80.7 % yield). Product purity typically reflects that of the bromohydrin starting material. If necessary, fractional vacuum distillation can be used for purification. ^1H NMR (CDCl_3 , 400 MHz): δ 4.36-4.22 (m, 4H); 3.67 (s, 2H); 1.35-1.31 (t, 6H). ^{13}C NMR (CDCl_3 , 100 MHz): 166.75, 62.21, 52.01, 14.01.

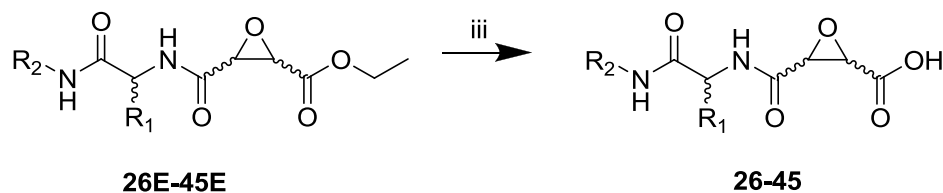
(2R,3R)-diethyl oxirane-2,3-dicarboxylate (3b). Followed general procedure for **3a** using the following quantities: **2b** (34.6 g, 129 mmol); Et_2O (100 ml); DBU (29.4 g, 193 mmol, in Et_2O [50

ml]); yielded **3b** as a colorless oil (18.1 g, 74.8 %). ^1H NMR (CDCl_3 , 400 MHz): δ 4.36-4.22 (m, 4H); 3.67 (s, 2H); 1.35-1.31 (t, 6H). ^{13}C NMR (CDCl_3 , 100 MHz): 166.75, 62.21, 52.01, 14.01.

(2S,3S)-3-(ethoxycarbonyl)oxirane-2-carboxylic acid (4a). An ethanolic solution of KOH (4.2 g, 64 mmol, in EtOH [50 ml]) was added dropwise to the **3a** (9.7 g, 63 mmol) in EtOH (20 ml) at 0 °C for 30 min, and then the reaction was continued at r.t. for 8 h. The resulting viscous solution was diluted with ice water (150 ml), extracted with EA (2 x 200 ml). The aqueous layer was acidified with 1N HCl to pH~4, and extracted with EA (3 x 150 ml). Combined organic extracts washed with brine (2 x 50 ml), dried over Na_2SO_4 , and concentrated to afford the pure epoxide monoester **4a** as colorless oil (8.9 g, 86.9 %). ^1H NMR (CDCl_3 , 400 MHz): δ 7.57 (br, 1H); 4.35-4.24 (m, 2H); 3.73(s, 1H); 3.72 (s, 1H); 1.36-1.32 (t, 3H). ^{13}C NMR (CDCl_3 , 100 MHz): 171.61, 166.40, 62.45, 52.20, 51.45, 13.89.

(2R,3R)-3-(ethoxycarbonyl)oxirane-2-carboxylic acid (4b). Followed general procedure for **4a** using the following quantities: **3b** (15.2 g, 81 mmol); KOH (4.53 g, 81 mmol, in EtOH [50 ml]); yielded **4b** as a colorless oil (9.5 g, 73.5 %). ^1H NMR (CDCl_3 , 400 MHz): δ 7.57 (br, 1H); 4.35-4.24 (m, 2H); 3.73(s, 1H); 3.72 (s, 1H); 1.36-1.32 (t, 3H). ^{13}C NMR (CDCl_3 , 100 MHz): 171.61, 166.40, 62.45, 52.20, 51.45, 13.89.

Scheme 2



Reagents: iii) LiOH, THF/MeOH/H₂O, 0°C, 50-85 %.

Table 1. Structure designations of Scheme 2 analogs

Compound	R1	R2	Stereochem
26, 26E	L-Leucine	Phenyl	<i>S,S,S</i>
27, 27E	L-Leucine	2,6 difluorophenyl	<i>S,S,S</i>
28, 28E	L-Leucine	2,6 difluorophenyl	<i>S,R,R</i>
29 (BiEP), 29E	L-Leucine	D-Biotin-NH-(CH ₂) ₄ -NH ₂	<i>S,S,S</i>
30, 30E	L-Leucine	Lipoyl-NH-(CH ₂) ₄ -NH ₂	<i>S,S,S</i>
31 (NYC-131), 31E	L-Leucine	4-(4-Fluorophenyl)thiazol-2-amine	<i>S,S,S</i>
32, 32E	L-Leucine	4-(4-Fluorophenyl)thiazol-2-amine	<i>S,R,R</i>
33, 33E	L-Leucine	4-F-Phenyl-SO ₂ -NH-(CH ₂) ₄ -NH ₂	<i>S,S,S</i>
34, 34E	L-Histidine	Phenyl	<i>S,S,S</i>
35, 35E	L-Histidine	1,3,5 trimethylaniline	<i>S,S,S</i>
41 (NYC-215), 41E	L-Histidine	4-(4-Fluorophenyl)thiazol-2-amine	<i>S/R,S,S</i>
37, 37E	L-Histidine	4-(4-Fluorophenyl)thiazol-2-amine	<i>S/R,R,R</i>
38, 38E	L-Histidine	6-fluorobenzo[d]thiazol-2-amine	<i>S/R,S,S</i>
39, 39E	L-Histidine	6-fluorobenzo[d]thiazol-2-amine	<i>S/R,R,R</i>
40, 40E	L-Ala(4-thiazoyl)-OH	Phenyl	<i>S,S,S</i>
41 (NYC-438), 41E	L-Ala(4-thiazoyl)-OH	4-(4-Fluorophenyl)thiazol-2-amine	<i>S,S,S</i>
42, 42E	L-Ala(4-thiazoyl)-OH	Propargylamine	<i>S,S,S</i>
43, 43E	L-Ala(4-thiazoyl)-OH	4-(4-Ethynyl)thiazol-2-amine	<i>S,S,S</i>
44, 44E	L-His(2-Me)-OH	4-(4-Fluorophenyl)thiazol-2-amine	<i>S,S,S</i>
45, 45E	L-His(4-Me)-OH	4-(4-Fluorophenyl)thiazol-2-amine	<i>S,S,S</i>

Optimized procedure for the coupling of Arylamines to N-protected peptidomimetics.

A round bottom was charged with the appropriate Boc-protected carboxylic acid (1.0 eq) dissolved in minimal DMF (~3 ml/mmol) under argon and maintained at 0 °C. EDCI (1.2 eq) was then added in one portion and the suspension stirred until homogenous (typically < 5 min), followed by the addition of HOBt (1.5 eq). After stirring for an additional 15 min, the amine (1.0 eq) in DMF (~2 ml/mmol) was added dropwise, and the reaction allowed to warm to r.t., monitored by TLC. In cases where amine remained on TLC after 8 h, reaction was again brought to 0 °C, and additional EDCI (0.5 eq) was added, followed by stirring for an additional 4 h. Reaction was quenched acidified to pH ~ 4 with 1 N HCl, extracted CH₂Cl₂ (3x). Combined organic extracts were washed with 1 N HCl (2x), and brine (1x), dried over Na₂SO₄, concentrated in vacuo, and purified by column chromatography to give the desired peptidomimetic scaffolds.

General procedure for coupling of the epoxide monoester with the peptidomimetic amine.

TFA (10 eq) was added to a suspension of compound the boc protected peptidomimetic (1 eq) in CH₂Cl₂ (20 ml/ 1 mmol peptidomimetic) at 0 °C and the reaction mixture stirred at the same temperature for 2 h. Excess TFA and CH₂Cl₂ were removed under vacuo and the residual TFA-salt was either dried under high vacuum and subjected to next reaction without further purification, or dissolved in MeOH/H₂O and brought to pH of ~ 7 using a saturated NaHCO₃ solution, followed by extraction with CH₂Cl₂ (3 x 50 ml) and removal of solvent in vacuo to afford the pure free amine, which was used without further purification. The intermediate deprotected amine (1 eq), the epoxide monoester (1.0eq), and HOBt (1.1eq) were dissolved minimal DMF and then DIPEA (1 mL, 5.6 mmol) and EDCI (326 mg, 1.7 mmol) were added. After stirring at ambient temperature for 12 h water was added to the reaction mixture and

diluted with 200 mL of CH₂Cl₂. The organic layer was separated and washed with 1M HCl (20 mL), saturated NaHCO₃ solution (10 mL), water (30 mL), brine (10 mL), and dried over anhydrous Na₂SO₄ and concentrated in *vacuo*. Column purification of the crude mixture gave the title compounds.

Optimized procedure for coupling of the epoxide monoester with the peptidomimetic amine

TFA (10 eq) was added to a suspension of compound the boc protected peptidomimetic (1 eq) in freshly distilled CH₂Cl₂ (10 ml/ 1 mmol peptidomimetic) at 0 °C and the reaction mixture stirred at the same temperature for 6 h. If needed, additional TFA (5 eq) was added at 0 °C every 30 min until no starting material remained on TLC. The reaction was then concentrated under *vacuo* and the residual TFA-salt was dissolved in MeOH/H₂O and brought to pH of ~ 7 using a sat.

NaHCO₃ solution, followed by extraction with CH₂Cl₂ (3 x 50 ml) and removal of solvent in *vacuo* to afford the pure free amine, which was dried under high vacuum and used in the next reaction without further purification. A round bottom was charged with the epoxide monoacid (1.0 eq) dissolved in minimal DMF (~2 ml/mmol) with DIPEA (1.1 eq) under argon and maintained at 0 °C. EDCI (1.0 eq) was then added in one portion and the suspension stirred until homogenous (typically < 5 min), followed by the addition of HOBt (1.2 eq). After stirring for an additional 15 min, the free amine (1.0 eq) in DMF (~3 ml/mmol) was added dropwise, and the reaction allowed to warm to room temperature, monitored by TLC. After 12 h, the reaction was quenched acidified to pH ~ 4 with 1 N HCl, extracted CH₂Cl₂ (3x). Combined organic extracts were washed with 1 N HCl (2x), and brine (1x), dried over Na₂SO₄, concentrated in *vacuo*, and purified by column chromatography to give the desired peptidomimetic scaffolds.

(2S,3S)-ethyl-3-((S)-4-methyl-1-oxo-1-(phenylamino)pentan-2-ylcarbamoyl)oxirane-2-carboxylate (26E). General procedure using: Boc-protected peptidomimetic (570 mg, 1.1

mmol); (2*S*, 3*S*)-epoxysuccinic acid monoester (126 mg, 0.93 mmol), DIPEA (0.16 mL, 0.93 mmol), and HOBT (126 mg, 0.93 mmol) CH₂Cl₂ (10 ml)/DMF (2 ml); EDCI (220 mg, 1.1 mmol) in DMF (1 mL) gave the title compound (100 mg, 30.6 %) as white solid. ¹H NMR (CDCl₃, 400 MHz): δ 7.57-7.55 (d, 2H, J = 7.67 Hz); 7.34-7.30 (t, 2H); 7.13-7.10 (t, 1H); 4.63-4.61 (m, 1H); 4.30-4.24 (m, 2H); 3.729-3.725 (d, 1H, J = 1.67 Hz); 3.62-3.61 (d, 1H, J = 1.72 Hz); 1.76-1.63 (m, 3H); 1.33-1.29 (t, 3H); 1.02-1.00 (t, 6H). ¹³C NMR (CDCl₃, 100 MHz): 171.22, 169.07, 167.15, 137.98, 128.41, 124.12, 120.14, 52.90, 52.58, 52.50, 51.70, 40.70, 29.50, 24.65, 22.04, 20.60.

(2*S*,3*S*)-ethyl-3-((*S*)-1-(2,6-difluorophenylamino)-4-methyl-1-oxopentan-2-

ylcarbamoyl)oxirane-2-carboxylate (27E). General procedure using: Boc-protected peptidomimetic (600 mg, 1.7 mmol); (2*S*, 3*S*)-epoxysuccinic acid monoester (280 mg, 1.7 mmol), DIPEA (0.45 mL, 2.6 mmol), in CH₂Cl₂ (10 ml)/DMF (5 ml); EDCI (280 mg, 1.7 mmol) in DMF (1 mL) gave the title compound (210 mg, 31.6 %) as white solid. ¹H NMR (400 MHz, CDCl₃): δ 8.20 (s, 1H); 7.18-7.16 (t, 1H); 6.94-6.90 (t, 2H); 6.72-6.70 (d, 1H); 4.86-4.85 (q, 1H); 4.29-4.23 (m, 2H); 3.83-3.80 (d, 1H, J = 1.69 Hz); 3.72-3.55 (d, 1H, J = 1.69 Hz); 1.84-1.70 (m, 3H); 1.30-1.26 (t, 3H); 1.01-0.99(d, 6H). ¹³C NMR (DMSO-*d*₆, 100 MHz): 170.10, 166.5, 166.39, 158.92, 156.46, 127.73, 111.88, 111.54, 164.9, 62.27, 53.9, 52.9, 51.01, 41.2, 24.74, 22.5, 14.0.

(2*R*,3*R*)-ethyl-3-((*S*)-1-(2,6-difluorophenylamino)-4-methyl-1-oxopentan-2-

ylcarbamoyl)oxirane-2-carboxylate (28E). General procedure using: Boc-protected peptidomimetic (550 mg, 1.6mmol); (2*S*, 3*S*)-epoxysuccinic acid monoester (250 mg, 1.6 mmol), DIPEA (0.65 mL, 3.8 mmol), and HOBT (250 mg, 1.9 mmol) in CH₂Cl₂ (15 ml)/DMF (5 ml); EDCI (300 mg, 2.0 mmol) in DMF (1 mL) gave the title compound (25 mg, 41.6 %) as white

solid. ^1H NMR (400 MHz, CDCl_3): δ 8.20 (s, 1H); 7.19-7.17 (t, 1H); 6.94-6.90 (t, 2H); 6.72-6.70 (d, 1H); 4.86-4.85 (q, 1H); 4.31-4.25 (m, 2H); 3.84-3.81 (d, 1H, $J = 1.69$ Hz); 3.73-3.56 (d, 1H, $J = 1.69$ Hz); 1.84-1.69 (m, 3H); 1.32-1.28 (t, 3H); 1.02-1.00 (d, 6H). ^{13}C NMR (CDCl_3 , 100 MHz): 170.10, 166.67, 166.39, 158.92, 156.46, 127.73, 111.78, 111.54, 62.28, 53.67, 52.69, 51.21, 40.81, 24.74, 22.74, 22.11, 13.97.

(2S,3R)-ethyl-3-((S)-4-methyl-1-oxo-1-(4-(5-((3aS,4S,6aR)-2-oxohexahydro-1H-thieno[3,4-d]imidazol-4-yl)pentanamido)butylamino)pentan-2-ylcarbamoyl)oxirane-2-carboxylate (29E). General procedure using: Boc-protected peptidomimetic (570 mg, 1.1 mmol); (2S, 3S)-epoxysuccinic acid monoester (176 mg, 1.1 mmol), DIPEA (0.2 mL, 1.1 mmol), and HOBT (178 mg, 1.3 mmol) in DMF (5 mL); EDCI (232 mg, 1.2 mmol) in DMF (1 mL) gave the title compound (624 mg, 85 %) as white solid. ^1H NMR ($\text{DMSO}-d_6$, 400 MHz): δ 8.62 (d, 1H); 8.08 (t, 1H); 7.74 (t, 1H); 6.42 (s, 1H); 6.36 (s, 1H); 4.31 (m, 2H); 4.18 (m, 3H); 3.71 (d, 1H); 3.59 (d, 1H); 3.12 (m, 1H); 3.01 (m, 4H); 2.92 (dd, 1H); 2.58 (d, 1H); 2.04 (t, 2H); 1.49 (m, 7H); 1.35 (m, 6H); 1.23 (t, 3H); 0.89 (d, 3H); 0.83 (d, 3H). ^{13}C NMR ($\text{DMSO}-d_6$, 100 MHz): 171.7; 170.9; 167.1; 164.4; 162.6; 61.4; 60.9; 59.1; 55.3; 52.8; 51.1; 41.0; 38.2; 37.9; 35.1; 28.1; 27.9; 26.5; 26.4; 25.2; 24.1; 22.8; 21.5; 13.8. ESI-LRMS (m/z): $[\text{M}+\text{H}]^+ = 570$.

(2S,3S)-ethyl-3-((2S)-1-((5-(1,2-dithiolan-3-yl)pentanamido)methylamino)-4-methyl-1-oxopentan-2-ylcarbamoyl)oxirane-2-carboxylate (30E). General procedure using: Boc-protected peptidomimetic (170 mg, 0.35 mmol); (2S, 3S)-epoxysuccinic acid monoester (56 mg, 0.35 mmol), DIPEA (0.06 mL, 0.35 mmol), and HOBT (56 mg, 0.42 mmol) in DMF (2 mL); EDCI (73 mg, 1.2 mmol) in DMF (0.5 mL) gave the title compound (53 mg, 28 %) as white solid. ^1H NMR (CDCl_3 , 400 MHz): δ 7.23-7.21 (d, 1H, $J = 8.4$ Hz); 7.18-7.15 (t, 1H); 6.33 (t, 1H); 4.51-4.49 (q, 1H); 4.28-4.24 (m, 2H); 3.717-3.713 (d, 1H, $J = 1.60$ Hz); 3.60-3.57 (m, 1H);

3.524-3.520 (d, 1H, $J = 1.60$ Hz); 3.18-3.11 (m, 7H); 2.47-2.45 (m, 1H); 2.22-2.18 (t, 2H); 1.93-1.90 (m, 1H); 1.67-1.52 (m, 15H); 1.33-1.30 (dd, 4H); 0.94-0.90 (t, 6H). ^{13}C NMR (CDCl_3 , 100 MHz): 173.66, 171.94, 167.13, 166.52, 62.85, 56.95, 56.92, 54.28, 53.28, 52.01, 41.89, 40.73, 40.10, 39.72, 39.40, 39.23, 38.94, 36.87, 35.07, 29.38, 29.36, 27.65, 27.50, 26.89, 26.27, 25.90, 25.32, 23.41, 22.48, 14.52. ESI-LRMS (m/z): $[\text{M}+\text{H}]^+ = 532$.

(2S,3S)-ethyl-3-((S)-1-(4-(4-fluorophenyl)thiazol-2-ylamino)-4-methyl-1-oxopentan-2-ylcarbamoyl)oxirane-2-carboxylate (31E). General procedure using: Boc-protected

peptidomimetic (410 mg, 1.0 mmol); (2S, 3S)-epoxysuccinic acid monoester (160 mg, 1.0 mmol), DIPEA (0.18 mL, 1.0 mmol), and HOBT (163 mg, 1.2 mmol) in CH_2Cl_2 (10 mL); EDCI (211 mg, 1.1 mmol) in DMF (0.5 mL) gave the title compound (203 mg, 40.1 %) as white solid. ^1H NMR (400 MHz, CDCl_3): δ 9.96 (s, 1H); 7.79-7.76 (q, 2H); 7.11-7.07 (m, 3H); 6.57-6.55 (d, 1H, $J = 8.4$ Hz); 4.80-4.78 (t, 1H); 4.29-4.23 (m, 2H); 3.868-3.864 (d, 1H, $J = 1.60$ Hz); 3.522-3.581 (d, 1H, $J = 1.60$ Hz); 1.86-1.81 (m, 1H); 1.66-1.61 (m, 2H); 1.28-1.24 (m, 4H); 0.98-0.94 (t, 6H). ^{13}C NMR ($\text{DMSO}-d_6$, 100 MHz): 170.28, 167.48, 165.78, 163.43, 161.00, 158.23, 148.34, 135.36, 131.32, 128.17, 116.13, 108.52, 62.01, 53.71, 53.36, 51.82, 14.33. ESI-LRMS (m/z): $[\text{M}+\text{H}]^+ = 450$.

(2R,3R)-ethyl-3-((S)-1-(4-(4-fluorophenyl)thiazol-2-ylamino)-4-methyl-1-oxopentan-2-ylcarbamoyl)oxirane-2-carboxylate (32E). General procedure using: Boc-protected

peptidomimetic (290 mg, 0.71 mmol); (2S, 3S)-epoxysuccinic acid monoester (113 mg, 0.71 mmol), DIPEA (0.13 mL, 0.71 mmol), and HOBT (115 mg, 0.85 mmol) in DMF (3 mL); EDCI (150 mg, 0.78 mmol) in DMF (0.5 mL) gave the title compound (100 mg, 31.5 %) as white solid. ^1H NMR (400 MHz, CDCl_3): δ 9.96 (s, 1H); 7.79-7.76 (q, 2H); 7.11-7.06 (m, 3H); 6.48-6.46 (d, 1H, $J = 8.4$ Hz); 4.71-4.69 (t, 1H); 4.25-4.22 (m, 2H); 3.78-3.77 (d, 1H, $J = 1.20$ Hz); 3.60-3.59

(d, 1H, $J = 1.20$ Hz); 1.86-1.81 (m, 1H); 1.71-1.60 (m, 2H); 1.30-1.25 (m, 4H); 0.98-0.96 (t, 6H).

^{13}C NMR (DMSO- d_6 , 100 MHz): 170.24, 167.46, 165.58, 163.43, 161.00, 158.20, 148.34,

135.36, 131.29, 128.09, 115.92, 108.52, 62.01, 53.52, 53.41, 51.85, 14.33. ESI-LRMS (m/z):

$[\text{M}+\text{H}]^+ = 450$.

(2S,3S)-ethyl-3-((S)-1-(4-(4-fluorophenylsulfonamido)butylamino)-4-methyl-1-oxopentan-2-ylcarbamoyl)oxirane-2-carboxylate (33E). General procedure using: Boc-protected

peptidomimetic (442 mg, 1.0 mmol); (2S, 3S)-epoxysuccinic acid monoester (154.1 mg, 0.96

mmol), DIPEA (0.17 mL, 0.96 mmol), and HOBT (157 mg, 1.15 mmol) in DMF (5 mL); EDCI

(203 mg, 1.05 mmol) in DMF (0.5 mL) gave the title compound (321 mg, 60.5 %) as white solid.

^1H NMR (400 MHz, CDCl_3): δ 7.89-7.86 (m, 2H); 7.21-7.19 (t, 2H); 6.87-6.85 (d, 1H, $J = 8.40$

Hz); 6.32 (bs, 1H); 5.25 (t, 1H); 4.27-4.25 (q, 1H); 4.22-4.19 (m, 2H); 3.71-3.70 (d, 1H, $J = 1.60$

Hz); 3.48-3.47 (d, 1H, $J = 1.60$ Hz); 3.28-3.12 (m, 2H); 2.95-2.93 (d, 2H); 1.62-1.45 (m, 9H);

1.33-1.30 (t, 3H); 0.94-0.90 (t, 6H). ^{13}C NMR (CDCl_3 , 100 MHz): 171.52, 166.67, 166.63,

166.51, 163.98, 130.01, 129.92, 116.66, 116.44, 62.65, 53.99, 53.23, 51.75, 42.98, 41.20, 39.15,

26.80, 26.63, 25.06, 23.06, 22.19, 14.25. ESI-LRMS (m/z): $[\text{M}+\text{H}]^+ = 502$.

(2S,3S)-ethyl-3-((S)-3-(1H-imidazol-5-yl)-1-oxo-1-(phenylamino)propan-2-

ylcarbamoyl)oxirane-2-carboxylate (34E). General procedure using: Boc-protected

peptidomimetic (463 mg, 1.4 mmol); (2S, 3S)-epoxysuccinic acid monoester (220 mg, 1.4

mmol), DIPEA (0.24 mL, 1.4 mmol), and HOBT (230 mg, 1.7 mmol) in DMF (5 mL); EDCI

(300 mg, 1.5 mmol) in DMF (0.5 mL) gave the title compound (180 mg, 34.5 %) as white

solid. ^1H NMR (400 MHz, $\text{MeOD}-d^4$): δ 7.63 (s, 1H); 7.52-7.50 (d, 2H, $J = 7.72$ Hz); 7.33-7.31

(t, 2H); 7.13-7.11 (t, 1H); 6.90 (s, 1H); 4.76-4.75 (t, 1H); 4.29-4.24 (q, 2H); 3.69-3.68 (d, 1H, $J =$

1.56 Hz); 3.64-3.63 (d, 1H, $J = 1.56$ Hz); 3.17-3.05 (qd, 2H); 1.33-1.29 (t, 3H). ^{13}C NMR

(MeOD- d^4 , 100 MHz): 169.75, 167.25, 166.90, 137.85, 134.98, 127.36, 124.19, 119.88, 61.73, 54.15, 52.90, 51.60, 12.88.

(2S,3S)-ethyl-3-((S)-3-(1H-imidazol-5-yl)-1-(mesitylamino)-1-oxopropan-2-

ylcarbamoyl)oxirane-2-carboxylate (35E). General procedure using: Boc-protected

peptidomimetic (180 mg, 0.47 mmol); (2S, 3S)-epoxysuccinic acid monoester (75 mg, 0.47 mmol), DIPEA (0.12 mL, 0.7 mmol), and HOBT (76 mg, 0.56 mmol) in DMF (5 ml); EDCI (99 mg, 0.52 mmol) in DMF (0.5 mL) gave the title compound (55 mg, 28.3 %) as white solid. ^1H NMR (400 MHz, MeOD- d^4): δ 7.66 (s, 1H); 6.96 (s, 1H) ; 6.88 (s,1H); 4.27-4.25 (q, 2H); 3.68 (s, 1H); 3.32 (s, 1H); 3.21-3.07 (m, 2H); 2.25 (s, 3H); 2.06 (s, 6H); 1.32-1.29 (t, 3H). ^{13}C NMR (MeOD): ^{13}C NMR (MeOD- d^4 , 100 MHz): 167.22, 136.74, 135.14, 128.25, 61.74, 52.98, 51.80, 19.53, 16.77, 12.88. MS (ESI) m/z 415.2 (M+H) $^+$.

(2S,3S)-ethyl-3-(1-(4-(4-fluorophenyl)thiazol-2-ylamino)-3-(1H-imidazol-4-yl)-1-oxopropan-

2-ylcarbamoyl)oxirane-2-carboxylate (36E). General procedure using: the racemic Boc-

protected peptidomimetic (400 mg, 1.2 mmol); (2S, 3S)-epoxysuccinic acid monoester (160 mg, 1.0 mmol), DIPEA (0.43 mL, 2.5 mmol) and HOBT (76 mg, 0.56 mmol) in DMF (5 ml); EDCI (210 mg, 1.1 mmol) in DMF (0.5 mL) gave the title compound (217 mg, 45.8 %) as a racemic mixture in the form of a white solid. ^1H NMR (DMSO- d_6 , 400 MHz): δ 12.50 (bs, 1H); 11.90 (bs, 1H); 8.85-8.76 (dd, 1H, J = 7.14 Hz); 7.95-7.91 (q, 2H); 7.64-7.58 (m, 2H); 7.28-7.24 (t, 2H); 6.84 (bs, 1H); 4.79-4.75 (q, 1H); 4.22-4.18 (q, 2H); 3.74-3.73 (dd, 1H, J = 1.80 Hz); 3.63-3.62 (dd, 1H; J = 1.80 Hz); 3.17-3.08 (m, 2H); 1.25-1.21 (t, 3H). ^{13}C NMR (DMSO- d_6 , 100 MHz): 169.53, 168.87, 168.81, 165.98, 165.83, 162.89, 160.47, 157.65, 147.82, 134.58, 132.10, 127.64, 127.56, 116.40, 115.60, 115.40, 108.04, 52.98, 52.75, 51.90, 28.55, 28.42.

(2R,3R)-ethyl-3-(1-(4-(4-fluorophenyl)thiazol-2-ylamino)-3-(1H-imidazol-4-yl)-1-

oxopropan-2-ylcarbamoyl)oxirane-2-carboxylate (37E). General procedure using: the racemic Boc-protected peptidomimetic (400 mg, 1.0 mmol); (2*S*, 3*S*)-epoxysuccinic acid monoester (149 mg, 0.93 mmol), DIPEA (0.16 mL, 0.93 mmol) and HOBt (151 mg, 1.1 mmol) in DMF (5 mL); EDCI (196 mg, 1.0 mmol) in DMF (0.5 mL) gave the title compound (240 mg, 50.8 %) as a racemic mixture in the form of a white solid. ¹H NMR (DMSO-*d*₆, 400 MHz): δ 12.52 (bs, 1H); 11.86 (bs, 1H); 8.85-8.77 (dd, *J* = 7.21 Hz; *J* = 7.48 Hz); 7.95-7.91 (q, 2H); 7.62 (s, 1H); 7.57 (s, 1H); 7.28-7.24 (t, 2H); 6.84 (s, 1H); 4.81-4.76 (m, 1H); 4.23-4.15 (m, 1H); 3.76-3.74 (dd, 1H, *J* = 1.8 Hz; *J* = 1.8 Hz); 3.64-3.61 (dd, 1H, *J* = 1.8 Hz; *J* = 1.8 Hz); 3.08-2.99 (m, 2H); 1.25-1.17 (t, 3H). ¹³C NMR (DMSO-*d*₆, 100 MHz): 170.28 & 170.24, 167.48 & 167.46, 165.78 & 165.58, 163.43, 161.01, 158.53 & 158.20, 135.37, 131.32 & 131.29, 128.17 & 128.09, 116.13 & 115.92, 108.52, 62.01, 53.72 & 53.52, 53.41 & 53.36, 51.85 & 51.82, 14.33.

(2*S*,3*S*)-ethyl-3-(1-(6-fluorobenzo[*d*]thiazol-2-ylamino)-3-(1H-imidazol-4-yl)-1-oxopropan-

2-ylcarbamoyl)oxirane-2-carboxylate (38E). General procedure using: the racemic Boc-protected peptidomimetic (402 mg, 0.99 mmol); (2*S*, 3*S*)-epoxysuccinic acid monoester (159 mg, 0.99 mmol), DIPEA (0.18 mL, 0.99 mmol) and HOBt (161 mg, 1.18 mmol) in DMF (5 mL); EDCI (209 mg, 1.09 mmol) in DMF (0.5 mL) gave the title compound (229 mg, 51.5 %) as a racemic mixture in the form of a white solid. ¹H NMR (CDCl₃, 400 MHz): δ 7.96 (bs, 1H); 7.76-7.73 (m, 2H); 7.52-7.50 (d, 1H); 7.18-7.14 (m, 1H); 6.94 (s, 1H); 4.93 (bs, 1H); 4.32-4.27 (m, 2H); 3.78 (s, 1H); 3.63 (s, 1H); 3.26-3.22 (dd, 1H); 3.10-3.06 (dd, 1H); 1.36-1.32 (t, 3H). ¹³C NMR (CDCl₃, 100 MHz): 172.15, 168.52 & 168.50, 166.88 & 166.70, 161.31, 159.19 & 158.91, 146.53, 136.25, 134.04 & 133.93, 122.94 & 122.84, 115.55 & 115.30, 109.41 & 109.14, 62.40, 55.67, 54.20 & 53.98, 53.72 & 53.66, 52.17 & 52.12, 14.42.

(2R,3R)-ethyl-3-(1-(6-fluorobenzo[d]thiazol-2-ylamino)-3-(1H-imidazol-4-yl)-1-oxopropan-2-ylcarbamoyl)oxirane-2-carboxylate (39E). General procedure using: Boc-protected peptidomimetic (420 mg, 1.0 mmol); (2*S*, 3*S*)-epoxysuccinic acid monoester (162 mg, 1.01 mmol), DIPEA (0.18 mL, 1.01 mmol) and HOBt (164 mg, 1.21 mmol) in DMF (5 mL); EDCI (213 mg, 1.11 mmol) in DMF (0.5 mL) gave the title compound (226 mg, 50.5 %) as a racemic mixture in the form of a white solid. ¹H NMR (DMSO-*d*⁶, 400 MHz): δ 11.85 (bs, 1H); 8.89-8.81 (dd, 1H, *J* = 7.21 Hz; *J* = 7.42 Hz); 7.91-7.88 (dd, 1H, *J* = 2.5 Hz; *J* = 2.5 Hz); 7.77-7.74 (q, 1H); 7.57 (s, 1H); 7.32-7.27 (td, 1H, *J* = 2.5 Hz; *J* = 2.5 Hz; *J* = 2.5 Hz); 6.85 (s, 1H); 4.82-4.76 (m, 1H); 4.23-4.16 (m, 2H); 3.76-3.74 (dd, 1H, *J* = 1.8 Hz; *J* = 1.8 Hz); 3.65-3.61 (, 1H, *J* = 1.8 Hz; *J* = 1.8 Hz); 3.17-2.98 (m, 2H); 1.25-1.17 (t, 3H). ¹³C NMR (DMSO-*d*₆, 100 MHz): 171.13 & 171.09, 167.47 & 167.45, 165.83 & 165.65, 160.32, 158.21 & 157.93, 145.64, 135.40, 133.23 & 133.12, 122.17 & 122.08, 114.83 & 114.59, 108.74 & 108.47, 62.01, 53.86 & 53.65, 53.40 & 53.33, 51.86 & 51.81, 14.34.

(2*S*,3*S*)-ethyl-3-((*S*)-1-oxo-1-(phenylamino)-3-(thiazol-4-yl)propan-2-ylcarbamoyl)oxirane-2-carboxylate (40E). General procedure using: Boc-protected peptidomimetic (230 mg, 0.66 mmol); (2*S*, 3*S*)-epoxysuccinic acid monoester (106 mg, 0.66 mmol), DIPEA (0.12 mL, 0.66 mmol) and HOBt (110 mg, 0.79 mmol) in CH₂Cl₂ (5 mL); EDCI (130 mg, 0.66 mmol) in DMF (0.5 mL) gave the title compound (84 mg, 32.5 %) as white solid. ¹H NMR (MeOD-*d*⁴, 400 MHz): δ 8.94 (s, 1H); 7.52-7.50 (d, 2H); 7.33 (s, 1H); 7.30-7.26 (t, 3H); 7.11-7.07 (t, 1H); 4.98-4.95 (t, 1H); 4.24-4.20 (q, 2H); 3.69 (s, 1H); 3.54 (s, 1H); 3.43-3.28 (m, 2H); 1.28-1.24 (t, 3H). ¹³C NMR (MeOD-*d*⁴, 100 MHz): 169.43, 167.21, 166.84, 153.89, 152.24, 137.82, 128.45, 124.23, 120.24, 116.10, 61.82, 53.60, 53.11, 51.92, 32.94, 12.99.

(2S,3S)-ethyl-3-((S)-1-(4-(4-fluorophenyl)thiazol-2-ylamino)-1-oxo-3-(thiazol-4-yl)propan-2-ylcarbamoyl)oxirane-2-carboxylate (41E). Synthesized following the optimized coupling procedure using: (2S, 3S)-epoxysuccinic acid monoester (622 mg, 3.88 mmol), DIPEA (0.75 mL, 4.2 mmol) in DMF (5 ml); EDCI (890 mg, 4.7 mmol); HOBt (730 mg, 5.4 mmol); deprotected free amine (1.35 g, 3.9 mmol) in DMF (5 ml); after column chromatography afforded the title compound (isolated yield = 1.38 g, 72.4 %) as white solid. ¹H NMR (400 MHz, MeOD-*d*⁴): δ 8.98-8.98 (d, 1H, J = 1.75 Hz); 7.92-7.90 (q, 2H); 7.37 (s, 1H); 7.36 (s, 1H); 7.15-7.10 (t, 2H); 5.06-5.02 (q, 1H); 4.27-4.24 (q, 2H); 3.69-3.68 (d, 1H, J = 1.66 Hz); 3.55-3.54 (d, 1H, J = 1.66 Hz); 3.56-3.29 (m, 2H); 1.33-1.29. ¹³C NMR (DMSO-*d*₆, 100 MHz): 169.17, 167.17, 157.69, 154.00, 151.90, 148.90, 130.95, 127.55, 116.15, 114.99, 114.77, 107.20, 61.76, 52.97, 52.91, 51.82, 32.35, 12.89. ESI-HRMS (m/z): [M-H]⁺ calcd. for C₂₁H₁₉FN₄O₅S₂: 489.0781, observed: 489.0731.

(2S,3S)-ethyl-3-((S)-1-oxo-1-(prop-2-ynylamino)-3-(thiazol-4-yl)propan-2-ylcarbamoyl)oxirane-2-carboxylate (42E). General procedure using: Boc-protected peptidomimetic (740 mg, 3.5 mmol); (2S, 3S)-epoxysuccinic acid monoester (564 mg, 3.52 mmol), DIPEA (1.53 mL, 8.8 mmol); EDCI (740 mg, 3.9 mmol); HOBT (520 mg, 3.9 mmol) in DMF (10 ml); afforded the title compound (960 mg, 77.6 %) as white solid. ¹H NMR (CDCl₃, 400 MHz): δ 8.78 (s, 1H); 7.65-7.63 (d, 1H, J = 1.00 Hz); 7.14 (s, 1H); 7.04 (bs, 1H); 4.80-4.75 (q, 1H); 4.29-4.24 (m, 2H); 3.99-3.97 (q, 2H); 3.72-3.71 (d, 1H, J = 1.6 Hz); 3.53-3.52 (d, 1H, J = 1.6 Hz); 3.34-3.15 (m, 2H); 2.19 (bs, 1H); 1.33-1.30 (t, 3H). ¹³C NMR (CDCl₃, 100 MHz): 169.59, 166.49, 166.45, 153.22, 152.42, 116.20, 78.98, 71.59, 62.31, 53.77, 52.81, 52.44, 32.65, 29.20, 14.02.

(2S,3S)-ethyl 3-((S)-1-(4-(4-ethynylphenyl)thiazol-2-ylamino)-1-oxo-3-(thiazol-4-yl)propan-2-ylcarbamoyl)oxirane-2-carboxylate (43E). ^1H NMR (DMSO- d^6 , 400 MHz) δ = 12.56 (s, 1H); 9.04-9.03 (d, 1H, J = 1.8 Hz); 8.84-8.82 (d, 1H, J = 7.7 Hz); 7.93-7.91 (d, 2H, J = 8.3 Hz); 7.76 (s, 1H); 7.55-7.53 (d, 2H, J = 8.3 Hz); 7.45-7.44 (d, 1H, J = 1.6 Hz); 4.99-4.93 (q, 1H); 4.26 (s, 1H); 4.22-4.16 (m, 2H); 3.72-3.71 (d, 1H, J = 1.7 Hz); 3.56-3.55 (d, 1H, J = 1.7 Hz); 3.67-3.22 (m, 2H); 1.25-1.19 (t, 3H). ^{13}C NMR (DMSO- d^6 , 100 MHz): 170.04, 167.47, 165.62, 158.24, 154.25, 152.62, 148.47, 134.95, 132.61, 126.26, 121.33, 116.67, 110.21, 83.87, 81.99, 62.02, 53.36, 53.11, 51.81, 33.11, 14.33. ESI-HRMS (m/z): $[\text{M}+\text{H}]^+$ calcd. for $\text{C}_{23}\text{H}_{20}\text{N}_4\text{O}_5\text{S}_2$: 497.0948; observed, 497.0949; HPLC method 2: Purity = 96.7 %, R_t = 14.5 min (Ion-Trap HPLC).

(2S,3S)-ethyl-3-((S)-1-(4-(4-fluorophenyl)thiazol-2-ylamino)-3-(1-methyl-1H-imidazol-5-yl)-1-oxopropan-2-ylcarbamoyl)oxirane-2-carboxylate (44E). General procedure using: Boc-protected peptidomimetic (200 mg, 0.45 mmol); (2S, 3S)-epoxysuccinic acid monoester (72 mg, 0.44 mmol), DIPEA (0.078 mL, 0.44 mmol) and HOBt (73 mg, 0.53 mmol) in DMF (4 mL); EDCI (95 mg, 0.49 mmol) in DMF (0.5 mL) gave the title compound (152 mg, 69.3 %) as white solid. ^1H NMR (DMSO- d^6 , 400 MHz): δ 12.59 (bs, 1H); 8.97-8.95 (d, 1H, J = 7.82 Hz); 7.95-7.92 (q, 2H); 7.64 (s, 1H); 7.50 (s, 1H); 7.28-7.24 (t, 2H); 6.67 (s, 1H); 4.87-4.81 (q, 1H); 4.21-4.15 (m, 2H); 3.74-3.73 (d, 1H, J = 1.79 Hz); 3.59 (s, 3H), 3.55-3.54 (d, 1H, J = 1.79 Hz); 3.16-2.97 (m, 2H); 1.24-1.17 (t, 3H). ^{13}C NMR (DMSO- d^6 , 100 MHz): 169.95, 167.48, 165.56, 163.45, 161.02, 148.41, 138.56, 131.27, 128.18, 128.09, 127.82, 127.00, 116.16, 115.95, 108.70, 62.01, 53.24, 52.36, 51.70, 31.30, 26.40, 14.33. ESI-LRMS (m/z): $[\text{M}+\text{H}]^+$ calcd. for $\text{C}_{22}\text{H}_{22}\text{FN}_5\text{O}_5\text{S}$: 487.5, observed: 488.0.

(2S,3S)-ethyl-3-((S)-1-(4-(4-fluorophenyl)thiazol-2-ylamino)-3-(1-methyl-1H-imidazol-4-yl)-1-oxopropan-2-ylcarbamoyl)oxirane-2-carboxylate (45E). General procedure using: Boc-protected peptidomimetic (185.5mg, 0.41mmol); (2S, 3S)-epoxysuccinic acid monoester (67mg, 0.41mmol), DIPEA (0.07mL, 0.41mmol) and HOBT (68mg, 0.49mmol) in DMF (3ml); EDCI (88mg, 0.45mmol) in DMF (0.5mL) gave the title compound (104mg, 50.2%) as white solid. .
¹H NMR (DMSO-*d*⁶, 400 MHz): δ 12.49 (bs, 1H); 8.74-8.72 (d, 1H, J = 7.4 Hz); 7.95-7.92 (q, 2H); 7.62 (s, 1H); 7.49 (s, 1H); 7.27-7.24 (t, 2H); 6.89 (s, 1H); 4.77-4.74 (q, 1H); 4.22-4.17 (m, 2H); 3.75-3.74 (d, 1H, J = 1.8 Hz); 3.62-3.61 (d, 1H, J = 1.8 Hz); 3.58 (s, 3H); 3.02-2.91 (m, 2H); 1.26-1.22 (t, 3H). ¹³C NMR (DMSO-*d*⁶, 100 MHz): 170.31, 167.48, 165.56, 163.43, 161.00, 148.32, 137.89, 136.98, 131.31, 128.11 (d, J = 8.1 Hz); 118.45, 116.14, 115.92, 108.49, 62.01, 53.54, 53.40, 51.87, 33.24, 30.55, 14.34. ESI-LRMS (m/z): [M+H]⁺ calcd. for C₂₂H₂₂FN₅O₅S: 487.5, observed: 488.0.

General Procedure for Epoxide Ester hydrolysis.

The peptidomimetic epoxide ester (1eq) was dissolved in THF/MeOH/H₂O 3:1:1 and cooled to 0 °C and LiOH (1eq) was added and reaction allowed to warm to r.t. Additional LiOH (0.2 eq) was added at 0 °C every 3 h as needed until no starting material remained on TLC. The resulting solution was acidified with cold 1 N HCl and poured into CH₂Cl₂. In some cases the acid precipitated out and was filtered through sintered funnel and washed consecutively with CH₂Cl₂ and H₂O and isolated. In instances when the compound stayed in solution, the aqueous phase was extracted with CH₂Cl₂ (3 x 50 ml), combined organic extracts dried over Na₂SO₄ and concentrated to give the desired product. Typically, the purity of the desired product reflects the purity of the ester starting material. Hence, the purity of the initial ester is important to afford a sufficiently pure acid upon hydrolysis.

(2S,3S)-3-((S)-4-methyl-1-oxo-1-(phenylamino)pentan-2-ylcarbamoyl)oxirane-2-carboxylic acid (26). Followed general procedure using: **26E** (70 mg, 0.2 mmol); LiOH (4.8 mg, 0.2 mmol); after extraction afforded the desired product as a white solid (54 mg, 83.9 %). ^1H NMR (MeOD- d^4 , 400 MHz): δ 7.57-7.55 (d, 2H); 7.33-7.29 (t, 2H); 7.13-7.09 (t, 1H); 4.64-4.61 (m, 1H); 3.71 (s, 1H); 3.57 (s, 1H); 1.76-1.65 (m, 3H); 1.02-0.98 (t, 6H). ^{13}C NMR (MeOD- d^4 , 100 MHz): 171.22, 169.07, 167.14, 137.98, 128.41, 124.12, 120.14, 52.90, 52.58, 51.69, 40.70, 29.49, 24.64, 22.04, 20.59. ESI-HRMS (m/z): $[\text{M}-\text{H}]^+$ calcd. for $\text{C}_{16}\text{H}_{20}\text{N}_2\text{O}_5$: 319.3404, observed: 319.1332. HPLC Method 1: R_t = 21.0min, purity = 96.1 %.

(2S,3S)-3-((S)-1-(2,6-difluorophenylamino)-4-methyl-1-oxopentan-2-ylcarbamoyl)oxirane-2-carboxylic acid (27). Followed general procedure using: **27E** (28mg, 0.72mmol); LiOH (1.7mg, 0.072mmol); after extraction afforded the desired product as a white solid(20mg, 77.0%). ^1H NMR (MeOD- d^4 , 400 MHz): δ 7.91 (s, 1H); 7.36-7.31 (m, 1H); 7.07-7.02 (t, 2H); 4.72 (m, 1H); 3.65 (s, 1H); 3.52 (s, 1H); 1.74-1.68 (m, 3H); 1.01-0.99 (d, 6H). ^{13}C NMR (DMSO- d^6 , 100 MHz): 171.26, 169.20, 165.81, 159.49 (d, J = 5.2 Hz), 157.00 (d, J = 5.2 Hz), 128.98 (t, J = 19.7 Hz); 115.34 (t, J = 34.0 Hz); 113.10 (d, J = 5.2 Hz), 107.43, 106.22, 52.96, 51.51, 51.32, 41.30, 24.71, 23.81. ESI-HRMS (m/z): $[\text{M}-\text{H}]^+$ calcd. for $\text{C}_{16}\text{H}_{20}\text{N}_2\text{O}_5$: 355.3216, observed: 355.3101. HPLC Method 1: R_t = 19.7 min, purity = 95.0 %.

(2R,3R)-3-((S)-1-(2,6-difluorophenylamino)-4-methyl-1-oxopentan-2-ylcarbamoyl)oxirane-2-carboxylic acid (28). Followed general procedure using: **28E** (85 mg, 0.22 mmol); LiOH (5.2 mg, 0.22 mmol); after extraction afforded the desired product as a white solid (59 mg, 74.8 %). ^1H NMR (DMSO- d^6 , 400 MHz): δ 9.88 (s, 1H); 8.81-8.79 (d, 1H, J = 8.21Hz); 7.38-7.33 (m, 1H); 7.17-7.13 (t, 2H); 4.61-4.56 (q, 1H); 3.70-3.69 (d, 1H, J = 1.79 Hz); 3.52-3.51 (d, 1H, J = 1.79 Hz); 1.66-1.58 (m, 3H); 0.93-0.88 (dd, 6H). ^{13}C NMR (DMSO- d_6 , 100 MHz): 171.35,

169.20, 165.79, 159.48 (d, J = 5.16Hz); 157.01 (d, J = 5.21Hz); 128.58 (t, 19.7 Hz); 114.63 (t, J = 34.0 Hz); 112.39 (d, J = 22.6Hz); 53.05, 51.71, 51.62, 41.32, 24.71, 21.96. ESI-HRMS (m/z): [M-H]⁺ calcd. for C₁₆H₂₀N₂O₅: 355.3216, observed: 355.3201. HPLC Method 1: R_t = 18.9 min, purity = 96.5 %.

(2S,3S)-3-((S)-4-methyl-1-oxo-1-(4-(5-((3aS,4S,6aR)-2-oxohexahydro-1H-thieno[3,4-d]imidazol-4-yl)pentanamido)butylamino)pentan-2-ylcarbamoyl)oxirane-2-carboxylic acid (29, BiEP). Synthesized following general saponification procedure using the following quantities: **29E** (155 mg, 0.3 mmol); LiOH (14 mg, 0.58 mmol); MeOH/H₂O (1.5 mL:0.5 mL:0.5 mL); yielded **29** as a white solid (40 mg, 27.1 %). ¹H NMR (DMSO-*d*₆, 400 MHz): 8.56 (d, 1H); 8.06 (t, 1H); 7.76 (t, 1H); 6.41 (s, 1H), 6.35 (s, 1H); 4.57 (m, 2H); 4.31 (m, 1 H); 3.66 (d, 1H); 3.31 (d, 1H); 3.08 (m, 1H); 3.01 (m, 3H); 2.80 (dd, 1H); 2.56 (d, 1H); 2.04 (t, 2H); 1.53 (m, 6H); 1.43 (m, 3H); 1.36 (m, 2H); 0.89 (d, 3H); 0.84 (d, 3H). ¹³C NMR (DMSO-*d*₆, 100 MHz): 171.80, 171.06, 168.78, 164.85, 162.68, 61.00, 59.16, 55.36, 52.65, 51.19, 41.14, 35.17, 28.17, 27.98, 26.59, 26.45, 25.28, 24.24, 22.87, 21.61. ESI-HRMS (m/z): no ionization, mass not seen. HPLC Method 1: R_t = 14.8 min, purity = 95.6 %.

(2S,3S)-3-((2S)-1-(4-(5-(1,2-dithiolan-3-yl)pentanamido)butylamino)-4-methyl-1-oxopentan-2-ylcarbamoyl)oxirane-2-carboxylic acid (30). **30E** (53 mg, 0.1 mmol) was dissolved in 2 mL of 3:1:1 mixture THF, methanol and water and cooled to 0 °C and LiOH (5 mg, 0.2 mmol) was added. After stirring at the same temperature for 15 min the resulting solution was acidified with 1M HCl and extracted with dichloromethane. The organic layer was washed with water, brine, and dried over anhydrous Na₂SO₄ and concentrated in *vacuo*. Column purification of the crude mixture (SiO₂, 15% MeOH/CHCl₃) gave the title compound as a white solide. ¹H NMR (CDCl₃, 400 MHz): δ 8.01-7.99 (d, 1H, J = 10.8 Hz); 7.26 (s, 1H); 6.25 (bs, 1H); 4.57-4.53 (q, 1H); 3.69

(s, 1H); 3.59 (s, 1H); 3.21-3.31 (m, 5H); 2.45-2.42 (m, 1H); 2.24-2.20 (t, 2H); 1.94-1.92 (m, 1H); 1.66-1.51 (m, 12H); 1.25-1.21 (m, 2H); 0.94-0.91 (m, 6H). ^{13}C NMR (CDCl_3 , 100 MHz): 174.12, 172.13, 168.92, 166.64, 56.52, 53.57, 52.57, 51.62, 41.19, 40.31, 39.09, 38.93, 38.50, 36.24, 34.63, 28.93, 26.56, 26.42, 25.55, 24.85, 22.80, 21.87. ESI-HRMS (m/z): $[\text{M}+\text{H}]^+$ calcd. for $\text{C}_{22}\text{H}_{37}\text{N}_3\text{O}_6\text{S}_2$: 504.2197, observed: 504.2192. HPLC Method 1: R_t = 21.7 min, purity = 95.4 %.

(2S,3S)-3-((S)-1-(4-(4-fluorophenyl)thiazol-2-ylamino)-4-methyl-1-oxopentan-2-ylcarbamoyl)oxirane-2-carboxylic acid (31, NYC-131). Followed general procedure using: **31E** (203 mg, 0.45 mmol); LiOH (10.8 mg, 0.45 mmol); after extraction afforded the desired product as a white solid (150 mg, 78.8 %). ^1H NMR ($\text{DMSO}-d^6$, 400 MHz): δ 12.51 (bs, 1H); 8.64-8.61 (d, 1H, J = 12.0 Hz); 7.95-7.92 (t, 2H); 7.62 (s, 1H); 7.28-7.24 (t, 2H); 4.63-4.58 (m, 1H); 3.51-3.50 (d, 1H, J = 1.60 Hz); 3.34-3.33 (d, 1H, J = 1.60 Hz); 1.65-1.54 (m, 3H); 0.91-0.88 (t, 6H). ^{13}C NMR ($\text{MeOD}-d^4$, 100 MHz): 172.44, 165.32, 162.87, 159.37, 150.45, 132.60, 132.57, 129.14, 129.06, 116.56, 116.34, 108.69, 54.41, 53.55, 53.19, 41.79, 26.21, 23.54, 22.02. ESI-HRMS (m/z): $[\text{M}+\text{H}]^+$ calcd. for $\text{C}_{19}\text{H}_{20}\text{FN}_3\text{O}_5\text{S}$: 422.1180, observed: 422.1188. HPLC Method 1: R_t = 24.6 min, purity = 95.7 %.

(2R,3R)-3-((S)-1-(4-(4-fluorophenyl)thiazol-2-ylamino)-4-methyl-1-oxopentan-2-ylcarbamoyl)oxirane-2-carboxylic acid (32). Followed general procedure using: **30E** (76.4 mg, 0.16 mmol); LiOH (8 mg, 0.34 mmol); after extraction afforded the desired product as a white solid (51 mg, 71.5 %). ^1H NMR ($\text{DMSO}-d^6$, 400 MHz): δ 12.52 (s, 1H); 8.78-8.76 (d, 1H, J = 8.0 Hz); 7.94-7.92 (t, 2H); 7.63 (s, 1H); 7.29-7.24 (t, 2H); 4.58-4.57 (m, 1H); 3.62-3.61 (d, 1H, J = 1.80 Hz); 3.41-3.40 (d, 1H, J = 1.80 Hz); 1.64-1.51 (m, 3H); 0.91-0.88 (dd, 6H). ^{13}C NMR ($\text{DMSO}-d^6$, 100 MHz): 171.02, 166.26, 162.88, 160.46, 157.72, 147.81, 130.80, 130.77, 127.62,

127.54, 115.59 (d, $J = 21.6$ Hz); 107.97, 52.36, 52.08, 51.37, 28.89, 24.25, 22.82, 21.19. ESI-HRMS (m/z): $[M+H]^+$ calcd. for $C_{19}H_{20}FN_3O_5S$: 422.1180, observed: 422.1186. HPLC Method 1: $R_t = 23.8$ min, purity = 95.1 %.

(2S,3S)-3-((S)-1-(4-(4-fluorophenylsulfonamido)butylamino)-4-methyl-1-oxopentan-2-ylcarbamoyl)oxirane-2-carboxylic acid (33). Followed general procedure using: **31E** (213 mg, 0.42 mmol); LiOH (21 mg, 0.85 mmol); after extraction afforded the desired product as a white solid (110 mg, 54.7 %). 1H NMR (DMSO- d^6 , 400 MHz): δ 8.15 (s, 1H); 7.89-7.85 (m, 2H); 7.38 (s, 1H); 7.21-7.17 (t, 2H); 6.14 (s, 1H); 3.68-3.60 (d, 2H); 3.38-3.37 (d, 1H, $J = 1.60$ Hz); 3.10-3.09 (d, 1H, $J = 1.60$ Hz); 2.97 (s, 1H); 2.85 (s, 1H); 1.65-1.56 (m, 7H); 0.91-0.88 (m, 6H). ^{13}C NMR (DMSO- d^6 , 100 MHz): 173.41, 170.47, 166.90, 166.52, 163.99, 135.75, 135.72, 130.03, 129.93, 116.71, 116.48, 53.83, 52.32, 43.08, 41.34, 39.65, 26.76, 26.22, 24.95, 22.94, 22.06. ESI-HRMS (m/z): $[M+H]^+$ calcd. for $C_{20}H_{28}FN_3O_7S$: 474.1705, observed: 474.1707. HPLC Method 1: $R_t = 20.9$ min, purity = 99.0 %.

(2S,3S)-3-((S)-3-(1H-imidazol-4-yl)-1-oxo-1-(phenylamino)propan-2-ylcarbamoyl)oxirane-2-carboxylic acid (34). Synthesized following general saponification procedure using the following quantities: **34E** (155 mg, 0.3 mmol); LiOH (14 mg, 0.58 mmol); MeOH/H₂O (1.5 mL:0.5 mL: 0.5 mL); yielded **34** as a white solid (40 mg, 27.1 %). 1H NMR (MeOD- d^4 , 400 MHz): δ 8.66 (s, 1H); 7.57-7.55 (d, 2H, $J = 7.86$ Hz); 7.29-7.27 (t, 3H); 7.10-7.07 (t, 1H); 4.97-4.94 (q, 1H); 3.64-3.63 (d, 1H, $J = 1.66$ Hz); 3.529-3.525 (d, 1H, $J = 1.66$ Hz); 3.36-3.15 (m, 2H). ^{13}C NMR (MeOD- d^4 , 100 MHz): 169.79, 167.26, 166.95, 137.90, 134.99, 128.37, 124.10, 120.11, 54.13, 52.94, 51.67. ESI-HRMS (m/z): $[M+H]^+$ calcd. for $C_{16}H_{16}N_4O_5$: 345.1194, observed: 345.1185. HPLC Method 1: $R_t = 18.2$ min, purity = 95.2 %

(2S,3S)-3-((S)-3-(1H-imidazol-5-yl)-1-(mesitylamino)-1-oxopropan-2-ylcarbamoyl)oxirane-2-carboxylic acid (35). Synthesized following general saponification procedure using the following quantities: **35E** (51.6 mg, 0.1 mmol); LiOH (5 mg, 0.2 mmol); MeOH/H₂O (1.5 mL:0.5 mL: 0.5 mL); yielded **35** as a white solid (26.2 mg, 54.2 %). ¹H NMR (MeOD-*d*⁴, 400 MHz): δ 7.62 (s, 1H); 6.93 (s, 1H); 6.87 (s, 2H); 4.84-4.82 (m, 1H); 3.53-3.49 (d, 1H); 3.38-3.35 (d, 1H); 3.25-3.22 (m, 2H); 2.25 (s, 3H); 2.07 (s, 6H). ¹³C NMR (MeOD-*d*⁴, 100 MHz): 174.40, 172.62, 170.80, 168.89, 136.54, 135.74, 135.11, 133.43, 131.25, 128.18, 117.26, 54.20, 53.82, 53.69, 52.80, 29.34, 19.55, 16.86. ESI-HRMS (m/z): [M-H]⁻ calcd. for C₁₉H₂₂N₄O₅: 385.1517, observed: 385.1516. HPLC method 2: R_t = 16.4 min, purity = 95.4 %

(2S,3S)-3-(1-(4-(4-fluorophenyl)thiazol-2-ylamino)-3-(1H-imidazol-4-yl)-1-oxopropan-2-ylcarbamoyl)oxirane-2-carboxylic acid (36, NYC-215). Synthesized following general saponification procedure using the following quantities: **35E** (184 mg, 0.39 mmol); LiOH (14 mg, 0.58 mmol); MeOH/H₂O (1.5 mL:0.5 mL: 0.5 mL); yielded **35** as a white solid (40 mg, 27.1 %). ¹H NMR (DMSO-*d*⁶, 400 MHz): δ 12.50 (bs, 1H₊; 8.84-8.73 (dd, 1H, J = 7.3 Hz, 7.3 Hz)); 7.95-7.91 (q, 2H); 7.73 (s, 1H); 7.63 (s, 1H); 7.29-7.24 (t, 2H); 6.90 (s, 1H); 4.81-4.74 (m, 1H); 3.65-3.64 (dd, 2H, J = 1.68 Hz, 1.68 Hz); 3.46-3.42 (dd, 2H, J = 1.65 Hz, 1.65 Hz); 3.09-3.01 (m, 2H). ¹³C NMR (DMSO-*d*⁶, 100 MHz): 169.81, 165.89, 163.95, 157.92, 147.96, 134.99, 132.93, 132.91, 127.89, 127.72, 115.77, 115.56, 108.17, 99.59, 52.69, 51.85, 51.77. ESI-HRMS (m/z): [M+H]⁺ calcd. for C₁₉H₁₆FN₅O₅S: 446.0929, observed: 446.0922. HPLC method 2: R_t = 16.2 min (S-isomer) & 12.8 min (R-isomer), purity = 98.2%

(2R,3R)-3-((S)-1-(4-(4-fluorophenyl)thiazol-2-ylamino)-3-(1H-imidazol-4-yl)-1-oxopropan-2-ylcarbamoyl)oxirane-2-carboxylic acid (37). Synthesized following general saponification procedure using the following quantities: **37E** (200 mg, 0.42 mmol); LiOH (12 mg, 0.50 mmol);

THF/MeOH/H₂O (2.5 mL:1.5 mL: 1.5 mL); yielded **37** as a white solid (85 mg, 45.2 %). ¹H NMR (DMSO-*d*₆, 400 MHz): δ 12.52 (bs, 1H); 8.85-8.75 (dd, 2H, *J* = 6.9 Hz; *J* = 43.1 Hz); 7.94-7.91 (t, 2H); 7.80 (s, 1H); 7.62 (s, 1H); 7.28-7.24 (t, 2H); 6.93 (s, 1H); 4.80-4.76 (q, 1H); 3.65-3.64 (d, 1H, *J* = 4.40 Hz); 3.46-3.42 (d, 1H, *J* = 14.0 Hz); 3.09-2.96 (m, 2H). ¹³C NMR (DMSO-*d*₆, 100 MHz): 169.5, 168.8, 165.9, 162.9, 160.5, 157.6, 147.8, 134.6, 132.1, 130.7, 127.6, 116.4, 115.5 (d, *J* = 21.4 Hz), 108.0, 52.9, 52.7, 52.6, 51.9, 28.6. ESI-HRMS (*m/z*): [M+H]⁺ calcd. for C₁₉H₁₆FN₅O₅S: 446.0928, observed: 446.0939; HPLC method 2: R_t = 15.8 min, Purity = 97.2 %.

(2S,3S)-3-((S)-1-(6-fluorobenzo[d]thiazol-2-ylamino)-3-(1H-imidazol-4-yl)-1-oxopropan-2-ylcarbamoyl)oxirane-2-carboxylic acid (38). Synthesized following general saponification procedure using the following quantities: **38E** (153 mg, 0.32 mmol); LiOH (7.7 mg, 0.32 mmol); THF/MeOH/H₂O (3.5 mL:1.5 mL: 1.5 mL); yielded **38** as a white solid (103 mg, 71.5 %). ¹H NMR (DMSO-*d*₆, 400 MHz): δ 14.55 (bs, 1H); 14.36 (bs, 1H); 9.18-9.02 (m, 2H); 7.93-7.91 (m, 1H); 7.79-7.75 (m, 1H); 7.44 (s, 1H); 7.31-7.29 (t, 1H); 4.96-4.91 (q, 1H); 3.72-3.71 (d, 1H, *J* = 1.62 Hz); 3.51-3.50 (d, 1H, *J* = 1.62 Hz); 3.29-3.16 (m, 2H). ¹³C NMR (DMSO-*d*₆, 100 MHz): 169.50, 168.51, 165.84, 165.84, 159.82, 157.53, 157.44, 145.02, 133.67, 132.68, 132.57, 128.56, 121.63, 117.01, 114.40, 114.16, 108.27, 108.00, 52.67, 52.19, 51.34, 26.20. ESI-HRMS (*m/z*): [M+H]⁺ calcd. for C₁₇H₁₄FN₅O₅S: 420.0773, observed: 420.0777.

(2R,3R)-3-((S)-1-(6-fluorobenzo[d]thiazol-2-ylamino)-3-(1H-imidazol-4-yl)-1-oxopropan-2-ylcarbamoyl)oxirane-2-carboxylic acid (39). Synthesized following general saponification procedure using the following quantities: **39E** (125 mg, 0.26 mmol); LiOH (6.2 mg, 0.26 mmol); THF/MeOH/H₂O (1.5 mL:1.0 mL: 0.5 mL); yielded **39** as a white solid (46 mg, 39.1 %). ¹H NMR (400 MHz, MeOD-*d*⁴): δ 11.88 (bs, 1H), 8.89-8.83 (dd, 1H, *J* = 7.4 Hz, *J* = 7.4 Hz); 7.91-7.89

(d, 1H, J = 2.5 Hz); 7.78- 7.72 (q, 1H); 7.56 (s, 1H); 7.30 (td, 1H, J = 2.6 Hz); 6.85 (s, 1H); 4.81-4.76 (m, 1H); 3.76-3.74 (dd, 1H, J = 1.68 Hz); 3.45-3.43 (dd, 1H, J = 1.65 Hz); 3.11-3.00 (m, 2H). ^{13}C NMR (DMSO- d_6 , 100 MHz): 171.13, 167.48, 165.83, 160.32, 158.21, 145.64, 135.40, 133.23, 122.17, 114.83, 108.74, 53.86, 53.40, 51.86. ESI-HRMS (m/z): $[\text{M}+\text{H}]^+$ calcd. for $\text{C}_{17}\text{H}_{14}\text{FN}_5\text{O}_5\text{S}$: 420.0773, observed: 420.0769.

(2S,3S)-3-((S)-1-oxo-1-(phenylamino)-3-(thiazol-4-yl)propan-2-ylcarbamoyl)oxirane-2-carboxylic acid (40). Synthesized following general saponification procedure using the following quantities: **40E** (112 mg, 0.28 mmol); LiOH (6.9 mg, 0.29 mmol); THF/MeOH/ H_2O (2.5 mL:1.0 mL: 1.0 mL); yielded **40** as a white solid (45 mg, 43.3 %). ^1H NMR (MeOD- d^4 , 400 MHz): δ 8.97 (s, 1H); 7.52-7.50 (d, 2H); 7.32 (s, 1H); 7.30-7.26 (t, 3H); 4.94-4.92 (t, 1H); 3.62 (s, 1H); 3.52-3.45 (q, 2H); 3.43 (s, 1H). ^{13}C NMR (DMSO- d_6 , 100 MHz): 172.48, 169.65, 168.87, 153.83, 152.41, 138.16, 128.33, 124.04, 120.73, 115.89, 54.49, 53.60, 52.89 32.87. ESI-HRMS (m/z): $[\text{M}+\text{H}]^+$ calcd. for $\text{C}_{16}\text{H}_{15}\text{N}_3\text{O}_5\text{S}$: 360.0660, observed: 360.0673; HPLC method 2: R_t = 16.4 min; Purity: 95.2 %.

3-((S)-1-(4-(4-fluorophenyl)thiazol-2-ylamino)-1-oxo-3-(thiazol-4-yl)propan-2-ylcarbamoyl)oxirane-2-carboxylic acid (41, NYC-438). Synthesized following general saponification procedure using the following quantities: **41E** (974 mg, 2.0 mmol); LiOH (47.5 mg, 2.0 mmol); THF/MeOH/ H_2O (25 mL:5 mL: 2 mL); yielded **41** as a white solid (685 mg, 74.6 %). ^1H NMR (MeOD- d^4 , 400 MHz): δ 8.99-8.98(d, 1H, J = 1.67 Hz); 7.94-7.91 (q, 2H); 7.37 (s, 1H); 7.36 (s, 1H); 7.15-7.10 (t, 2H); 5.06-5.02 (q, 1H); 3.64-3.63 (d, 1H, J = 1.57 Hz); 3.49-3.45 (m, 3H). ^{13}C NMR (MeOD- d^4 , 100 MHz): 170.05, 169.01, 166.19, 163.43, 158.19, 154.25, 152.66, 148.36, 131.30, 128.18, 116.63, 116.15, 115.93, 108.62, 53.12, 53.05, 52.21, 33.09. ESI-

HRMS (m/z): $[M+H]^+$ calcd. for $C_{19}H_{15}FN_4O_5S_2$: 463.0541, observed: 463.0545; HPLC method 2: R_t = 23.3 min; purity = 96.3 %.

3-((S)-1-oxo-1-(prop-2-ynylamino)-3-(thiazol-4-yl)propan-2-ylcarbamoyl)oxirane-2-carboxylic acid (42). Synthesized following general saponification procedure to afford **42** as a white solid. 1H NMR (DMSO- d^6 , 400MHz): δ 9.02-9.01 (d, 1H, J = 1.94 Hz); 8.64-8.62 (d, 1H, J = 8.44 Hz); 8.57 (t, 1); 7.35-7.34 (d, 1H, J = 1.94 Hz); 4.67-4.62 (m, 1H); 4.21-4.14 (m, 2H); 3.85 (bs, 2H); 3.64-3.63 (d, 1H, J = 1.80 Hz); 3.50-3.49 (d, 1H). ESI-HRMS (m/z): $[M+H]^+$ calcd. for $C_{15}H_{17}N_3O_5S$: 352.0962, observed: 352.0975. **(2S,3S)-3-((S)-1-(4-(4-ethynylphenyl)thiazol-2-ylamino)-1-oxo-3-(thiazol-4-yl)propan-2-ylcarbamoyl)oxirane-2-carboxylic acid (43).**

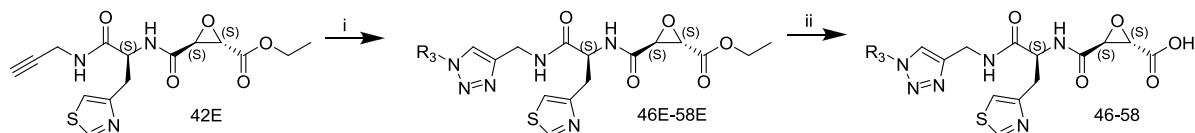
Synthesized following general saponification procedure using the following quantities: **43E** (115 mg, 0.23 mmol); LiOH (6.7 mg, 0.28 mmol); THF/MeOH/H₂O (4.5 ml:1.5 ml: 1.5 ml); yielded **43** as a white solid (48 mg, 44.2 %). 1H NMR (DMSO- d^6 , 400 MHz) : δ 12.57 (s, 1H); 9.06-9.05 (d, 1H, J = 1.92 Hz); 8.81-8.79 (d, 1H, J = 7.8 Hz); 7.93-7.91 (d, 2H, J = 8.4 Hz); 7.76 (s, 1H); 7.55-7.53 (d, 2H, J = 8.4 Hz); 7.45-7.44 (d, 1H, 1.8 Hz); 4.98-4.93 (q, 1H); 4.25 (s, 1H); 3.66-3.65 (d, 1H, J = 1.8 Hz); 3.42-3.41 (d, 1H, J = 1.8 Hz); 3.35-3.22 (m, 2H). ^{13}C NMR (DMSO- d^6 , 100 MHz): 170.08, 169.03, 165.98, 158.25, 154.33, 152.54, 148.47, 134.95, 132.61, 126.26, 121.32, 116.75, 110.20, 83.87, 81.99, 53.15, 53.08, 51.88, 33.05. ESI-HRMS (m/z): $[M+H]^+$ calcd. for $C_{21}H_{16}N_4O_5S_2$: 469.0635; observed, 469.0627; HPLC method 1: R_t = 12.5 min, Purity = 95.7 %.

(2S,3S)-3-((S)-1-(4-(4-fluorophenyl)thiazol-2-ylamino)-3-(1-methyl-1H-imidazol-5-yl)-1-oxopropan-2-ylcarbamoyl)oxirane-2-carboxylic acid (44). Synthesized following general saponification procedure using the following quantities: **44E** (129 mg, 0.26 mmol); LiOH (6.3 mg, 0.26 mmol); THF/MeOH/H₂O (2.5 mL:1.5 mL: 1.5 mL); yielded **44** as a white solid (56 mg,

46.1 %). ^1H NMR (DMSO- d_6 , 400 MHz): 8.92-8.90 (d, 1H); 7.96-7.91 (m, 2H); 7.68 (s, 1H); 7.35-7.24 (m, 3H); 4.94-4.87 (m, 1H); 4.64-4.56 (m, 2H); 3.82-3.50 (m, 5H). ^{13}C NMR (400 MHz, DMSO- d_6): 171.52, 167.50, 165.57, 162.45, 161.02, 148.42, 138.62, 131.27, 128.18, 128.01, 127.83, 127.05, 116.17, 115.99, 106.70, 53.24, 52.58, 51.90, 31.29, 29.52. ESI-HRMS (m/z): $[\text{M}+\text{H}]^+$ calcd. for $\text{C}_{20}\text{H}_{18}\text{FN}_5\text{O}_5\text{S}$: 460.1085; observed, 460.1092; R_t = 17.8 min, Purity = 93.6 %.

(2S,3S)-3-((S)-1-(4-(4-fluorophenyl)thiazol-2-ylamino)-3-(1-methyl-1H-imidazol-4-yl)-1-oxopropan-2-ylcarbamoyl)oxirane-2-carboxylic acid (45). Synthesized following general saponification procedure using the following quantities: **45E** (93 mg, 0.19 mmol); LiOH (4.5 mg, 0.19 mmol); THF/MeOH/H₂O (1.5 mL:0.5 mL: 0.5 mL); yielded **45** as a white solid (29 mg, 33.1 %). ^1H NMR (400 MHz, DMSO- d_6): 12.50 (bs, 1H), 8.82-8.80 (d, 1H); 7.93-7.91 (m, 2H); 7.76 (s, 1H); 7.63 (s, 1H); 7.46-7.24 (t, 2H); 6.99 (s, 1H); 4.79-4.74 (m, 1H); 3.67-3.66 (d, 1H); 3.62 (s, 3H); 3.49-3.48 (d, 1H); 3.12-2.90 (m, 2H). ^{13}C NMR (400 MHz, DMSO- d_6): 169.72, 168.60, 165.56, 162.97, 160.54, 157.78, 147.88, 137.17, 130.84, 127.71, 127.63, 118.35, 115.68, 115.47, 108.08, 53.07, 52.98, 51.56, 33.11, 29.60. ESI-HRMS (m/z): $[\text{M}+\text{H}]^+$ calcd. for $\text{C}_{20}\text{H}_{18}\text{FNO}_5\text{S}$: 460.1085, observed: 460.1090. R_t = 18.1 min, Purity = 95.3 %.

Scheme 3



Reagents: i) R_3-N_3 , $CuSO_4$, NaAsc, TBTA, $H_2O/t-BuOH/EtOH$ (2:1:1), r.t., 12 h, 90-100 %. ii) LiOH, THF/MeOH/ H_2O , 0°C, 95-100 %

Table 2. Structure designations of Scheme 6 analogs

Compound	R3
46, 46E	Phenyl
47 (NYC-488), 47E	4-fluorophenyl
48, 48E	4-phenylsulfonylpiperidine
49, 49E	1,3-methylenedioxyphenyl
50, 50E	4-phenylsulfonylamide
51, 51E	3,5-trifluoromethylphenyl
52 (NYC-106), 52E	4-bromophenyl
53, 53E	4-nitrophenyl
54, 54E	2,6 fluorophenyl
55, 55E	1,3,5 trimethylphenyl

General Procedure for Cycloaddition Reaction (34-44).

To the appropriate azide (1.2 eq [for preparation see supplemental materials]) and 16c (1.0 eq) were dissolved in *t*-BuOH/EtOH/H₂O (1:1:0.5). CuSO₄ (0.2 eq), Sodium Ascorbate (0.4 eq), and a catalytic amount of TBTA (Tris[(1-benzyl-1H-1,2,3-triazol-4-yl)methyl]amine) (0.01 eq) were added sequentially and the reaction stirred for 12 h. The resulting precipitate was filtered off, dissolved in CH₂Cl₂, filtered through Celite and concentrated in vacuo to afford the desired product in yields and quantities as follows.

(2S,3S)-ethyl 3-((S)-1-oxo-1-(1-phenyl-1H-1,2,3-triazol-4-yl)methylamino)-3-(thiazol-4-yl)propan-2-ylcarbamoyl)oxirane-2-carboxylate (46E). The general click procedure was used substituting the following quantities using: **42E** (25.0 mg, 0.077 mmol); phenylazide (9.5 mg, 0.071 mmol); CuSO₄ (2.0 mg, 0.01 mmol); NaAsc (6.0 mg, 0.03 mmol); TBTA (5.0 mg, 0.009 mmol); in *t*-BuOH/EtOH/H₂O (2:1:0.5); afforded the **46E** as a white solid (32 mg, 92.6 %). ¹H NMR (CDCl₃, 400 MHz): δ = 8.74-7.73 (d, 1H, J = 1.90 Hz), 7.93 (s, 1H); 7.73-7.71 (d, 3H, J = 8.68 Hz); 7.55-7.52 (t, 2H); 7.47-7.39 (m, 2H); 7.07-7.06 (d, 1H, J = 1.71 Hz); 4.84-4.79 (q, 1H); 4.56-4.54 (d, 2H, J = 5.87 Hz); 4.32-4.21 (m, 2H); 3.71-3.70 (d, 1H, J = 1.78 Hz); 3.57-3.56 (d, 1H, J = 1.78 Hz); 3.39-3.18 (m, 2H); 1.33-1.31 (t, 3H). ¹³C NMR (CDCl₃, 100 MHz): 170.06, 166.52, 166.39, 153.25, 152.36, 145.11, 136.91, 129.75, 128.81, 120.57, 120.46, 115.97, 62.27, 53.80, 52.79, 52.58, 34.98, 32.76, 14.01.

(2S,3S)-ethyl 3-((S)-1-((1-(4-fluorophenyl)-1H-1,2,3-triazol-4-yl)methylamino)-1-oxo-3-(thiazol-4-yl)propan-2-ylcarbamoyl)oxirane-2-carboxylate (47E, NYC-488E). The general

click procedure was used substituting the following quantities using: **42E** (27.3 mg, 0.077 mmol); 1-azido-4-fluorobenzene (10.4 mg, 0.078 mmol); CuSO₄ (2.0 mg, 0.01 mmol); NaAsc (6.0 mg, 0.03 mmol); TBTA (5.0 mg, 0.009 mmol); in *t*-BuOH/EtOH/H₂O (2:1:0.5); afforded the **47E** as a white solid (35 mg, 92.2 %). ¹H NMR (CDCl₃, 400 MHz): δ = 8.73-8.72 (d, 1H, J = 1.91 Hz); 7.90 (s, 1H); 7.74-7.67 (m, 3H); 7.58-7.55 (t, 1H); 7.24-7.18 (t, 2H); 7.07-7.06 (d, 1H, J = 1.71 Hz); 4.84-4.79 (q, 1H); 4.54-4.50 (d, 2H, J = 5.90 Hz); 4.29-4.21 (m, 2H); 3.68-3.67 (d, 1H, J = 1.78 Hz); 3.53-3.52 (d, 1H, J = 1.78 Hz); 3.37-3.18 (m, 2H); 1.30-1.26 (t, 3H). ¹³C NMR (CDCl₃, 100 MHz): 169.82, 166.17, 166.03, 163.28, 160.81, 152.86, 152.00, 144.94, 132.78, 122.10, 122.01, 120.48, 116.45, 116.22, 115.59, 61.91, 53.43, 52.40, 52.24, 34.55, 32.42, 13.63.

(2S,3S)-ethyl 3-((S)-1-oxo-1-((1-(4-(piperidin-1-ylsulfonyl)phenyl)-1H-1,2,3-triazol-4-yl)methylamino)-3-(thiazol-4-yl)propan-2-ylcarbamoyl)oxirane-2-carboxylate (48E). The general click procedure was used substituting the following quantities using: **42E** (28.1 mg, 0.079 mmol); 4-piperidinophenylazide (10.7 mg, 0.079 mmol); CuSO₄ (3.0 mg, 0.02 mmol); NaAsc (6.0 mg, 0.03 mmol); TBTA (5.0 mg, 0.009 mmol); in *t*-BuOH/EtOH/H₂O (2:1:0.5); afforded the **48E** as a white solid (31 mg, 79.8 %). ¹H NMR (CDCl₃, 400 MHz): δ = 8.76-8.75 (d, 1H, J = 1.84 Hz); 8.05 (s, 1H); 7.93 (s, 4H); 7.76-7.74 (d, 1H, J = 7.04 Hz); 7.38-7.36 (t, 1H); 7.10-7.09 (d, 1H, J = 1.70 Hz); 4.79-4.76 (q, 1H); 4.58-4.55 (q, 2H); 4.30-4.25 (m, 2H); 3.72-3.71 (d, 1H, J = 1.78 Hz); 3.55-3.54 (d, 1H, J = 1.78 Hz); 3.38-3.17 (abq, 2H); 3.07-3.04 (t, 3H); 1.75-1.60 (m, 1H); 1.31-1.26 (t, 3H). ¹³C NMR (CDCl₃, 100 MHz): 170.31, 169.65, 166.52, 166.44, 153.30, 152.40, 152.34, 145.93, 139.64, 136.68, 129.40, 120.61, 120.41, 116.20, 116.02, 79.01, 71.57, 62.31, 53.77, 52.80, 52.45, 46.94, 32.70, 29.19, 25.11, 23.42, 14.02.

(2S,3S)-ethyl 3-((S)-1-(1-(benzo[d][1,3]dioxol-5-yl)-1H-1,2,3-triazol-4-yl)methylamino)-1-oxo-3-(thiazol-4-yl)propan-2-ylcarbamoyl)oxirane-2-carboxylate (49E). The general click

procedure was used substituting the following quantities using: **42E** (25.0 mg, 0.071 mmol); 5-azidobenzo[d][1,3]dioxole (9.5 mg, 0.071 mmol); CuSO₄ (2.0 mg, 0.01 mmol); NaAsc (6.0 mg, 0.03 mmol); TBTA (5.0 mg, 0.009 mmol); in *t*-BuOH/EtOH/H₂O (2:1:0.5); afforded the **49E** as a white solid (31 mg, 89.7 %). ¹H NMR (CDCl₃, 400 MHz): δ = 8.76-8.75 (d, 1H, J = 1.86 Hz); 7.79 (s, 1H); 7.73-7.71 (d, 1H, J = 7.16 Hz); 7.24-7.21 (dd, 2H); 7.14-7.11 (dd, 1H); 7.08-7.07 (d, 1H, J = 1.63 Hz); 6.93-6.91 (d, 1H, J = 8.32 Hz); 6.09 (s, 2H); 4.79-4.76 (q, 1H); 4.54-4.53 (d, 2H, J = 5.90 Hz); 4.31-4.25 (m, 2H); 3.72-3.71 (d, 1H, J = 1.76 Hz); 3.55-3.54 (d, 1H, J = 1.76 Hz); 3.38-3.15 (ab, 2H, J = 92.8 Hz, 57.57 Hz); 1.35-1.30 (t, 3H). ¹³C NMR (CDCl₃, 100 MHz): 169.49, 169.05, 164.22, 155.01, 153.30, 148.84, 147.92, 148.27, 130.98, 121.72, 116.26, 114.17, 109.12, 102.60, 102.33, 62.14, 52.95, 52.54, 51.90, 34.78, 33.49, 14.23.

(2S,3S)-ethyl 3-((S)-1-oxo-1-((1-(4-sulfamoylphenyl)-1H-1,2,3-triazol-4-yl)methylamino)-3-(thiazol-4-yl)propan-2-ylcarbamoyl)oxirane-2-carboxylate (50E): The general click procedure was used substituting the following quantities using: **42E** (109.0 mg, 0.31 mmol); 4-azidobenzenesulfonamide (61.5 mg, 0.31 mmol); CuSO₄ (10.0 mg, 0.06 mmol); NaAsc (20.0 mg, 0.03 mmol); TBTA (10.0 mg, 0.018 mmol); in *t*-BuOH/EtOH/H₂O (4:4:2); afforded the **50E** as a white solid (119 mg, 69.8 %). ¹H NMR (CDCl₃, 400 MHz): δ = 8.93 (s, 1H); 8.45 (s, 1H); 8.19-8.05 (q, 4H); 7.33 (s, 1H); 4.81-4.77 (t, 1H); 4.57-4.48 (q, 2H); 4.28-4.23 (q, 2H); 3.64 (s, 1H); 3.50 (s, 1H); 3.40-3.21 (m, 2H); 1.28-1.23 (t, 3H). ¹³C NMR (MeOD-*d*⁴, 100 MHz): 170.94, 166.80, 166.72, 153.45, 151.92, 145.70, 143.49, 138.85, 127.31, 120.74, 119.76, 115.56, 61.42, 52.72, 52.67, 51.47, 33.93, 31.91, 12.52.

(2S,3S)-ethyl 3-((S)-1-((1-(3,5-bis(trifluoromethyl)phenyl)-1H-1,2,3-triazol-4-yl)methylamino)-1-oxo-3-(thiazol-4-yl)propan-2-ylcarbamoyl)oxirane-2-carboxylate (51E).

The general click procedure was used substituting the following quantities using: **42E** (93.7 mg,

0.27 mmol); 1-azido-3,5-bis(trifluoromethyl)benzene (82.5 mg, 0.32 mmol); CuSO₄ (0.6 mg, 0.0043 mmol); NaAsc (3.5 mg, 0.018 mmol); TBTA (15.0 mg, 0.028 mmol); in *t*-BuOH/EtOH/H₂O (4:4:2) with an additional 3 drops of DMF; afforded the **51E** as a white solid (142 mg, 87.8 %). ¹H NMR (CDCl₃, 400 MHz): δ = 8.77 (s, 1H); 8.25 (s, 2H); 8.09 (s, 1H); 7.96 (s, 1H); 7.77-7.75 (d, 1H, *J* = 7.09 Hz); 7.34-7.32 (t, 1H); 7.11 (s, 1H); 4.81-4.76 (q, 1H); 4.59-4.57 (d, 2H, *J* = 5.90 Hz); 4.31-4.25 (m, 2H); 3.72-3.711 (d, 1H, *J* = 1.64 Hz); 3.55-3.54 (d, 1H, *J* = 1.64 Hz); 3.41-3.17 (m, 2H); 1.01-0.99 (t, 3H). ¹³C NMR (DMSO-*d*⁶, 100 MHz): 170.62, 167.49, 165.37, 154.06, 153.24, 146.92, 138.31, 124.57, 122.37, 121.85, 121.09, 116.21, 61.97, 53.44, 52.97, 51.74, 34.64, 33.49, 14.29.

(2S,3S)-ethyl 3-((S)-1-((1-(4-bromophenyl)-1H-1,2,3-triazol-4-yl)methylamino)-1-oxo-3-(thiazol-4-yl)propan-2-ylcarbamoyl)oxirane-2-carboxylate (52E). The general click procedure was used substituting the following quantities using: **42E** (60 mg, 0.17 mmol); 1-azido-4-bromobenzene (51 mg, 0.26 mmol); CuSO₄ (4.4 mg, 0.027 mmol); NaAsc (22 mg, 0.11 mmol); TBTA (20.0 mg, 0.037 mmol); in *t*-BuOH/EtOH/H₂O (2:2:1); afforded the **52E** as a white solid (40 mg, 42.6 %). ¹H NMR (DMSO-*d*⁶, 400 MHz): δ = 9.00-8.99 (d, 1H, *J* = 1.66 Hz); 8.74-8.71 (t, 1H); 8.63-8.61 (d, 1H, *J* = 8.22 Hz); 8.54 (s, 1H); 7.60-7.56 (d, 2H, *J* = 14.85 Hz); 7.345-7.341 (d, 1H, *J* = 1.63 Hz); 7.11-7.07 (d, 2H, *J* = 14.85 Hz); 4.69-4.66 (q, 1H); 4.40-4.38 (d, 2H, *J* = 5.59 Hz); 4.20-4.13 (m, 2H); 3.66-3.66 (d, 1H, *J* = 1.73 Hz); 3.52-3.51 (d, 1H, *J* = 1.73 Hz); 3.33-3.12 (m, 2H); 1.23-1.20 (t, 3H). ¹³C NMR (100 MHz, DMSO-*d*⁶): 170.57, 167.51, 165.36, 154.07, 153.27, 146.56, 139.39, 136.25, 122.30, 121.54, 117.51, 116.23, 61.97, 53.46, 52.99, 51.76, 34.75, 33.50, 14.32.

(2S,3S)-ethyl 3-((S)-1-((1-(4-nitrophenyl)-1H-1,2,3-triazol-4-yl)methylamino)-1-oxo-3-(thiazol-4-yl)propan-2-ylcarbamoyl)oxirane-2-carboxylate (53E). The general click

procedure was used substituting the following quantities using: **42E** (60 mg, 0.17 mmol); 1-azido-4-nitrobenzene (42 mg, 0.26 mmol); CuSO₄ (4.4 mg, 0.027 mmol); NaAsc (22 mg, 0.11 mmol); TBTA (20.0 mg, 0.037 mmol); in *t*-BuOH/EtOH/H₂O (2:2:1); afforded the **53E** as an orange solid (40 mg, 45.6 %). ¹H NMR (DMSO-*d*⁶, 400 MHz): δ = 9.00-8.99 (d, 1H, *J* = 1.8 Hz); 8.77-8.74 (t, 1H); 8.73 (s, 1H); 8.63-8.61 (d, 1H, *J* = 8.17 Hz); 8.47-8.44 (d, 2H, *J* = 9.13 Hz); 8.21-8.19 (d, 2H, *J* = 9.13 Hz); 7.36 (d, 1H, *J* = 1.78 Hz); 4.71-4.65 (q, 1H); 4.42-4.40 (d, 2H, *J* = 5.50 Hz); 4.20-4.09 (m, 2H); 3.66-3.65 (d, 1H, *J* = 1.75 Hz); 3.52-3.51 (d, 1H, *J* = 1.75 Hz); 3.28-3.06 (m, 2H); 1.22-1.17 (t, 3H). ¹³C NMR (CDCl₃, 100 MHz): 170.25, 167.14, 165.00, 153.70, 152.87, 146.77, 146.68, 140.89, 125.70, 121.59, 120.42, 115.86, 61.60, 53.09, 52.61, 51.40, 34.32, 33.12, 13.94.

(2S,3S)-ethyl 3-((S)-1-((1-(2,6-difluorophenyl)-1H-1,2,3-triazol-4-yl)methylamino)-1-oxo-3-(thiazol-4-yl)propan-2-ylcarbamoyl)oxirane-2-carboxylate (54E). The general click procedure was used substituting the following quantities using: **42E** (48 mg, 0.14 mmol); 2-azido-1,3-difluorobenzene (24 mg, 0.15 mmol); CuSO₄ (3.5 mg, 0.022 mmol); NaAsc (18 mg, 0.09 mmol); TBTA (12 mg, 0.013 mmol); in *t*-BuOH/EtOH/H₂O (1:1:0.5); afforded **54E** as a white solid (20 mg, 31.6 %). ¹H NMR (DMSO-*d*⁶, 400 MHz): δ = 8.74-8.73 (d, 1H, *J* = 1.79 Hz); 7.74-7.72 (m, 2H); 7.55-7.45 (m, 1H); 7.34-7.32 (m, 1H); 7.17-7.13 (t, 2H); 7.04-7.03 (d, 1H, *J* = 1.72 Hz); 4.82-4.80 (q, 1H); 4.57-4.56 (d, 2H, *J* = 5.97 Hz); 4.29-4.24 (m, 2H); 3.71-3.70 (d, 1H, *J* = 1.78 Hz); 3.55-3.54 (d, 1H, *J* = 1.78 Hz); 3.35-3.18 (m, 2H); 1.33-1.30 (t, 3H). ¹³C NMR (CDCl₃, 100 MHz): 170.16, 166.65, 166.30, 158.01, 155.46, 153.29, 152.24, 144.36, 131.48, 129.14, 125.10, 116.01, 112.64, 62.24, 53.81, 52.74, 52.62, 34.74, 32.91, 13.99.

(2S,3S)-ethyl 3-((S)-1-((1-mesityl-1H-1,2,3-triazol-4-yl)methylamino)-1-oxo-3-(thiazol-4-yl)propan-2-ylcarbamoyl)oxirane-2-carboxylate (55E). The general click procedure was used

substituting the following quantities using: **42E** (48 mg, 0.14 mmol); 2-azido-1,3-difluorobenzene (24 mg, 0.15 mmol); CuSO₄ (3.5 mg, 0.022 mmol); NaAsc (18 mg, 0.09 mmol); TBTA (12 mg, 0.013 mmol); in *t*-BuOH/EtOH/H₂O (1:1:0.5); afforded **55E** as a white solid (30 mg, 42.8 %). ¹H NMR (400 MHz, DMSO-*d*⁶): δ = 8.79-8.74 (d, 1H, *J* = 1.79 Hz); 7.68-7.64 (m, 2H); 7.50 (s, 1H); 7.36-7.34 (d, 2H); 7.28-7.26 (d, 2H), 7.15-7.10 (m, 2H), 6.98 (s, 1H); 5.50 (s, 1H); 4.83-4.78 (m, 1H); 4.59-4.58 (d, 1H); 4.29-4.25 (m, 2H); 3.99-3.97 (q, 1H); 3.81 (s, 3H); 3.69-3.68 (m, 3H); 3.55-3.54 (d, 1H); 3.37-3.19 (abq, 2H); 2.35 (s, 3H); 1.93 (s, 3H) 1.33-1.29 (t, 3H). ¹³C NMR (DMSO-*d*⁶, 100 MHz): 169.25, 165.62, 153.65, 152.98, 144.93, 140.11, 134.51, 134.50, 128.12, 124.69, 115.88, 63.51, 52.69, 52.78, 51.98, 48.66, 34.54, 33.10, 20.69, 16.89, 13.52.

(2S,3S)-3-((S)-1-oxo-1-((1-phenyl-1H-1,2,3-triazol-4-yl)methylamino)-3-(thiazol-4-yl)propan-2-ylcarbamoyl)oxirane-2-carboxylic acid (46). Followed general procedure using: **42E** (23 mg, 0.47 mmol); LiOH (1.2 mg, 0.047 mmol); after extraction afforded the desired product as a white solid (18 mg, 84.9 %). ¹H NMR (DMSO-*d*⁶, 400 MHz) = δ 9.00-8.99 (d, 1H, *J* = 1.76 Hz); 8.73-8.70 (t, 1H); 8.58-8.56 (d, 1H, *J* = 8.24 Hz); 8.50 (s, 1H); 7.87-7.85 (d, 2H, *J* = 7.76 Hz); 7.61-7.49 (m, 3H); 7.344-7.341 (d, 1H, *J* = 1.21 Hz); 4.69-4.66 (q, 1H); 4.41-4.39 (d, 2H, *J* = 5.49 Hz); 3.59-3.59 (d, 1H, *J* = 1.58 Hz); 3.35-3.10 (m, 3H). ¹³C NMR (DMSO-*d*⁶, 100 MHz): 170.62, 169.06, 165.75, 154.05, 153.31, 146.36, 137.07, 130.38, 129.06, 131.48, 120.41, 116.19, 53.25, 52.96, 51.90, 34.80, 29.42. HRMS-ESI: *m/z* [M+H]⁺ calculated for C₁₈H₁₆N₆O₅S: 443.1137, observed: *m/z* 443.1135. HPLC method 2: R_t = 16.7 min; purity = 97.9 %

(2S,3S)-3-((S)-1-((1-(4-fluorophenyl)-1H-1,2,3-triazol-4-yl)methylamino)-1-oxo-3-(thiazol-4-yl)propan-2-ylcarbamoyl)oxirane-2-carboxylic acid (47). Followed general procedure using:

47E (25 mg, 0.51 mmol); LiOH (1.3 mg, 0.06 mmol); after extraction afforded the desired product as a white solid (18 mg, 76.2 %). ^1H NMR (DMSO- d^6 , 400 MHz) = δ 8.98 (s, 1H); 8.72-8.70 (t, 1H); 8.57-8.55 (d, 1H, J = 8.06); 8.48 (s, 1H); 7.93-7.90 (q, 2H); 7.48-7.44 (t, 2H); 7.34 (s, 1H); 4.70-4.65 (q, 1H); 4.40-4.38 (d, 2H; J = 5.52); 3.66 (s, 1H); 3.54-3.06 (m, 3H). ^{13}C NMR (DMSO- d^6 , 100 MHz): 170.62, 165.75, 163.24, 160.80, 154.06, 153.32, 146.40, 133.62, 122.81, 122.72, 121.76, 117.33, 117.10, 53.24, 53.01, 52.94, 34.77, 33.50. HRMS-ESI: m/z $[\text{M}+\text{H}]^+$ calculated for $\text{C}_{19}\text{H}_{17}\text{FN}_6\text{O}_5\text{S}$: 461.1043, observed: m/z 461.1049. HPLC method 2: R_t = 17.9 min; purity = 97.2 %.

(2S,3S)-3-((S)-1-oxo-1-((1-(4-(piperidin-1-ylsulfonyl)phenyl)-1H-1,2,3-triazol-4-yl)methylamino)-3-(thiazol-4-yl)propan-2-ylcarbamoyl)oxirane-2-carboxylic acid (48).

Followed general procedure using: **48E** (26 mg, 0.42 mmol); LiOH (1.0 mg, 0.04 mmol); after extraction afforded the desired product as a white solid (12 mg, 48.3 %). ^1H NMR (Acetone- d^6 , 400 MHz): δ = 8.98 (bs, 1H); 8.48 (s, 1H); 8.16-8.12 (d, 2H, 8.48); 8.02-8.00 (d, 2H, J = 8.48 Hz); 7.37 (bs, 1H); 4.81 (bs, 1H); 4.52 (s, 2H); 3.85-3.79 (m, 4H); 3.61 (s, 1H); 3.55 (s, 1H); 1.82-1.60 (m, 6H). ^{13}C NMR (Acetone- d^6 , 100 MHz): 170.07, 169.01, 165.12, 153.52, 139.36, 136.19, 129.47, 120.84, 120.21, 107.39, 107.25, 66.62, 53.44, 52.80, 52.77, 46.83, 32.52, 30.07, 25.02, 23.13. HRMS-ESI: m/z $[\text{M}+\text{H}]^+$ calculated for $\text{C}_{24}\text{H}_{27}\text{N}_7\text{O}_7\text{S}_2$: 589.64, observed: m/z 590.1050 ($\text{M}+\text{H}^+$); HPLC method 2: R_t = 21.7 min; purity = 96.3 %.

(2S,3S)-3-((S)-1-((1-(benzo[d][1,3]dioxol-5-yl)-1H-1,2,3-triazol-4-yl)methylamino)-1-oxo-3-(thiazol-4-yl)propan-2-ylcarbamoyl)oxirane-2-carboxylic acid (49). Followed general procedure using: **49E** (10 mg, 0.16 mmol); LiOH (0.35 mg, 0.016 mmol); after extraction afforded the desired product as a white solid (7 mg, 73.1 %). ^1H NMR (DMSO- d^6 , 400 MHz) = δ 9.00-8.99 (d, 1H, J = 1.88 Hz); 8.71-8.68 (t, 1H); 8.57-8.55 (d, 1H, J = 8.28 Hz); 8.38 (s, 1H);

7.46-7.45 (d, 1H, $J = 2.15$ Hz); 7.33-7.31 (m, 2H); 7.11 (s, 1H); 7.09 (s, 1H); 6.15 (s, 2H); 4.67-4.65 (m, 1H); 4.38-4.36 (d, 2H); 3.60-3.58 (d, 1H, $J = 1.72$ Hz); 3.50-3.17 (m, 3H). ^{13}C NMR (DMSO- d^6 , 100 MHz): 170.59, 169.06, 165.75, 154.05, 153.31, 148.65, 147.81, 146.07, 131.53, 121.69, 116.19, 114.15, 109.11, 102.58, 102.33, 53.24, 52.94, 51.90, 34.78, 33.49. HRMS-ESI: m/z $[\text{M}+\text{H}]^+$ calculated for $\text{C}_{20}\text{H}_{18}\text{N}_6\text{O}_7\text{S}$: 486.46, observed: m/z 487.1050 ($\text{M}+\text{H})^+$; HPLC method 2: $R_t = 18.1$ min; Purity = 97.7 %.

(2S,3S)-3-((S)-1-oxo-1-((1-(4-sulfamoylphenyl)-1H-1,2,3-triazol-4-yl)methylamino)-3-(thiazol-4-yl)propan-2-ylcarbamoyl)oxirane-2-carboxylic acid (50). Followed general procedure using: **50E** (30 mg, 0.55 mmol); LiOH (1.3 mg, 0.055 mmol); product goes into aqueous layer during work up. Aqueous layer washed with CH_2Cl_2 and lyophilized to give the desired product as a white solid (8 mg, 45.1 %). ^1H NMR (DMSO- d^6 , 400 MHz) = δ 9.00-8.99 (d, 1H, $J = 1.92$ Hz); 8.79-8.76 (t, 1H); 8.70-8.68 (d, 1H, $J = 8.0$ Hz); 8.66 (s, 1H); 8.12-8.01 (m, 4H); 7.55 (s, 2H); 7.36 (s, 1H); 4.70-4.65 (m, 1H); 4.41-4.40 (d, 2H, $J = 5.20$ Hz); 3.61 (s, 1H); 3.44-3.10 (m, 3H). ^{13}C NMR (DMSO- d^6 , 100 MHz): 172.25, 170.66, 169.06, 165.74, 154.10, 152.52, 138.29, 146.80, 144.19, 128.01, 121.75, 120.59, 116.29, 53.25, 52.98, 51.84, 49.01, 33.43. HRMS-ESI: m/z $[\text{M}+\text{H}]^+$ calculated for $\text{C}_{19}\text{H}_{19}\text{N}_7\text{O}_7\text{S}_2$: 522.0865, observed: m/z 522.0858 ($\text{M}+\text{H})^+$; HPLC method 2: $R_t = 14.8$ min; Purity = 95.1 %.

(2S,3S)-3-((S)-1-((1-(3,5-bis(trifluoromethyl)phenyl)-1H-1,2,3-triazol-4-yl)methylamino)-1-oxo-3-(thiazol-4-yl)propan-2-ylcarbamoyl)oxirane-2-carboxylic acid (51). Followed general procedure using: **51E** (94 mg, 0.15 mmol); LiOH (3.7 mg, 0.15 mmol); after extraction afforded the desired product as a white solid (72 mg, 80.3 %). ^1H NMR (DMSO- d^6 , 400 MHz) = δ 8.99-8.98 (d, 1H, $J = 1.92$ Hz); 8.92 (s, 1H); 8.79-8.77 (t, 1H); 8.63 (s, 2H); 8.57-8.55 (d, 1H, $J = 8.27$ Hz); 8.27 (s, 1H); 7.34-7.33 (d, 1H, $J = 1.85$ Hz); 4.71-4.66 (m, 1H); 4.43-4.42 (d, 2H, $J = 5.67$

Hz); 3.58-3.57 (d, 1H, J = 1.73 Hz); 3.36-3.35 (d, 1H, J = 1.70 Hz); 3.28-3.10 (m, 2H). ¹³C NMR (DMSO-*d*⁶, 100 MHz): 170.67, 169.07, 165.80, 154.06, 153.29, 146.93, 138.32, 132.48, 132.14, 122.38, 121.11, 116.18, 53.22, 52.90, 51.96, 34.64, 33.51. HRMS-ESI: *m/z* [M+H]⁺ calculated for C₂₁H₁₆F₆N₆O₅S: 578.44, observed: *m/z* 579.0890 (M+H)⁺; *m/z* 577.0775 (M-H)⁺. HPLC method 2: R_t = 24.5 min; Purity = 95.3 %.

(2S,3S)-3-((S)-1-((1-(4-bromophenyl)-1H-1,2,3-triazol-4-yl)methylamino)-1-oxo-3-(thiazol-4-yl)propan-2-ylcarbamoyl)oxirane-2-carboxylic acid (52). Followed general procedure using: **52E** (25 mg, 0.04 mmol); LiOH (1.1 mg, 0.04 mmol); after extraction afforded the desired product as a white solid (18 mg, 75.9 %). ¹H NMR (DMSO-*d*⁶, 400 MHz) = δ 8.99-8.98 (d, 1H, J = 1.87 Hz); 8.74-8.71 (t, 1H); 8.58-8.56 (d, 1H, J = 8.27 Hz); 8.54 (s, 1H); 7.86-7.79 (q, 4H); 7.34-7.33 (d, 1H, J = 1.75 Hz); 4.70-4.65 (q, 1H); 4.40-4.38 (d, 2H, J = 5.59 Hz); 3.60-3.59 (d, 1H, J = 1.77 Hz); 3.38-3.37 (d, 1H, J = 1.77 Hz); 3.28-3.10 (m, 2H). ¹³C NMR (DMSO-*d*⁶, 100 MHz): 170.62, 169.08, 165.74, 154.06, 153.29, 146.57, 136.25, 133.27, 122.31, 121.67, 121.54, 116.20, 53.25, 52.94, 51.89, 34.76, 33.49. HRMS-ESI: *m/z* [M+H]⁺ calculated for C₁₉H₁₇BrN₆O₅S: 521.34, observed: *m/z* 523.0229 (M+H)⁺; *m/z* 519.0123 (M-H)⁺; HPLC method 2: R_t = 21.8; 97.2 %

(2S,3S)-3-((S)-1-((1-(4-nitrophenyl)-1H-1,2,3-triazol-4-yl)methylamino)-1-oxo-3-(thiazol-4-yl)propan-2-ylcarbamoyl)oxirane-2-carboxylic acid (53). Followed general procedure using: **53E** (27 mg, 0.05 mmol); LiOH (1.2 mg, 0.05 mmol); after extraction afforded the desired product as a white solid (20 mg, 78.3 %). ¹H NMR (DMSO-*d*⁶, 400 MHz) = δ 9.00-8.99 (d, 1H, J = 1.79 Hz); 8.74-8.71 (t, 1H); 8.59 (s, 1H); 8.48-8.47 (d, 1H, J = 8.42 Hz); 8.47-8.45 (d, 2H, J = 9.15 Hz); 8.21-8.19 (d, 2H, J = 9.15 Hz); 7.34-7.33 (d, 1H, J = 1.78 Hz); 4.69-4.66 (q, 1H); 4.42-4.41 (d, 2H, J = 5.60 Hz); 3.60-3.59 (d, 1H, J = 1.79 Hz); 3.50-3.10 (m, 3H). ¹³C NMR

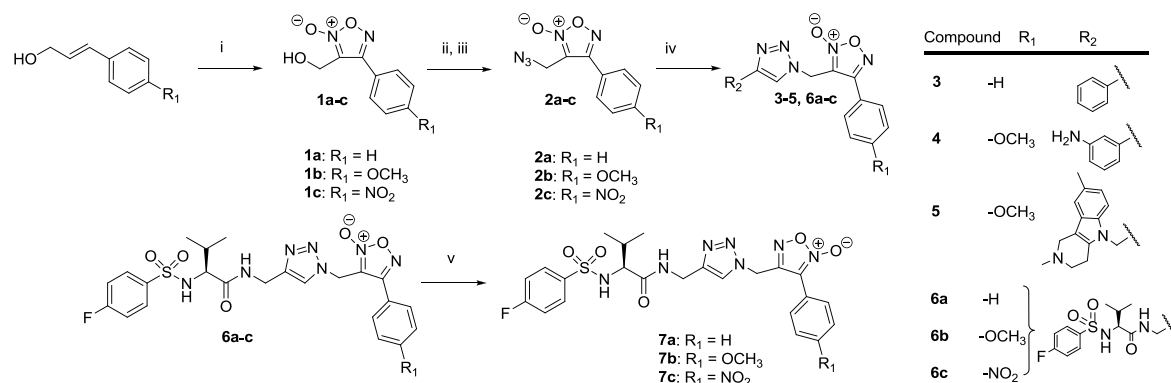
(DMSO- d^6 , 100 MHz):170.68, 169.07, 165.75, 154.10, 153.25, 147.11, 147.05, 141.26, 126.08, 121.95, 120.94, 116.23, 53.24, 52.95, 51.85, 34.69, 33.44. HRMS-ESI: m/z $[M+H]^+$ calculated for $C_{19}H_{17}N_7O_7S$: 487.45, observed: m/z 488.0986 ($M+H$) $^+$; m/z 486.0864 ($M-H$) $^+$. HPLC method 2: R_t = 20.4; 93.4 %.

(2S,3S)-3-((S)-1-((1-(2,6-difluorophenyl)-1H-1,2,3-triazol-4-yl)methylamino)-1-oxo-3-(thiazol-4-yl)propan-2-ylcarbamoyl)oxirane-2-carboxylic acid (54). Followed general procedure using: **54E** (24 mg, 0.047 mmol); LiOH (1.1 mg, 0.047 mmol); after extraction afforded the desired product as a white solid (13 mg, 57.3 %). 1H NMR (DMSO- d^6 , 400 MHz) = δ 9.00-8.99 (d, 1H, J = 1.90 Hz); 8.78-8.76 (t, 1H); 8.60-8.58 (d, 1H, J = 8.29 Hz); 8.27 (s, 1H); 7.77-7.69 (m, 1H); 7.49-7.45 (t, 2H); 7.36-7.27 (m, 2H); 4.71-4.65 (m, 1H); 4.44-4.42 (d, 2H, J = 5.63 Hz); 3.598-3.593 (d, 1H, J = 1.78); 3.360-3.355 (d, 1H, J = 1.78); 3.27-3.22 (m, 2H). ^{13}C NMR DMSO: 170.69, 169.07, 165.69, 158.07, 158.04, 155.56, 155.53, 154.05, 153.31, 145.67, 136.62, 129.17, 128.48, 126.17, 116.17, 53.23, , 52.93, 51.83, 34.67, 33.51. HRMS-ESI: m/z $[M+H]^+$ calculated for $C_{19}H_{16}F_2N_6O_5S$: 478.43, observed: m/z 479.0960 ($M+H$) $^+$: HPLC method 2: R_t = 17.32 min; 95.9 %

(2S,3S)-3-((S)-1-((1-mesityl-1H-1,2,3-triazol-4-yl)methylamino)-1-oxo-3-(thiazol-4-yl)propan-2-ylcarbamoyl)oxirane-2-carboxylic acid (55). Followed general procedure using: **55E** (24 mg, 0.046 mmol); LiOH (1.1 mg, 0.046 mmol); after extraction afforded the desired product as a white solid (15 mg, 66.1 %). 1H NMR (DMSO- d^6 , 400 MHz) = δ 8.98-8.97 (d, 1H, J = 1.87 Hz); 8.72-8.70 (t, 1H, J = 11.2 Hz); 8.55-8.53 (d, 1H, J = 8.23 Hz); 7.93 (s, 1H); 7.34 (s, 1H); 7.08 (s, 1H); 4.68-4.63 (m, 1H); 4.42-4.40 (d, 2H, J = 5.50 Hz); 3.61-3.50 (m, 4H); 2.32 (s, 3H); 1.86 (s, 6H). ^{13}C NMR (DMSO- d^6 , 100 MHz):170.29, 165.60, 153.65, 152.98, 144.93, 139.46, 134.51, 133.50, 128.90, 124.69, 115.78, 52.79, 52.58, 48.66, 34.54, 33.10, 20.69, 16.89.

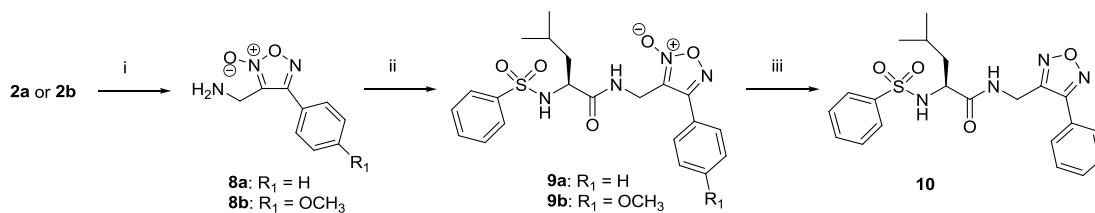
HRMS-ESI: m/z $[M+H]^+$ calculated for $C_{22}H_{24}N_6O_5S$: 484.53, observed: m/z 485.1622 $(M+H)^+$:
 m/z 483.1600 $(M-H)^+$; HPLC method 2: R_t = 23.6; 97.4 %.

Scheme 4. Synthesis of furoxan-triazole incorporating peptidomimetics



^aReagents and Conditions: i) $NaNO_2$, acetic acid, $< 20\text{ }^\circ\text{C}$; ii) $TsCl$, TEA, CH_2Cl_2 , $0\text{ }^\circ\text{C}$; iii) NaN_3 , DMF, $60\text{ }^\circ\text{C}$; iv) CuI , DIPEA, toluene, with phenylacetylene for **3**; 2,8-Dimethyl-5-(prop-2-ynyl)-2,3,4,5-tetrahydro-1H-pyrido[4,3-b]indole for **5**; (S)-2-(4-Fluorophenylsulfonyl)-3-methyl-N-(prop-2-ynyl)butanamide for **6a-c**; or $CuSO_4$, sodium ascorbate, 3-ethynylaniline, t -BuOH/EtOH/ H_2O for **4**; v) toluene, $120\text{ }^\circ\text{C}$, 3 d.

Scheme 5. Synthesis of furoxan peptidomimetics with methylene linker



^aReagents and Conditions: i) $P(Ph_3)$, 35 % NH_4OH , DMF, r.t.; ii) EDCI, DMAP, (S)-4-Methyl-2-(phenylsulfonyl)pentanoic acid, CH_2Cl_2 , $0\text{ }^\circ\text{C}$; iii) **9a**, Zn, ammonium formate, MeOH, $60\text{ }^\circ\text{C}$.

General Methods (Furoxans):

Purity and/or low resolution mass spectral (ESI or APCI) analysis was measured using an Advantage ARMOR C18; 5 μ M; 150 x 4.6 mm analytical column, on either a Shimadzu UFLC (Instrument 1) or Agilent 1100 Series HPLC in tandem with an Agilent 6310 Ion Trap LC/MS (Instrument 2). HPLC Method: Solvents: 0.05 % FA in CH₃CN (Solvent A); 0.05 % FA in 9:1 mixture of H₂O and MeOH (Solvent B); Flow rate 1.0 mL/min; Gradient: t = 0 min, 10 % B; t = 5 min, 30 % B; t = 15 min, 70 % B; t = 30 min, 90 % B; t = 35 min, 50% B, t = 38, 10% B; stop time 45 min.

General procedure for arylfuroxan-3-methanol cyclization: The appropriate cinnamyl alcohol (100 mmol) was dissolved in acetic acid (25 ml) under argon at 0 °C. NaNO₂ (300 mmol) was added dropwise over 30 min, while maintaining reaction temperature < 20 °C. The reaction was then allowed to warm to rt and monitored by TLC. After 4 h, the rxn was diluted with ice water, and extracted with ethyl acetate (3 x 175 ml). The combined organic extracts were washed with brine (2 x 75 ml), dried over Na₂SO₄ and concentrated to afford orange oil. The residual oil was then purified by column chromatography (hexane/ethyl acetate [10:1→5:1]) to yield the desired products in each circumstance as described below.

3-(Hydroxymethyl)-4-phenyl-1,2,5-oxadiazole 2-oxide (1a). yellow solid (4.8 g, 24.9 %); ¹H NMR (CDCl₃, 400 MHz): δ 7.85-7.82 (m, 2H); 7.61-7.54 (m, 3H); 4.77-4.76 (d, 2H, J = 4.89 Hz); 2.82 (bs, 1H). ¹³C NMR (CDCl₃, 100 MHz): 157.05, 131.58, 130.38, 129.62, 129.36, 127.99, 126.36, 115.07, 56.93.

3-(Hydroxymethyl)-4-(4-methoxyphenyl)-1,2,5-oxadiazole 2-oxide (1b). white solid (5.8 g, 26.1 %); ^1H NMR (CDCl_3 , 400 MHz): δ 7.79-7.77 (d, 2H, $J = 9.75$ Hz); 7.08-7.02 (d, 2H, $J = 9.75$ Hz); 4.77-4.75 (d, 2H); 3.90-3.86 (s, 3H); 2.64-2.60 (t, 1H). ^{13}C NMR (CDCl_3 , 100 MHz): 161.97, 156.48, 129.28, 118.42, 114.82, 114.74, 55.45, 53.42.

3-(Hydroxymethyl)-4-(4-nitrophenyl)-1,2,5-oxadiazole 2-oxide (1c). white solid (6.9 g, 29.1 %); ^1H NMR (CDCl_3 , 400 MHz): δ 8.44-8.42 (d, 2H, $J = 8.8$ Hz); 8.13-8.10 (d, 2H, $J = 8.8$ Hz); 4.79 (s, 2H); 2.45-2.18 (bs, 1H). ^{13}C NMR (CDCl_3 , 100 MHz): 154.75, 149.15, 131.76, 128.55, 124.15, 113.21, 52.94.

General procedure for alcohol activation: Triethylamine (0.62 ml, 4.43 mmol) was added to furoxan alcohol (284 mg, 1.48 mmol) in freshly distilled CH_2Cl_2 (10 ml) at 0 °C. TsCl (380 mg, 2.2 mmol) was separately dissolved in CH_2Cl_2 (5 ml) and added dropwise over 10 min. The mixture was allowed to warm to rt and stirred for 3 h. The reaction was quenched w/ saturated aqueous NH_4OH (10 ml), and extracted with ethyl acetate (3 x 75 ml). Combined organic layers washed with brine (2 x 15 ml), dried over Na_2SO_4 and concentrated to give yellow oil. Reaction products were isolated by column chromatography (hexane/ethyl acetate [8:1 \rightarrow 4:1]). Once products were confirmed by NMR, subsequent crude mixtures of the tosyl and chloro intermediates were submitted to next reaction without further purification.

General procedure for preparation of the azide: NaN_3 (1.5 eq) was added to the a mixture of the tosyl and chloro derivatives (1.0 eq) in DMF (10 ml) and the reaction brought to 50 °C and reaction progress monitored by TLC. After completion of reaction (typically 4-12 h) the reaction was quenched with ice water (150 ml), extracted with ethyl acetate (3 x 50 ml). The combined organic extracts were washed with brine (2 x 50 ml), water (3 x 250 ml), dried over Na_2SO_4 and concentrated to give orange oil. Crude oil was purified by column chromatography (hexane/ethyl acetate [5:1]) to give a mixture of the desired azides described below.

3-(Azidomethyl)-4-phenyl-1,2,5-oxadiazole 2-oxide (2a). Synthesized using the general procedure with the following values: Crude mixture of tosylated and chlorinated **1a** (366 mg, 1.06 mmol); NaN₃ (100 mg, 1.6 mmol); afforded **2a** as a white solid (175 mg, 76.3 %). ¹H NMR (CDCl₃, 400 MHz): δ 7.76-7.74 (d, 2H); 7.63-7.56 (m, 3H); 4.48 (s, 2H). ¹³C NMR (CDCl₃, 100 MHz): 156.51, 131.54, 129.51, 127.67, 125.80, 111.75, 42.83. Analytical HPLC (Instrument 1): Purity = 97.9 %, t_R = 22.8 min.

3-(Azidomethyl)-4-(4-methoxyphenyl)-1,2,5-oxadiazole 2-oxide (2b). Synthesized using general the procedure with the following values: Crude mixture of tosylated and chlorinated **1b** (560 mg, 1.5 mmol); NaN₃ (150 mg, 2.2 mmol); afforded **2b** as a white solid (310 mg, 84.3 %). ¹H NMR (CDCl₃, 400 MHz): δ 7.70-7.67 (d, 2H); 7.09-7.05 (d, 2H); 4.47 (s, 2H); 3.90 (s, 3H). ¹³C NMR (CDCl₃, 100 MHz): 162.10, 156.20, 129.15, 118.01, 114.94, 111.71, 55.47, 42.91. Analytical HPLC (Instrument 1): Purity = 99.2 %, t_R = 23.5 min.

3-(Azidomethyl)-4-(4-nitrophenyl)-1,2,5-oxadiazole 2-oxide (2c). Synthesized using the general procedure with the following values: Crude mixture of tosylated and chlorinated **1c** (612 mg, 1.63 mmol); NaN₃ (160 mg, 2.4 mmol); afforded **2c** as a white solid (345 mg, 85.8 %). ¹H NMR (CDCl₃, 400 MHz): δ 8.45-8.42 (d, 2H); 8.01-7.99 (d, 2H); 4.52 (s, 2H). ¹³C NMR (CDCl₃, 100 MHz): 154.68, 149.55, 131.71, 128.81, 124.65, 111.22, 42.85. Analytical HPLC (Instrument 1): Purity = 97.4 %, t_R = 23.4 min.

General procedure for click reaction A: The azide (25 mg, 0.12 mmol) was dissolved in toluene (5 ml) followed under argon, by the addition of phenylacetylene (15 mg, 0.15 mmol) and copper (I) iodide (10 mg, 0.032 mmol). N, N-Diisopropylethylamine (0.02 ml, 0.115 mmol) was then added to the solution. The reaction was allowed to stir at room temperature until TLC analysis (hexane/ethyl acetate [1:1]) indicated completion. The solution was filtered through

celite and concentrated to give a crude brown solid which was purified by column chromatography to give the title compound.

General procedure for click reaction B: The furoxan azide (1.0 eq), 3-ethynylaniline (1.0 eq), sodium ascorbate (0.4 eq), and CuSO₄ (0.2 eq) were stirred in *t*-BuOH/EtOH/H₂O (3:1:1) for 12 h. Reaction was filtered through celite, and concentrated. Residual oil was purified by column chromatography to give the title compound.

4-Phenyl-3-((4-phenyl-1H-1,2,3-triazol-1-yl)methyl)-1,2,5-oxadiazole 2-oxide (3).

Synthesized using the general click procedure with the following values: Click reaction A: furoxan-azide (25 mg, 0.12 mmol); phenylacetylene (15 mg, 0.15 mmol) and copper (I) iodide (10 mg, 0.032 mmol); and N, N-diisopropylethylamine (0.02 ml, .115 mmol); afforded **3** as a white solid (30 mg, 81.6 %). ¹H NMR (DMSO-*d*⁶, 400 MHz): δ 8.69 (s, 1H); 7.83-7.81 (t, 4H); 7.61-7.59 (m, 3H); 7.44-7.31 (m, 3H); 5.81 (s, 2H). ¹³C NMR (DMSO-*d*⁶, 100 MHz): 157.46, 146.90, 131.94, 130.63, 129.82, 129.38, 128.56, 128.23, 125.84, 125.65, 122.93, 112.54, 42.62.

3-((4-(3-Aminophenyl)-1H-1,2,3-triazol-1-yl)methyl)-4-(4-methoxyphenyl)-1,2,5-oxadiazole 2-oxide (4). Click reaction B: *p*-methoxyphenylfuroxan azide (65 mg, 0.26 mmol), 3-ethynylaniline (30.8 mg, 0.26 mmol), sodium ascorbate (20 mg, 0.1 mmol), and CuSO₄ (8 mg, 0.05 mmol); afforded **4** as a white solid (72 mg, 75.0 %). ¹H NMR (CDCl₃, 400 MHz): δ 8.02 (s, 1H); 7.87-7.84 (d, 2H, *J* = 6.8 Hz); 7.22-7.21 (t, 1H); 7.20-7.18 (d, 1H, *J* = 7.63 Hz); 7.17-7.15 (dt, 1H); 7.09-7.06 (d, 2H, *J* = 6.8 Hz); 6.68-6.55 (dq, 1H); 5.59 (s, 2H); 3.87 (s, 3H). ¹³C NMR (CDCl₃, 100 MHz): 162.23, 156.27, 148.81, 146.96, 130.71, 129.85, 129.65, 120.74, 117.41, 116.05, 115.28, 115.06, 112.18, 111.61, 55.47, 42.09. ESI-HRMS (*m/z*): [M+H]⁺ calcd. for C₁₈H₁₆N₆O₃: 365.1356, observed: 365.1360. Analytical HPLC (Instrument 1): Purity = 97.3 %, *t*_R = 12.7 min.

3-((4-((2,8-Dimethyl-3,4-dihydro-1H-pyrido[4,3-b]indol-5(2H)-yl)methyl)-1H-1,2,3-triazol-1-yl)methyl)-4-(4-methoxyphenyl)-1,2,5-oxadiazole 2-oxide (5). Click reaction A: carbazole alkyne (26 mg, 0.105 mmol [see supplemental materials for preparation]), furoxan azide (34 mg, 0.143 mmol), DIPEA (0.03 ml, 0.18 mmol) and CuI (20 mg, 0.06 mmol); yielded **5** as a white solid (52 mg, 75.1 %). ¹H NMR (CDCl₃, 400 MHz): δ 7.79-7.76 (d, 2H, 8.83 Hz); 7.50 (s, 1H); 7.22-7.19 (m, 2H); 7.05-7.02 (d, 2H, J = 8.83 Hz); 7.01-6.99 (d, 1H, J = 8.28 Hz); 5.40 (s, 2H); 5.31 (s, 2H); 3.88 (s, 3H); 3.80 (s, 2H); 3.00 (s, 4H); 2.89 (s, 3H); 2.63 (s, 3H); 2.43 (s, 3H). ¹³C NMR (CDCl₃, 100 MHz): 161.81, 155.80, 145.21, 134.28, 131.96, 129.20, 128.57, 125.62, 122.65, 122.61, 117.30, 117.04, 114.65, 110.84, 108.31, 106.64, 55.09, 51.60, 51.00, 44.38, 41.67, 38.17, 21.69, 21.00. ESI-HRMS (m/z): [M+H]⁺ calcd. for C₂₆H₂₇N₇O₃: 486.2248, observed: 486.2258. Analytical HPLC (Instrument 1): Purity = 99.0 %, *t*_R = 8.3 min.

(R)-3-((4-((2-(4-Fluorophenylsulfonamido)-3-methylbutanamido)methyl)-1H-1,2,3-triazol-1-yl)methyl)-4-phenyl-1,2,5-oxadiazole 2-oxide (6a). Click reaction A: peptidomimetic alkyne (140 mg, 0.44 mmol [see supplemental materials for preparation]), **2a** (100 mg, 0.40 mmol), DIPEA (0.07 ml, 0.44 mmol) and CuI (10 mg, 0.04 mmol); yielded **6a** (*R*_f = 0.37, hexane/ethyl acetate [1:2]) as a white solid (174 mg, 76.8 %). ¹H NMR (DMSO-*d*⁶, 400 MHz): δ 8.80-8.60 (t, 1H); 7.94 (s, 1H); 7.89-7.81 (bs, 1H); 7.89-7.76 (m, 4H); 7.65-7.58 (m, 3H); 7.34-7.29 (t, 2H); 5.72 (s, 2H); 4.19-3.93 (abq, 2H); 3.44 (bs, 1H); 1.78-1.76 (q, 1H); 0.77-0.70 (dd, 6H). ¹³C NMR (DMSO-*d*⁶, 100 MHz): 170.27, 157.41, 145.02, 131.97, 130.54, 129.95, 129.86, 128.20, 125.84, 124.34, 116.27, 116.05, 112.64, 62.25, 42.18, 34.21, 31.12, 19.36, 18.78. ESI-HRMS (m/z): [M+H]⁺ calcd. for C₂₃H₂₄FN₇O₅S: 530.1567; observed, 530.1636; [M-H]⁺ calcd. for C₂₃H₂₄FN₇O₅S: 528.1519; observed, 528.1541. Analytical HPLC (Instrument 1): Purity = 97.1 %, *t*_R = 24.4 min.

(R)-3-(((4-((2-(4-Fluorophenylsulfonamido)-3-methylbutanamido)methyl)-1H-1,2,3-triazol-1-yl)methyl)-4-(4-methoxyphenyl)-1,2,5-oxadiazole 2-oxide (6b): Click reaction A:

peptidomimetic alkyne (140 mg, 0.44 mmol), **2b** (100 mg, 0.40 mmol), DIPEA (0.07 ml, 0.44 mmol) and CuI (10 mg, 0.04 mmol); yielded **6b** (R_f = 0.36, hexane/ethyl acetate [1:2]) as a white solid (yield = 58%). ^1H NMR ($\text{CD}_3\text{CN}-d^3$, 400 MHz): δ 7.85-7.82 (q, 2H); 7.79-7.77 (d, 2H, J = 8.83); 7.69 (s, 1H); 7.24-7.20 (t, 2H); 7.15-7.13 (d, 2H, J = 8.78); 6.91 (bs, 1H); 5.93-5.91 (d, 1H, J = 8.80); 5.57 (s, 2H); 4.24-4.07 (qd, 2H); 3.89 (s, 3H); 3.55-3.47 (t, 1H); 1.95-1.78 (m, 1H); 0.82-0.79 (q, 6H). ^{13}C NMR ($\text{CD}_3\text{CN}-d^3$, 100 MHz): 170.29, 163.11, 162.08, 157.02, 145.07, 137.88, 130.05, 129.95, 129.78, 124.26, 117.97, 116.27, 116.05, 115.33, 112.53, 62.26, 55.92, 49.03, 42.24, 34.23, 31.11, 19.34, 18.77. ESI-HRMS (m/z): $[\text{M}+\text{H}]^+$ calcd. for $\text{C}_{24}\text{H}_{26}\text{FN}_7\text{O}_6\text{S}$: 560.1673; observed, 560.1739; $[\text{M}-\text{H}]^+$ calcd. for $\text{C}_{24}\text{H}_{26}\text{FN}_7\text{O}_6\text{S}$: 558.1625; observed, 558.1649. Analytical HPLC (Instrument 1): Purity = 98.5 %, t_R = 24.9 min.

(R)-3-(((4-((2-(4-Fluorophenylsulfonamido)-3-methylbutanamido)methyl)-1H-1,2,3-triazol-1-yl)methyl)-4-(4-nitrophenyl)-1,2,5-oxadiazole 2-oxide (6c). **2c** (200 mg, 1 mmol) dissolved in toluene (5 ml) was added the terminal alkyne (340 mg, 1.1 mmol) in 4 ml of toluene/methanol (3:1) at room temperature. To this suspension CuI (30 mg, 0.1 mmol) was added followed by DIPEA (0.18 ml, 1 mmol) and the reaction stirred for 8 h. The reaction was then filtered through celite and concentrated. The corresponding oil was dissolved in CH_2Cl_2 and successively washed with 1 N HCl (2 x 15 ml), brine (2 x 30 ml), dried over Na_2SO_4 and concentrated to give a yellow solid. The solid then washed with CHCl_3 , giving the desired product as a white solid (352 mg, 63 %). R_f = 0.38 (hexane/ethyl acetate [1:2]). ^1H NMR ($\text{DMSO}-d^6$, 400 MHz): δ 8.39-8.37 (d, 2H, J = 8.0 Hz); 8.34-8.31 (t, 1H); 8.26 (s, 1H); 8.07-8.05 (d, 2H, J = 8.0 Hz); 7.92 (s, 1H); 7.85-7.83 (d, 1H, J = 9.2 Hz); 7.31-7.26 (t, 2H); 5.78 (s, 2H); 4.08-3.89 (qd, 2H); 3.42-3.38 (t, 1H); 1.76-1.71 (m, 1H); 0.73-0.66 (dd, 6H). ^{13}C NMR ($\text{DMSO}-d^6$, 100 MHz): 170.29, 156.09, 149.57,

145.04, 131.77, 130.05, 129.95, 129.91, 124.81, 124.42, 116.27, 116.24, 112.66, 62.26, 34.21, 31.09, 19.34. ESI-HRMS (m/z): $[M+H]^+$ calcd. for $C_{23}H_{23}FN_8O_7S$: 575.1418; observed, 575.1477; $[M-H]^+$ calcd. for $C_{23}H_{23}FN_8O_7S$: 573.1370; observed, 573.1384. Analytical HPLC (Instrument 1): Purity = 95.7 %, t_R = 24.7 min.

General procedure for the isomerization to the tautomeric oxadiazole-N-oxides: The appropriate oxadiazole-2N-oxide (1 mmol) was suspended in anhydrous toluene (10 ml) and heated to 120 °C for 3 d. The reaction was allowed to cool to rt, toluene removed under vacuo, and the mixture of isomers was purified by column chromatography (hexane/ethyl acetate [2:1 → 1:2]) to give the corresponding tautomeric furoxans.

(R)-4-(((4-((2-(4-fluorophenylsulfonamido)-3-methylbutanamido)methyl)-1H-1,2,3-triazol-1-yl)methyl)-3-phenyl-1,2,5-oxadiazole 2-oxide (7a). white solid (33% conversion); R_f = 0.27 (hexane/ethyl acetate [1:2]). 1H NMR ($CDCl_3$, 400 MHz): δ 7.85-7.81 (q, 2H); 7.71 (s, 1H); 7.66-7.65 (m, 2H); 7.61-7.54 (m, 3H); 7.13-7.08 (t, 2H); 6.84 (bs, 1H); 5.80-5.72 (q, 2H); 5.60-5.58 (d, 1H, J = 8.54); 4.45-4.36 (m, 2H); 3.55-3.51 (q, 1H); 2.06-2.01 (m, 1H); 0.83-0.79 (q, 6H). ^{13}C NMR ($CDCl_3$, 100 MHz): 170.55, 151.25, 145.15, 131.20, 130.08, 129.87, 129.54, 127.69, 122.78, 121.33, 116.27, 116.05, 62.24, 45.17, 34.76, 31.33, 19.09, 17.31. ESI-HRMS (m/z): $[M+H]^+$ calcd. for $C_{23}H_{24}FN_7O_5S$: 530.1567; observed, 530.1624; $[M-H]^+$ calcd. for $C_{23}H_{24}FN_7O_5S$: 528.1519; observed, 528.1557. Analytical HPLC (Instrument 2): Purity = 97.0 %, t_R = 23.68 min.

(S)-4-(((4-((2-(4-fluorophenylsulfonamido)-3-methylbutanamido)methyl)-1H-1,2,3-triazol-1-yl)methyl)-3-(4-methoxyphenyl)-1,2,5-oxadiazole 2-oxide (7b). white solid (25% conversion); R_f = 0.26 (hexane/ethyl acetate [1:2]); 1H NMR ($CDCl_3$, 400 MHz): δ 8.14-8.12 (d, 1H); 7.84-7.81 (t, 3H); 7.69 (s, 1H); 7.63-7.61 (d, 2H); 7.52-7.48 (t, 1H); 7.12-7.04 (m, 5H); 6.82 (bs, 1H); 5.76-5.74 (q, 2H); 5.59-5.50 (m, 2H); 3.60 (s, 3H); 3.54-3.51 (m, 2H); 2.10-2.02 (m, 3H); 0.82-

0.79 (q, 6H). ^{13}C NMR (CDCl_3 , 100 MHz): 170.50, 161.57, 151.4, 145.07, 135.48, 133.57, 130.13, 130.01, 129.23, 128.47, 122.60, 116.27, 116.04, 115.06, 62.20, 55.47, 45.29, 34.73, 31.38, 29.67, 19.09, 17.27. ESI-HRMS (m/z): $[\text{M}+\text{H}]^+$ calcd. for $\text{C}_{24}\text{H}_{26}\text{FN}_7\text{O}_6\text{S}$: 560.1673; observed, 560.1723; $[\text{M}-\text{H}]^+$ calcd. for $\text{C}_{24}\text{H}_{26}\text{FN}_7\text{O}_6\text{S}$: 558.1625; observed, 558.1664.

Analytical HPLC (Instrument 2): Purity = 95.9 %, t_R = 23.9 min.

(R)-4-(((4-((2-(4-fluorophenylsulfonamido)-3-methylbutanamido)methyl)-1H-1,2,3-triazol-1-yl)methyl)-3-(4-nitrophenyl)-1,2,5-oxadiazole 2-oxide (7c). white solid (52 % conversion); R_f = 0.28 (hexane/ethyl acetate [1:2]). ^1H NMR (CDCl_3 , 400 MHz): δ 8.41-8.39 (d, 2H, J = 8.96); 7.96-7.94 (d, 2H, J = 8.96); 7.86-7.82 (q, 2H); 7.77 (s, 1H); 7.17-7.13 (t, 2H); 6.76 (bs, 1H); 5.84-5.76 (q, 2H); 5.41-5.39 (d, 1H, J = 8.00); 4.46-4.41 (q, 2H); 3.50-3.46 (q, 1H); 2.06-2.01 (m, 1H); 0.80-0.78 (q, 6H). ^{13}C NMR (CDCl_3 , 100 MHz): 170.69, 150.75, 148.82, 145.70, 130.09, 130.00, 128.77, 124.54, 122.81, 116.40, 116.17, 112.81, 62.36, 60.38, 45.12, 34.90, 31.07, 19.07, 17.26, 14.17. ESI-HRMS (m/z): $[\text{M}+\text{H}]^+$ calcd. for $\text{C}_{23}\text{H}_{23}\text{FN}_8\text{O}_7\text{S}$: 575.1418; observed, 575.1456; $[\text{M}-\text{H}]^+$ calcd. for $\text{C}_{23}\text{H}_{23}\text{FN}_8\text{O}_7\text{S}$: 573.1370; observed, 573.1380.

Analytical HPLC (Instrument 2): Purity = 95.1 %, t_R = 24.2 min.

General procedure for Staudinger Reduction, yielding 8a & 8b.

The appropriate azide (1 eq) and $\text{P}(\text{Ph})_3$ (15.8 eq) were dissolved in DMF and stirred at rt for 1 h. 35 % NH_4OH (4 eq) was added dropwise and reaction continued for an additional hour. The mixture was then diluted with ice water, extracted with ethyl acetate (3 x 100 ml). Combined organic layers were then extracted with 1 N HCl (3 x 100 ml). Combined acidic extracts were washed with CHCl_3 (3 x 75 ml), brought to pH ~ 10 using 1 N NaOH, extracted with ethyl acetate (3 x 150 ml), concentrated under vacuo and purified by column chromatography to give the desired products as white solids.

3-(aminomethyl)-4-phenyl-1,2,5-oxadiazole 2-oxide (8a). Synthesized following the general procedure with the following quantities: **57a** (70 mg, 0.32 mmol); P(Ph)₃ (1.33 g, 5.06 mmol); 35 % NH₄OH (1.26 ml); DMF (8.4 ml, 0.038M reaction concentration); yielded **63a** (78 mg, 33.3 %). ¹H NMR (CDCl₃, 400 MHz): δ 7.66-7.61 (m, 3H); 7.57-7.52 (m, 2H); 3.94 (s, 2H), 1.60 (bs, 2H). ¹³C NMR (CDCl₃, 100 MHz): 156.54, 131.54, 129.51, 127.64, 125.79, 111.78, 42.82.

3-(aminomethyl)-4-(4-methoxyphenyl)-1,2,5-oxadiazole 2-oxide (8b). Synthesized following the general procedure with the following quantities: **57b** (284 mg, 1.48 mmol); P(Ph)₃ (6.13 g, 23.4 mmol); 35 % NH₄OH_(aq) (6.0 ml); DMF (32 ml); yielded **63b** (98 mg, 38.5 %). ¹H NMR (CDCl₃, 400 MHz): δ 7.71-7.68 (d, 2H); 7.09-7.05 (d, 2H); 4.10 (s, 2H). ¹³C NMR (CDCl₃, 100 MHz): 161.10, 155.15, 129.19, 118.11, 114.54, 112.71, 48.52.

General coupling procedure: The appropriate carboxylic acid (1 eq) was dissolved in anhydrous CH₂Cl₂ and brought to 0 °C under argon. DMAP (0.5 eq) and EDCI (1.1 eq) were added and the suspension stirred for 15 min at 0 °C. The furoxan amine (1.0 eq) dissolved in anhydrous CH₂Cl₂ (5 ml) was added slowly at 0 °C. The reaction was allowed to warm to rt and stirred overnight. The mixture was quenched w/ 1 N HCl, diluted with ice water, extracted with CH₂Cl₂ (3 x 50 ml). Combined organic layers were washed with brine (2 x 25 ml), dried over Na₂SO₄ and concentrated to give crude yellow oil. The residual oil purified by column chromatography to give the corresponding furoxan peptidomimetics.

(R)-3-((4-Methyl-2-(phenylsulfonamido)pentanamido)methyl)-4-phenyl-1,2,5-oxadiazole 2-oxide (9a). Synthesized using the general procedure with the following values: **63a** (111 mg, 0.58 mmol); EDCI (130 mg, 0.69 mmol); DMAP (40 mg, 0.3 mmol); peptidomimetic acid (190 mg, 0.69 mmol); afforded **64a** as a white solid (244 mg, 95.4 %). ¹H NMR (CDCl₃, 400 MHz): δ 7.85-7.79 (m, 4H); 7.59-7.42 (m, 6H); 6.85-6.83 (t, 1H); 5.154-5.135 (d, 1H); 4.53-4.30 (m, 2H); 3.75-3.71 (m, 1H); 1.59-1.52 (m, 1H); 1.45-1.41 (m, 2H); 0.851-0.834 (d, 3H); 0.703-0.687

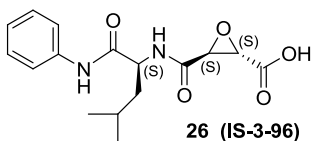
(3H). ^{13}C NMR (CDCl_3 , 100 MHz): 171.91, 156.24, 139.00, 133.17, 131.30, 129.37, 129.05, 127.93, 127.24, 125.80, 112.94, 55.39, 42.25, 32.28, 24.27, 22.88, 20.98. ESI-HRMS (m/z): $[\text{M}+\text{H}]^+$ calcd. for $\text{C}_{21}\text{H}_{24}\text{N}_4\text{O}_5\text{S}$: 445.1491; observed, 445.1556; $[\text{M}-\text{H}]^+$ calcd. for $\text{C}_{21}\text{H}_{24}\text{N}_4\text{O}_5\text{S}$: 443.1443; observed, 443.1447. Analytical HPLC (Instrument 2): Purity = 98.5 %, t_{R} = 25.2 min.

(R)-4-(4-Methoxyphenyl)-3-((4-methyl-2-(phenylsulfonamido)pentanamido)methyl)-1,2,5-oxadiazole 2-oxide (9b). Synthesized using the general procedure with the following values: **63a** (40 mg, 0.21 mmol); EDCI (48 mg, 0.25 mmol); DMAP (20 mg, 0.25 mmol); peptidomimetic acid (68 mg, 0.25 mmol); afforded **64b** as a white solid (75 mg, 80.7 %). ^1H NMR ($\text{MeOD}-d^4$, 400 MHz): δ 7.81-7.80 (m, 2H); 7.70-7.68 (d, 2H, J = 9.2 Hz); 7.57-7.46 (m, 3H); 7.09-7.07 (d, 2H, J = 9.2 Hz); 5.5 (s, 1H); 4.28-4.05 (q, 2H); 3.68-3.65 (q, 1H); 1.49-1.41 (m, 1H); 1.29-1.21 (m, 1H); 1.08-1.03 (m, 1H); 0.78-0.76 (d, 3H, J = 6.8 Hz); 0.66-0.65 (d, 3H, J = 6.8 Hz). ^{13}C NMR ($\text{MeOD}-d^4$, 100 MHz): 171.91, 161.97, 155.83, 150.45, 145.07, 138.95, 133.20, 130.85, 129.42, 129.04, 128.78, 127.23, 117.96, 114.84, 112.85, 55.39, 42.25, 32.28, 24.27, 22.88, 20.98. ESI-HRMS (m/z): $[\text{M}+\text{H}]^+$ calcd. for $\text{C}_{22}\text{H}_{26}\text{N}_4\text{O}_6\text{S}$: 475.1597; observed, 475.1650; $[\text{M}-\text{H}]^+$ calcd. for $\text{C}_{22}\text{H}_{26}\text{N}_4\text{O}_6\text{S}$: 473.1549; observed, 473.1530. Analytical HPLC (Instrument 2): Purity = 99.5 %, t_{R} = 25.7 min.

(R)-4-Methyl-N-((4-phenyl-1,2,5-oxadiazol-3-yl)methyl)-2-(phenylsulfonamido)pentanamide (10). Activated zinc dust (40 mg, 0.5 mmol) was added to a solution of **64a** (120 mg, 0.27 mmol) in anhydrous MeOH (5 ml) and the reaction stirred for 15 min. Ammonium formate (50 mg, 0.8 mmol) was then added in one portion and the reaction refluxed at 60 °C for 8 h. The reaction mixture was then cooled to room temperature, filtered through celite, concentrated, and purified by column chromatography to give the desired product as a white solid (15 mg, 13.0 %). ^1H NMR (CDCl_3 , 400 MHz): δ 7.85-7.85 (d, 2H, J = 1.6 Hz);

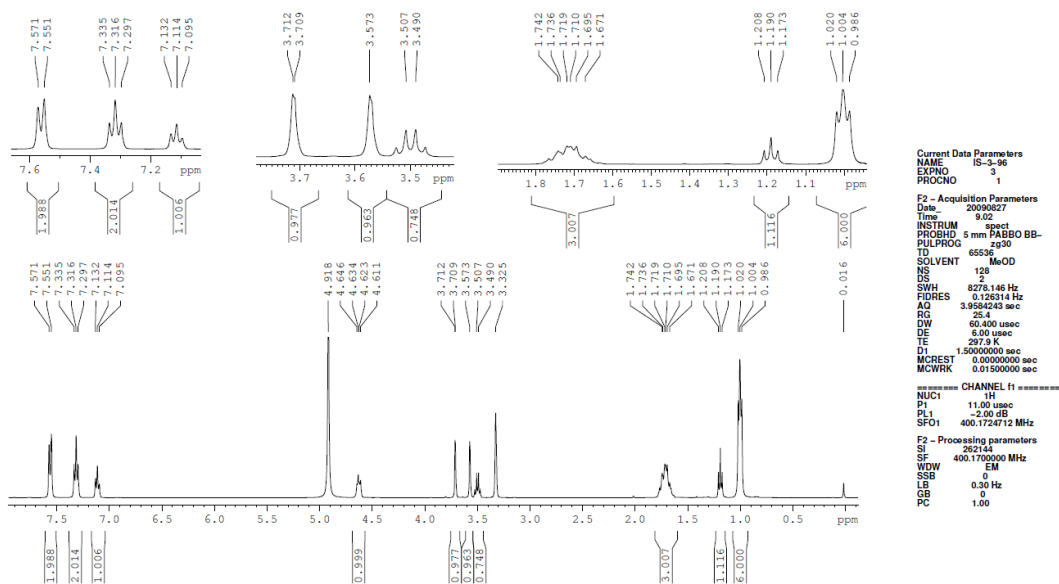
7.69-7.66 (m, 2H); 7.57-7.44 (m, 6H); 6.76-6.75 (t, 1H); 4.73-4.60 (m, 2H); 3.76-3.72 (m, 1H); 1.51-1.46 (m, 2H); 1.39-1.36 (m, 1H); 0.84-0.81 (d, 3H, J = 6.8 Hz); 0.68-0.63 (d, 3H, J = 6.8 Hz). ^{13}C NMR (CDCl_3 , 100 MHz): 171.55, 153.05, 150.29, 139.05, 133.15, 130.85, 129.33, 129.19, 128.14, 127.27, 125.03, 55.43, 41.98, 34.11, 24.26, 22.86, 21.01. ESI-HRMS (m/z): $[\text{M}+\text{H}]^+$ calcd. for $\text{C}_{21}\text{H}_{24}\text{N}_4\text{O}_4\text{S}$: 429.1542; observed, 429.1573. Analytical HPLC (Instrument 1): Purity = 95.2 %, t_{R} = 19.9 min.

APPENDIX B. COMPOUND CHARACTERIZATION SPECTRA

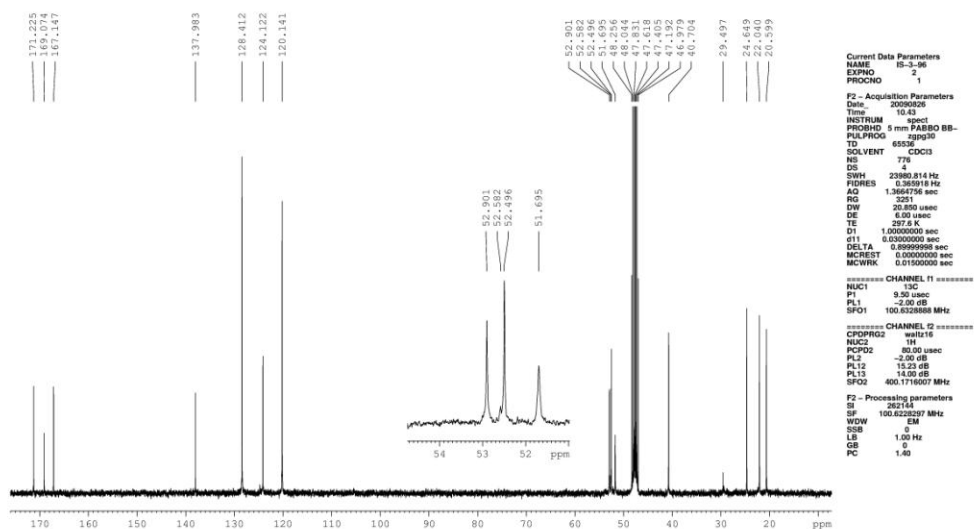


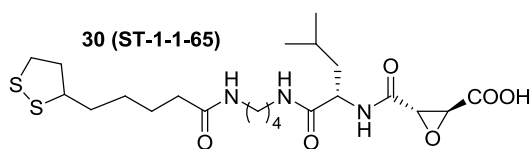
Chemical Formula: C₁₆H₂₀N₂O₅
Molecular Weight: 320.34040

Sample: IS-3-96
Solvent: MeOD
Standard Survey 1-D Proton NMR Spectrum
Bruker AVANCE-400 NMR Spectrometer



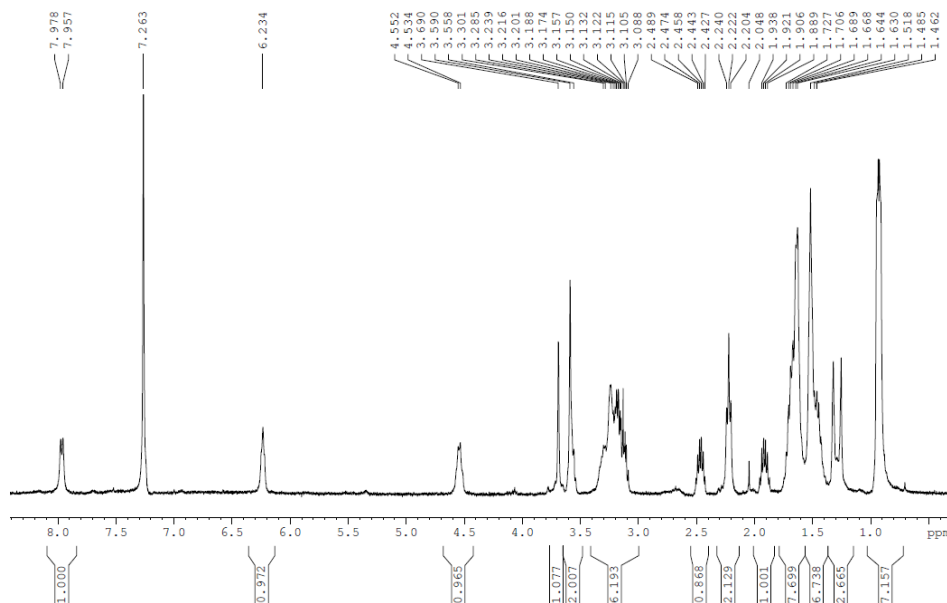
Sample: IS-3-96
Solvent: MeOD
Standard Carbon-13 Parameters with
Composite Pulse Decoupling (Waltz-16)
Bruker AVANCE-400 NMR Spectrometer





Chemical Formula: $C_{19}H_{31}N_3O_6S_2$
Molecular Weight: 461.59594

Sample: ST-1-1-65
Solvent: CDCl₃
09/29/2009



Current Data Parameters
NAME BP-1-162-diazide
EXPNO 131
PROCNO 1

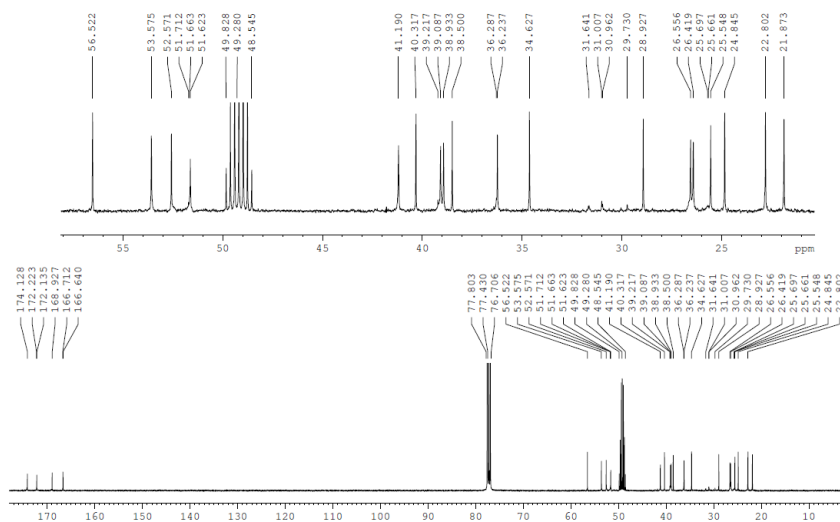
F2 - Acquisition Parameters
Date_ 20090929
Time 13.36
INSTRUM spect
PROBHD 5 mm PABBO BB-
PULPROG zg30
TD 65536
SOLVENT CDCl₃
NS 8
DS 2
SWH 8278.146 Hz
FIDRES 0.126314 Hz
AQ 3.9584243 sec
RG 64
DW 60.400 usec
DE 6.00 usec
TE 296.4 K
D1 1.50000000 sec
MCREST 0.00000000 sec
MCWRK 0.01500000 sec

===== CHANNEL f1 =====
NUC1 1H
P1 12.75 usec
PL1 -2.00 dB
SFO1 400.1724712 MHz

F2 - Processing parameters
SI 262144
SF 400.1700066 MHz
WDW EM
SSB 0
LB 0.30 Hz
GB 0
PC 1.00

1D NMR plot parameters
CX 28.00 cm
CY 5.00 cm
F1P 8.688 ppm
F1 3476.78 Hz
F2P 0.352 ppm
F2 140.81 Hz
PPMCM 0.29773 ppm/cm
HZCM 119.14176 Hz/cm

Sample: ST-1-65
Solvent: CDCl₃ + MeOD
1-D Carbon-13 NMR Spectrum
with Waltz-16 (CPD) Decoupling
Bruker DXP-400 NMR Spectrometer



Current Data Parameters
NAME BP-1-162-diazide
EXPNO 245
PROCNO 1

F2 - Acquisition Parameters
Date_ 20090929
Time 13.39
INSTRUM spect
PROBHD 5 mm QNP 1H/1
PULPROG zgpg30
TD 65536
SOLVENT CDCl₃
NS 15360
DS 8
SWH 23980.814 Hz
FIDRES 0.343918 Hz
AQ 1.344711 sec
RG 64
DW 20.810 usec
DE 6.00 usec
TE 298.2 K
D1 1.00000000 sec
DELTA 0.89999999 sec
MUSEY 0.00000000 sec
MUSEY 0.01000000 sec

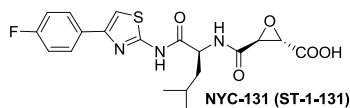
===== CHANNEL f1 =====
NUC1 13C
P1 12.00 usec
PL1 0.00 dB
SFO1 100.6283500 MHz

===== CHANNEL f2 =====
NAME waltz16
NUC2 1H
P2 80.00 usec
PL2 0.00 dB
PL12 17.00 dB
SFO2 400.1314000 MHz

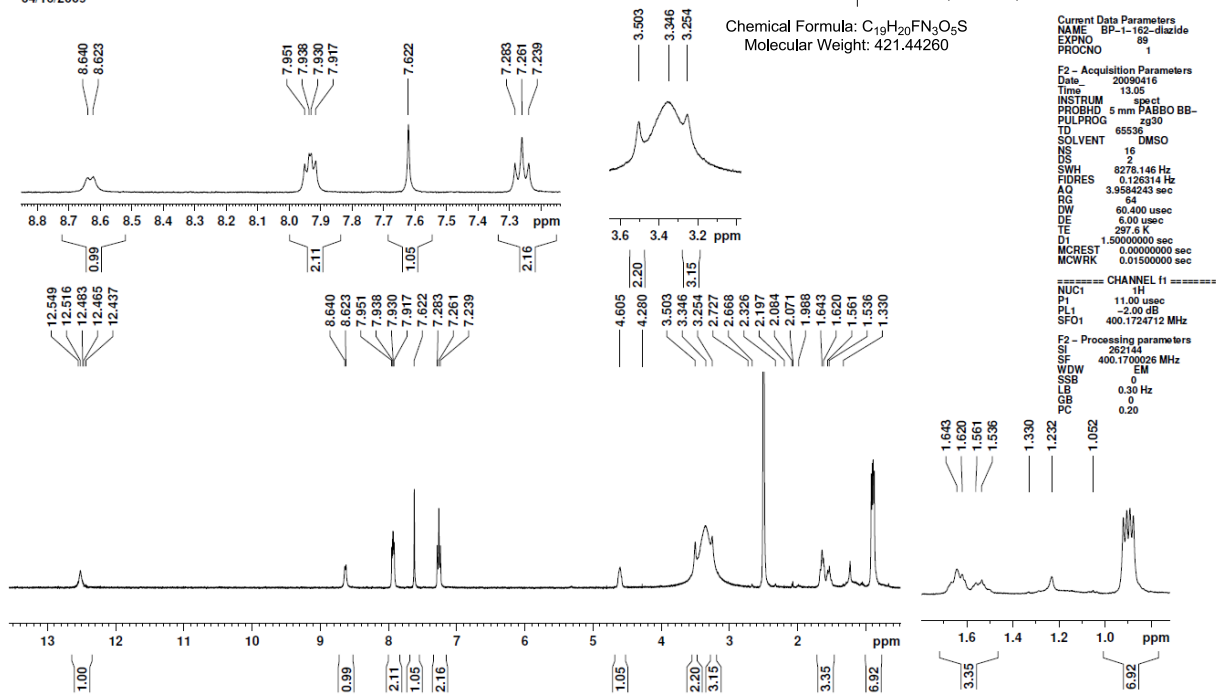
F2 - Processing parameters
SI 57312
SF 100.6127000 MHz
WDW EM
SSB 0
LB 1.00 Hz
GB 0
PC 0.25

1D NMR plot parameters
CX 28.00 cm
CY 5.00 cm
F1P 8.688 ppm
F1 3476.78 Hz
F2P 0.352 ppm
F2 140.81 Hz
PPMCM 0.29773 ppm/cm
HZCM 119.14176 Hz/cm

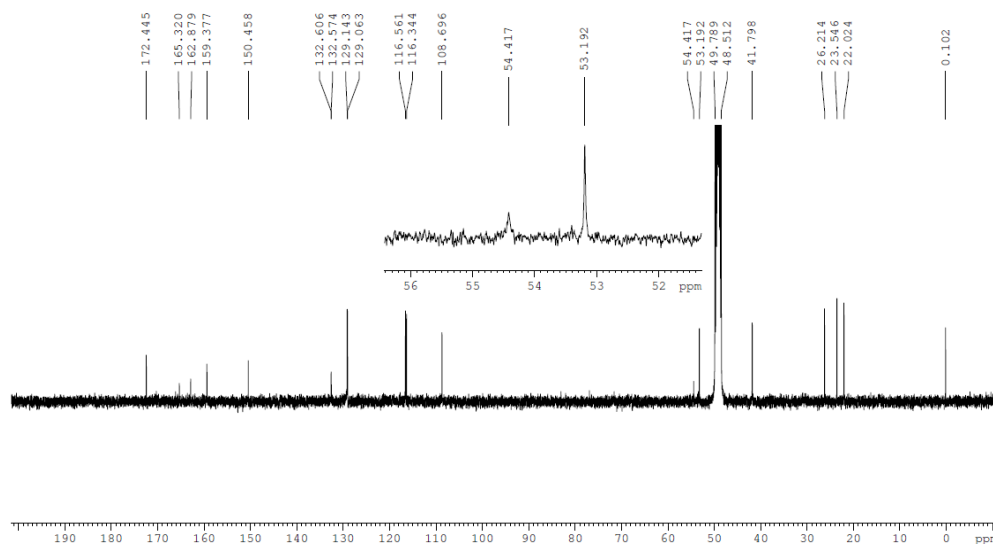
Sample: ST-1-1-131
Solvent: DMSO
04/16/2009



Chemical Formula: $C_{19}H_{20}FN_3O_5S$
Molecular Weight: 421.44260



ST-1-131
MeOD
01/20/2010



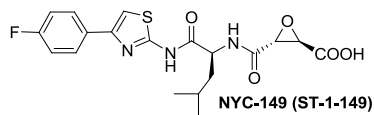
Current Data Parameters
NAME BP-1-162-diazide
EXPNO 140
PROCNO 1

F2 - Acquisition Parameters
Date_ 20100120
Time 8.57
INSTRUM spect
PROBHD 5 mm PABBO BB-
PULPROG zgpg30
TD 65536
SOLVENT MeOD
NS 20480
DS 4
SWH 23980.814 Hz
FIDRES 0.365918 Hz
AQ 1.3664759 sec
RG 1625.5
DW 20.650 usec
DE 6.00 usec
TE 298.3 K
D1 1.00000000 sec
d11 0.03000000 sec
DELTA 0.89999998 sec
MCREST 0.00000000 sec
MCWRK 0.01500000 sec

===== CHANNEL f1 =====
NUC1 13C
P1 9.50 usec
PL1 -2.00 dB
SFO1 100.625169 MHz

===== CHANNEL f2 =====
CPDPRG2 waltz16
NUC2 1H
PCPD2 80.00 usec
PL2 -2.00 dB
PL12 15.23 dB
PL13 14.00 dB
SFO2 400.1716007 MHz

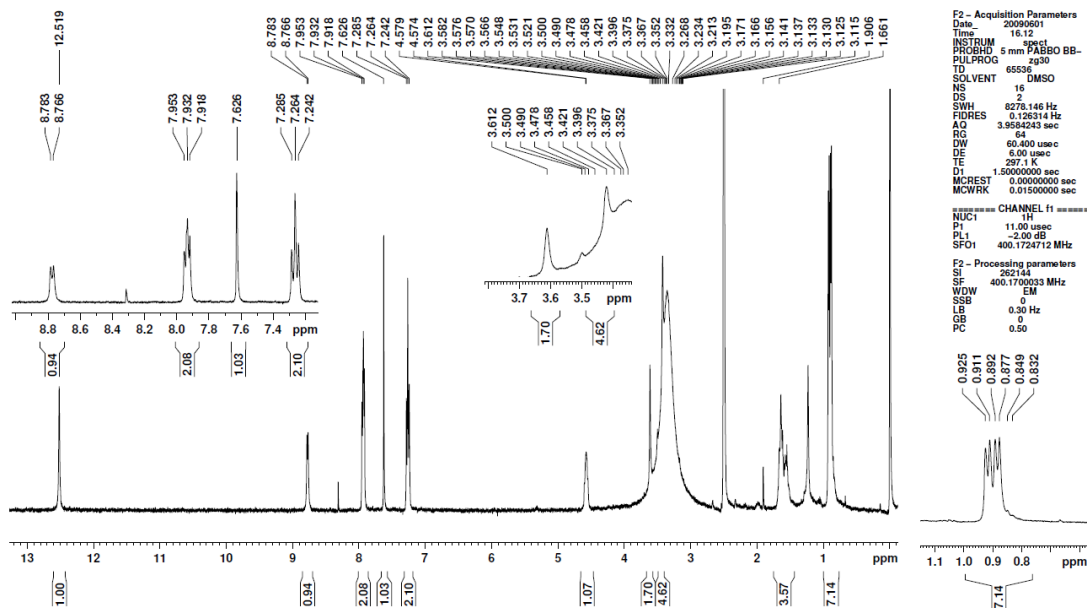
F2 - Processing parameters
SI 262144
SF 100.625169 MHz
WDW EM
SSB 0
LB 1.00 Hz
GB 0
PC 1.40



NYC-149 (ST-1-149)

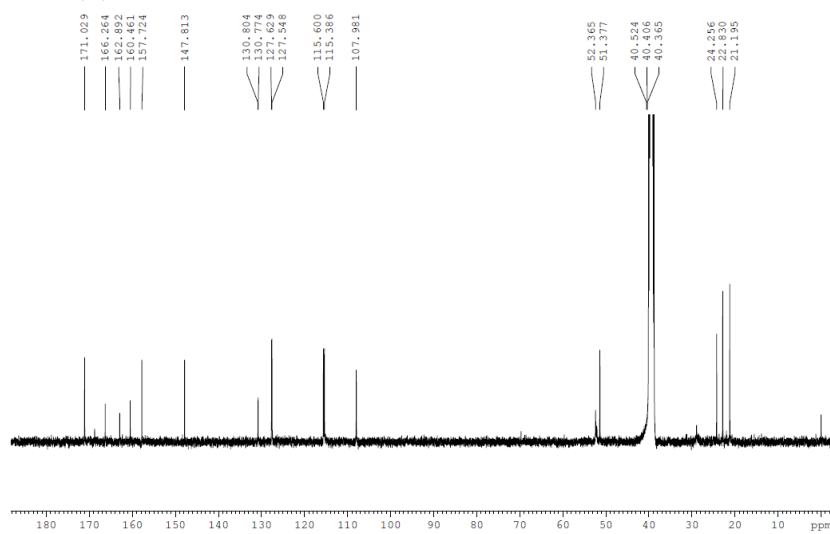
Chemical Formula: $C_{19}H_{20}FN_3O_5S$
Molecular Weight: 421.44260

Sample: ST-1-149
Solvent: DMSO
06/01/2009

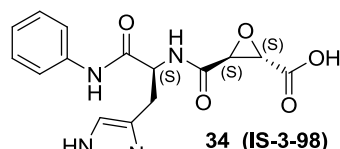


Current Data Parameters
NAME BP-1-162-diazide
EXPNO 103
PROCNO 1
F2 - Acquisition Parameters
Date_ 20090901
Time 16.12
INSTRUM spect
PROBHD 5 mm PABBO BB-
PULPROG zg30
TD 65536
SOLVENT DMSO
NS 16
DS 2
SWH 8276.146 Hz
FIDRES 0.126314 Hz
AQ 3.9584243 sec
RG 64
DW 60.400 usec
DE 6.00 usec
TE 297.1 K
D1 1.50000000 sec
MCREST 0.00000000 sec
MCWRK 0.01500000 sec
===== CHANNEL f1 =====
NUC1 1H
P1 11.00 usec
PL1 -2.00 dB
SFO1 400.1724712 MHz
F2 - Processing parameters
SI 262144
SF 400.1700033 MHz
WDW EM
SSB 0
LB 0.30 Hz
GB 0
PC 0.50

ST-1-149 R,R-epoxy acid
DMSO
01/26/2010



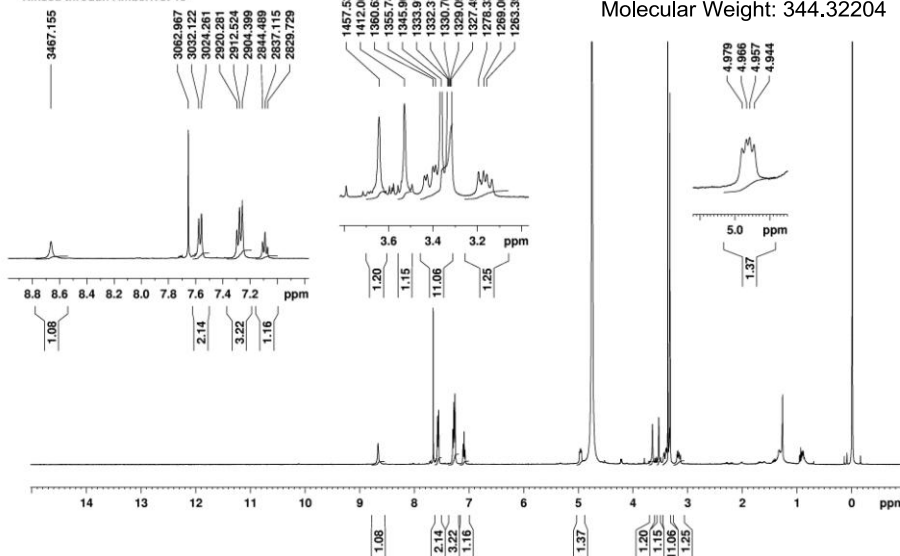
Current Data Parameters
NAME BP-1-162-diazide
EXPNO 142
PROCNO 1
F2 - Acquisition Parameters
Date_ 20100127
Time 6.25
INSTRUM spect
PROBHD 5 mm PABBO BB-
PULPROG zgpg30
TD 65536
SOLVENT DMSO
NS 18432
DS 4
SWH 23980.814 Hz
FIDRES 0.365918 Hz
AQ 1.3664756 sec
RG 1024
DW 20.859 usec
DE 6.00 usec
TE 299.1 K
D1 1.00000000 sec
d11 0.03000000 sec
DELTA 0.89999998 sec
MCREST 0.00000000 sec
MCWRK 0.01500000 sec
===== CHANNEL f1 =====
NUC1 13C
P1 9.50 usec
PL1 -2.00 dB
SFO1 100.6328888 MHz
===== CHANNEL f2 =====
CPDPRG2 waltz16
NUC2 1H
PCPD2 80.00 usec
PL2 -2.00 dB
PL12 15.23 dB
PL13 14.00 dB
SFO2 400.1716007 MHz
F2 - Processing parameters
SI 262144
SF 100.6228840 MHz
WDW EM
SSB 0
LB 1.00 Hz
GB 0
PC 0.50



34 (IS-3-98)

Chemical Formula: $C_{16}H_{16}N_4O_5$
Molecular Weight: 344.32204

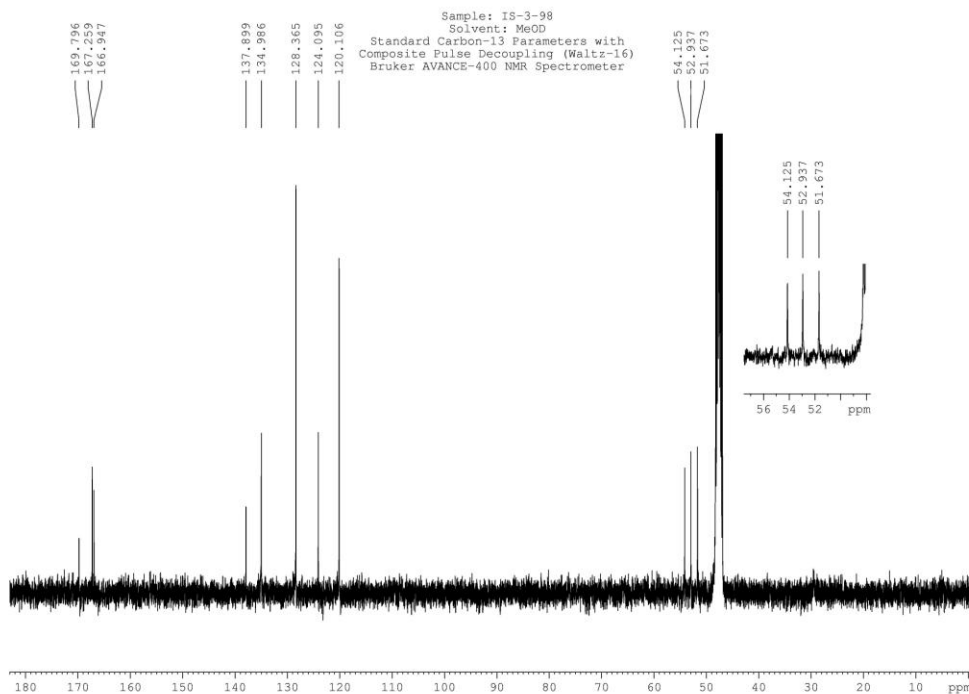
Sample: IS-3-98
Solvent: MeOD/ $CDCl_3$
Standard Survey 1-D Proton NMR Spectrum
Bruker AVANCE-400 NMR Spectrometer
Rinsed through Amberlyst 15



Current Data Parameters
NAME IS-3-98
EXPNO 1
PROCNO 1
F2 - Acquisition Parameters
Date_ 20090908
Time 11.20
INSTRUM spect
PROBHD 5 mm PABBO BB-
PULPROG zgpg30
TD 65536
SOLVENT H₂O-D₂O
NS 105
DS 2
SWH 8278.146 Hz
FIDRES 0.130314 Hz
AQ 3.9504263 sec
RG 64
DW 60.400 usec
DE 6.50 usec
TE 297.4 K
D1 1.5000000 sec
MCREST 0.0000000 sec
MCWRK 0.0150000 sec

===== CHANNEL f1 =====
NUC1 1H
P1 12.75 usec
PL1 -2.00 dB
SFO1 400.1264712 MHz
F2 - Processing parameters
SI 262144
SF 400.1700000 MHz
WDW EM
SSB 0
LB 0.30 Hz
GB 0
PC 1.00
TD NMR plot parameters
CX 20.00 cm
CY 30.00 cm
F1P 16.518 ppm
F1 6610.29 Hz
F2P -4.116 ppm
F2 -1667.86 Hz
PPMCM 0.73881 ppm/cm
HZCM 295.64807 Hz/cm

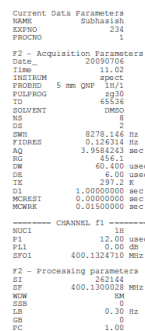
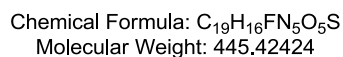
Sample: IS-3-98
Solvent: MeOD
Standard Carbon-13 Parameters with
Composite Pulse Decoupling (Waltz-16)
Bruker AVANCE-400 NMR Spectrometer



Current Data Parameters
NAME IS-3-98
EXPNO 2
PROCNO 1
F2 - Acquisition Parameters
Date_ 20090907
Time 12.43
INSTRUM spect
PROBHD 5 mm PABBO BB-
PULPROG zgpg30
TD 65536
SOLVENT $CDCl_3$
NS 10000
DS 4
SWH 23980.814 Hz
FIDRES 0.365918 Hz
AQ 1.3684756 sec
RG 3649.1
DW 20.850 usec
DE 6.50 usec
TE 297.3 K
D1 1.0000000 sec
d11 0.0300000 sec
DELTA 0.8999998 sec
MCREST 0.0000000 sec
MCWRK 0.0150000 sec

===== CHANNEL f1 =====
NUC1 13C
P1 9.50 usec
PL1 -2.00 dB
SFO1 100.6264688 MHz
===== CHANNEL f2 =====
CPDPRG2 waltz16
NUC2 1H
PCPD2 80.00 usec
PL2 -2.00 dB
PL12 15.23 dB
PL13 14.00 dB
SFO2 400.1716007 MHz

F2 - Processing parameters
SI 262144
SF 100.6262829 MHz
WDW EM
SSB 0
LB 1.00 Hz
GB 0
PC 1.40



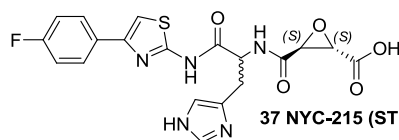
Current Data Parameters
 NAME RD-1-15j-diazide
 EXPNO 149
 PROCNO 1

F2 - Acquisition Parameters
 Date_ 20100216
 Time 9.55
 INSTRUM spect
 PROBHD 5 mm PABBO BB
 PULPROG zgpg30
 TO 65536
 SOLVENT DMSO
 NS 18432
 DS 4
 SWH 23980.814 Hz
 FIDRES 0.365918 Hz
 AQ 1.3664756 sec
 RG 1024
 OW 20.000 usec
 DE 6.00 usec
 TE 298.5 K
 D1 1.00000000 sec
 d11 0.00000000 sec
 DELTA 0.00000000 sec
 MCREST 0.00000000 sec
 MCWPRG 0.01000000 sec

===== CHANNEL f1 =====
 NUC1 ¹³C
 P1 9.50 usec
 PL1 -2.00 dB
 SFO1 100.622888 MHz

===== CHANNEL f2 =====
 CPDPRG2 waltz16
 NUC2 ¹H
 PCPD2 80.00 usec
 PL2 -2.00 dB
 PL12 15.23 dB
 PL13 14.00 dB
 SFO2 400.1716007 MHz

F2 - Processing parameters
 SI 282144
 SF 100.6228839 MHz
 WDW EM
 SSB 0
 LB 1.00 Hz
 GB 0
 PC 1.40



37 NYC-215 (ST-2-15)

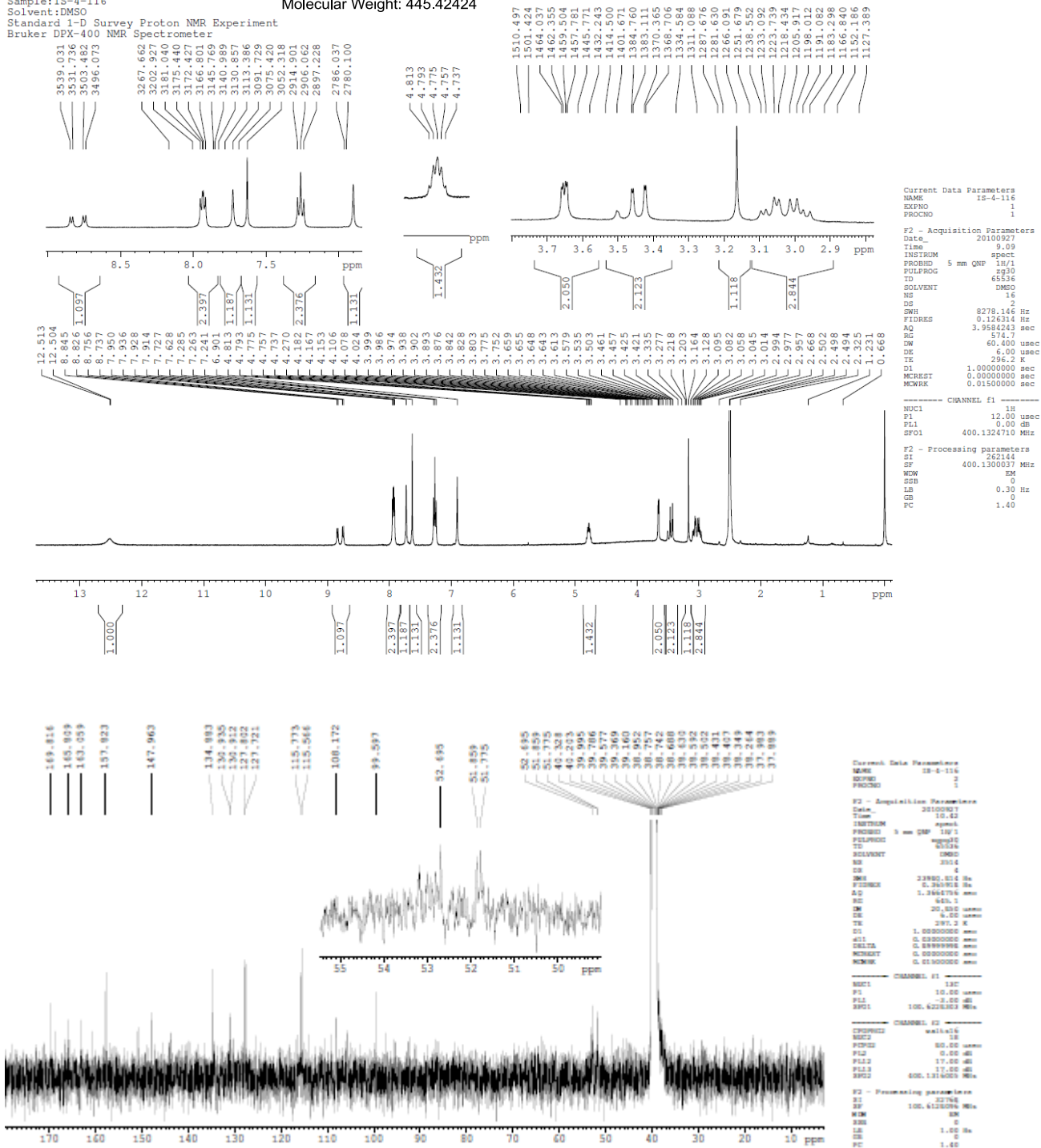
Chemical Formula: $C_{19}H_{16}FN_5O_5S$
Molecular Weight: 445.42424

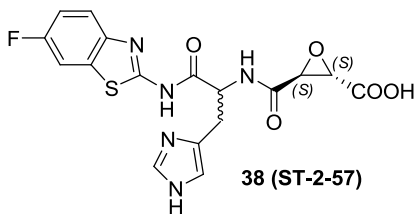
Sample: IS-4-116

Solvent: DMSO

Standard 1-D Survey Proton NMR Experiment

Bruker DPX-400 NMR Spectrometer

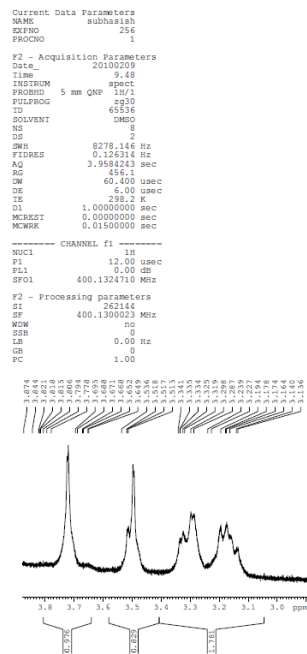
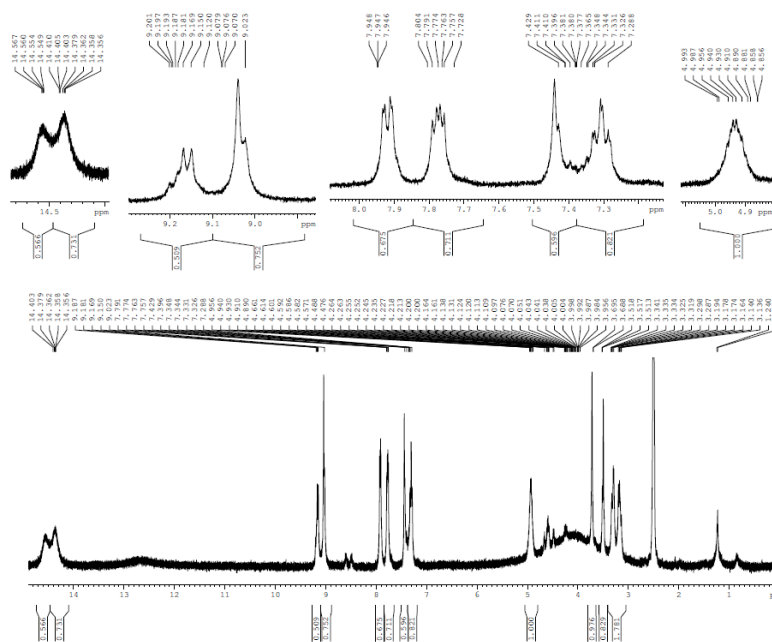




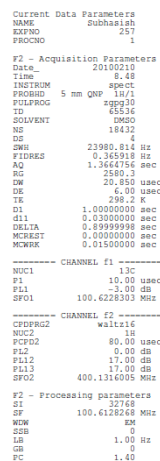
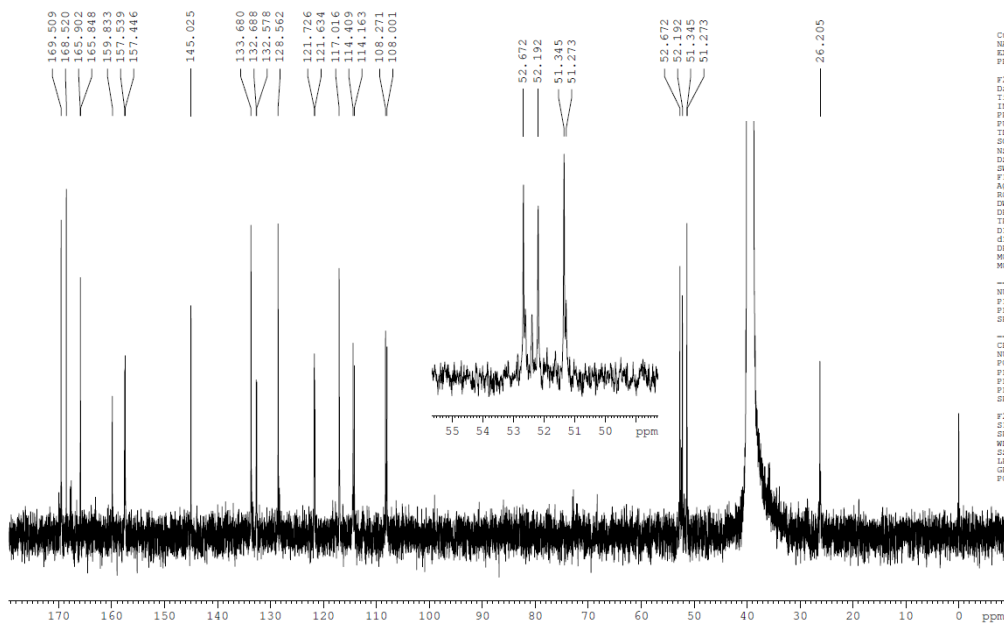
38 (ST-2-57)

Chemical Formula: $C_{17}H_{14}FN_5O_5S$
Molecular Weight: 419.38696

Sample: ST-2-59
Solvent: DMSO
02/09/2010

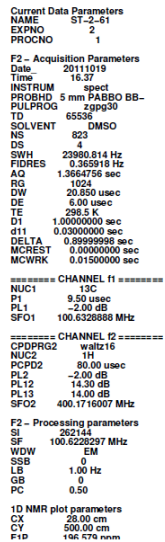
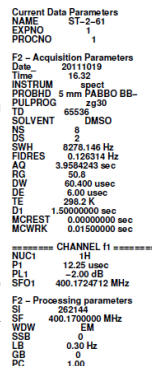


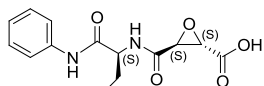
Sample: ST-2-57
Solvent: DMSO-d6
02/10/2010





Molecular Weight: 419.38696

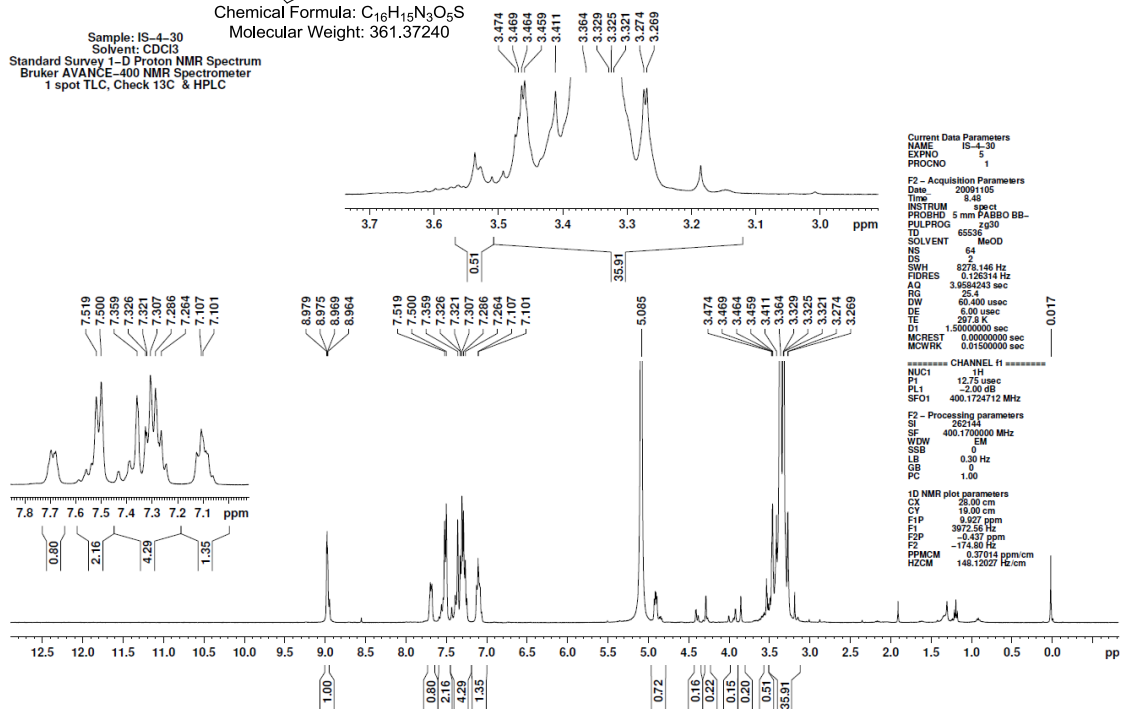




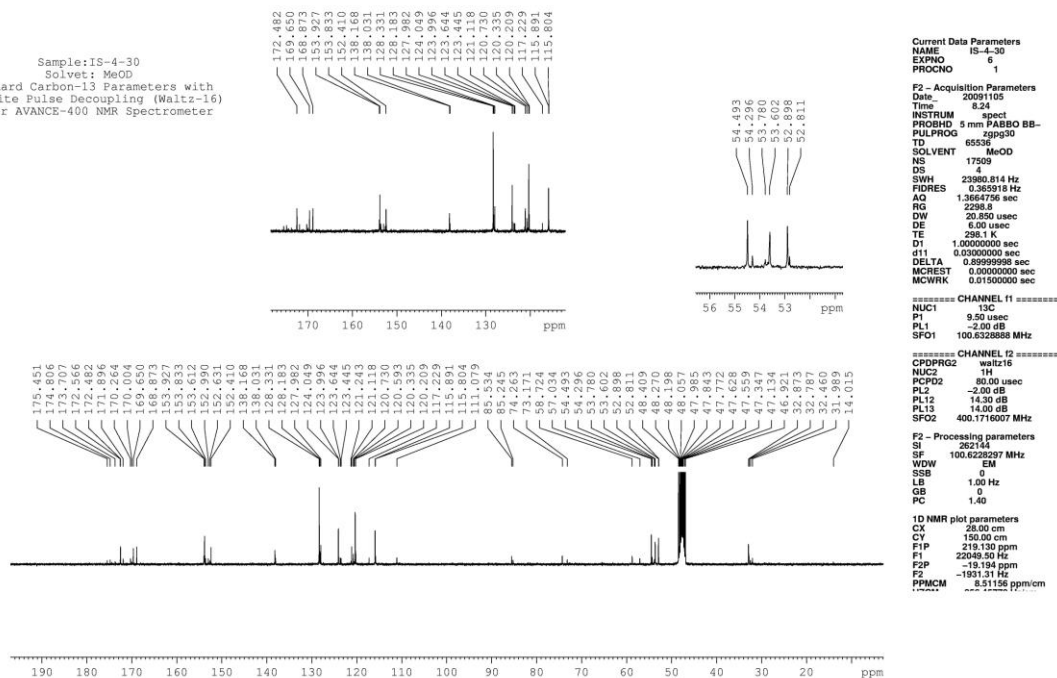
40 (IS-4-30)

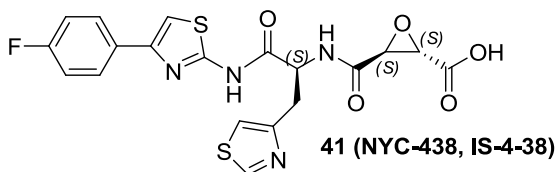
Chemical Formula: $C_{16}H_{15}N_3O_5S$
Molecular Weight: 361.37240

Sample: IS-4-30
Solvent: $CDCl_3$
Standard Survey 1-D Proton NMR Spectrum
Bruker AVANCE-400 NMR Spectrometer
1 spot TLC, Check ^{13}C & HPLC



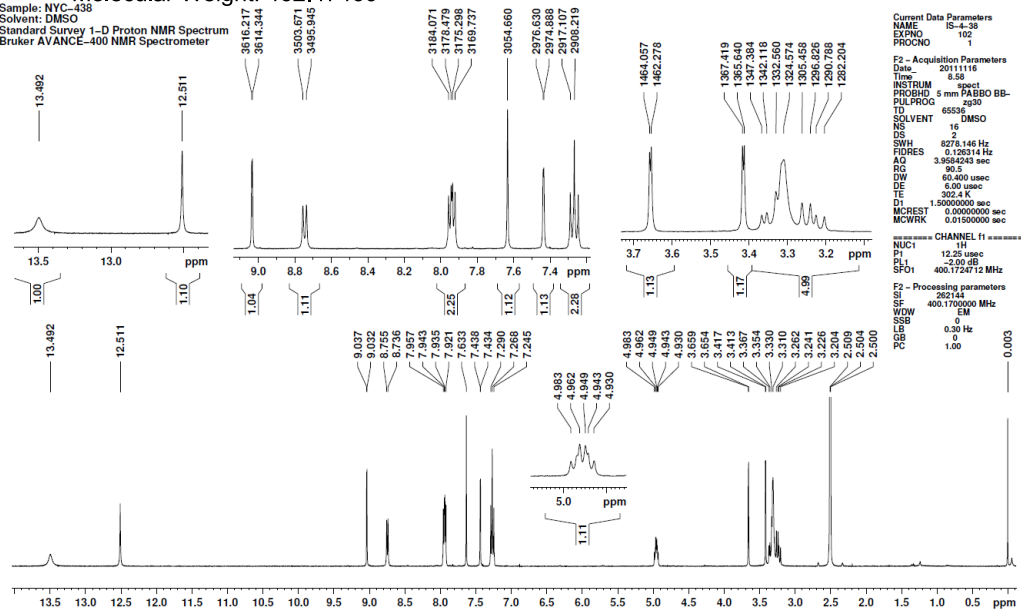
Sample: IS-4-30
Solvent: MeOD
Standard Carbon-13 Parameters with
Composite Pulse Decoupling (Waltz-16)
Bruker AVANCE-400 NMR Spectrometer



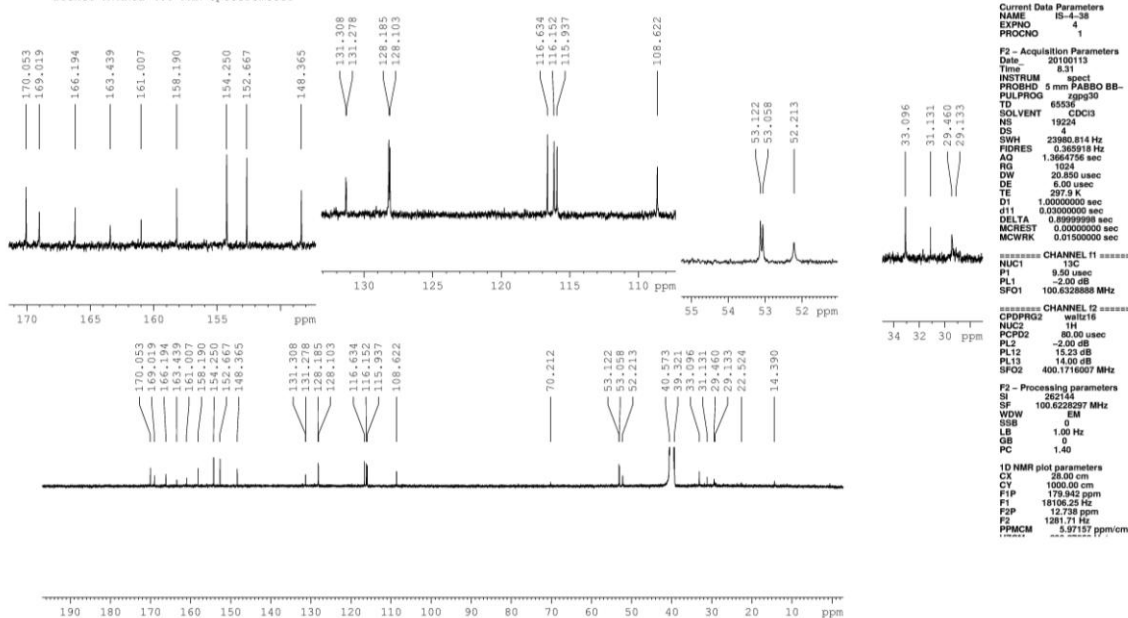


Chemical Formula: $C_{19}H_{15}FN_4O_5S_2$
Molecular Weight: 462.47460

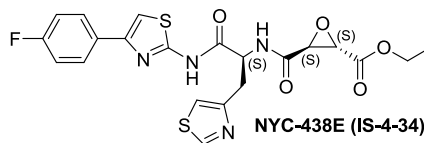
Sample: NYC-438
Solvent: DMSO
Standard Survey 1-D Proton NMR Spectrum
Bruker AVANCE-400 NMR Spectrometer



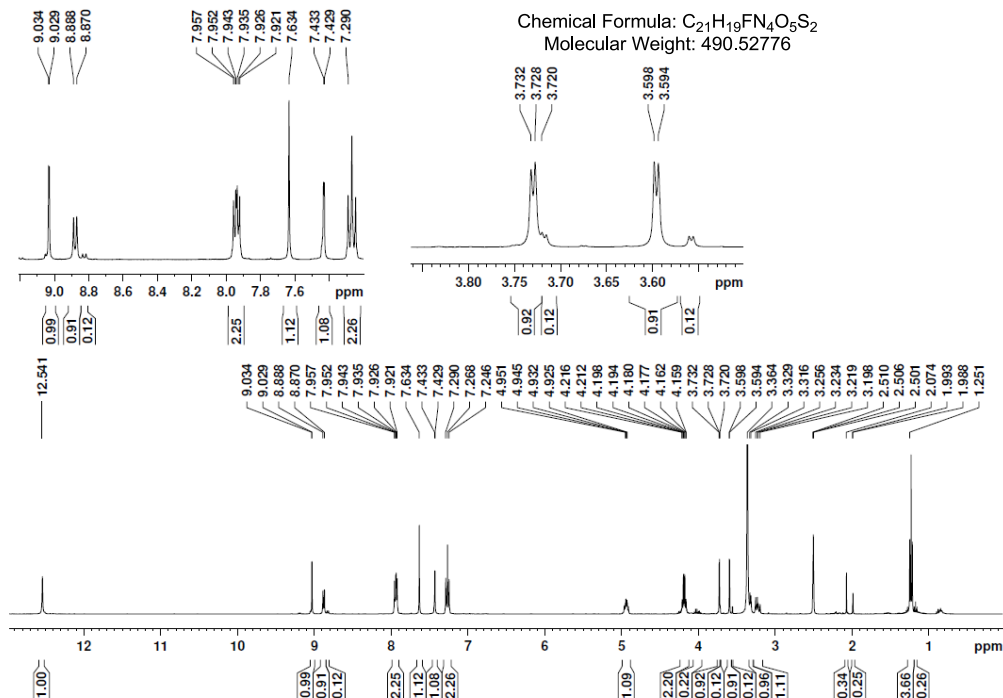
Sample: IS-4-38
Solvent: DMSO
Standard Carbon-13 Parameters with
Composite Pulse Decoupling (Waltz-16)
Bruker AVANCE-400 NMR Spectrometer



Sample: NYC-438E 072911 to Columbia Pending HPI
Solvent: DMSO
Standard Survey 1-D Proton NMR Spectrum
Bruker AVANCE-400 NMR Spectrometer

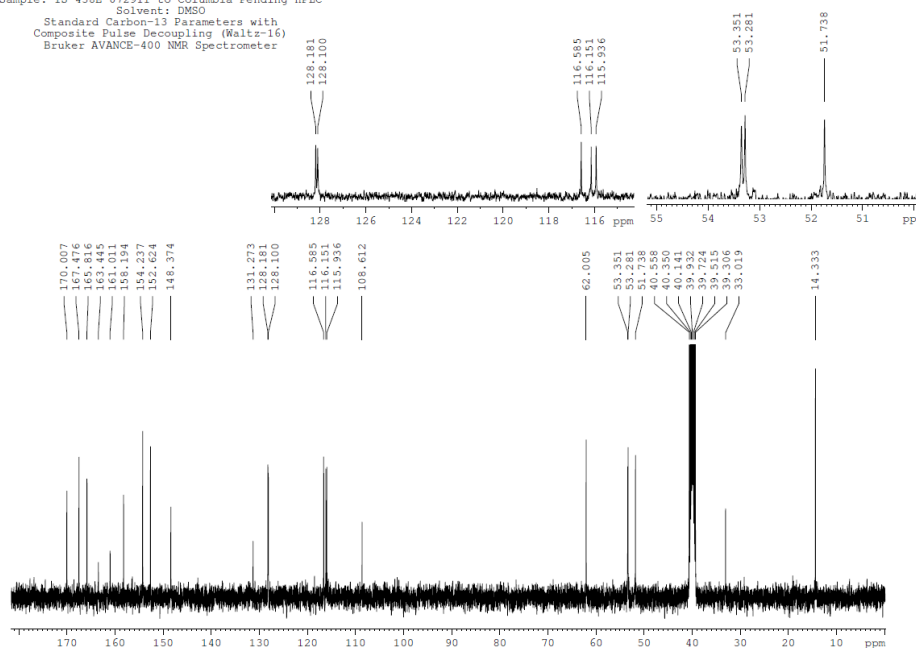


Chemical Formula: C₂₁H₁₉FN₄O₅S₂
Molecular Weight: 490.52776

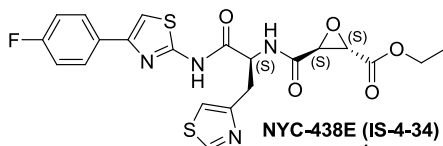


Current Data Parameters
NAME IS-4-38E 072911
EXPNO 1
PROCNO 1
F2 - Acquisition Parameters
Date_ 20110729
Time 6.46
INSTRUM spect
PROBHD 5 mm PABBO BB-
PULPROG zg30
TD 65536
SOLVENT DMSO
NS 16
DS 2
SWH 8278.146 Hz
FIDRES 0.125314 Hz
AQ 3.9584243 sec
RG 22.6
DW 60.400 usec
DE 6.00 usec
TE 297.4 K
D1 1.50000000 sec
MCREST 0.00000000 sec
MCWRK 0.01500000 sec
===== CHANNEL f1 =====
NUC1 1H
P1 12.25 usec
PL1 -2.00 dB
SFO1 400.1724712 MHz
F2 - Processing parameters
SI 262144
SF 400.1700000 MHz
WDW EM
SSB 0
LB 0.30 Hz
GB 0
PC 1.00
1D NMR plot parameters
CX 28.00 cm
CY 19.00 cm
F1P 13.466 ppm
F1 5401.45 Hz
F2P 0.134 ppm
F2 53.53 Hz
FPMCM 0.47729 ppm/cm
HZCM 190.6663 Hz/cm

Sample: IS-438E 072911 to Columbia Pending HPLC
Solvent: DMSO
Standard Carbon-13 Parameters with
Composite Pulse Decoupling (Waltz-16)
Bruker AVANCE-400 NMR Spectrometer

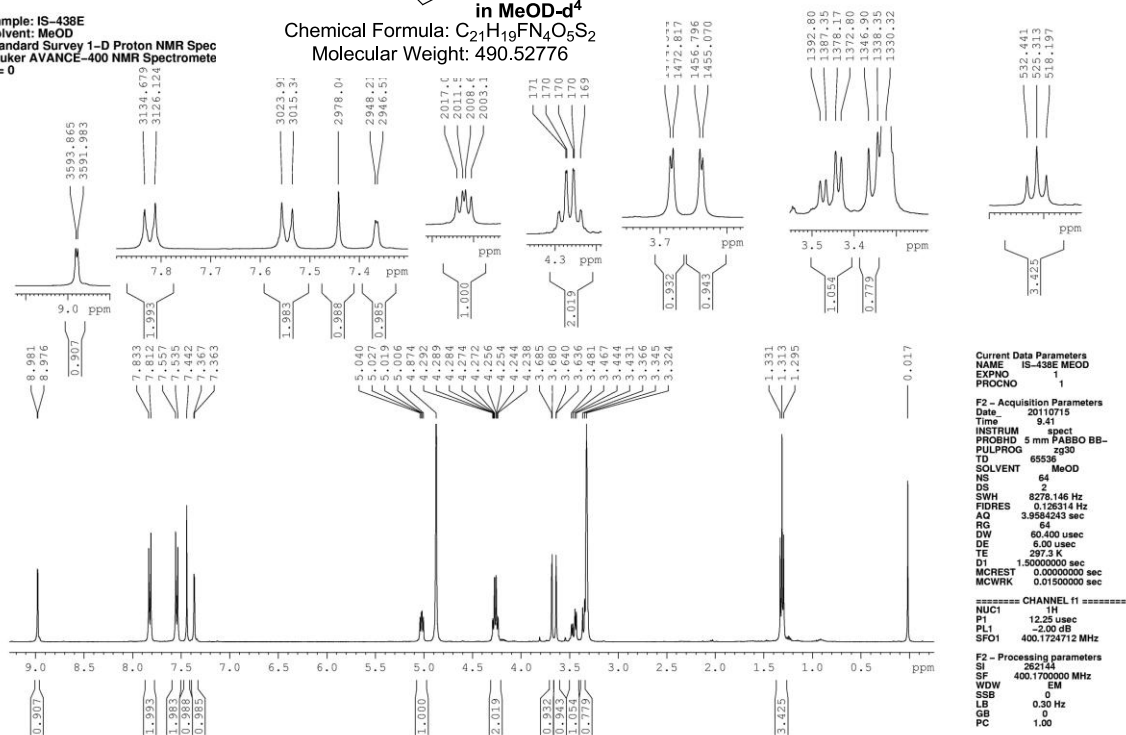


Current Data Parameters
NAME IS-4-38E 072911
EXPNO 2
PROCNO 1
F2 - Acquisition Parameters
Date_ 20110729
Time 6.53
INSTRUM spect
PROBHD 5 mm PABBO BB-
PULPROG zg30
TD 65536
SOLVENT DMSO
NS 522
DS 4
SWH 23980.814 Hz
FIDRES 0.365918 Hz
AQ 1.3664756 sec
RG 1024
DW 20.850 usec
DE 6.00 usec
TE 297.4 K
D1 1.00000000 sec
d11 0.03000000 sec
DELTA 0.89999998 sec
MCREST 0.00000000 sec
MCWRK 0.01500000 sec
===== CHANNEL f1 =====
NUC1 13C
P1 6.50 usec
PL1 -2.00 dB
SFO1 100.626088 MHz
===== CHANNEL f2 =====
CPDPRG2 waltz16
NUC2 1H
PCPD2 80.00 usec
PL2 -2.00 dB
PL12 14.30 dB
PL13 14.30 dB
SFO2 400.1716007 MHz
F2 - Processing parameters
SI 262144
SF 100.626088 MHz
WDW EM
SSB 0
LB 1.00 Hz
GB 0
PC 1.40
1D NMR plot parameters
CX 28.00 cm
CY 19.00 cm
F1P 181.895 ppm

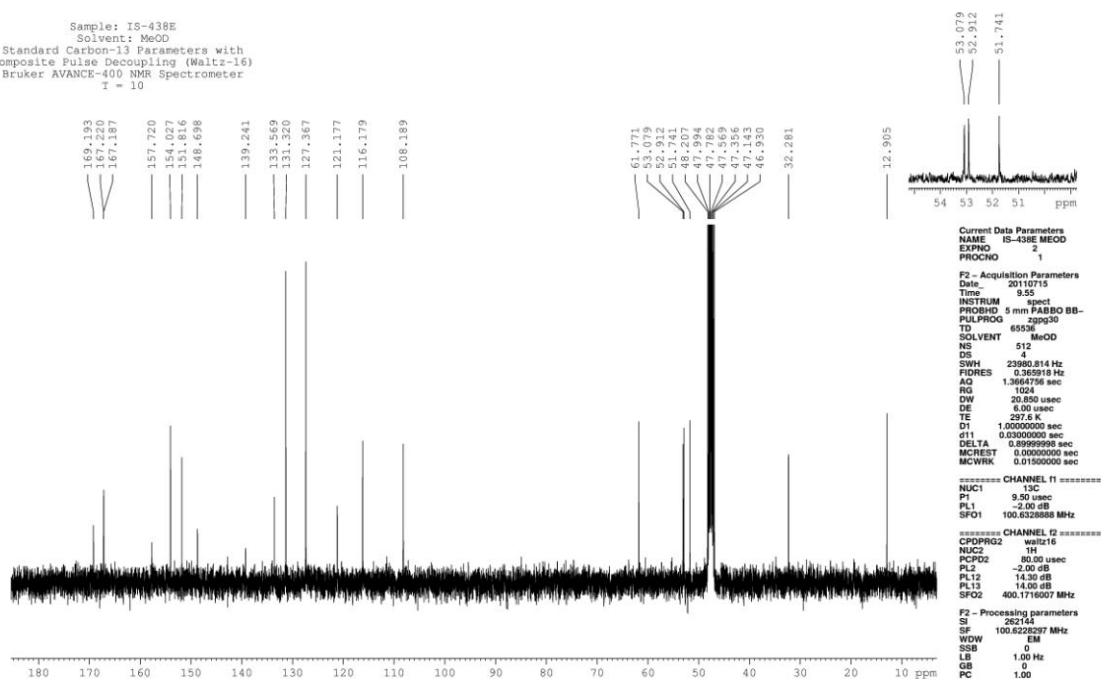


NYC-438E (IS-4-34)
in MeOD- d_4
Chemical Formula: $C_{21}H_{19}FN_4O_5S_2$
Molecular Weight: 490.52776

Sample: IS-438E
Solvent: MeOD
Standard Survey 1-D Proton NMR Spec
Bruker AVANCE-400 NMR Spectrometer
T = 0

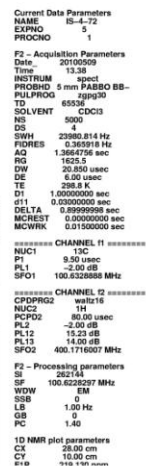
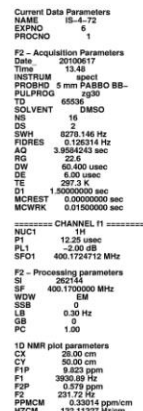


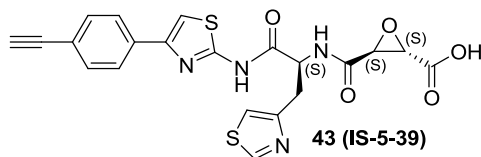
Sample: IS-438E
Solvent: MeOD
Standard Carbon-13 Parameters with
Composite Pulse Decoupling (Waltz-16)
Bruker AVANCE-400 NMR Spectrometer
T = 10





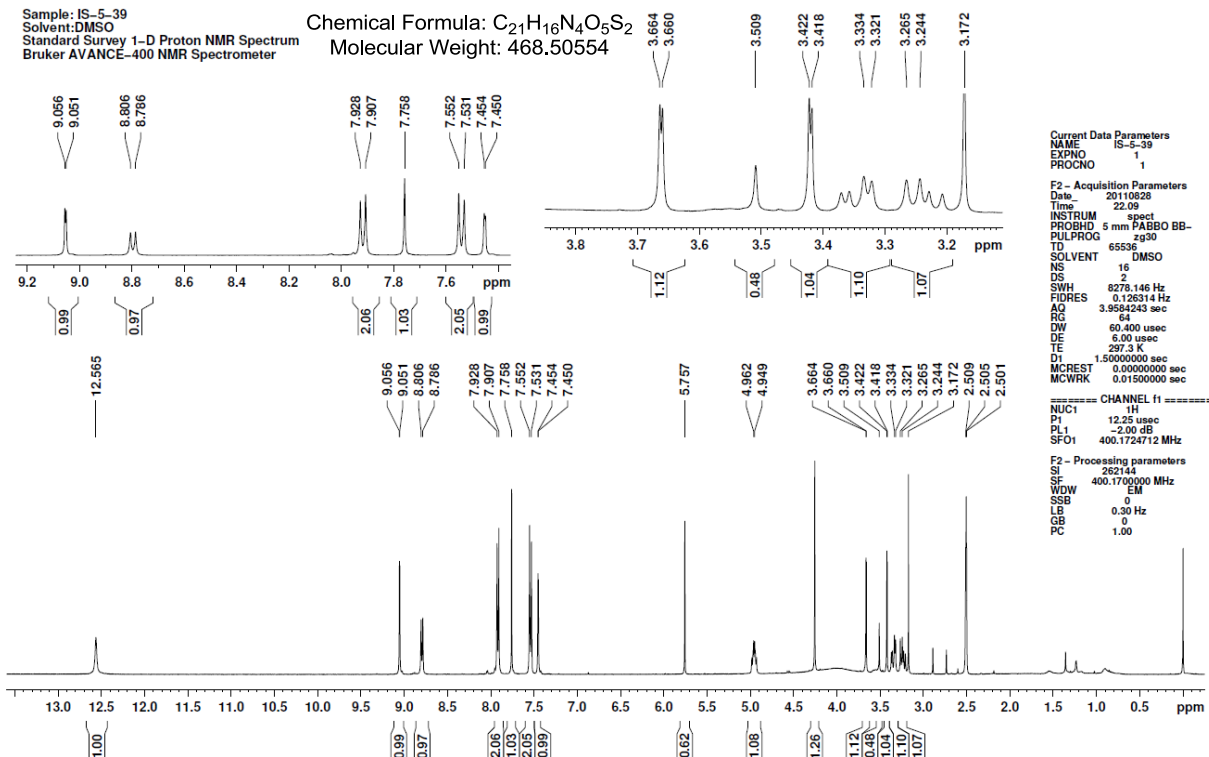
Molecular Weight: 351.37758





Sample: IS-5-39
Solvent: DMSO
Standard Survey 1-D Proton NMR Spectrum
Bruker AVANCE-400 NMR Spectrometer

Chemical Formula: $C_{21}H_{16}N_4O_5S_2$
Molecular Weight: 468.50554



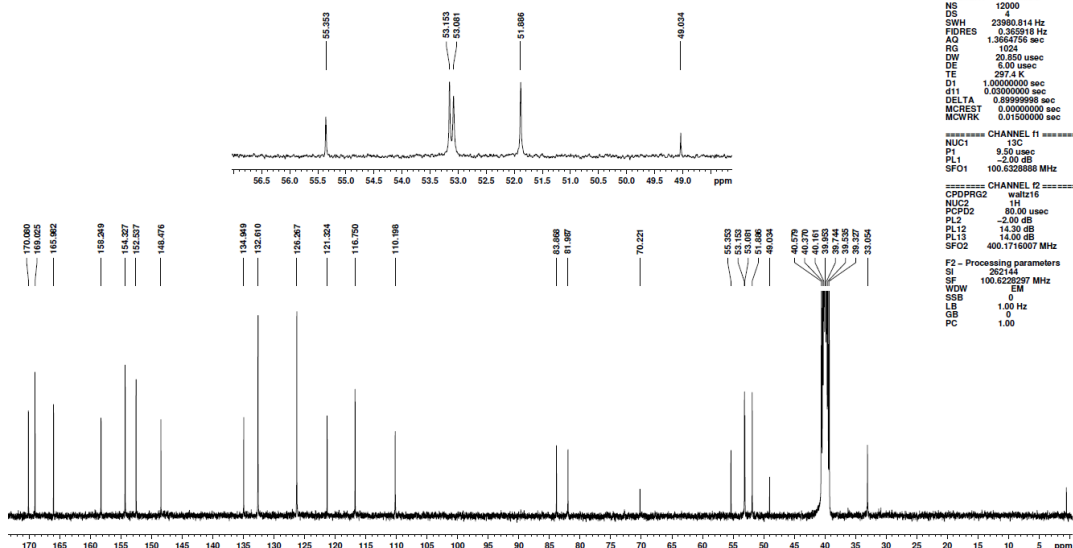
Current Data Parameters
NAME IS-5-39
EXPNO 1
PROCNO 1

F2 - Acquisition Parameters
Date_ 20110828
Time 22.08
INSTRUM spect
PROBHD 5 mm PABBO BB-
PULPROG zg30
TD 65536
SOLVENT DMSO
DS 16
NS 2
SWH 8278.146 Hz
FIDRES 0.126314 Hz
AQ 3.9584243 sec
RG 64
DW 60.400 usec
DE 6.90 usec
TE 297.3 K
D1 1.50000000 sec
MCREST 0.00000000 sec
MCWRK 0.01500000 sec

===== CHANNEL f1 =====
NUC1 1H
P1 12.25 usec
PL1 -2.00 dB
SFO1 400.1724712 MHz

F2 - Processing parameters
SI 262144
SF 400.1700000 MHz
WDW EM
SSB 0
LB 0.30 Hz
GB 0
PC 1.00

Sample: IS-5-39
Solvent: DMSO
Standard Carbon-13 Parameters with
Composite Pulse Decoupling (Waltz-16)
Bruker AVANCE-400 NMR Spectrometer



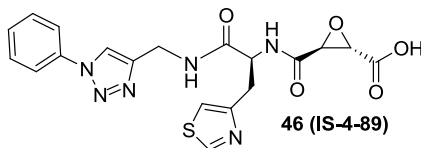
Current Data Parameters
NAME IS-5-39
EXPNO 2
PROCNO 1

F2 - Acquisition Parameters
Date_ 20110828
Time 22.46
INSTRUM spect
PROBHD 5 mm PABBO BB-
PULPROG zgpg30
TD 65536
SOLVENT DMSO
DS 4
NS 12000
SWH 23980.814 Hz
FIDRES 0.365918 Hz
AQ 1.3624756 sec
RG 1024
DW 20.650 usec
DE 6.90 usec
TE 297.4 K
D1 1.00000000 sec
d11 0.00000000 sec
DELTA 0.89999998 sec
MCREST 0.00000000 sec
MCWRK 0.01500000 sec

===== CHANNEL f1 =====
NUC1 13C
P1 9.50 usec
PL1 -2.00 dB
SFO1 100.6289888 MHz

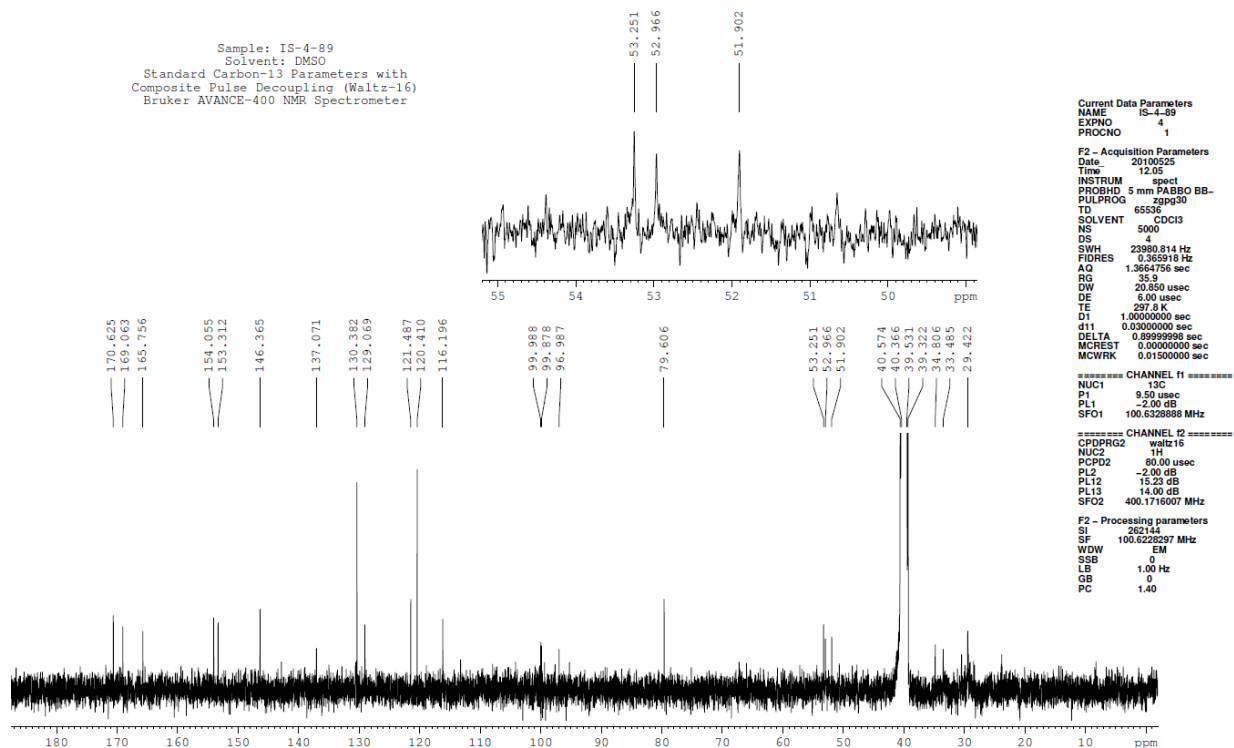
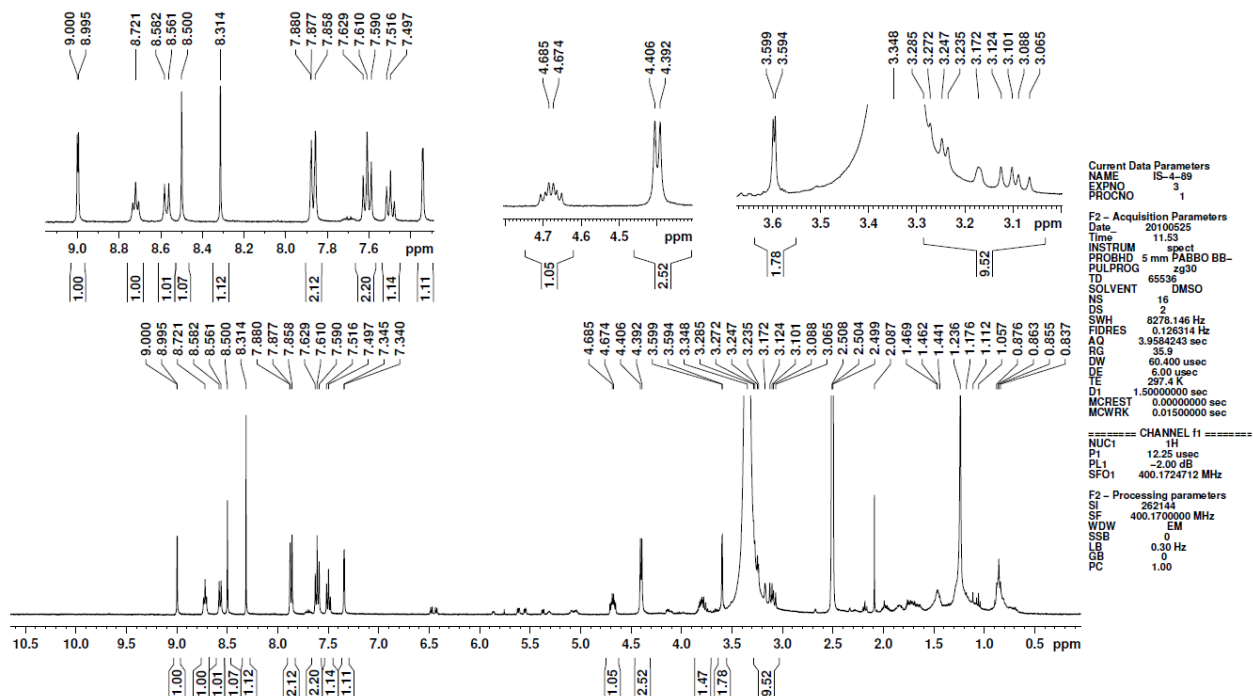
===== CHANNEL f2 =====
CPDPRG2 waltz16
NUC2 1H
PCPDZ 20.00 usec
PL2 -2.00 dB
PL12 14.30 dB
PL13 14.00 dB
SFO2 400.1716007 MHz

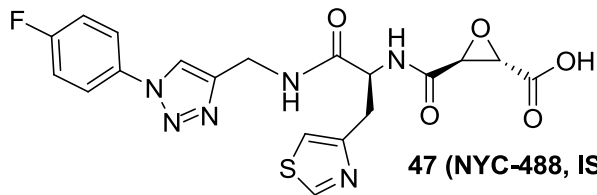
F2 - Processing parameters
SI 262144
SF 100.6289888 MHz
WDW EM
SSB 0
LB 1.80 Hz
GB 0
PC 1.00



Sample: IS-4-89
Solvent: DMSO
Standard Survey 1-D Proton NMR Spectrum
Bruker AVANCE-400 NMR Spectrometer

Chemical Formula: $C_{19}H_{18}N_6O_5S$
Molecular Weight: 442.44842

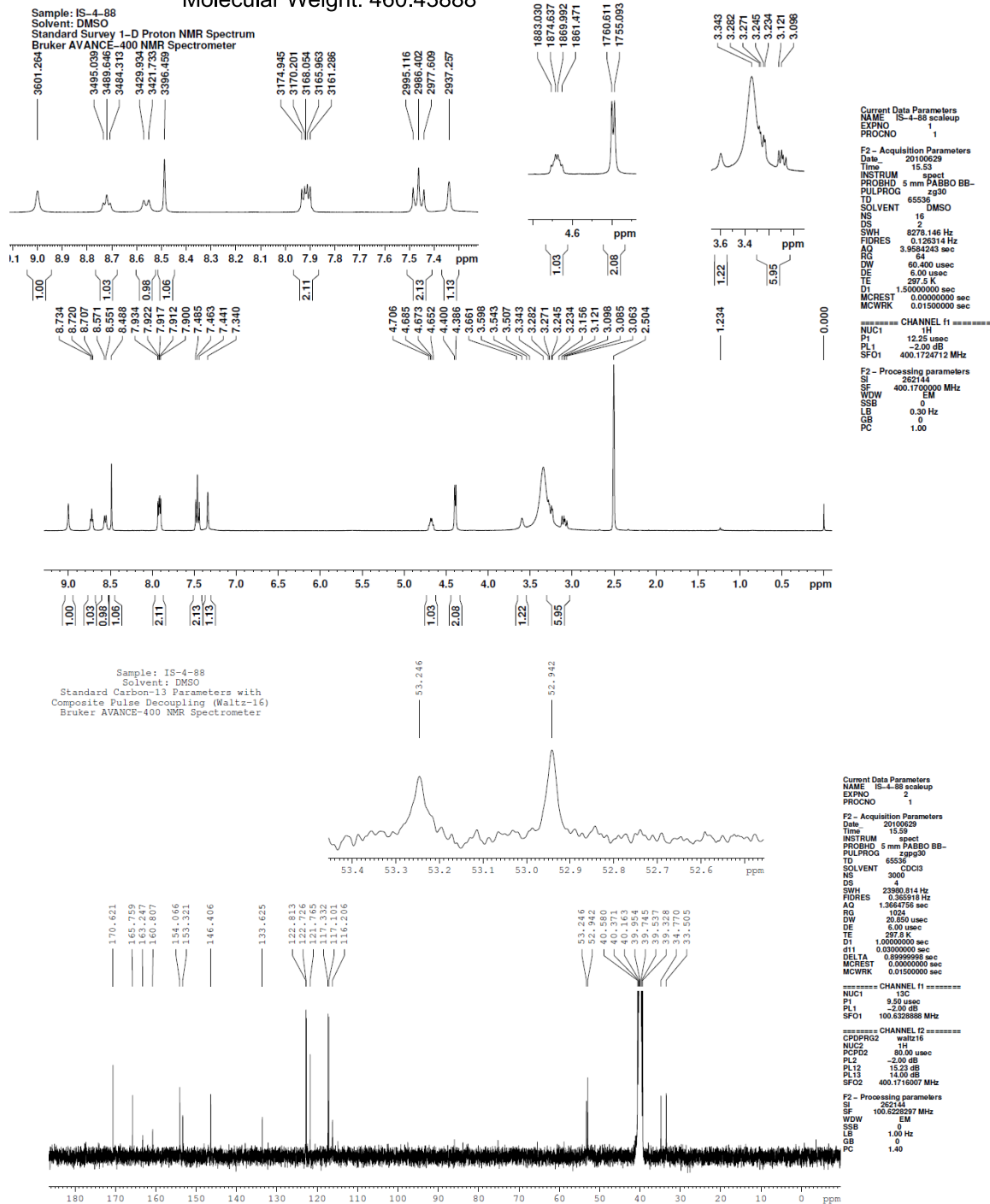


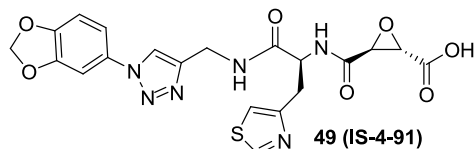


47 (NYC-488, IS-4-88)

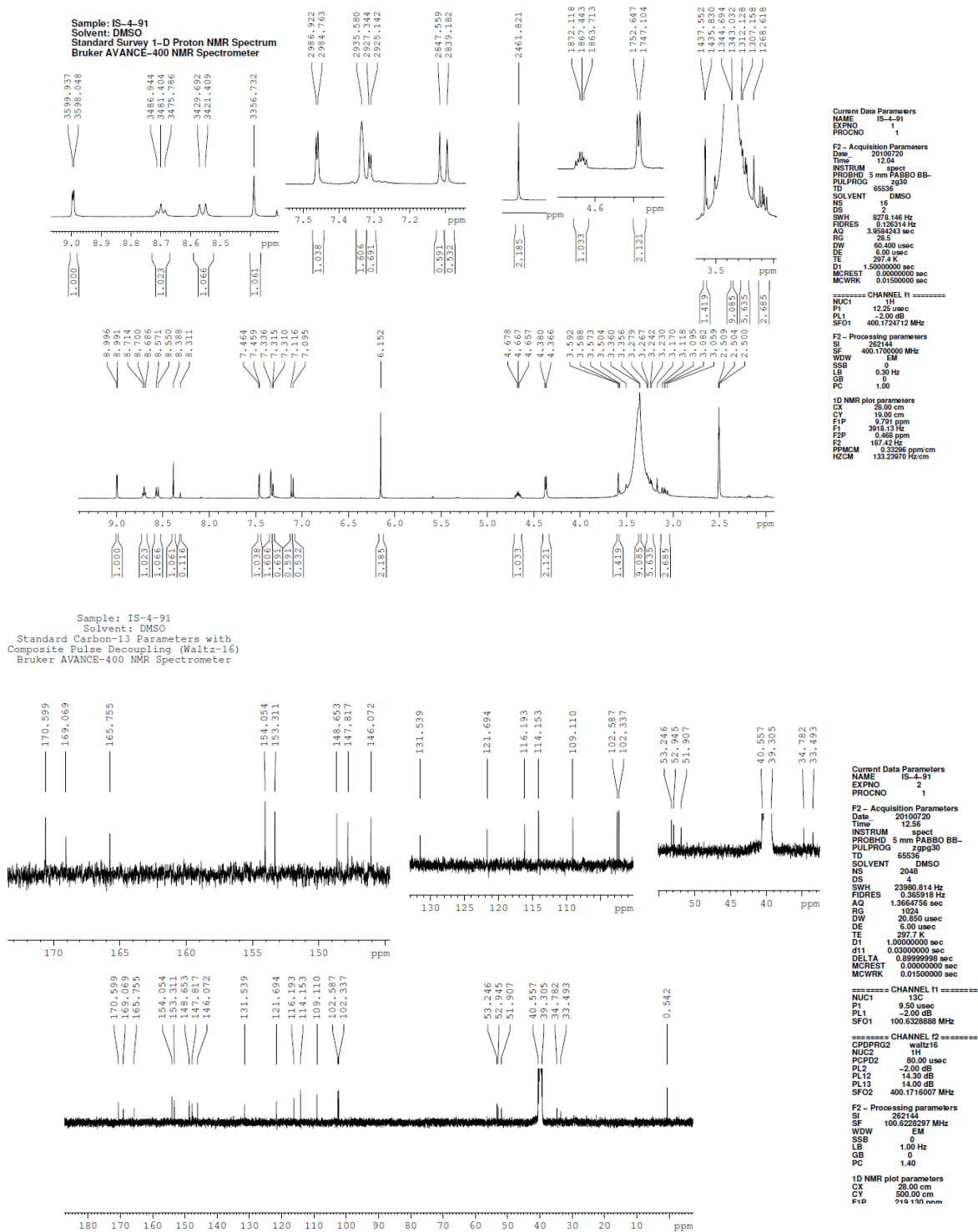
Chemical Formula: $C_{19}H_{17}FN_6O_5S$

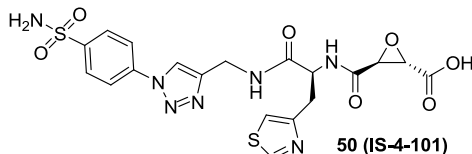
Molecular Weight: 460.43888





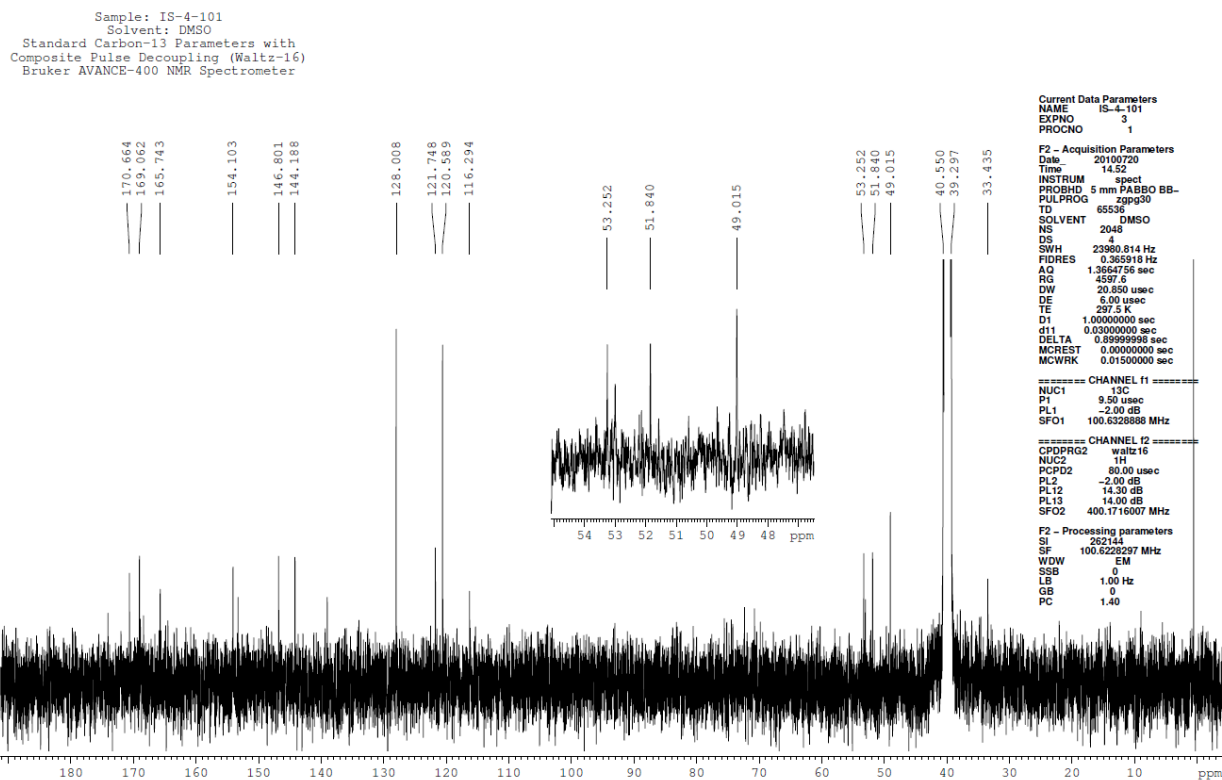
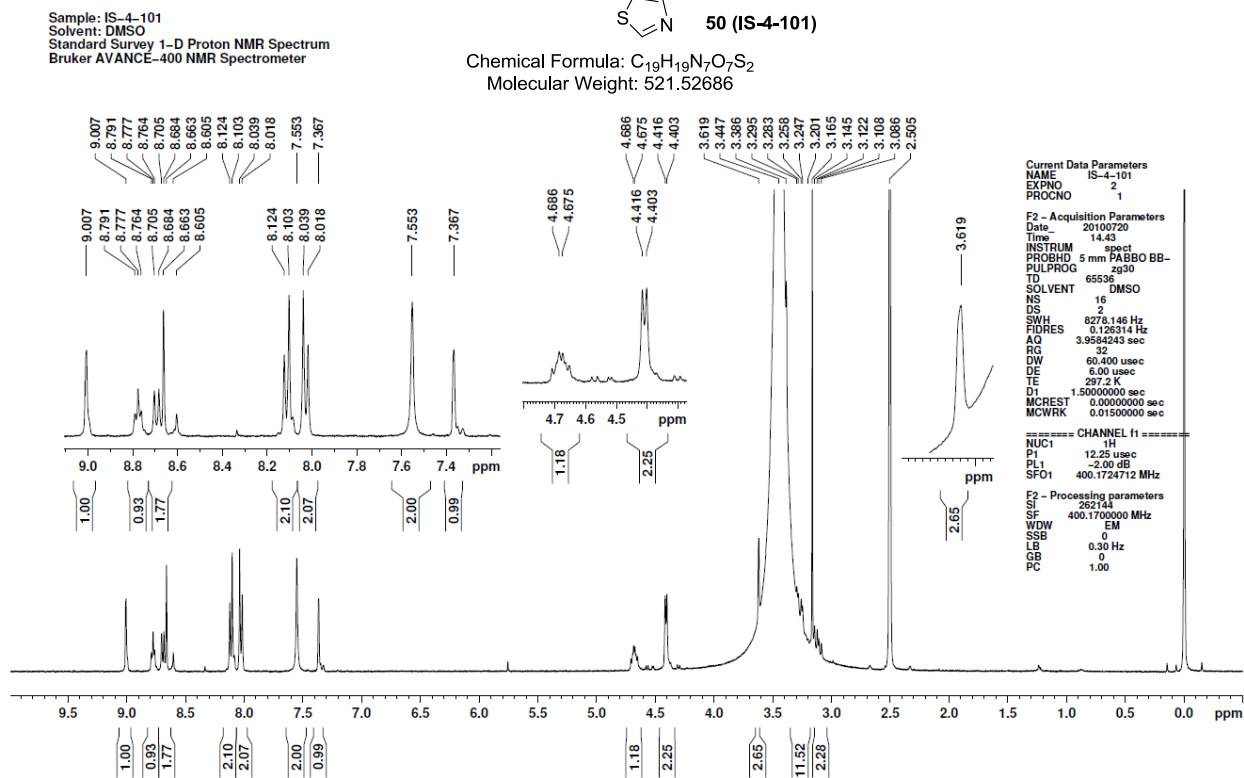
Chemical Formula: C₂₀H₁₈N₆O₇S
Molecular Weight: 486.45792

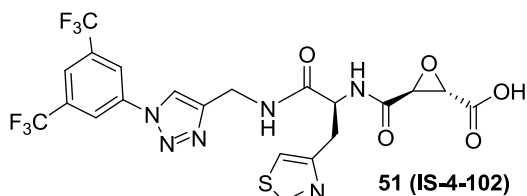




50 (IS-4-101)

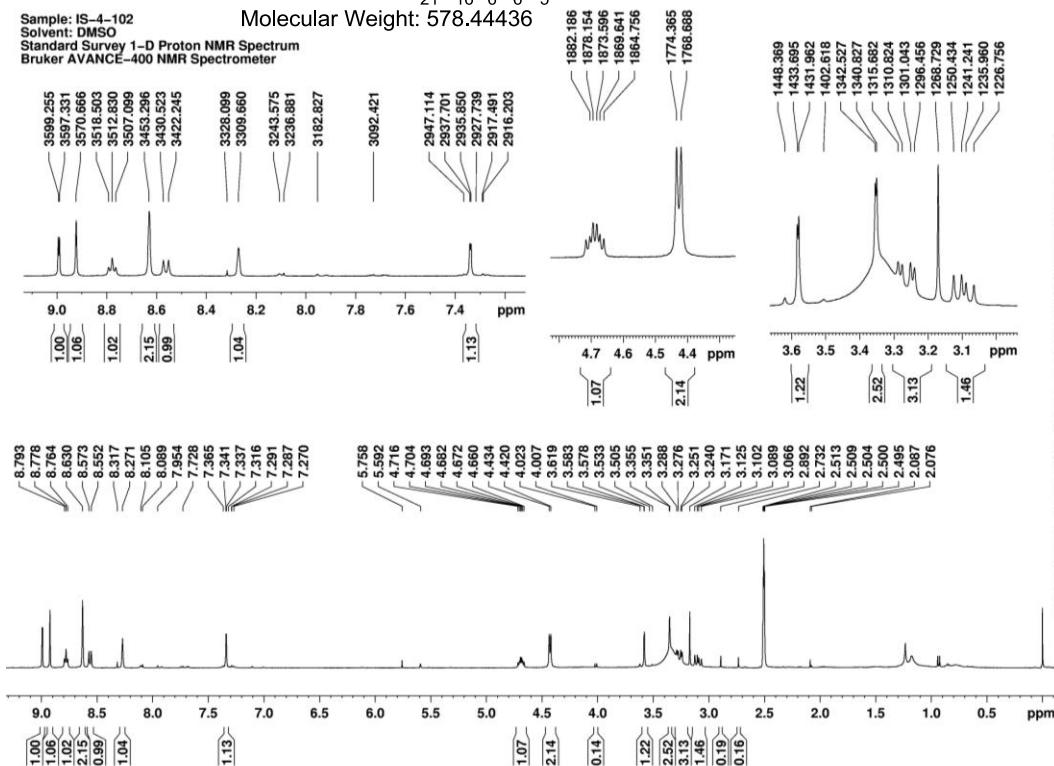
Chemical Formula: C₁₉H₁₉N₇O₇S₂
Molecular Weight: 521.52686





Chemical Formula: C₂₁H₁₆F₆N₆O₅S
Molecular Weight: 578.44436

Sample: IS-4-102
Solvent: DMSO
Standard Survey 1-D Proton NMR Spectrum
Bruker AVANCE-400 NMR Spectrometer



Current Data Parameters
NAME IS-4-102
EXPNO 3
PROCNO 1

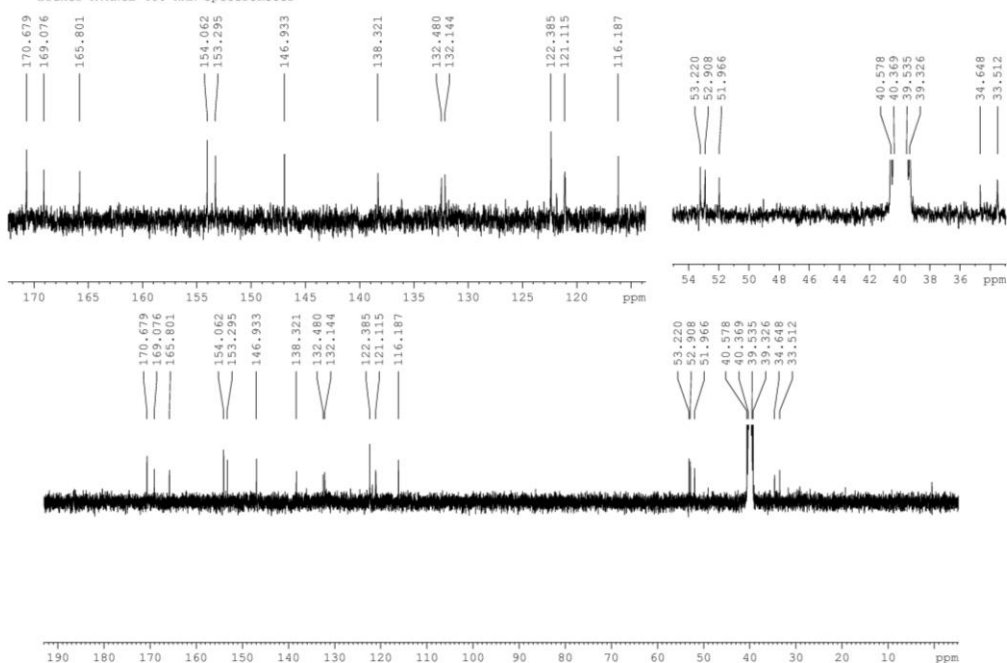
F2 - Acquisition Parameters
Date_ 20100714
Time 19.26
INSTRUM spect
PROBHD 5 mm PABBO BB-
PULPROG zgpg30
TD 65536
SOLVENT DMSO
NS 16
DS 2
SWH 8278.146 Hz
FIDRES 0.126314 Hz
AQ 3.9584243 sec
RG 64
DW 60.400 usec
DE 6.00 usec
TE 296.8 K
D1 1.5000000 sec
MCREST 0.0000000 sec
MCWRK 0.01500000 sec

===== CHANNEL f1 =====
NUC1 1H
P1 12.25 usec
PL1 2.00 dB
SFO1 400.126412 MHz

F2 - Processing Parameters
SI 262144
SF 400.1700000 MHz
WDW EM
SSB 0
LB 0 Hz
GB 0
PC 1.00

1D NMR plot parameters
CX 26.00 cm
CY 19.00 cm
F1P 9.531 ppm
F1 3014.17 Hz
F2P 1.469 ppm
F2 595.94 Hz
PPMCM 0.28723 ppm/cm
HZCM 114.94024 Hz/cm

Sample: IS-4-102
Solvent: DMSO
Standard Carbon-13 Parameters with
Composite Pulse Decoupling (Waltz-16)
Bruker AVANCE-400 NMR Spectrometer



Current Data Parameters
NAME IS-4-102
EXPNO 4
PROCNO 1

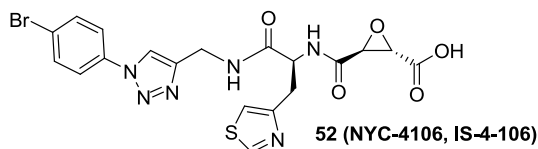
F2 - Acquisition Parameters
Date_ 20100714
Time 19.51
INSTRUM spect
PROBHD 5 mm PABBO BB-
PULPROG zgpg30
TD 65536
SOLVENT DMSO
NS 4
DS 4
SWH 23980.814 Hz
FIDRES 0.365918 Hz
AQ 1.3664756 sec
RG 1024
DW 20.850 usec
DE 6.00 usec
TE 297.4 K
D1 1.0000000 sec
D11 0.0300000 sec
DELTA 0.89999998 sec
MCREST 0.0000000 sec
MCWRK 0.01500000 sec

===== CHANNEL f1 =====
NUC1 13C
P1 9.50 usec
PL1 -2.00 dB
SFO1 100.626886 MHz

===== CHANNEL f2 =====
CPDPRG2 waltz16
NUC2 1H
PCPD2 80.10 usec
PL2 -2.00 dB
PL12 14.30 dB
PL13 14.00 dB
SFO2 400.1716007 MHz

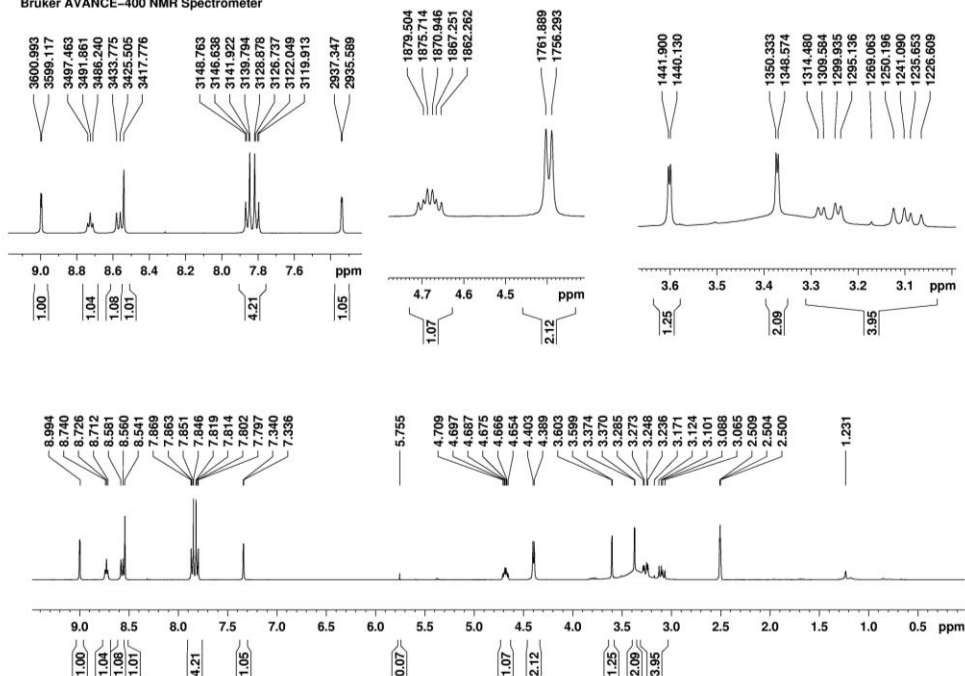
F2 - Processing parameters
SI 262144
SF 100.626886 MHz
WDW EM
SSB 0
LB 1.00 Hz
GB 0
PC 1.40

1D NMR plot parameters
CX 26.00 cm
CY 250.00 cm
F16 114.94024 Hz/cm



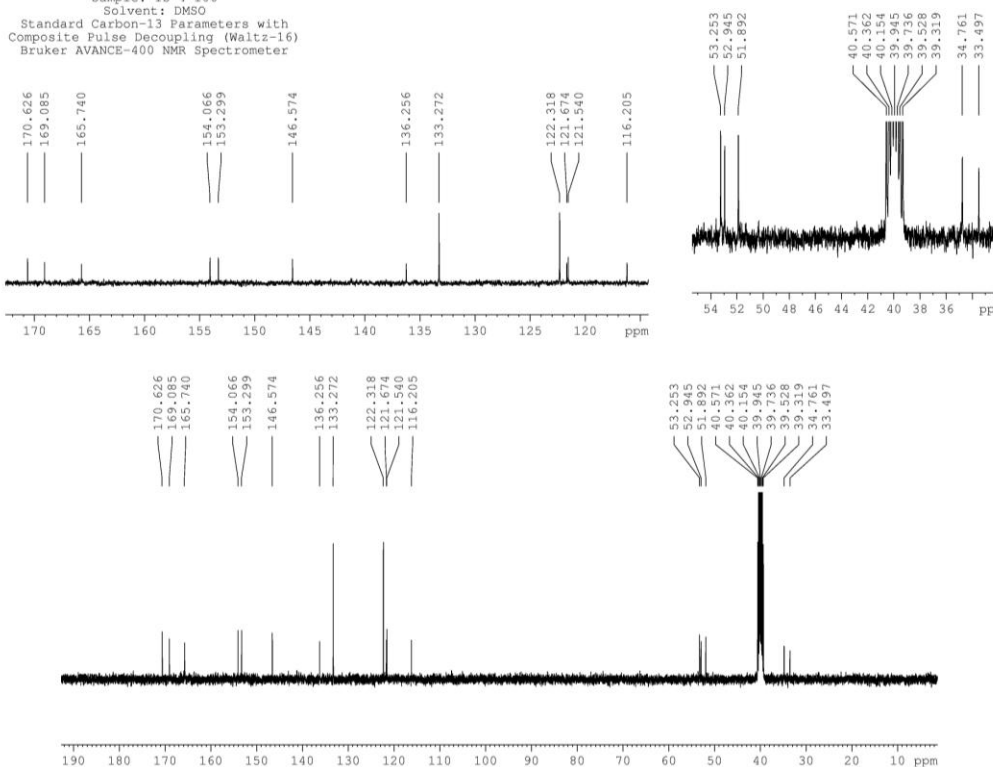
Sample: IS-4-106
Solvent: DMSO
Standard Survey 1-D Proton NMR Spectrum
Bruker AVANCE-400 NMR Spectrometer

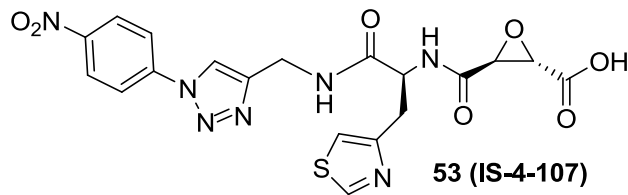
Chemical Formula: $C_{19}H_{17}BrN_5O_5S$
Molecular Weight: 521.34448



Current Data Parameters
NAME IS-4-106
EXPNO 1
PROCNO 1
F2 - Acquisition Parameters
Date_ 20100712
Time 18.29
INSTRUM spect
PROBHD 5 mm PABBO BB-
PULPROG zgpg30
TD 65536
SOLVENT DMSO
NS 16
DS 2
SWH 8278.146 Hz
FIDRES 0.126314 Hz
AQ 3.9584243 sec
RG 28.5
DW 60.400 usec
DE 6.00 usec
TE 297.3 K
D1 1.50000000 sec
MCREST 0.00000000 sec
MCWRK 0.01500000 sec
===== CHANNEL f1 =====
NUC1 1H
P1 12.25 usec
PL1 -2.00 dB
SFO1 400.1724712 MHz
F2 - Processing parameters
SI 262144
SF 400.17000000 MHz
WDW EM
SSB 0
LB 0.30 Hz
GB 0
PC 1.00
1D NMR plot parameters
CX 28.00 cm
CY 18.00 cm
F1 6615.28 Hz
F2 -4.168 ppm
F2 -1667.86 Hz
PPMCM 0.73881 ppm/cm
HZCM 295.64807 Hz/cm

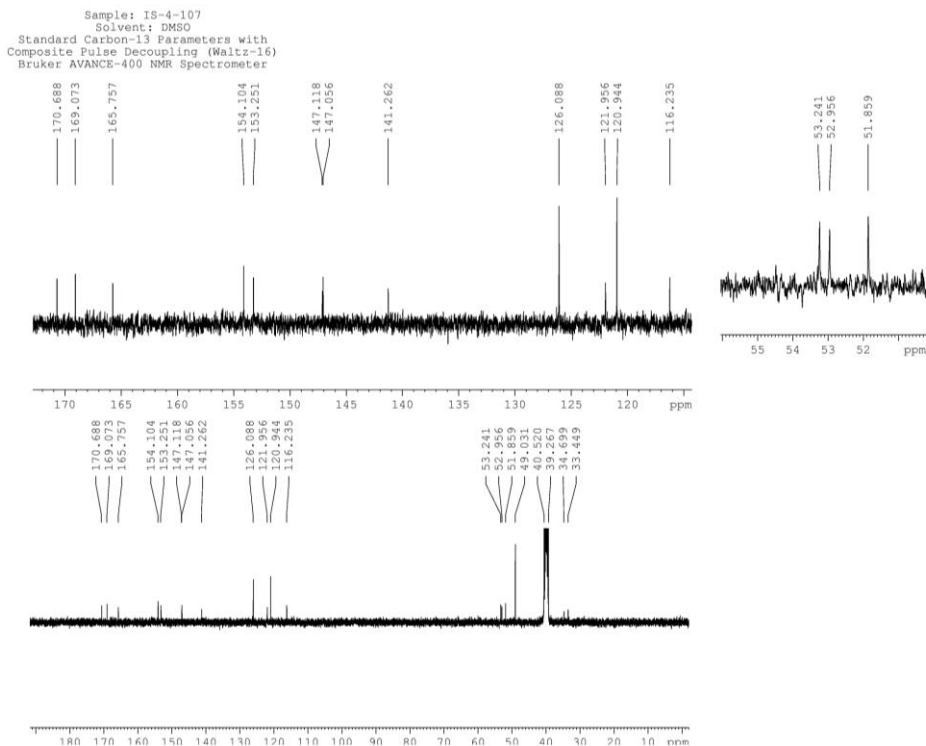
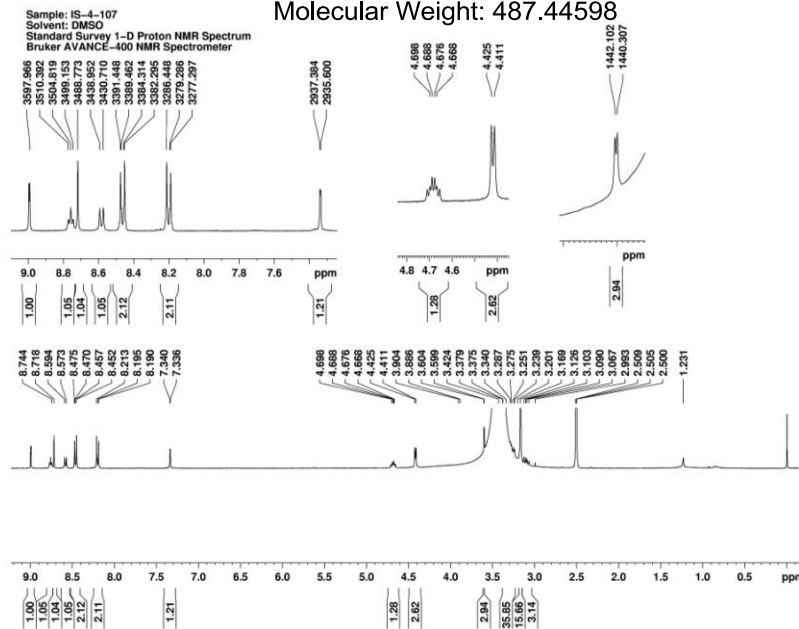
Sample: IS-4-106
Solvent: DMSO
Standard Carbon-13 Parameters with
Composite Pulse Decoupling (Waltz-16)
Bruker AVANCE-400 NMR Spectrometer

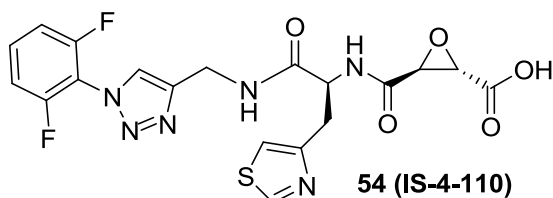




Chemical Formula: $C_{19}H_{17}N_7O_7S$

Molecular Weight: 487.44598





Chemical Formula: $C_{19}H_{16}F_2N_6O_5S$

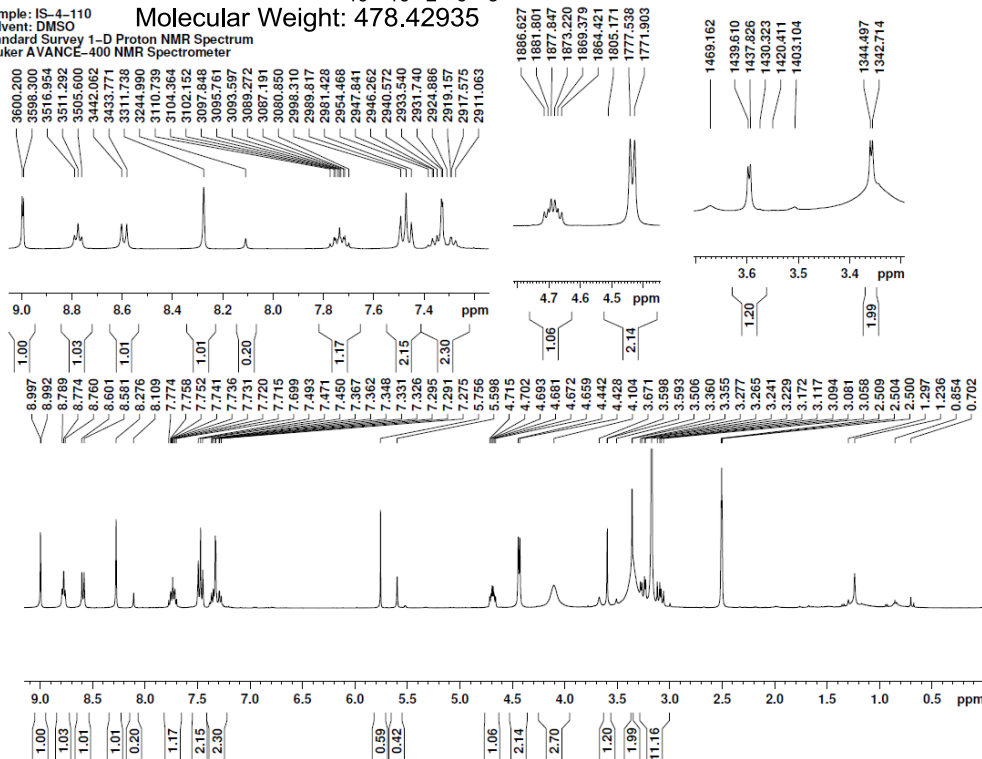
Molecular Weight: 478.42935

Sample: IS-4-110

Solvent: DMSO

Standard Survey 1-D Proton NMR Spectrum

Bruker AVANCE-400 NMR Spectrometer



Current Data Parameters
NAME IS-4-110
EXPNO 2
PROCNO 1

F2 - Acquisition Parameters
Date_ 20100717
Time 21.01
INSTRUM spect
PROBHD 5 mm PABBO BB-
PULPROG zgpg30
TD 65536
SOLVENT DMSO
NS 16
DS 2
SWH 8273.146 Hz
FIDRES 0.126314 Hz
AQ 3.6594243 sec
RG 28.5
DW 60.400 usec
DE 6.00 usec
TE 297.3 K
D1 1.5000000 sec
MCREST 0.0000000 sec
MCWRK 0.0150000 sec

===== CHANNEL f1 =====
NUC1 1H
P1 12.25 usec
PL1 -2.00 dB
SFO1 400.1724712 MHz

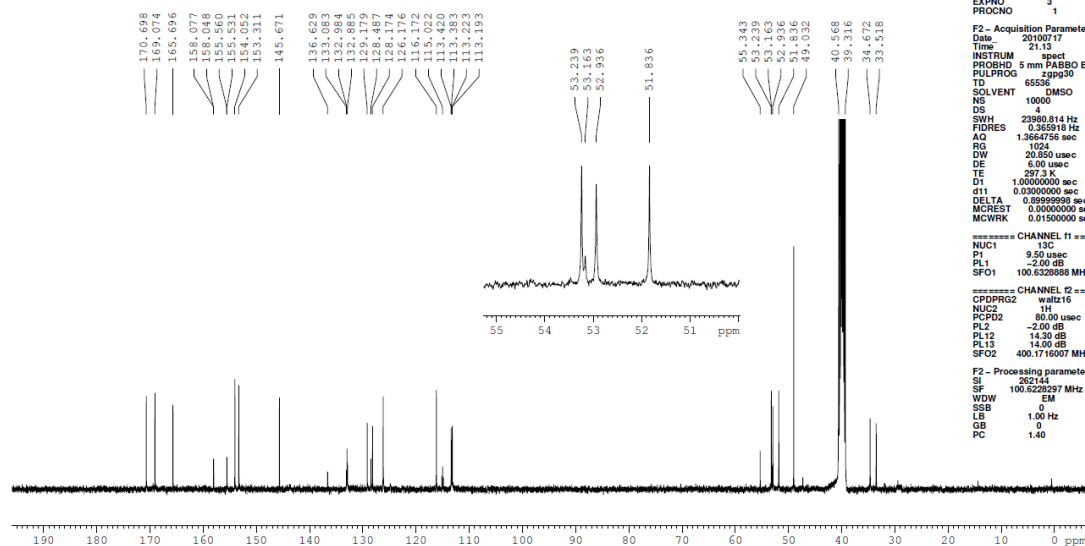
F2 - Processing parameters
SI 262144
SF 400.1724712 MHz
WDW EM
SSB 0
GB 0
PC 1.00

1D NMR plot parameters
CX 28.00 cm
CY 50.00 cm
F1P 3835.45 Hz
F2P 0.293 ppm
F2 104.22 Hz
PPMCM 0.33300 ppm/cm
HCM 133.25812 Hz/cm

3.277
3.265
3.241
3.229
3.172
3.117
3.084
3.081
3.058
2.509
2.504
2.500
1.297
1.286
0.854
0.702

11.16

Sample: IS-4-110
Solvent: DMSO
Standard Carbon-13 Parameters with
Composite Pulse Decoupling (Waltz-16)
Bruker AVANCE-400 NMR Spectrometer



Current Data Parameters
NAME IS-4-110
EXPNO 3
PROCNO 1

F2 - Acquisition Parameters
Date_ 20100717
Time 21.13
INSTRUM spect
PROBHD 5 mm PABBO BB-
PULPROG zgpg30
TD 65536
SOLVENT DMSO
NS 10000
DS 4
SWH 23980.814 Hz
FIDRES 0.365918 Hz
AQ 1.3664756 sec
RG 1024
DW 20.850 usec
DE 6.00 usec
TE 297.3 K
D1 1.0000000 sec
d11 0.0300000 sec
DELTA 0.8999999 sec
MCREST 0.0000000 sec
MCWRK 0.0150000 sec

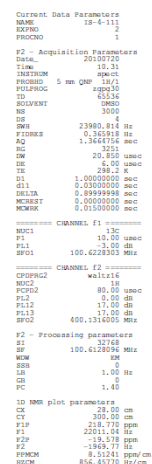
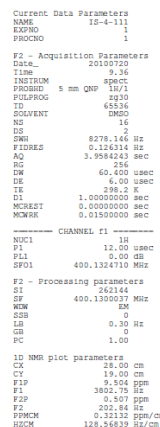
===== CHANNEL f1 =====
NUC1 13C
P1 9.50 usec
PL1 -2.00 dB
SFO1 100.6262287 MHz

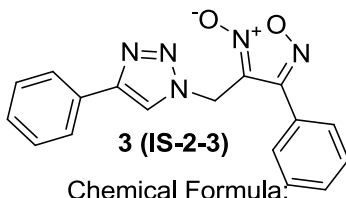
===== CHANNEL f2 =====
CPDPRG2 waltz16
NUC2 1H
PCPD2 80.00 usec
PL2 -2.00 dB
PL12 14.30 dB
PL13 14.00 dB
SFO2 400.1716807 MHz

F2 - Processing parameters
SI 262144
SF 100.6262287 MHz
WDW EM
SSB 1.00 Hz
GB 0
PC 1.40



Sample: IS-4-111
Solvent: DMSO
Standard 1-D Survey Proton NMR Experiment
Bruker DPX-400 NMR Spectrometer

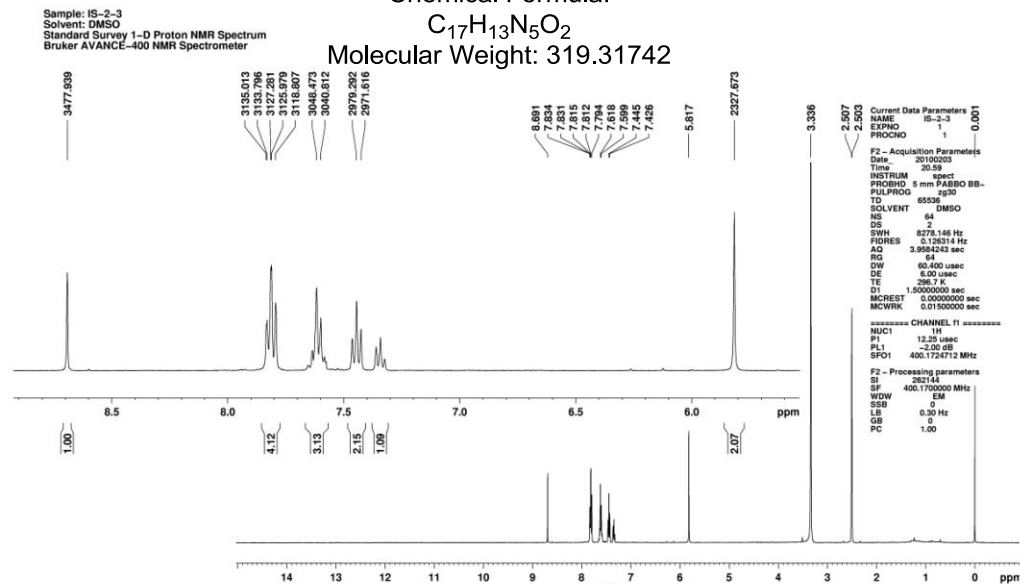




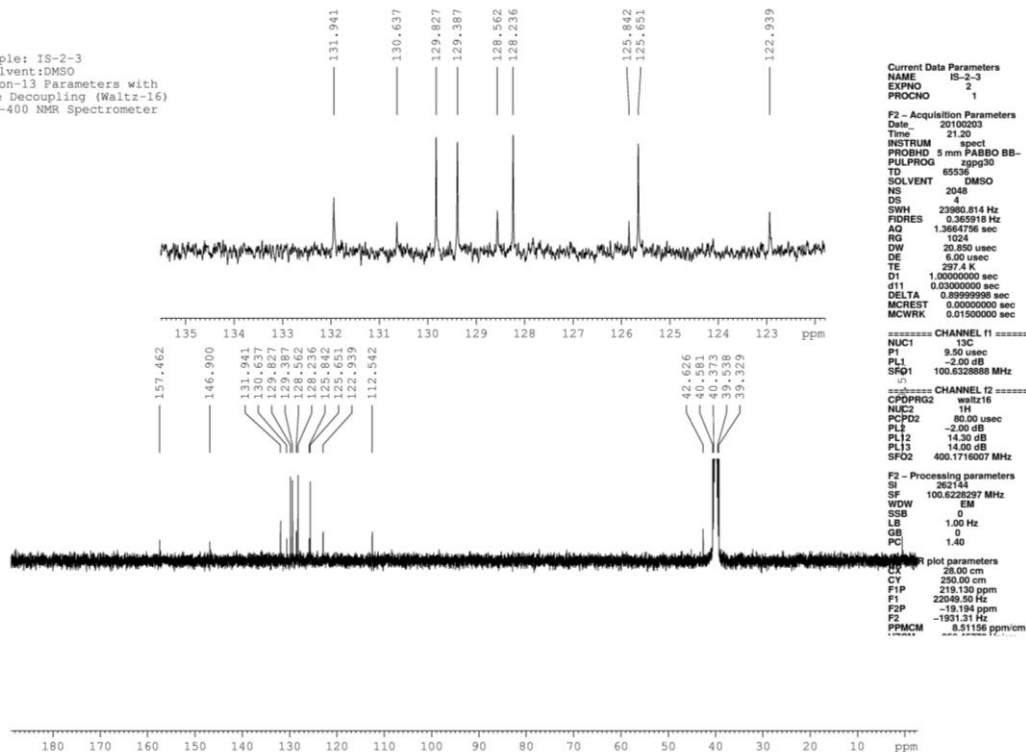
Chemical Formula:

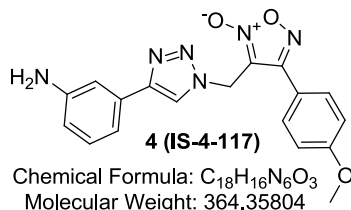
$C_{17}H_{13}N_5O_2$

Molecular Weight: 319.31742

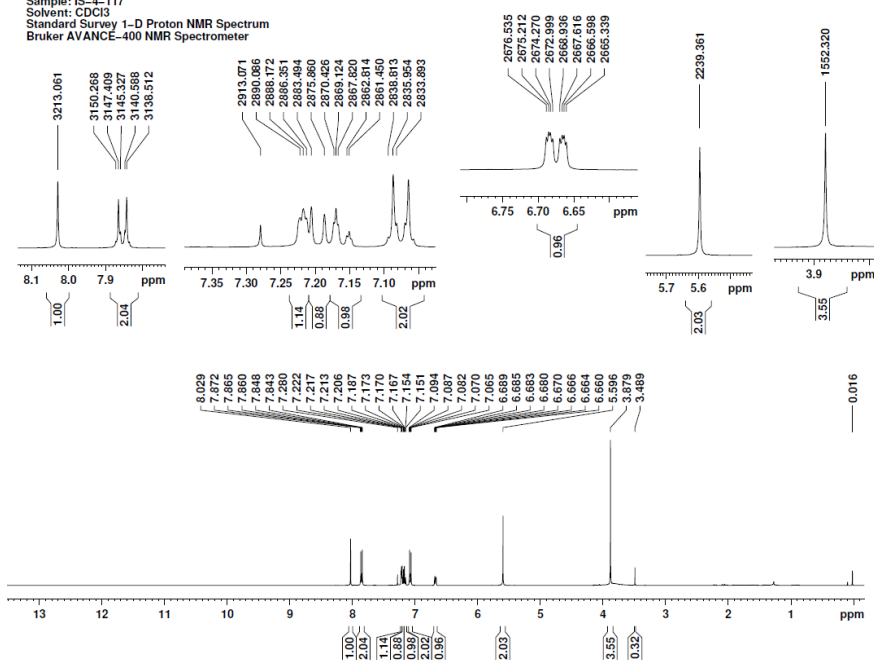


Sample: IS-2-3
Solvent: DMSO
Standard Carbon-13 Parameters with
Composite Pulse Decoupling (Waltz-16)
Bruker AVANCE-400 NMR Spectrometer



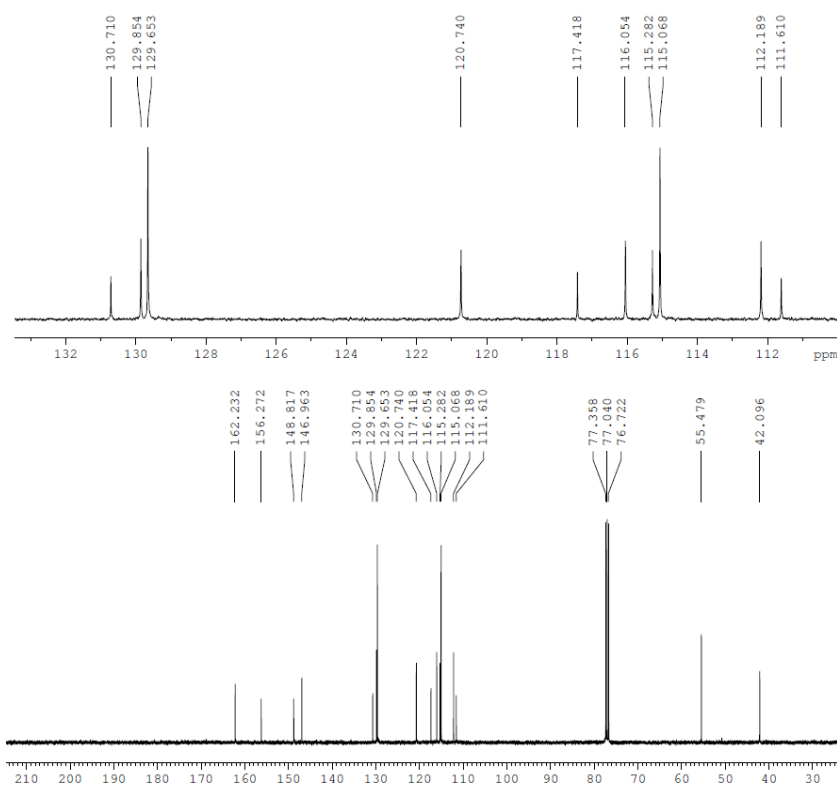


Sample: IS-4-117
 Solvent: CDCl₃
 Standard Survey 1-D Proton NMR Spectrum
 Bruker AVANCE-400 NMR Spectrometer

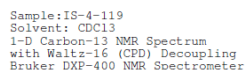
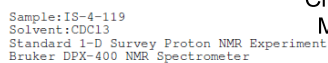


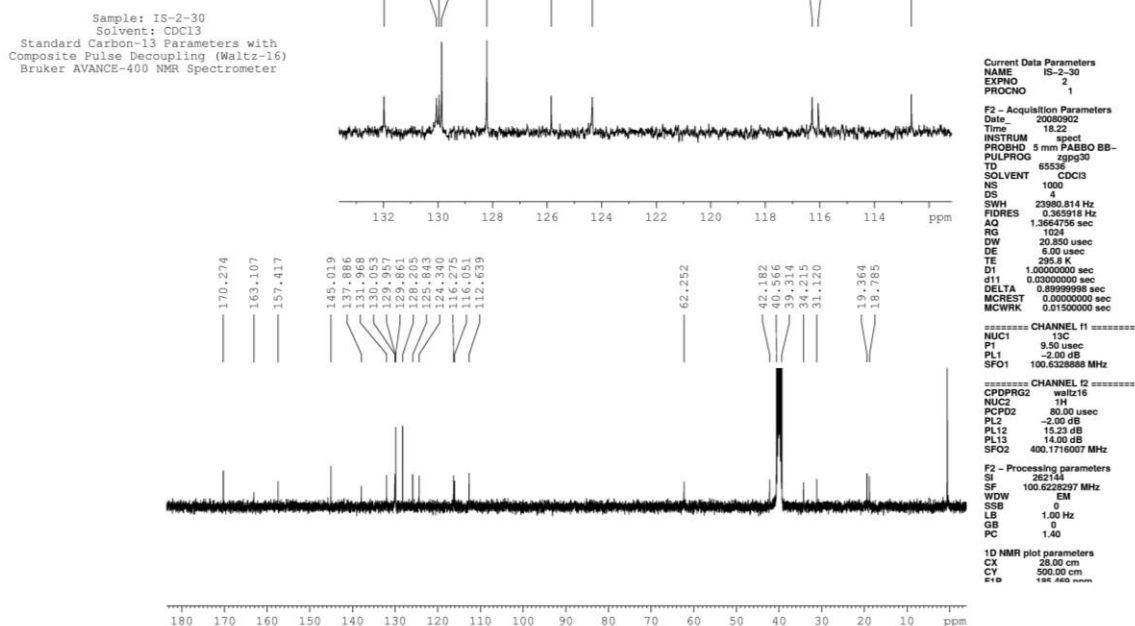
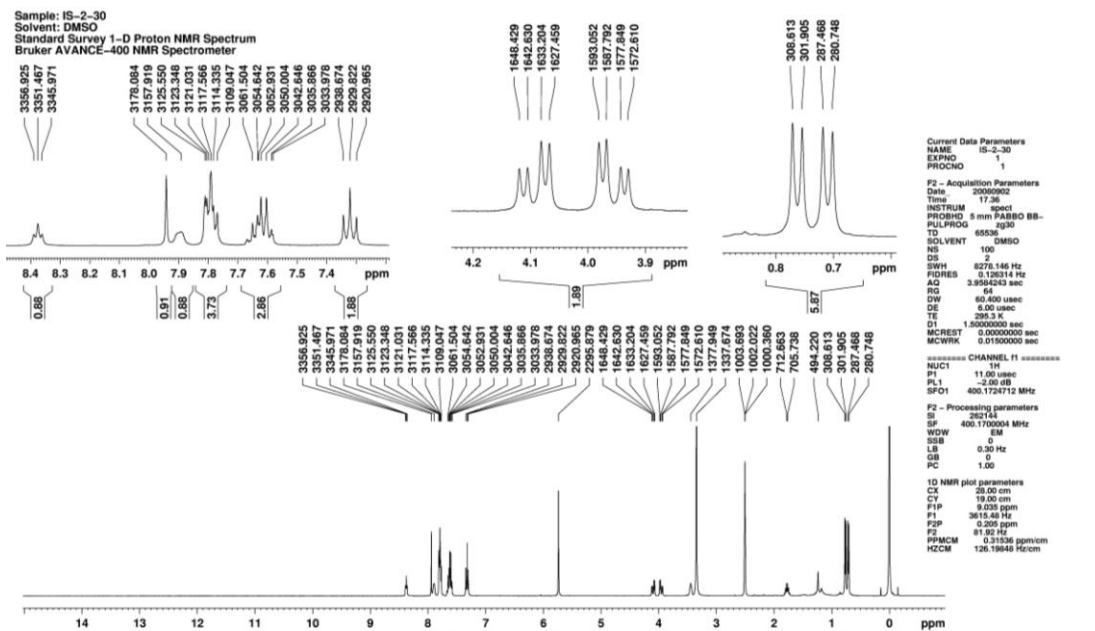
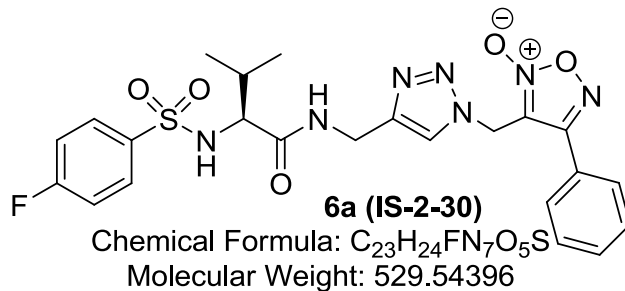
Current Data Parameters
 NAME IS-4-117
 EXPNO 1
 PROCNO 1
 F2 - Acquisition Parameters
 Date_ 20100929
 Time 8.41
 INSTRUM spect
 PROBHD 5 mm PABBO BB-
 PULPROG zg30
 TD 65536
 TO SOLVENT CDCl₃
 NS 16
 DS 2
 SWH 8276.146 Hz
 FIDRES 0.138314 Hz
 AQ 3.9584243 sec
 RG 26.2
 DW 60.400 usec
 DE 6.00 usec
 TE 298.2 K
 D1 1.50000000 sec
 MCREST 0.00000000 sec
 MCWRK 0.01500000 sec
 ===== CHANNEL f1 =====
 NUC1 1H
 P1 12.25 usec
 PL1 -2.00 dB
 SFO1 400.1724712 MHz
 F2 - Processing parameters
 SI 262144
 SF 400.1700000 MHz
 WDW EM
 SSB 0
 LB 0.30 Hz
 GB 0
 PC 1.00

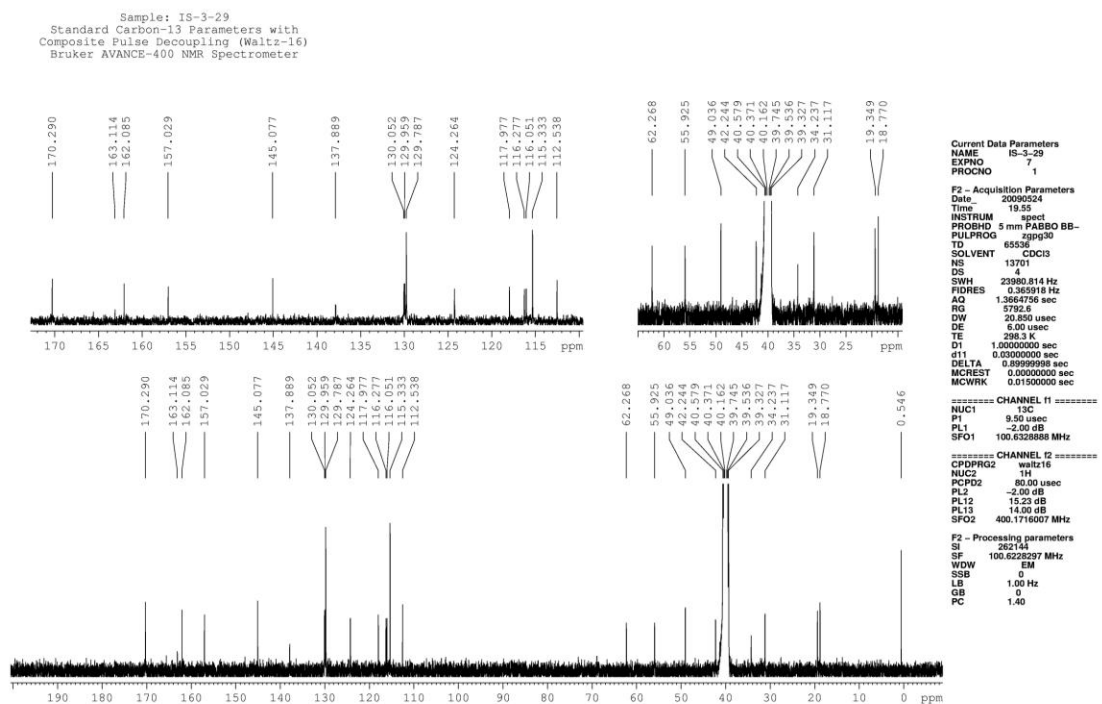
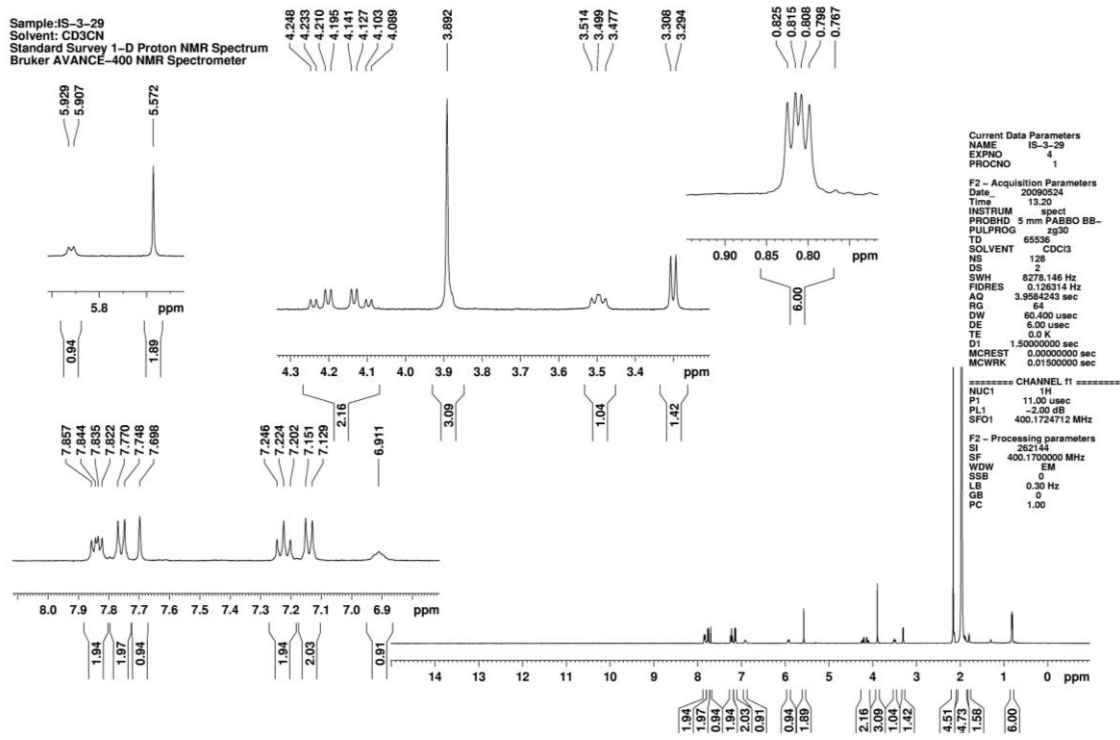
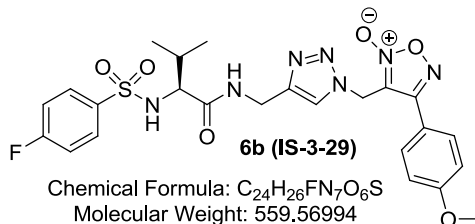
Sample: IS-4-117
 Solvent: CDCl₃
 Standard Carbon-13 Parameters with
 Composite Pulse Decoupling (Waltz-16)
 Bruker AVANCE-400 NMR Spectrometer

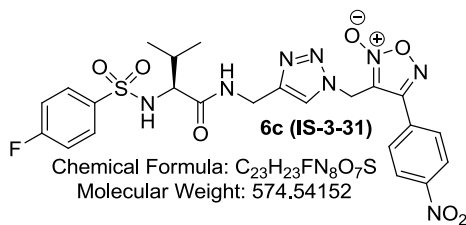


Current Data Parameters
 NAME IS-4-117
 EXPNO 2
 PROCNO 1
 F2 - Acquisition Parameters
 Date_ 20100929
 Time 8.47
 INSTRUM spect
 PROBHD 5 mm PABBO BB-
 PULPROG zgpg30
 TD 65536
 TO SOLVENT CDCl₃
 NS 663
 DS 4
 SWH 23980.814 Hz
 FIDRES 0.365918 Hz
 AQ 1.3664756 sec
 RG 1024
 DW 29.650 usec
 DE 6.00 usec
 TE 298.2 K
 D1 1.00000000 sec
 d11 0.03000000 sec
 DELTA 0.89999999 sec
 MCREST 0.00000000 sec
 MCWRK 0.01500000 sec
 ===== CHANNEL f1 =====
 NUC1 13C
 P1 9.50 usec
 PL1 -2.00 dB
 SFO1 100.6228888 MHz
 ===== CHANNEL f2 =====
 CPDPRG2 waltz16
 NUC2 1H
 PCPD2 80.00 usec
 PL2 -2.00 dB
 PL12 14.30 dB
 PL13 14.00 dB
 SFO2 400.1716007 MHz
 F2 - Processing parameters
 SI 262144
 SF 100.6228237 MHz
 WDW EM
 SSB 0
 LB 1.00 Hz
 GB 0
 PC 1.40
 1D NMR plot parameters
 CX 28.00 cm
 CY 10.00 cm
 FID 294.814 mm

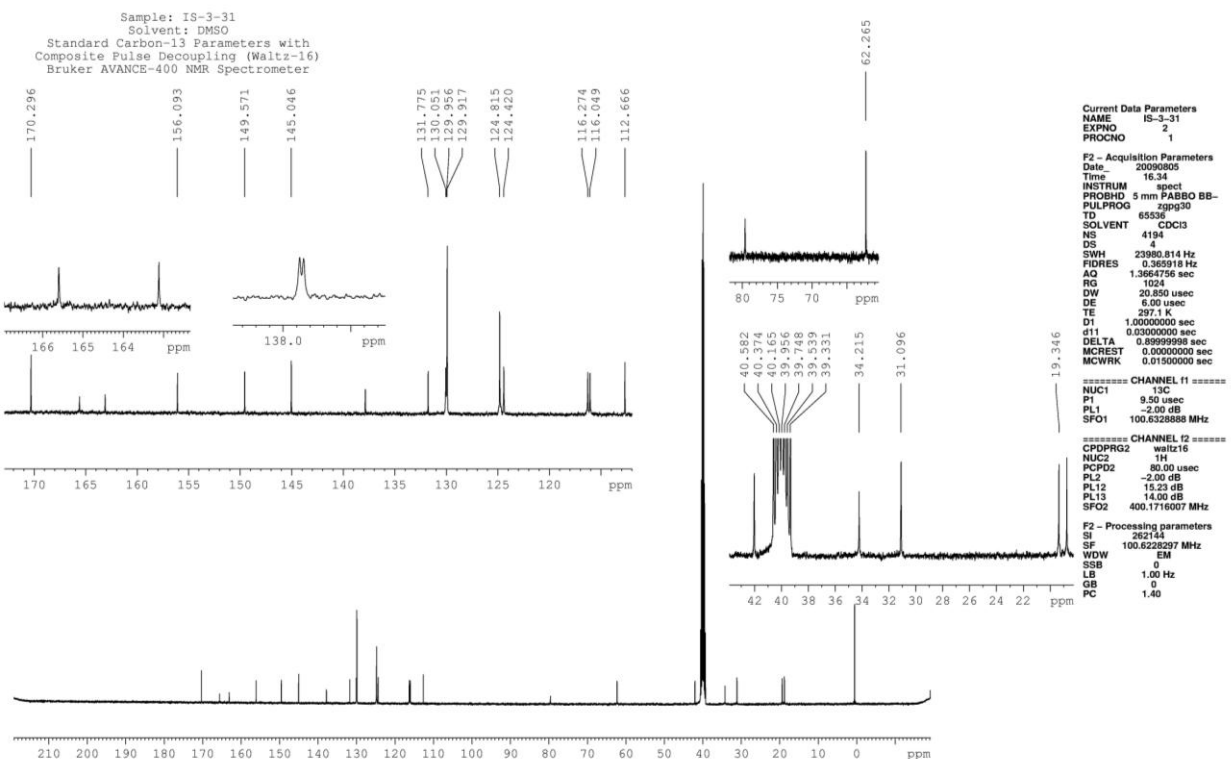
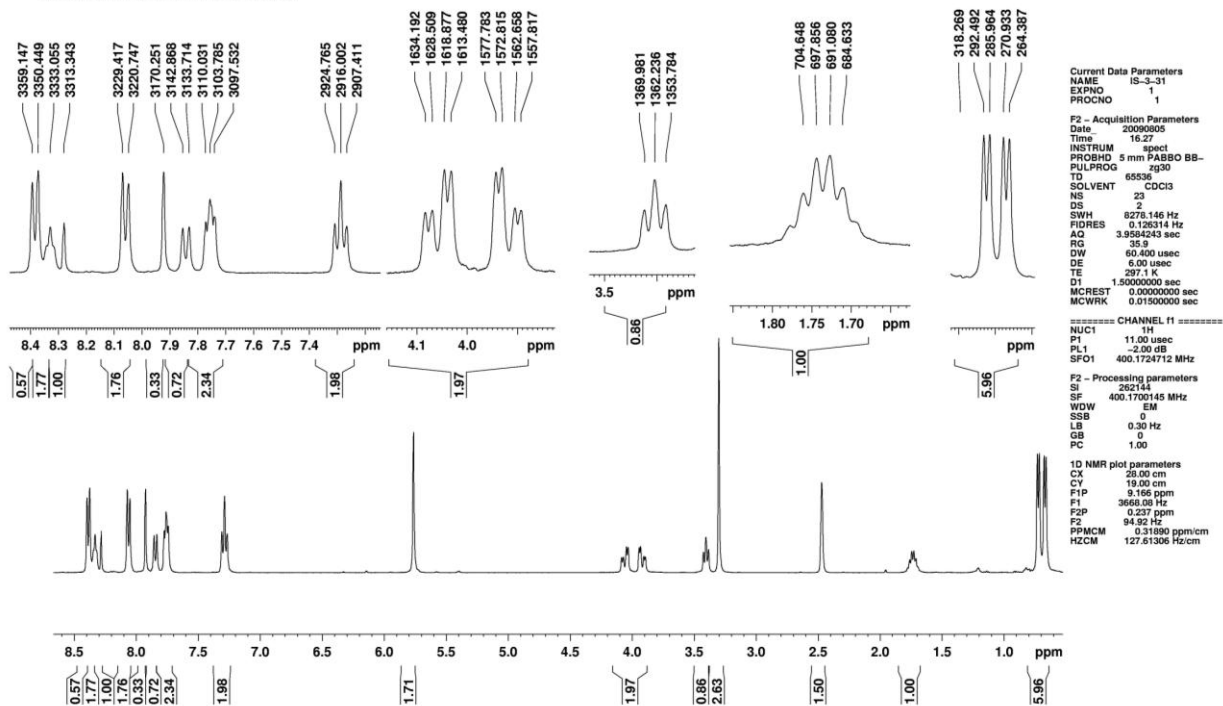


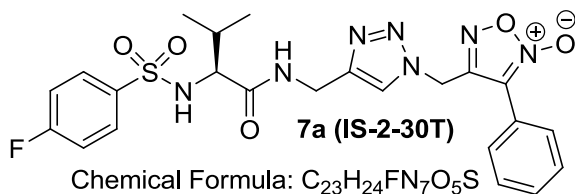




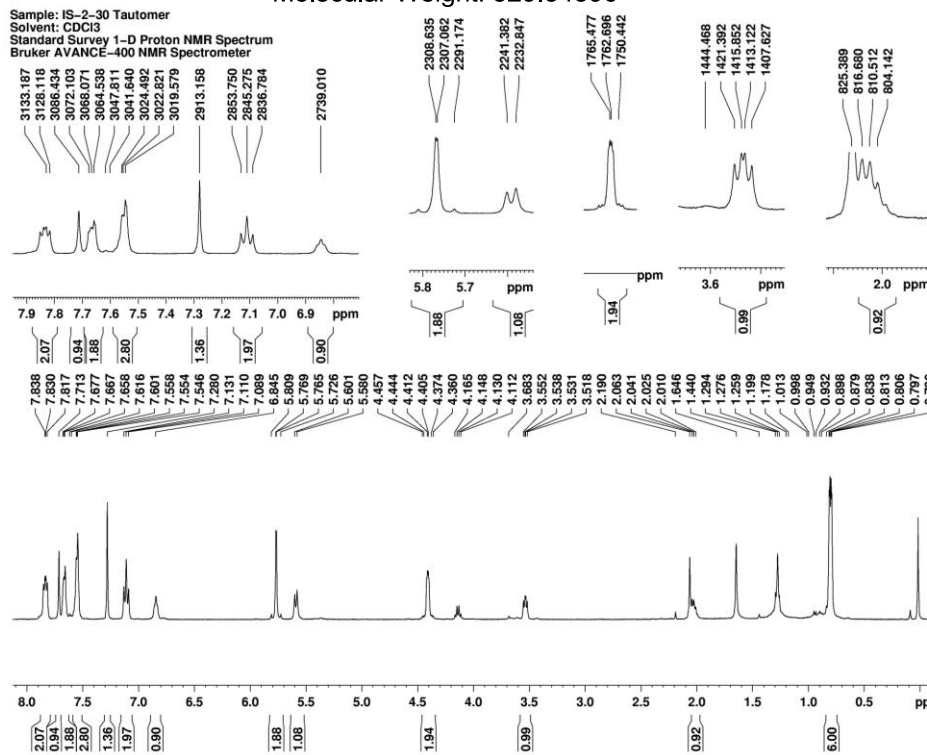


Sample: IS-3-31
 Solvent: DMSO
 Standard Survey 1-D Proton NMR Spectrum
 Bruker AVANCE-400 NMR Spectrometer

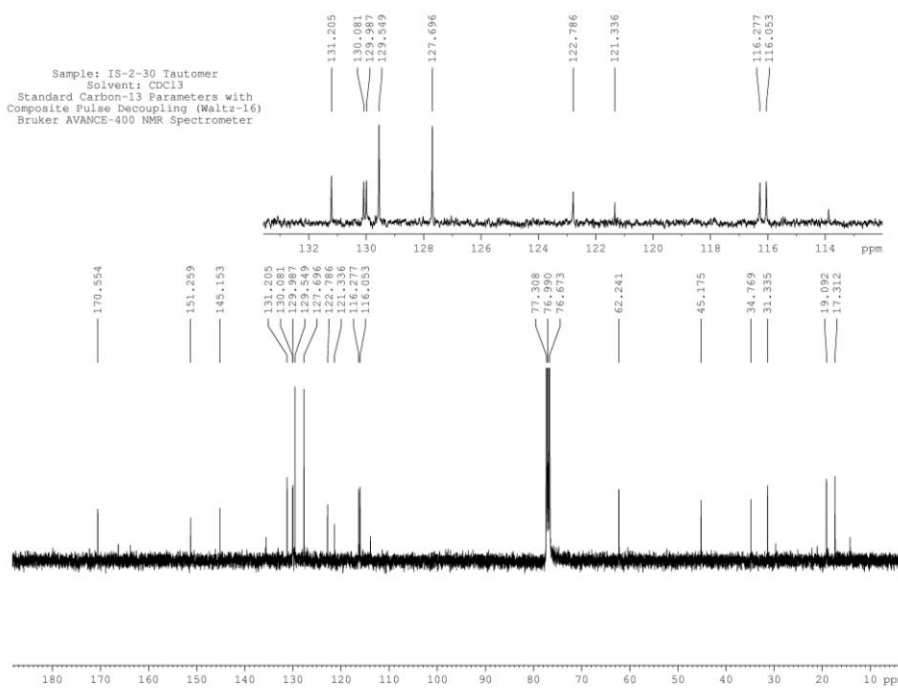




Sample: IS-2-30 Tautomer
 Solvent: CDCl₃
 Standard Survey 1-D Proton NMR Spectrum
 Bruker AVANCE-400 NMR Spectrometer



Current Data Parameters
 NAME: IS-2-30Tautomer
 EXPNO: 1
 PROCNO: 1
 F2 - Acquisition Parameters
 Date_: 20100220
 Time: 19.57
 INSTRUM: spect
 PROBHD: 5 mm PABBO BB-
 PULPROG: zg30
 TD: 65536
 SOLVENT: CDCl₃
 NS: 16
 DS: 2
 SWH: 8278.146 Hz
 FIDRES: 0.130314 Hz
 AQ: 3.9584243 sec
 RG: 64
 DW: 60.400 usec
 DE: 6.00 usec
 TE: 297.5 K
 D1: 1.50000000 sec
 MCREST: 0.01500000 sec
 MCWRK: 0.01500000 sec
 ===== CHANNEL f1 =====
 NUC1: ¹H
 P1: 12.25 usec
 PL1: -2.00 dB
 SFO1: 400.1724712 MHz
 F2 - Processing parameters
 SI: 362144
 SF: 400.1700000 MHz
 WDW: EM
 SSB: 0
 LB: 0.30 Hz
 GB: 0
 PC: 1.00



Sample: IS-2-30 Tautomer
 Solvent: CDCl₃
 Standard Carbon-13 Parameters with
 Composite Pulse Decoupling (Waltz-16)
 Bruker AVANCE-400 NMR Spectrometer

Current Data Parameters
 NAME: IS-2-30Tautomer
 EXPNO: 2
 PROCNO: 2
 F2 - Acquisition Parameters
 Date_: 20100220
 Time: 20.05
 INSTRUM: spect
 PROBHD: 5 mm PABBO BB-
 PULPROG: zgpg30
 TD: 65536
 SOLVENT: CDCl₃
 NS: 2682
 DS: 4
 SWH: 23980.814 Hz
 FIDRES: 0.369918 Hz
 AQ: 1.3664796 sec
 RG: 1024
 DW: 20.350 usec
 DE: 6.00 usec
 TE: 297.5 K
 D1: 1.00000000 sec
 d11: 0.03000000 sec
 DELTA: 0.89999998 sec
 MCREST: 0.03000000 sec
 MCWRK: 0.01500000 sec
 ===== CHANNEL f1 =====
 NUC1: ¹³C
 P1: 9.50 usec
 PL1: -2.00 dB
 SFO1: 100.6260888 MHz
 ===== CHANNEL f2 =====
 CPDPRG2: waltz16
 NUC2: ¹H
 PCPD2: 80.00 usec
 PL2: -2.00 dB
 PL12: 15.23 dB
 PL13: 16.00 dB
 SFO2: 400.1716007 MHz
 F2 - Processing parameters
 SI: 362144
 SF: 100.6260287 MHz
 WDW: EM
 SSB: 0
 LB: 1.00 Hz
 GB: 0
 PC: 1.40
 1D NMR plot parameters
 CX: 28.00 cm
 CY: 10.00 cm
 F1P: 219.130 ppm
 F1: 22048.50 Hz
 F2P: -19.194 ppm
 F2: -1891.31 Hz
 PPMCM: -6.51156 ppm/cm

```

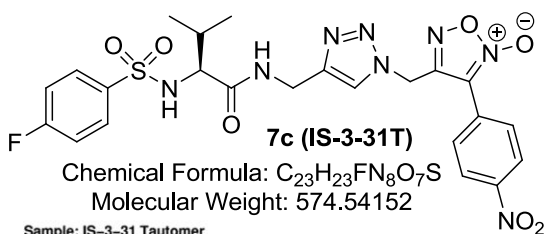
Current Data Parameters
Name    IS-3-29 Isoamer
EXPNO   1
PROCNO   1
F2 - Acquisition Parameters
Time    20100302
P1       1.0000000
INSTRUM  spect
PROBHD   5mm HBBBO BB
PULPROG  zgpg30
SFOF      400.130
SOLVENT   DMSO
DS         4
SWH        16379.814 Hz
FIDRES    0.365918 Hz
AQ         1.26954 sec
RG          1024
WDW         2
SSB         0
GB          0
PC         298.1 K
D1         1.0000000
d11         0.0300000 sec
DE         0.0000000
AQ1        0.0000000 sec
MCREST    0.0000000 sec
MWRK       0.0000000 sec

===== CHANNEL 12 =====
NUC1      13C
P1         8.000000
PC         -2.000000
SFO1      100.6238888 MHz

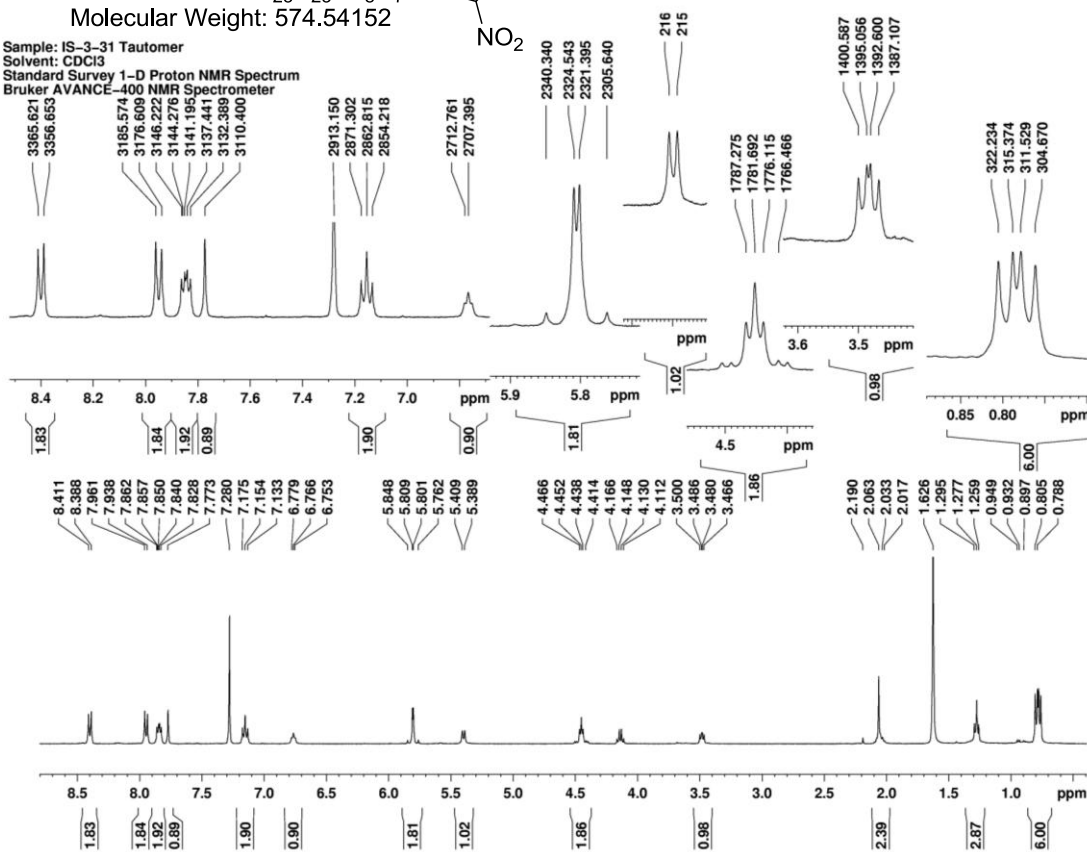
===== CHANNEL 12 =====
NUC2       1H
P2         80.000000
PC         -2.000000
PL1        15.25 dB
PL2        15.25 dB
PL3        14.90 dB
SFO2       500.1716007 MHz

F2 - Processing parameters
SI         262.145
SF         62.8262857 MHz
WDW         EM
SSB         0
LB          1.0 Hz
GB          0
PC          1.000000
DC          0

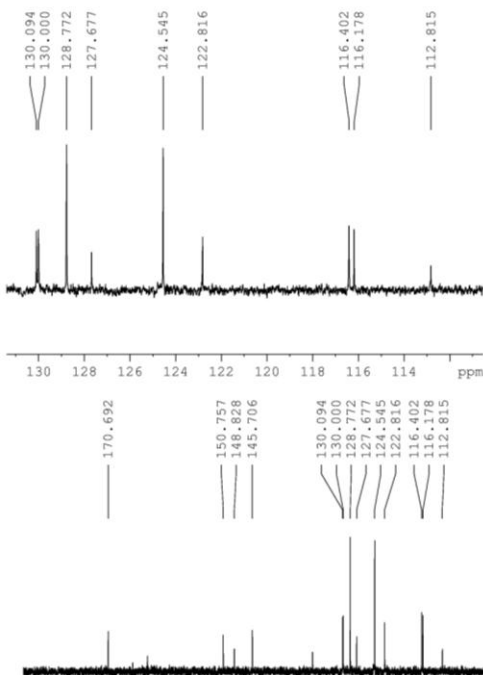
```



Sample: IS-3-31 Tautomer
 Solvent: CDCl₃
 Standard Survey 1-D Proton NMR Spectrum
 Bruker AVANCE-400 NMR Spectrometer

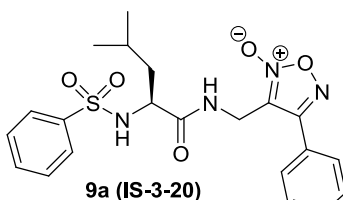


Current Data Parameters
 NAME IS-3-31Tautomer
 EXPNO 1
 PROCNO 1
 F2 - Acquisition Parameters
 Date 20100220
 Time 22.03
 INSTRUM spect
 PROBHD 5 mm PABBO BB-
 PULPROG zg30
 TD 65536
 SOLVENT CDCl₃
 NS 32
 DS 2
 SWH 8278.146 Hz
 FIDRES 0.126314 Hz
 AQ 3.9584243 sec
 RG 64
 DW 60.400 usec
 DE 6.00 usec
 TE 297.4 K
 D1 1.50000000 sec
 MCREST 0.00000000 sec
 MCWRK 0.01500000 sec
 ===== CHANNEL f1 =====
 NUC1 1H
 P1 12.75 usec
 PL1 -2.00 dB
 SFO1 400.1724712 MHz
 F2 - Processing parameters
 SI 32768
 SF 400.1700000 MHz
 WDW EM
 SSB 0
 LB 0.30 Hz
 GB 0
 PC 1.00
 1D NMR plot parameters
 CX 28.00 cm
 CY 19.00 cm
 F1P 3599.37 Hz
 F2P 0.534 ppm
 F2 213.54 Hz
 PPMCM 0.29661 ppm/cm
 HZCM 119.49413 Hz/cm



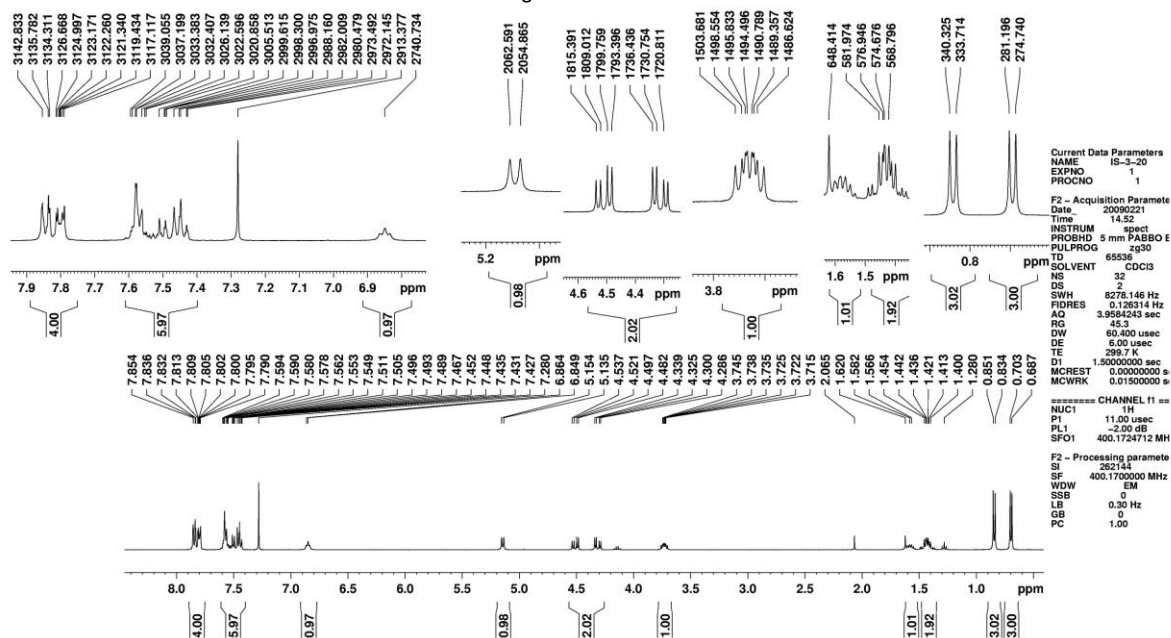
Sample: IS-3-31 Tautomer
 Solvent: CDCl₃
 Standard Carbon-13 Parameters with
 Composite Pulse Decoupling (Waltz-16)
 Bruker AVANCE-400 NMR Spectrometer

Current Data Parameters
 NAME IS-3-31Tautomer
 EXPNO 2
 PROCNO 1
 F2 - Acquisition Parameters
 Date 20100220
 Time 22.11
 INSTRUM spect
 PROBHD 5 mm PABBO BB-
 PULPROG zgpg30
 TD 65536
 SOLVENT CDCl₃
 NS 15000
 DS 4
 SWH 23980.814 Hz
 FIDRES 0.365918 Hz
 AQ 1.3664756 sec
 RG 1024
 DW 20.850 usec
 DE 6.00 usec
 TE 297.9 K
 D1 1.00000000 sec
 d11 0.03000000 sec
 DELTA 0.89999998 sec
 MCREST 0.00000000 sec
 MCWRK 0.01500000 sec
 ===== CHANNEL f1 =====
 NUC1 13C
 P1 9.50 usec
 PL1 -2.00 dB
 SFO1 100.632888 MHz
 ===== CHANNEL f2 =====
 NUC2 1H
 P2 80.00 usec
 PL2 -2.00 dB
 PL12 15.23 dB
 PL13 14.00 dB
 SFO2 400.1716007 MHz
 F2 - Processing parameters
 SI 262144
 SF 100.6228297 MHz
 WDW EM
 SSB 0
 LB 1.00 Hz
 GB 0
 PC 1.40
 1D NMR plot parameters
 CX 28.00 cm
 CY 10.00 cm
 F1P 256.760 ppm
 F1 29835.94 Hz
 F2P -56.824 ppm
 F2 -5717.76 Hz
 PPMCM 11.19943 ppm/cm
 HZCM 119.49413 Hz/cm

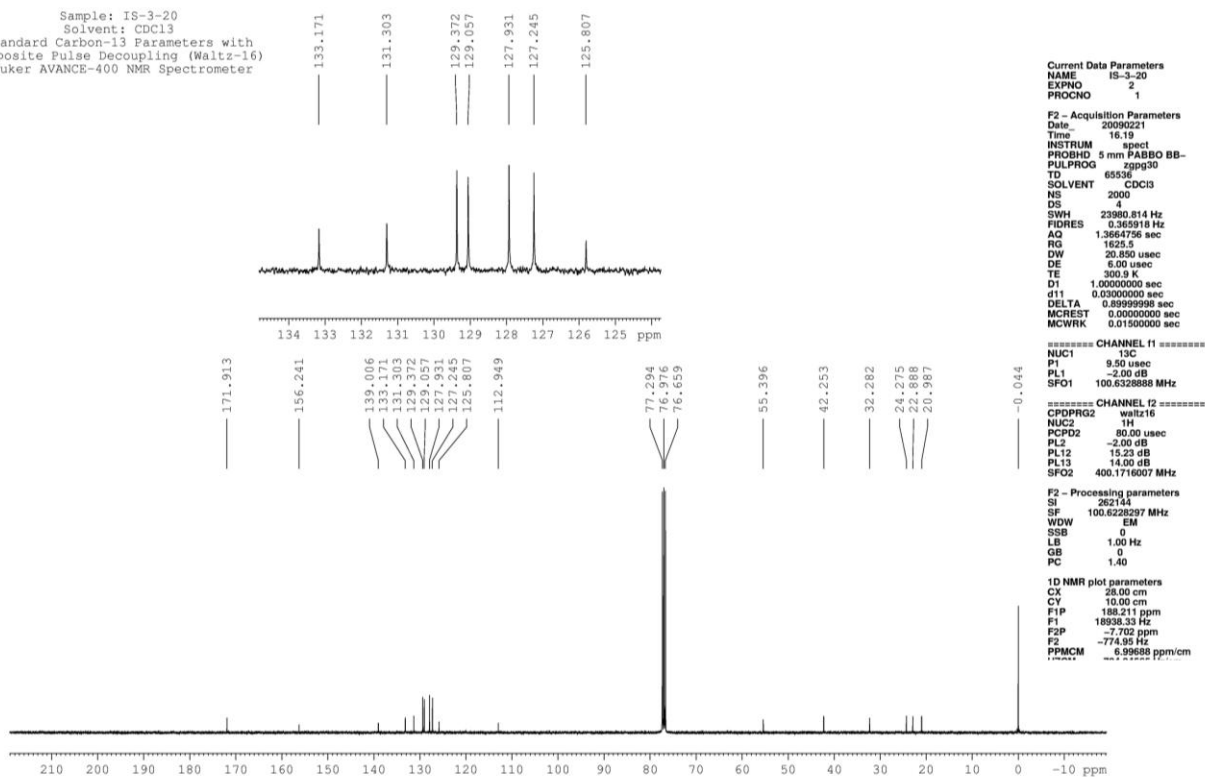


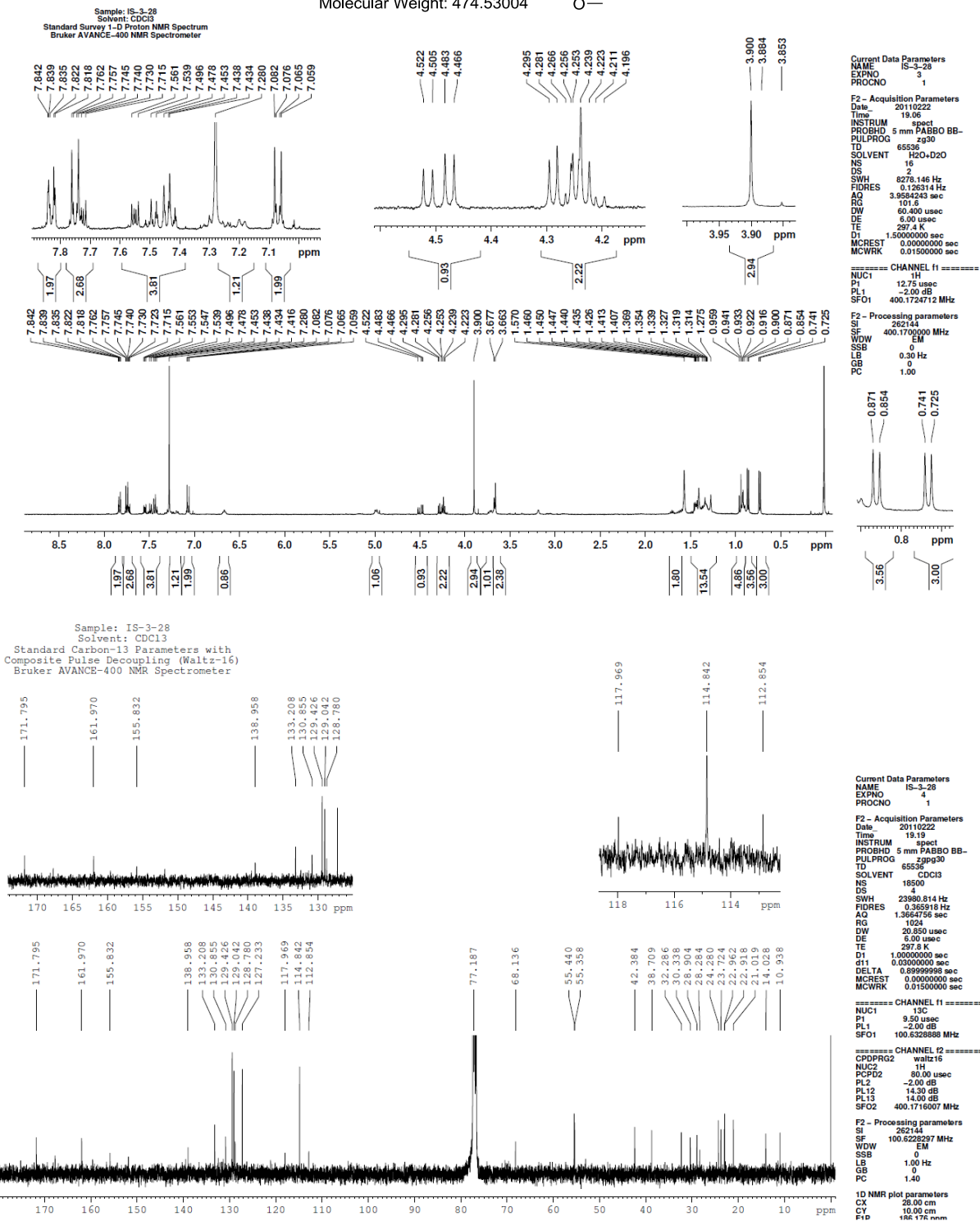
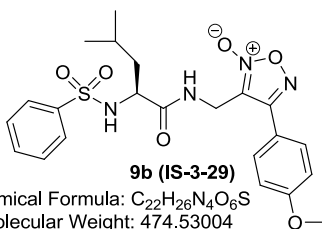
Chemical Formula: $C_{21}H_{24}N_4O_5S$
Molecular Weight: 444.50406

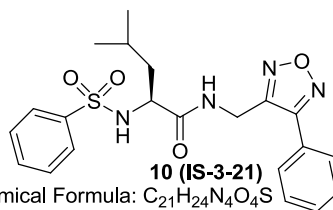
Sample: IS-3-20
Solvent: CDCl₃
Standard Survey 1-D Proton NMR Spectrum
Bruker AVANCE-400 NMR Spectrometer
HY compound



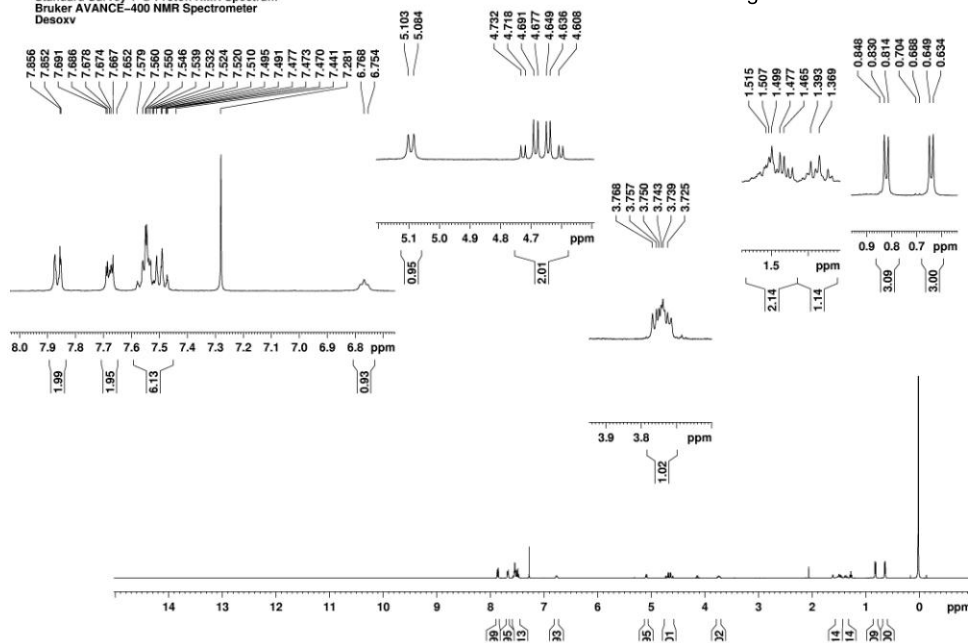
Sample: IS-3-20
Solvent: CDCl₃
Standard Carbon-13 Parameters with
Composite Pulse Decoupling (Waltz-16)
Bruker AVANCE-400 NMR Spectrometer





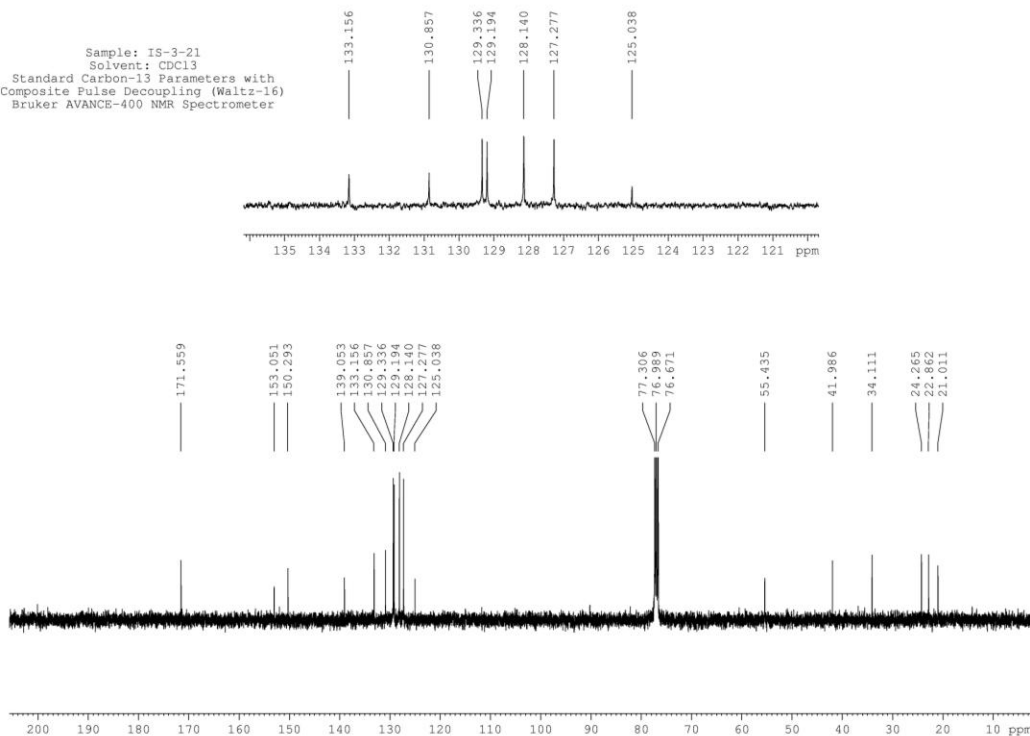


Sample: IS-3-21
Solvent: CDCl₃
Standard Survey 1-D Proton NMR Spectrum
Bruker AVANCE-400 NMR Spectrometer
Desoxy



Current Data Parameters
NAME IS-3-21
EXPNO 2
PROCNO 1
F2 - Acquisition Parameters
Date_ 20090225
Time 11.18
INSTRUM spect
PROBHD 5 mm PABBO BB-
PULPROG zgpg30
TD 65536
SOLVENT CDCl₃
NS 16
DS 4
SWH 8278.146 Hz
FIDRES 0.126214 Hz
AQ 3.894243 sec
RG 64
RG 64
DW 60.400 usec
DE 6.00 usec
TE 297.3 K
D1 1.5000000 sec
MCREST 0.0000000 sec
MCWRK 0.0150000 sec
===== CHANNEL f1 =====
NUC1 1H
P1 11.00 usec
PL1 -2.00 dB
SFO1 400.1724712 MHz
F2 - Processing parameters
SI 262144
SF 400.1700000 MHz
WDW EM
SSB 0
LB 0.30 Hz
GB 0
PC 1.00
1D NMR plot parameters
CX 28.00 cm
CY 19.00 cm
F1P 9.015 ppm
F2P 3607.59 Hz
F2P -1.411 ppm
PPMCM -864.66 Hz
H2CM 149.00900 Hz/cm

Sample: IS-3-21
Solvent: CDCl₃
Standard Carbon-13 Parameters with
Composite Pulse Decoupling (Waltz-16)
Bruker AVANCE-400 NMR Spectrometer



Current Data Parameters
NAME IS-3-21
EXPNO 3
PROCNO 1
F2 - Acquisition Parameters
Date_ 20090225
Time 11.41
INSTRUM spect
PROBHD 5 mm PABBO BB-
PULPROG zgpg30
TD 65536
SOLVENT CDCl₃
NS 1442
DS 4
SWH 23980.814 Hz
FIDRES 0.365918 Hz
AQ 1.3664756 sec
RG 2560.3
RG 20.850 usec
DE 6.00 usec
TE 297.3 K
D1 1.0000000 sec
d11 0.0300000 sec
DELTA 0.8999999 sec
MCREST 0.0000000 sec
MCWRK 0.0150000 sec
===== CHANNEL f1 =====
NUC1 13C
P1 9.50 usec
PL1 -2.00 dB
SFO1 100.6238888 MHz
===== CHANNEL f2 =====
CPDPRG2 waltz16
NUC2 1H
PCPD2 80.00 usec
PL2 -2.00 dB
PL12 15.23 dB
PL13 14.00 dB
SFO2 400.1716007 MHz
F2 - Processing parameters
SI 262144
SF 100.6228297 MHz
WDW EM
SSB 0
LB 1.00 Hz
GB 0
PC 1.40
1D NMR plot parameters
CX 28.00 cm
CY 10.00 cm
F1P 215.130 ppm
F2P 22048.80 Hz
F2P -19.194 ppm
F2P -1931.31 Hz
PPMCM 8.51156 ppm/cm

Vita
Isaac T. Schiefer
University of Illinois at Chicago
Department of Medicinal Chemistry and Pharmacognosy
833 S. Wood St. Rm. 539
Chicago, Illinois, 60612

EDUCATION

August 2003 - June 2007 *Bachelor of Science in Pharmaceutical Sciences,
Medicinal and Biological Chemistry*
University of Toledo, **Toledo, Ohio**
• **Minor in Chemistry**
• **Honors Thesis: "Design and Synthesis
of Muscarinic Agonist Derivatives"**



August 2007 - May 2012 *Doctor of Philosophy in Medicinal Chemistry*
University of Illinois at Chicago, **Chicago, Illinois**
• **Thesis Title: "Synthesis, Optimization,
and Evaluation of Thiophilic Peptidomimetics
as Novel AD Therapies"**



RESEARCH EXPERIENCE

Research Assistant, University of Illinois at Chicago,
Faculty Advisor: Gregory R. J. Thatcher, Ph.D., Hans W. Vahlteich 06/2008 to present
Chair of Medicinal Chemistry, Professor & Assistant Head for Research
Department of Medicinal Chemistry & Pharmacognosy, College of
Pharmacy

Primary Project:

1) Three years as **Medicinal Chemistry Team Leader** of a successful UO1 project in collaboration with the lab of Ottavio Arancio (Columbia University, New York, NY), focusing on evaluating peptidomimetic epoxide based cysteine protease inhibitors for the treatment of Alzheimer's disease. *Personally designed, synthesized and optimized over 50 analogs of the selected lead compound during the duration of the project* (all compounds fully characterized by ¹H NMR, ¹³C NMR, HRMS, and > 95 % pure by HPLC). Examined stability and reactivity of selected compounds by HPLC-UV. Characterized *in vitro* metabolites and measured *in vivo* bioavailability using LC-MS/MS. Acted as the key intermediary between the neurobiologist, bioanalytical chemist, computational chemist, and the **PI/synthetic chemistry team**. Actively corresponded with collaborators to define deadlines and ensure the timely delivery of compounds to colleagues and collaborators in order to advance the project. The highest endeavor culminated in the identification of two novel, synthetically accessible molecules that show promising efficacy and negligible toxicity *in vivo* (Therapeutic Index > 100, in murine model). Further drug development efforts are ongoing.

Selected Secondary Projects:

- 2) Synthesized novel NO-NSAID derivatives as selective amyloid lowering agents [Published Manuscript: Schiefer, I. T.; et al. *J. Med. Chem.*, **2011**, *54*, 2293-2306];
- 3) Performed synthetic chemistry troubleshooting and analyzed brain bioavailability of chimeric NO-SSRI molecules [Published Manuscript: Abdul-Hay, S.; Schiefer, I. T.; et al. *ACS Med. Chem. Lett.*, **2011**, *2*, 656-661];
- 4) Designed, and synthesized novel neuroprotective NO mimetic furoxan (oxadiazole-N-oxides) containing peptidomimetics. Monitored reactivity of selected furoxans with cysteine using HPLC and identified reaction products by LC-MS/MS. Examined NO release and cysteine reaction rate using colorimetric assays, and correlated reactivity/NO release to observed neuroprotection [Schiefer, I. T.; et al. *J. Med. Chem.*, Accepted Manuscript, Spring **2012**].

NMR Facility Technician, University of Illinois at Chicago, Supervisor:
Alec Krunić, Shared Laboratories Director, Department of Medicinal
Chemistry & Pharmacognosy, College of Pharmacy

06/2009 to
present

Primarily responsible for regular NMR facility maintenance, including: spectrometer troubleshooting; training new users in 1D and 2D NMR; filling with liquid Nitrogen & Helium; *etc.*
Most importantly, this experience afforded the ability to quickly and accurately acquire/interpret ^1H and ^{13}C NMR, and therefore enhanced my ability to understand and troubleshoot complex chemical reactions.

Undergraduate Honors Student Lab Technician, University of Toledo,
Faculty Advisor: William S. Messer Jr, Ph.D., Professor and Chair,
Department of Pharmacology, College of Pharmacy

05/2006 to
06/2007

Performed scale up synthesis of muscarinic agonist currently in clinical development for AD and Schizophrenia. Designed and synthesized novel bivalent muscarinic ligands for further development.
Honors Thesis Title: “*Design and Synthesis of Muscarinic Agonist Derivatives*”.

ACADEMIC TRAINING AND EXPERIENCE

Graduate Student/Clinical Fellow Teaching Certificate Program: a semester long course initiated and facilitated by renowned pharmaceutical educator, **Nicholas Popovich, Ph.D.**, (current Head of the Department of Pharmacy Practice at the University of Illinois at Chicago, and Emeritus Professor of the College of Pharmacy at Purdue University) to address the general lack of instructional education training among academic research faculty.

Constructed a personal teaching philosophy (available upon request), developed and refined teaching/lecture style, and produced a teaching portfolio to aide in the transition to an academic teaching/research position.

Teaching Assistant, Experiential IPPE (Spring 2008, Fall 2008, Spring 2009)
Department of Pharmacy Practice
University of Illinois at Chicago, Chicago, Illinois

Teaching Assistant, Principles of Drug Action and Therapeutics (Fall 2007)
Department of Medicinal Chemistry and Pharmacognosy
University of Illinois at Chicago, Chicago, Illinois

HONORS AND AWARDS

Departmental Honors in Medicinal and Biological Chemistry, University of Toledo, 2007
Graduate Student/Clinical Fellow Teaching Certificate, University of Illinois at Chicago, 2009
Oscar Robert Olberg Prize for Excellence in Medicinal Chemistry, University of Illinois at Chicago, 2011
Young Investigator Scholarship, Alzheimer's Drug Discovery Foundation (ADDF), 2012

MEMBERSHIPS IN PROFESSIONAL SOCIETIES

American Chemical Society
• Medicinal Chemistry Division
Society for Neuroscience
Kappa Psi Pharmaceutical Fraternity
American Association of Pharmaceutical Scientists
Phi Kappa Delta Honors Society
International Union of Pure and Applied Chemistry

PUBLICATIONS/PATENTS/ABSTRACTS (in chronological order)

Published and Pending Manuscripts

Schiefer, I. T.; et al. ...and Thatcher, G. R. J. Design, Synthesis, and Optimization of Epoxide Based Calpain Inhibitors as Preclinical Candidates for Alzheimer's Disease Therapy, *Manuscript in Preparation*.

Schiefer, I. T.; VandeVrede, L.; Fa', M.; Arancio, O.; Thatcher, G.R.J. Furoxans (1, 2, 5 Oxadiazole-N-Oxides) as Novel NO Mimetic Neuroprotective and Procognitive Agents, *Accepted Manuscript, J. Med. Chem.*, **2012**, DOI: 10.1021/jm201504.

Abdul-Hay, S.; **Schiefer, I. T.**, Chandrasena, R. E. P.; Li, M.; Abdelhamid, R.; Wang, Y.; Tavassoli, E.; Michalsen, B.; Luo, J.; and Thatcher, G. R. J. NO-SSRIs: Nitric Oxide Chimera Drugs Incorporating a Selective Serotonin Reuptake Inhibitor. *ACS Med. Chem. Lett.*, **2011**, 2, 656-661. DOI: 10.1021/ml2000033

Schiefer, I. T.; Abdul-Hay, S.; Wang, H.; Vanni, M.; Qin, Z.; Thatcher, G. R. J. Inhibition of Amyloidogenesis by Nonsteroidal Anti-inflammatory Drugs and Their Hybrid Nitrates. *J. Med. Chem.*, **2011**, 54, 2293-2306. DOI: 10.1021/jm101450p

Abdelhamid, R.; Luo, J.; VandeVrede, L.; Kundu, I.; Michalsen, B.; Litosh, V. A.; **Schiefer, I. T.**; Gherezghiher, T.; Yao, P.; Qin, Z.; Thatcher, G. R. J. Benzothiophene Selective Estrogen Receptor Modulators Provide Neuroprotection by a Novel GPR30-Dependent Mechanism. *ACS Chem. Neuro.*, **2011**, 2, 256-268. DOI: 10.1021/cn100106a

Anand, S.; **Schiefer, I. T.**; Thatcher, G.R. J. Nitric Oxide Donor and Mimetic Molecules in Cancer Chemotherapy and Chemoprevention. *Forum on Immunopathological Diseases and Therapeutics*, **2010**, *1*, 251-279.

Sinha, V.; Wijewickrama, G. T.; Chandrasena, R. E. P.; Xu, H.; Edirisinghe, P. D.; **Schiefer, I. T.**; Thatcher, G. R. J. Proteomic and Mass Spectroscopic Quantitation of Protein S-Nitrosation Differentiates NO-Donors. *ACS Chem. Biol.*, **2010**, *5*, 667-680.

Patents and Pending Applications

Thatcher, G.R.J. , **Schiefer, I. T.**; Fa', M.; Arancio, O. Preparation of Epoxide Based Cysteine Protease Inhibitors for the Treatment of Neurodegenerative Diseases and Uses Thereof. *Provisional Patent Disclosure February 2012*.

Thatcher, G.R.J. , **Schiefer, I. T.**; Arancio, O. Furoxans (1, 2, 5 Oxadiazole-N-Oxides) as Novel NO Mimetic Neuroprotective and Procognitive Agents; *Provisional Patent Disclosure, March 2011*.

Selected Abstracts & Oral Presentations

Schiefer, I. T.; et al...and Thatcher, G. R. J. *Design, Synthesis, and Optimization of Epoxide Based Calpain Inhibitors as Preclinical Candidates for Alzheimer's Disease Therapy*, 6th Drug Discovery for Neurodegeneration Conference, Alzheimer's Drug Discovery Foundation, New York, United States, Feb 12-14, 2012

Schiefer, I. T.; VandeVrede, L.; Fa', M.; Arancio, O.; Thatcher, G.R.J., *Furoxans (1, 2, 5 Oxadiazole-N-Oxides) as Novel NO Mimetic Neuroprotective and Procognitive Agents*, 7th Canadian Nitric Oxide Society Conference, Queens University, Kingston, Ontario, Canada, June 10-11, 2011.

Schiefer, I. T.; VandeVrede, L.; Fa', M.; Arancio, O.; Thatcher, G.R.J. *Furoxans (1, 2, 5 Oxadiazole-N-Oxides) as Novel NO Mimetic Neuroprotective and Procognitive Agents*, 49th annual MIKI medicinal chemistry meeting, University of Kansas, United States, April 8-10, 2011.

Litosh, Vladislav A.; Michalsen, Bradley T.; Gandhi, Ronak P.; Abdelhamid, Ramy; Luo, Jia; Van de Vrede, Lawren; Kundu, Indraneel; **Schiefer, I. T.**; Gherezghiher, Teshome; Yao, Ping; Qin, Zhihui; Thatcher, Gregory R. *Synthesis of novel benzothiophene selective estrogen receptor modulators (BT-SERMs) that provide neuroprotection by a novel GPR30-dependent mechanism*. Abstracts of Papers, 242nd ACS National Meeting&Exposition, Denver, CO, United States, August 28-September 1, **2011**.

Mendonca, Emma L.; Pieffet, Gilles; **Schiefer, I.**; Sinha, Vaishali; Ranepuradewage, Chandrasena E.; Tapadar, Subhasish; Gihani, Thakshala W.; Edirisinghe, Praneeth; Arancio, Ottavio; Thatcher, G. R. J.; Petukhov, Pavel A. Binary QSAR model for classification of calpain inhibitors. Abstracts of Papers, 237th ACS National Meeting, Salt Lake City, UT, United States, March 22-26, **2009**.

Statement of Teaching Philosophy

Emphasizing the clinical impact of basic medicinal chemistry concepts is vital to teaching of medicinal chemistry successfully within a college of pharmacy. The basic pharmaceutical sciences, i.e., medicinal chemistry, biochemistry, pharmacology, form the necessary foundation of pharmacy students' education. Medicinal chemistry plays the important role of bridging the gap between pharmacology and biochemistry. Unfortunately, educators engaged in teaching medicinal chemistry sometimes struggle to demonstrate clearly the importance of this discipline to pharmacy students. As a result, students frequently associate medicinal chemistry with organic chemistry, which some consider as "boring" or "irrelevant" to their eventual career goals. Disengaged students will often resort to rely heavily on memorization rather than genuinely studying to learn the course materials. The ability to secure the attention and interest of students must be a top priority. This can be accomplished through constant "side bars," or reminders of the clinical consequences of the medicinal chemistry topics being presented.

I believe a central agenda of teaching medicinal chemistry to pharmacy students must focus on highlighting the relationships between medicinal chemistry concepts and clinical outcomes.

To educate students more successfully, faculty must work together to help "connect the dots" for their students. Frequently, educators focus primarily on their own content area and expertise and fail to relate their course material with other courses in the students' curriculum. It is important, therefore, for faculty to be familiar with the entire curriculum, especially when content from other courses overlaps with their own. The importance of creating a strong interdisciplinary approach and the need for a team effort is crucial. Communication is the backbone to achieve a comprehensive and ideal interdisciplinary teaching environment. However, communication among faculty is often neglected due to scheduling conflicts and differences in faculty priorities.

I believe that taking the time engage other faculty members to more effectively relate the materials of the curriculum as interconnected is of great importance.

The emergence of new technological and social media platforms presents opportunities for the future of higher education. The rise of social media platforms (e.g. facebook [845 million users], twitter [350 million users]) can be harnessed to help educate students using structured and unstructured approaches. The guided use of these platforms can aide in increasing the accessibility of educators to students. Alternatively, back channel communications by students can also allow for a free back-and-forth exchange of questions and discussion. Typically, students refrain from asking questions during a course lecture due to a fear of "looking stupid", and the appropriate use of technology could alleviate this concern through anonymous postings on a course twitter feed.

Creating opportunities for students to engage classmates and teachers actively using social media can assist in developing a more successful learning environment.

Isaac Schiefer
University of Illinois at Chicago
March 2012

